



UNIVERSITY OF <sup>TM</sup>  
**KWAZULU-NATAL**

---

INYUVESI  
**YAKWAZULU-NATALI**

**A STUDY ON THE ATMOSPHERIC AND  
ENVIRONMENTAL IMPACTS OF AEROSOL,  
CLOUD AND PRECIPITATION INTERACTION**

**ABDULAZIZ TUNDE YAKUBU**

**216076172**

**2022**

**A STUDY ON THE ATMOSPHERIC AND  
ENVIRONMENTAL IMPACTS OF AEROSOL, CLOUD  
AND PRECIPITATION INTERACTION**

By

**ABDULAZIZ TUNDE YAKUBU**

Under the supervision of

**PROF. NAVEN CHETTY**

Submitted in partial fulfillment of the requirements for the degree of

**Doctor of Philosophy in Physics**

School of Chemistry and Physics

College of Agriculture, Engineering and Science

University of KwaZulu-Natal

Pietermaritzburg Campus

South Africa

**2022**

## **ABSTRACT**

Understanding the mechanisms and processes of aerosol-cloud-precipitation interactions (ACPI) is essential in the determination of the specific role of aerosols in modulating extreme weather events and climate change in the long run. Atmospheric aerosols are mainly of various types and are emitted from differing sources. Considering they commonly exist in the heterogeneous forms in most environments, they significantly influence the incoming solar energy and the general perturbation of the clouds depending on their constituents. Thus, a systemic identification and characterisation of these particles are essential for proper representation in climate models. To better understand the process of climate change, this research explores the climate diversity of South Africa to examine aerosol sources and types concerning the atmospheric aerosol suspension over the region and their role in clouds and precipitation formation. The study further provided answers to the cause of extreme precipitation events, including drought and occasional flooding experienced over the region. Also, an insightful explanation of the process of ACPI is provided in the context of climate change. Furthermore, the research found that the effective radiative forcing (RF) over South Africa as monitored in Cape Town and Pretoria is negative (i.e., cooling effect) and provided an analysis of the cause. Similarly, the validation of some satellite datasets from MISR (Multiangle Imaging Spectroradiometer) and MODIS (Moderate Resolution Imaging Spectroradiometer) instruments against AERONET (Aerosol Robotic Network) is conducted over the region. Although a significant level of agreement is observed for the two instruments, intense improvements are needed, especially regarding measurements over water surfaces. Finally, the study demonstrated the proficiency of effective rainfall prediction from satellite instrument cloud datasets using machine learning algorithms.

## **PREFACE**

The work contained in this thesis was carried out by Abdulaziz Yakubu at the School of Chemistry and Physics, University of KwaZulu-Natal, Pietermaritzburg campus, South Africa under the supervision of Professor Naven Chetty.

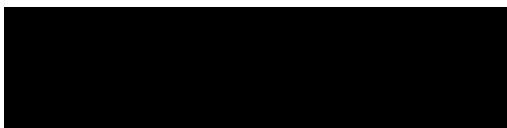
The entire thesis, unless specifically indicated in the text, is the work of the author and has not been submitted in whole or in part to any other institution. Where use has been made of the work of others, it is duly acknowledged in the text.



06/12/2022

**Signature (Student)**

**Date**



06 December 2022

**Signature (Supervisor)**

**Date**

## DECLARATION: PLAGIARISM

I, Abdulaziz Tunde Yakubu, declare that;

1. The research reported in this thesis, except where otherwise indicated, is my original research.
2. This thesis has not been submitted in full or in part for any degree or examination at any other university.
3. This thesis does not contain other persons' data, pictures, graphs or other information unless specifically acknowledged as being sourced from other persons.
4. This thesis does not contain other persons' writing unless specifically acknowledged as being sourced from other researchers. Where other written sources have been quoted, then:
  - a. Their words have been rewritten but the general information attributed to them has been referenced.
  - b. Where their exact words have been used, then their writing has been placed inside quotation marks and referenced.
5. This thesis does not contain text, graphics or tables copied and pasted from the internet, unless specifically acknowledged, and the source is detailed in the thesis and the References sections.

.....

Signed

.....06/12/2022.....

Date

## **DECLARATION 2 – PUBLICATIONS**

### **Articles submitted to Journal**

The work listed below are submitted articles currently undergoing peer-review with a reputable journal, they form part of this thesis and are original work of the author.

Yakubu, A. T., and Chetty, N. 2022. A decadal assessment of the climatology of aerosol and cloud properties over South Africa. (Submitted to Journal of Atmospheric Chemistry and Physics)

Yakubu, A. T., and Chetty, N. 2022. Atmospheric aerosol optical properties and radiative forcing over two metros in South Africa. (Submitted to Journal of Geophysical Research: Atmosphere)

Yakubu, A. T., Abayomi, A., and Chetty, N. 2022. Machine learning-based precipitation prediction using cloud properties. (Submitted to Springer Lecture Notes in Networks and Systems)

## **ACKNOWLEDGEMENT**

In the name of Allah, the most gracious and the most merciful. Blessed is he in whose hand is the dominion and he can do all things, who has created death and life that he may test you for which of you is best in deeds. And he is the all-mighty, the oft-forgiving. I give all thanks and adoration to Almighty Allah (SWT) for this accomplishment. Also, may the peace and blessings of Allah (SWT) be upon our beloved prophet Muhammad (SAW) as my role model in spirituality, knowledge, steadfastness, moral uprightness and true guidance to the proper way of life critical to this achievement and beyond.

Special thanks to my supervisor Prof. N. Chetty for the moral, financial and academic support he offered me. His inspiration has not only been instrumental to the success of this work, but it has also earned me a landmark in my career. I want to thank all members and staff of the Physics Department (Pietermaritzburg Campus) for their tolerance and support. My thank is also due to my uncle Dr. K.T. Omopupa, a scholar of this prestigious university who recommended it as worthy of learning. I wish him continuous success in his endeavours.

My profound gratitude goes to my parents Mr. & Mrs. Yakubu, for their love, prayers and support towards my success. I pray to Allah (SWT) to reward you abundantly in this life and the hereafter. Also, my gratitude to my wife, Khadijah and the children (Maryam, Aisha, and Ibrahim) for their patience, endurance, and steadfastness while I sojourn in pursuit of excellence. I cannot thank you enough for the roles you all played, and I pray Allah (SWT) makes you all a continuous blessing in this world and hereafter. Finally, my appreciations are due to my brothers and sisters, Alfa Lateef, Bar. Fashina, Ahmed, Rasheedat, Mariam, Abdulrasaq, and others for their financial and moral support during the programme. May Allah (SWT) elevate and reward you all.

## LIST OF ABBREVIATIONS AND SYMBOLS

$\alpha$	Ångström exponent
$A$	amplitude
ACI	aerosol-cloud interactions
ACIS	Advance CCD Imaging Spectrometre
ACPI	aerosol-cloud-precipitation interactions
AERONET	Aerosol Robotic Network
ANN	artificial neural network
AOD	aerosol optical depth ( $\tau$ )
$A_{\text{abs}}$	absorption AOD
ARI	aerosol-radiation interactions
ATSR	Along-Track Scanning Radiometre
AVIRIS	Airborne Visible/Infrared Imaging Spectrometre
AWV	atmospheric water vapour
$\beta$	backscatter coefficient
$BB$	blackbody

BB	biomass burning
BC	black carbon
BOA	bottom of the atmosphere
BSOA	biogenic secondary organic aerosol
$c$	speed of light
CALIPSO	Cloud-Aerosol Lidar and Infrared Pathfinder Satellite Observations
CCN	cloud condensation nuclei
$C_d$	cloud droplet
CER, $R_e$	cloud effective radius
CF	cloud fraction
COD	cloud optical depth
CTH	cloud top height
CTT	cloud top temperature
$C_w$	cloud liquid water
$D$	diameter
DARF	direct aerosol radiative forcing

DMA	differential mobility analyzers
DMS	dimethyl sulfide
E	electric field
<i>E</i>	energy
EEB	earth's energy budget
EM	electromagnetic
EME	electromagnetic energy
EMR	electromagnetic radiation
EOS	earth observing system
FF	fossil fuel
FMF	fine mode fraction
GHG	greenhouse gases
HOCR	Hyperspectral Ocean Colour Radiometre
<i>I</i>	light intensity
IN	ice nuclei
<i>L</i>	precipitation water content

LWP	liquid water path
LWR	longwave radiation
M	magnetic field
MD	mineral dust
MISR	Multangle Imaging Spectroradiometer
MLR	multiple linear regression
MLP-ANN	multilayer perceptron ANN
MODIS	Moderate Resolution Imaging Spectroradiometer
$n$	refractive index
NASA	National Aeronautics and Space Administration
$N_d$	number of cloud droplets
$\theta$	scattering angle
OC	organic carbon
OPC	optical particle counter
$P$	momentum
$\rho_w$	water density

PBA	primary biogenic aerosol
PM	particulate matter
PRECP	precipitation
$R$	range
RF	radiative forcing
RH	relative humidity
RMSE	root mean square error
SAWS	South Africa Weather Service
SS	sea salt
SSA, $\omega$	single scattering albedo
SWR	shortwave radiation
$T$	period
$T_b$	brightness temperature
$\tau^*$	residence time
$\tau_c$	coarse mode AOD
$\tau_f$	fine mode AOD

$\lambda$	wavelength
TEMP	temperature
TOA	top of the atmosphere
TOMS	Total Ozone Mapping Spectrometre
$\nu$	frequency
VA	volcanic aerosols
VBG	volatile biogenic gases
VIIRS	Visible Infrared Imaging Radiometre Suite
VOC	volatile organic compounds
WS	wind speed
WVC	water vapor content
XRD	X-ray diffraction

# LIST OF FIGURES

Figure 2.1 An illustration of the different classes and sources of aerosols [4]. .....- 13 -

Figure 2.2 Typical aerosol particle size distribution that bases on the log-normal function.....- 16 -

Figure 2.3 An illustration of EMR travelling in x-direction, with the electric field E (red) and magnetic field B (blue) propagating in directions y and z respectively [74]. .....- 29 -

Figure 2.4 An illustration of the EM-spectrum highlighting the visible light spectrum [77]. .....- 32 -

Figure 2.5 The atmospheric windows illustrated from the EM-spectrum [78]......- 33 -

Figure 2.6 A graphical illustration of the basic elements of remote sensing. ....- 35 -

Figure 2.7 Bands of wavelength for different remote sensors within the atmospheric windows of the EM-spectrum [80]......- 37 -

Figure 2.8 An artistic illustration of an active remote sensor setup.....- 37 -

Figure 2.9 An artistic depiction of a passive remote sensing setup. ....- 41 -

Figure 2.10 A graphical display of the ten types of clouds along with their altitude and shapes [87].  
.....- 49 -

Figure 2.11 An illustration of the types of precipitation; (a) convective (b) cyclonic and (c) orographic precipitation systems.....- 53 -

Figure 2.12 Images of a recording (left) and non-recording (right) gauges.....- 55 -

Figure 2.13 A graphical description of ARI and ACI modified from [36]. .....- 60 -

Figure 3.1 Map of South Africa divided into three sub-regions based on the distribution of aerosol loading. ....- 80 -

Figure 3.2 Average spatial distribution of aerosol optical depth (AOD) at  $\lambda = 555\text{nm}$  over South Africa from MISR data for 10 years. ....- 84 -

Figure 3.3 Average aerosol absorbing optical depth ( $A_{\text{abs}}$ ) over South Africa from MISR data for 10 years. ....- 85 -

Figure 3.4 Average Ångström exponent (AE) over South Africa from MISR data for 10 years. ....	86 -
Figure 3.5 Average spatial distribution of atmospheric water vapour (AWV) in cm over South Africa from MODIS data for 10 years. ....	87 -
Figure 3.6 Average cloud water path (LWP) in gm-2 over South Africa from MODIS data for 10 years. ....	89 -
Figure 3.7 Average cloud optical depth (COD) over South Africa from MODIS data for 10 years.-	91 -
-	
Figure 3.8 Average spatial distribution of cloud fraction (CF) over South Africa from MODIS data for 10 years. ....	93 -
Figure 3.9 Average cloud effective radius (CER) in $\mu\text{m}$ over South Africa from MODIS data for 10 years. ....	94 -
Figure 3.10 Average cloud top height (CTH) over South Africa from MODIS data for 10 years. ...	95 -
Figure 3.11 Intercomparison of average monthly variation of aerosol (AOD, AE, $A_{\text{abs}}$ ), AWV, cloud (CF, LWP, COD, CTH, CER) and meteorology (WS, TEMP, PRECP) parameters over upper South Africa. ....	98 -
Figure 3.12 Intercomparison of average monthly variation of aerosol (AOD, AE, $A_{\text{abs}}$ ), AWV, cloud (CF, LWP, COD, CTH, CER) and meteorology (WS, TEMP, PRECP) parameters over central South Africa. ....	100 -
Figure 3.13 Intercomparison of average monthly variation of aerosol (AOD, AE, $A_{\text{abs}}$ ), AWV, cloud (CF, LWP, COD, CTH, CER) and meteorology (WS, TEMP, PRECP) parameters over lower South Africa. ....	102 -
Figure 3.14 Interannual variation of monthly means for aerosol (AOD, AE, $A_{\text{abs}}$ ), AWV, cloud (CF, LWP, COD, CTH, CER) and meteorology (WS, TEMP, PRECP) parameters over upper (U), central I and lower (L) South Africa. ....	104 -
Figure 3.15 Correlation analysis of (a) AOD vs cloud (CF, LWP, COD, CTH, CER) properties, (b) AI vs cloud (CF, LWP, COD, CTH, CER) properties, and (c) PRECP vs cloud (CF, LWP, COD, CTH, CER) properties for upper, central and lower South Africa.....	106 -
Figure 4.1 A map of South Africa showing the locations of Cape Town and Pretoria.....	120 -

Figure 4.2 The graphs of the multiyear monthly mean AOD, AE and FMF for Cape Town; (a), (c) and I, and Pretoria; (b), (d) and (f).....- 124 -

Figure 4.3 The plot of monthly mean  $AOD_{abs}$ , SSA440 and WVC for Cape Town; (a), (c) and I, and Pretoria; (b), (d) and (f) over their respective study periods.....- 126 -

Figure 4.4 The plots of comparisons amongst AERONET, MISR and MODIS instrument data on AOD, AE,  $AOD_{abs}$ , SSA and WVC for CPT (left panels) and PTR (right panels).....- 128 -

Figure 4.5 The plots of the relationships between AERONET, MISR and MODIS instrument measurement of the parameters AE vs AOD, SSA vs AOD, AE vs  $AOD_{abs}$  and AI vs WVC for CPT; (a), (c), (e) and (g), and PRT; (b), (d), (f) and (h). .....- 130 -

Figure 4.6 The illustration of monthly and seasonal average particle size distribution for CPT; (a), (b) and (e), and PRT; (c), (d) and (f). .....- 132 -

Figure 4.7 The graph showing the monthly and seasonal average spectral variation of SSA,  $AOD_{abs}$ ,  $RI_r$  and  $RI_i$ . .....- 134 -

Figure 4.8 The plot of SSA, AOD and  $\tau_{abs}$  (colourbar) for (a) CPT and (b) PTE.....- 136 -

Figure 4.9 The graph of RF at BOA, TOA and average over CPT (a, c and e) and Pretoria (b, d and f).....- 138 -

Figure 5.1 Map of South Africa showing the study areas locations. ....- 151 -

Figure 5.2 Summary of the correlations amongst the predictors and the targets. ....- 152 -

Figure 5.3 The ANN architecture for precipitation prediction. ....- 154 -

Figure 5.4 Plots of model outputs based on MLR (left panels) and ANN (right panels) for (a) CPT (b) DBN, and (c) PTE.....- 158 -

Figure 5.5 Comparison plots of observed precipitation and prediction for MLR (left panels) and ANN (right panels) models for January – December 2005: (a) CPT (b) DBN (c) PTE.....- 159 -

## LIST OF TABLES

Table 2.1 A summary of aerosol types predominantly found in different environments [3, 14, 20]. .....	- 17 -
Table 2.2 Examples of remote sensors and their operational principle [11, 69, 72].....	- 44 -
Table 2.3 Cloud classification by altitude over different latitudes [63, 84].....	- 46 -
Table 2.4 Cloud classification by structure [63, 84]. .....	- 46 -
Table 3.1 A summary of the different states of cloud properties and the corresponding effects on precipitation over the region. ....	- 106 -
Table 5.1 The statistical summary of filtered data samples available for each location.....	- 153 -
Table 5.2 Summary of training parameters and results of the models for the locations.....	- 156 -
Table 5.3 Summary of models. ....	- 157 -

# Contents

ABSTRACT.....	i
PREFACE .....	ii
DECLARATION: PLAGIARISM.....	iii
DECLARATION 2 – PUBLICATIONS.....	iv
ACKNOWLEDGEMENT .....	v
LIST OF ABBREVIATIONS AND SYMBOLS .....	vi
LIST OF FIGURES .....	xii
LIST OF TABLES .....	xii
Chapter 1 – General Introduction.....	- 1 -
1.1 Introduction .....	- 1 -
1.2 Challenges of climate change assessments .....	- 4 -
1.3 Motivation .....	- 5 -
1.4 Problem statements .....	- 6 -
1.5 Research questions .....	- 7 -
1.6 Aims and objectives .....	- 7 -
1.7 Thesis structure .....	- 8 -
References .....	- 10 -
Chapter 2 – Background theory and Literature review .....	- 13 -
2.1 Aerosols.....	- 13 -
2.1.1 Descriptions of different aerosol types .....	- 18 -

2.1.2 Importance of aerosol.....	- 21 -
2.1.3 Processes modifying atmospheric aerosol .....	- 24 -
2.1.4 Measurements of aerosol.....	- 25 -
2.1.5 In-situ and Remote sensing of aerosol.....	- 27 -
2.2 Principle of remote sensing .....	- 28 -
2.2.1 EM-spectrum .....	- 31 -
2.2.2 Atmospheric interactions .....	- 32 -
2.2.3 Components of remote sensing .....	- 35 -
2.2.4 Types of remote sensor .....	- 36 -
2.3 Clouds and classification.....	- 45 -
2.3.1 Types of clouds .....	- 46 -
2.3.2 Importance of clouds .....	- 49 -
2.3.3 Processes modifying the clouds .....	- 50 -
2.3.4 Measurements of cloud.....	- 51 -
2.4 Precipitation .....	- 51 -
2.4.1 Types of precipitation .....	- 52 -
2.4.2 Importance of precipitation .....	- 54 -
2.4.3 Processes that modify precipitation .....	- 54 -
2.4.4 Measurements of precipitation .....	- 55 -
2.5 Aerosol-cloud-precipitation interaction (ACPI): A general review .....	- 58 -
References .....	- 62 -

Chapter 3 – A decadal assessment of the climatology of aerosol and cloud properties over South Africa .....	- 76 -
3.1 Abstract .....	- 77 -
3.2 Introduction .....	- 77 -
3.3 Data and methods .....	- 80 -
3.3.1 MISR .....	- 80 -
3.3.2 MODIS .....	- 81 -
3.3.3 Meteorology data .....	- 81 -
3.4 Results and discussion .....	- 82 -
3.4.1 Climatology of aerosol properties .....	- 82 -
3.4.2 Climatology of the atmospheric vapour and cloud optical properties .....	- 86 -
3.4.3 Climatology of aerosol-cloud interrelationship and meteorology characteristics .....	- 96 -
3.4.4 Interannual characteristics of aerosol, cloud, and meteorology parameters ..	- 102 -
3.4.5 Correlation analysis of parameters .....	- 104 -
3.5 Summary and conclusion .....	- 107 -
Acknowledgment .....	- 108 -
Reference .....	- 108 -
Chapter 4 – Atmospheric aerosol optical properties and radiative forcing over two metros in South Africa .....	- 114 -
4.1 Abstract .....	- 115 -
4.2 Introduction .....	- 115 -
4.3 Method .....	- 119 -

4.3.1 Sites.....	- 119 -
4.3.2 Data .....	- 120 -
4.4 Results .....	- 122 -
4.4.1 Aerosol optical properties statistics .....	- 122 -
4.4.2 Validation of satellite retrieved data .....	- 126 -
4.4.3 Relationships amongst optical properties .....	- 128 -
4.4.4 Particle size distributions .....	- 131 -
4.4.5 Spectral Characteristics .....	- 132 -
4.4.6 Identification of different aerosol types .....	- 134 -
4.4.7 Radiative forcing (RF).....	- 136 -
4.5 Conclusion.....	- 139 -
Acknowledgments .....	- 140 -
References .....	- 140 -
Chapter 5 – Machine Learning-Based Precipitation Prediction Using Cloud Properties...-	146 -
5.1 Abstract. ....	- 147 -
5.2 Introduction .....	- 147 -
5.3 Literature Review .....	- 148 -
5.4 Materials and Method.....	- 150 -
5.4.1 Study Areas’ Descriptions .....	- 150 -
5.4.2 Data Acquisition and Processing .....	- 151 -
5.5 Results and Discussion.....	- 155 -

5.6 Conclusion.....	- 160 -
References .....	- 160 -
Chapter 6 – Summary and challenges .....	- 163 -
6.1 Summary .....	- 163 -
6.2 Challenges .....	- 164 -
6.3 Future work .....	- 165 -

## Chapter 1 –

# General Introduction

### 1.1 Introduction

Amidst the dramatic change (e.g., rising global temperature and change in precipitation pattern) in the regional and global climate trend, different opinions regarding the cause of climate change have quickly resulted in a worldwide debate amongst scholars, researchers, government, and other stakeholders. Consequently, several platforms such as the United Nations Climate Change Conference (UN-COP) and Intergovernmental Panel on Climate Change (IPCC) have emerged as a meeting point between the scientist, government and public stakeholders to review the challenges of climatic change. These include demonstrating the evidence, identifying the cause, projecting the future, and proffering mitigating and adapting strategies to manage the phenomenon effectively. According to [1-3], aerosol, cloud and precipitation dynamics constitute a vital climate change driver. However, the interaction between these three components is complex and remains ambiguous due to factors like poor quantification, high sensitivity and large spatial extent.

Therefore, the enhanced knowledge of aerosol, cloud, and precipitation interactions is critical to understanding the various atmospheric phenomenon and environmental dynamics. Studies of these interactions have been found helpful by the scientific community in explaining the immediate changes in the regional and global atmospheric and environmental conditions [4-6]. Further, aerosol-cloud-precipitation interactions (ACPI) influence climate change and constitutes an essential diagnostic tool in understanding, modelling, and predicting global climatic changes [6]. These include having a clear picture of historical or past climate state and the future expected condition based on current activities. Besides, the ACPI plays a vital role in environmental changes, especially its impacts on human wellbeing and adaptability [7-9].

Generally, the belief that solar energy is the primary energy source for the earth is well established in theory and reality [10, 11]. Thus, the interaction of aerosol and cloud with the incoming solar energy impacts the earth's energy budget (EEB), thereby altering the short-run weather state and long-run climate condition [12, 13]. Studies have shown that aerosols and clouds interact with solar radiation directly, indirectly, and semi-directly [4, 14-16]. The

result is the change in the amount of energy received by the earth and the changing climate patterns. The consequence varies regionally depending on activities in each region. However, the effects are mainly global due to transport activities by air motion [3]. The aftermath of climate change expense different levels of burden to the atmosphere and environmental state, thus invoking varying hardships on the earth's inhabitants.

Climate changes pose several challenges and continue to be a subject of concern that requires appropriate and proactive actions on the international scale [3]. The effects are felt in all environmental and socio-economic wellbeing of the world. Even though the impact sometimes varies due to local activities and external influence, the consequences transverses the global scene [2, 17]. Apart from aerosol-cloud interaction, several other factors identified to induce climate change include greenhouse and trace gases emission such as carbon dioxide (CO<sub>2</sub>), methane (CH<sub>4</sub>), nitrous oxide (N<sub>2</sub>O), ozone (O<sub>3</sub>), and related gases [3]. Besides, the changes in the sea surface temperature form another significant factor. These identified causes directly or indirectly link to the EEB. Even though some of the underlying causes are known with uncertainties, several other factors persistently aggravate the associated ambiguities. Thus, the proper assessment, mitigation, and management constitute a global challenge that demands decisive actions. Nevertheless, understanding ACPI is essential for studying climate variation and patterns to provide suitable solution options for decision-makers on mitigation and adaptivity.

Further to climate change, ACPI is crucial to human health and environmental wellbeing. Studies have been able to associate different health cases and environmental changes with ACPI [18, 19]. Direct and indirect mechanisms characterise these effects influenced positively or negatively by aerosols. ACPI regulates air pollution exposure to humans and the environment through aerosol removal by cloud and precipitation formation following the direct process [7, 20]. On the other hand, the indirect mechanism is mainly based on feedback from ACPI, which can result in diseases due to water shortages, heatwaves, drought leading to soil cracks, hurricanes, etc. Therefore, understanding ACPI is crucial to know how the changes affect humans and their environment and the most effective management method.

Africa is considered one of the most vulnerable regions to climate change and other impacts of violent changes in ACPI due to a high poverty level [21]. Yet, the continent is burdened by immense pollution from anthropogenic emissions, both internal (wildly indiscriminate biomass burning and fossil fuel combustion) and external, from the industrialised parts of the

world [21, 22]. According to a study affiliated with the World Bank in 2020, the number of people pushed down below hunger and poverty level is expected to increase by more than 131 million globally by the end of 2030 due to climate change if appropriate actions are not taken [23]. Prediction points Africa alone to contributing more than 33% of the quoted figure [23], which will significantly impact the continent and thus be of great concern. Africa represents the least studied region related to the factors that could induce climate change and all associated studies mainly due to poor infrastructure to establish such studies, reoccurring conflicts and limited government commitments [24, 25]. Therefore, more studies are required in this field over the African continent, including setting up more in-situ experiments and monitoring instruments to effectively assess factors that exacerbate negative climate variability [25, 26].

During the last decade, climatic change has been more evident than in the previous few decades due to the continuous rise in global average temperature and sea level and increasing extreme climate events [3]. Yet, there is a lack of sufficient information to understand factors that influence climate variability to tackle the challenges presented by the event effectively. For instance, dramatic variations in the climate pattern have been experienced over the Southern Africa region, with the footprint of changes (such as flooding, drought, and heatwave) in the last two decades being more prominent. Changes in the components of climate, such as precipitation, land and sea temperature profiles, air motion, and sea levels, which have resulted in different atmospheric/environmental hazards, have been reported over Southern Africa in the last few decades [5, 17]. Trends such as flooding, water shortages, drought, heatwaves, increased air pollution, and loss of vegetation have been experienced from Cape Town, the southernmost coast, to the border parts around Eastern and Central Africa [17]. These trends call for intuitive and decisive actions from regional and international communities to efficiently address climate change issues. However, such measures are difficult to come by, mainly due to several uncertainties such as poor quantification of aerosols due to anthropogenic sources, the effective radiative forcing due to aerosols and deficient characterisation of mixed-phase clouds, revolving around the circumstances influencing climatic change [3, 13].

This work intends to understand better the atmospheric and environmental impacts of climate change due to aerosol-cloud-precipitation interactions by examining the general atmospheric aerosol characteristics with cloud properties and how they impact precipitation mainly over

Southern Africa, focusing on South Africa. The study will follow the context of aerosol and cloud variation, their impacts on incoming solar radiation, EEB, precipitation, and other environmental response to changes, and finally, how they drive climate variability. Special attention will be devoted to the aerosol sources and cloud characteristics over the investigated regions.

## **1.2 Challenges of climate change assessments**

Climate change is a critical yet complex phenomenon of diverse nature that has become a global concern. The phenomenon constitutes a potent modifier of the earth's atmospheric and environmental conditions, leading to varying detriments to inhabitants' normal development and behaviour, including humans [3]. Over several decades, rigorous studies on the evidence of climate change and its causes have been ongoing in different parts of the world [2, 3]. Despite the considerable number of valuable results such as greenhouse effect quantification, understanding of aerosol effects on radiative forcing and knowledge improvement on global hydrology cycle, and the effect on global warming/cooling, a substantial knowledge gap still exist in climatic change proper assessment [3]. Critical deficiencies include poor quantification of global warming/cooling due to anthropogenic emissions, inadequate understanding of aerosol-cloud interactions (ACI) and the resulting impact on precipitation, and weak models due to insufficient observation and characterisation of components' properties [6, 20, 27].

Although researchers have attempted to define the factors that induce changes in the climate pattern, ambiguity in climate model outcomes and poor quantification of the main culprits sometimes lead such efforts to vast susceptibility. In summary, the bulk of these challenges is mainly on the uncertainty accompanying evidence presented by climate researchers and the lack of public trust and support to implement recommended actions. Therefore, to address the grand challenge of adequate understanding of the physical science of climate change, this work examined ACI and its role in precipitation formation over South Africa. This effort will enhance the proper assessment of climate change and boost the public confidence in supporting recommended actions. The study explained the cause of flooding and drought experienced in parts of South Africa. Further, the work defined the process of aerosol-cloud-precipitation interactions (ACPI) based on findings to enhance models.

Also, by examining the optical properties of aerosols over South Africa, this work improved the characterisation of different aerosol types, including providing insight into their sources and how they influence the earth's radiative forcing. Furthermore, the study conducted a validation exercise on satellite observation data to enhance reliability since this medium offers more spatio-temporal coverage to address the issue of poor observation. Finally, the research presented a possible way of improving precipitation prediction/projection through machine learning techniques.

### **1.3 Motivation**

Recently, the intensifying burden of climate change impacts continues to be a critical challenge globally. Meanwhile, researchers have identified several factors that induce climate change even though their processes are not well understood and call for more studies [3]. One crucial factor is the aerosol-cloud-precipitation interactions (ACPI), which are associated with significant uncertainties due to the complex mechanisms and processes involving cloud dynamics, thermodynamics and microphysical changes [2, 3]. From general knowledge, aerosols act as cloud condensation (CCN) and ice nuclei (IN) in forming cloud droplets and subsequently forming clouds [3, 4, 16]. Also, the clouds evolve to form precipitation droplets and consequently cause precipitating events [12]. However, transitions along the different process stages are complex and poorly understood due to reasons including accounting for the aerosol amount acting as CCN/IN, the microphysical changes due to additional aerosol emission, changes in the atmospheric dynamic and thermodynamic properties, and the effect of different aerosol types on cloud development and precipitation formation [3, 6].

Apart from the dynamic and thermodynamic processes centred on cloud development, changes in the amount of energy available to the earth also constitute a significant factor in the atmospheric and environmental stability. Acknowledging the sun as the primary energy source for the earth, ACPI influences the global radiative budget by directly and indirectly modifying the amount of solar radiation reaching the surface and longwave terrestrial radiation leaving the earth, thus inducing climatic change [12, 15]. Therefore, the significant variation in aerosol emission, types and concentration, and cloud development over different regions compound the poor assessment and evaluation of climate change and impacts in observations and likewise models, which even require solving complex physics and mathematics for effective projection. Although atmospheric physicists and climate scientists have made tremendous progress studying ACPI and radiation budget over time, a significant

knowledge gap persists and requires drastic improvements to divulge climate models of uncertainties and ambiguity [3].

As a starting point, improving our understanding of aerosol characteristics and the mechanisms and processes of ACPI in detail over different locations is vital to enhancing models that seek a solution to complex physics and mathematics involving proper climate change assessment and projection. Therefore, this work will investigate the atmospheric and environmental effects of ACPI over South Africa with a focus on the cause of occasional drought and flooding over the region. Furthermore, the study will improve the characterisation and validate satellite instruments observation of aerosols for better data quality and efficient models. Subsequently, the work will demonstrate the effectiveness of machine learning in improving weather prediction.

#### **1.4 Problem statements**

- Climate change events continue to pose hardships to the global community and the environment amid uncertainties, especially those concerning the factors influencing climate change with the mechanisms, thereby affecting the proper assessments of the potential impacts.
- Effectively estimating the likely climatic consequences of aerosol-cloud-precipitation interactions (ACPI) and evaluating the global net radiative forcing as an effective way of climate change assessments remains unsolved and needs strong evidence or backing.
- A wide gap still exists in satellite measurements compared to in-situ and ground measurements of the atmosphere, land, and ocean properties; hence, reducing the uncertainty or data inconsistency is required to harness the spatio-temporal benefits of satellite observations effectively.
- Africa is still less studied in climate change despite being perceived as one of the most vulnerable amongst peers. For instance, studies from different world regions have demonstrated that increased aerosol enhances rainfall and possibly flooding in one environment but affects the same event sometimes till drought extent in another location, concisely what is wrong or what has changed and the cause. Then what is the case in South Africa with a similar experience?
- The insinuation and debate (among public opinion) of humans as the cause or culprit or significant contributors to current global warming remained contested. Hence, poor policy emanates from public mistrust of scientific claims, especially regarding research methods

and models due to the vagueness of data. To this end, more effective and less complex communication of trends on climate change becomes paramount to enhance public trust, compliance, and support of policymakers and researchers.

### **1.5 Research questions**

- As a case study, what are the evidence and impacts of climate change on the South African region?
- What is the role of aerosol-cloud-precipitation interactions (ACPI) in the context of the identified evidence and impacts of climate change over the region?
- What are the main types and sources of atmospheric aerosols over South Africa, the immediate and long-time atmosphere and the environmental effects based on their characteristics, and the strength of satellite instruments in monitoring events towards enhancing the spatio-temporal coverage and data quality?
- What ways to improve weather and climate prediction/projection using machine learning techniques?
- What is the agreement level of the mechanisms and processes of ACPI in defining the short and long-time climate pattern over South Africa compared to the observations in other regions of the world for improvement of general climate models?
- How can scientific claims be divulged of misinterpretation and gain public confidence in the short and long run based on current data and findings to improve the government strategies on climate change adaptation?

### **1.6 Aims and objectives**

The aims include to;

- demonstrate the evidence and impacts of climatic change over South Africa as a case study and improve the methods of climate diagnosis towards early detection and model enhancements for better regional and global climate projection.
- enhance the understanding of the mechanisms and processes of how ACPI influences climate variability regionally and globally.
- better characterise the different aerosol types, identify their primary sources and understand their roles in atmospheric and environmental variability for better representation in models.

- increase the footprint of satellite data validation by defining the alignment level of satellite observations with the ground and in-situ-based measurement towards enhancing satellite instruments' data quality (e.g., reducing uncertainty) to harness their spatio-temporal coverage advantage.
- demonstrate the potential of machine learning techniques (as a vital big data tool) and the robustness of satellite data in the effective prediction/projection of climate patterns over varying specified periods.
- improve the communication on results and findings for easy adoption in the development of blueprints suitable to enhance models and policies targeted at the efficient management, mitigation, and prediction of climate variability for stronger adaptiveness and sustainability and to earn more public trust.

The objectives include to;

- identify and define the evidence and impacts of climate change over South Africa (SA) and compare them with trends reported in other regions.
- use ground and satellite data, investigate ACPI over SA by considering different aerosol and cloud properties from multiple instruments, focusing on their role in precipitating and non-precipitating events.
- investigate the optical properties, primary sources, potential atmospheric and environmental impacts, and characterise aerosol suspended over SA. Then, use the findings information to assess the radiative forcing on the region.
- validate aerosol data products from various satellite instruments such as MODIS (Moderate Resolution Imaging Spectroradiometer) and MISR (Multi-angle Imaging SpectroRadiometer) over SA and establish the level of agreement with ground observation instrument.
- conduct assessments of the capabilities of machine learning methods to enhance weather prediction models.
- downscale various scientific data on climate change through proper interpretation to ease public consumption.

## **1.7 Thesis structure**

This thesis contains works covering the intensive understanding of climate change and the impacts from the perspective of ACPI. The conclusions drawn from the investigation will be

of great use in developing frameworks for climate change assessments and the eventual development of policies and implementation strategies.

To this effect, the write-up is presented in six (6) distinct chapters, including three (3) paper-based chapters (Chapters 3-5) and documented as follows;

Chapter 1 briefly introduces the main description of the project's rationale, goals, and expected outcome. The chapter begins by presenting climate change as a holistic concern, linked to ACPI being a vital factor influencing the change and a crucial problem to be addressed. Subsequently, the chapter terminates after defining the problem statements, benefits of studies, key objectives, and the target output.

As a follow-up to chapter 1, the background theory and the literature review of ACPI components in climate change are presented in chapter 2. At the beginning of the chapter, definitions, terms, descriptions of characteristics and features in real scenarios, and how they influence one another are detailed. Besides, the chapter further discusses the measurement methods, including the advantages and disadvantages. Subsequently to these descriptions, a literature review of critical components of the study is presented to include past, current, and potential future research to understand them better. Meanwhile, a general summary is documented towards the end of the chapter to provide quick insight into future studies.

Chapter 3 presents a study conducted on analysing aerosol-cloud climatology over South Africa. Based on satellite data, the study attempts to identify and understand the characteristics of aerosol and cloud over the study region. The investigation covers aerosol sources, dispersion, transport processes, and the effect on clouds, precipitation, and climate. In the end, the study explained the process of ACPI and its impacts on the environment.

In Chapter 4, a study on the aerosol optical properties and validation of satellite and model data over South Africa is presented. The investigation becomes necessary because of the wide use of satellite aerosol data due to the limited coverage of ground monitoring stations. Several climatic change-related studies depend on these data types, particularly in remote areas. Therefore, assessing these datasets is essential to enhance the confidence level of those studies and the scientific stance on climatic change.

Chapter 5 presents a study on machine learning as a form of future weather prediction tool. The study examined the capabilities and prospects of satellite-acquired data as input to

predict precipitation. Besides, the result provides insight into adopting this method for weather prediction mainly to assist farmers in rural communities.

Finally, in Chapter 6, a general summary of results and findings from studies carried out throughout this thesis is presented. Furthermore, the presentation includes the challenges and achievements associated with the project.

## References

- [1] IPCC, Climate Change 2001: The Scientific Basis. Contribution of Working Group I to the Third Assessment Report of the Intergovernmental Panel on Climate Change, in: J.T. Houghton, Y. Ding, D.J. Griggs, M. Noguer, P.J. van der Linden, X. Dai, K. Maskell, C.A. Johnson (Eds.), Intergovernmental Panel on Climate Change, Cambridge, United Kingdom New York, NY, USA, 2001, pp. 881.
- [2] IPCC, The Physical Science Basis. Contribution of Working Group I to the Fourth Assessment Report of the Intergovernmental Panel on Climate Change in, Cambridge University Press, Cambridge, 2007.
- [3] IPCC, Climate Change 2013: The Physical Science Basis. Contribution of Working Group I to the Fifth Assessment Report of the Intergovernmental Panel on Climate Change, Cambridge University Press, Cambridge, United Kingdom and New York, NY, USA, 2013.
- [4] B.A. Albrecht, Aerosols, Cloud Microphysics, and Fractional Cloudiness, *Science*, 245 (1989) 1227-1230.
- [5] A.J. Adesina, K.R. Kumar, V. Sivakumar, Aerosol-Cloud-Precipitation Interactions over Major Cities in South Africa: Impact on Regional Environment and Climate Change, *Aerosol and Air Quality Research*, 16 (2016) 195-211.
- [6] J. Fan, Y. Wang, D. Rosenfeld, X. Liu, Review of Aerosol–Cloud Interactions: Mechanisms, Significance, and Challenges, *Journal of the Atmospheric Sciences*, 73 (2016) 4221-4252.
- [7] U. Pöschl, Atmospheric aerosols: Composition, transformation, climate and health effects., *Angewandte Chemie International Edition*, 44 (2005) 7520-7540.

- [8] I.B. Tager, Health effects of aerosols: mechanisms and epidemiology, in: L.S. Ruzer, N.H. Harley (Eds.) *Aerosols Handbook: Measurement, Dosimetry, and Health Effects* seconded, CRC Press, Boca Raton, 2013, pp. 565–636.
- [9] D. Wang, B. Jiang, F. Li, W. Lin, Investigation of the air pollution event in Beijing-Tianjin-Hebei region in December 2016 using WRF-Chem, *Advances in Meteorology*, 2018 (2018) 1-12.
- [10] R.G. Barry, R.J. Chorley, *Atmosphere, weather and climate*, 8 ed., Routledge, London, 2003.
- [11] K. Tempfli, N. Kerle, G.C. Huurneman, L.L.F. Janssen, *Principles of remote sensing*, The International Institute for Geo-Information Science and Earth Observation (ITC), Enschede, The Netherlands, 2009.
- [12] J. Haywood, O. Boucher, Estimates of the direct and indirect radiative forcing due to tropospheric aerosols: A review, *Rev Geophys*, 38 (2000) 513-543.
- [13] IPCC, Anthropogenic and Natural Radiative Forcing, in: T.F. Stocker, D. Qin, G.-K. Plattner, M. Tignor, S.K. Allen, J. Boschung, A. Nauels, Y. Xia, V. Bex, P.M. Midgley (Eds.) *Climate Change 2013 - The Physical Science Basis*, Cambridge University Press, Cambridge, United Kingdom and New York, NY, USA, 2014, pp. 659-740.
- [14] O. Boucher, *Atmospheric aerosols: Properties and climate impacts*, 1 ed., Springer, Netherlands, 2015.
- [15] J. Hansen, M. Sato, R. Ruedy, Radiative forcing and climate response, *Journal of Geophysical Research: Atmospheres*, 102 (1997) 6831-6864.
- [16] S. Twomey, Pollution and the planetary albedo, *Atmospheric Environment* (1967), 8 (1974) 1251-1256.
- [17] A.T. Yakubu, N. Chetty, Optical properties of atmospheric aerosol over Cape Town, Western Cape of South Africa: Role of biomass burning, *Atmósfera*, 34 (2020) 395–416.
- [18] C.A. Pope, R.T. Burnett, M.J. Thun, E.E. Calle, D. Krewski, K. Ito, G.D. Thurston, Lung Cancer, Cardiopulmonary Mortality, and Long-term Exposure to Fine Particulate Air Pollution, *JAMA*, 287 (2002) 1132-1141.

- [19] J.P. Putaud, European aerosol phenomenology-3: Physical and chemical characteristics of particulate matter from 60 rural, urban, and kerbside sites across Europe, *Atmospheric Environment*, 44 (2010) 13.
- [20] G. Myhre, C.E.L. Myhre, B.H. Samset, T. Storelvmo, Aerosols and their relation to global climate and climate sensitivity, *Nature Education Knowledge*, 4 (2013).
- [21] IPCC, Impacts, Adaptation, and Vulnerability. Part A: Global and Sectoral Aspects. Contribution of Working Group II to the Fifth Assessment Report of the Intergovernmental Panel on Climate Change, in: C.B. Field, V.R. Barros, D.J. Dokken, K.J. Mach, M.D. Mastrandrea, T.E. Bilir, M. Chatterjee, K.L. Ebi, Y.O. Estrada, R.C. Genova, B. Girma, E.S. Kissel, A.N. Levy, S. MacCracken, P.R. Mastrandrea, L.L. White (Eds.) *Climate Change 2014*, Cambridge University Press, Cambridge, 2014.
- [22] M. Tesfaye, V. Sivakumar, J. Botai, G. Mengistu Tsidu, Aerosol climatology over South Africa based on 10 years of Multiangle Imaging Spectroradiometer (MISR) data, *Journal of Geophysical Research: Atmospheres*, 116 (2011).
- [23] B.A. Jafino, B. Walsh, J. Rozenberg, S. Hallegatte, Revised Estimates of the Impact of Climate Change on Extreme Poverty by 2030, in, World Bank, Washington, DC, 2020.
- [24] S.J. Piketh, R.J. Swap, W. Maenhaut, H.J. Annegam, P. Formenti, Chemical evidence of long-range atmospheric transport over southern Africa, *J Geophys Res-Atmos*, 107 (2002).
- [25] J.M. Haywood, J. Pelon, P. Formenti, N. Bharmal, M. Brooks, G. Capes, P. Chazette, C. Chou, S. Christopher, H. Coe, J. Cuesta, Y. Derimian, K. Desboeufs, G. Greed, M. Harrison, B. Heese, E.J. Highwood, B. Johnson, M. Mallet, B. Marticorena, J. Marsham, S. Milton, G. Myhre, S.R. Osborne, D.J. Parker, J.-L. Rajot, M. Schulz, A. Slingo, D. Tanré, P. Tulet, Overview of the Dust and Biomass-burning Experiment and African Monsoon Multidisciplinary Analysis Special Observing Period-0, *Journal of Geophysical Research: Atmospheres*, 113 (2008).
- [26] S.P. Hersey, R.M. Garland, E. Crosbie, T. Shingler, A. Sorooshian, S. Piketh, R. Burger, An overview of regional and local characteristics of aerosols in South Africa using satellite, ground, and modeling data, *Atmos Chem Phys*, 15 (2015) 4259-4278.
- [27] A.T. Yakubu, N. Chetty, A decadal assessment of the climatology of aerosol and cloud properties over South Africa, *Atmos. Chem. Phys. Discuss.*, 2022 (2022) 1-36.

## Chapter 2 –

# Background theory and Literature review

## 2.1 Aerosols

Atmospheric aerosols are suspensions of mixed particles of solid and liquid with heterogeneous physical and chemical composition in the air [1, 2]. The particles are highly variable in time and space due to numerous factors such as the size distribution, sources, mode of formation, and atmospheric dynamics. Examples of aerosols include mineral dust, sea salt, pollen, fumes, and smoke. Due to the dynamic nature and heterogeneous interactions amongst individual aerosol types in most environments, identifying and distinguishing the spatial distribution amongst aerosol types are quite complex [3]. Aerosols are generally described and classified by their size, formation mechanism, concentration, emission source, chemical composition, and localisation. An illustration of different aerosol classes is as in Figure 2.1.

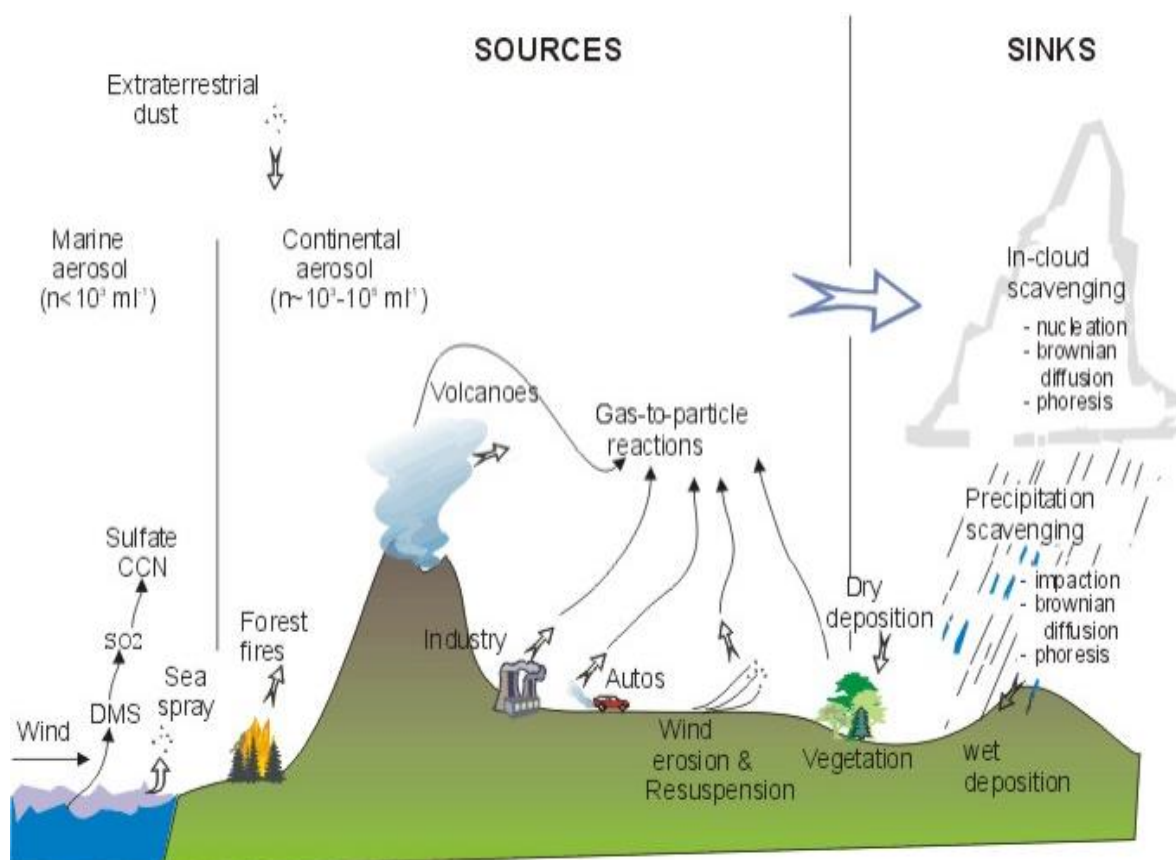


Figure 2.1 An illustration of the different classes and sources of aerosols [4].

Aerosols are classified into two groups regarding the formation mechanism or method of emission, namely primary and secondary aerosols. Primary aerosols mainly result from fragmentation or combustion processes and are usually emitted directly into the atmosphere. They exist as organic (particles made-up of carbon typically from living things) and inorganic (particles from non-living things such as mineral sources) components and can change structure due to gas-to-particle conversion, coagulation, and humidification. Organic primary aerosols such as smoke from burning or combustion, spores, and pollen are typically less than 1  $\mu\text{m}$  in diameter and have long atmospheric lifetimes [2]. However, primary inorganic aerosols, including mineral dust, volcanic ashes, and sea salts, are bigger than 1  $\mu\text{m}$  in diameter and exhibit shorter residence time (typically days) in air. The larger portion of aerosols found in the atmosphere originates from primary sources [2, 5].

Secondary aerosols are formed in the earth's atmosphere through transformation processes of precursor gases to create new particles (gas-to-particle conversion) [2, 6]. They are mainly formed through heterogeneous nucleation of water vapour by pre-existing particles [7, 8]. Secondary aerosol particles are primarily made up of a mixture of compounds such as organic carbon (OC), sulphate, and nitrate, which are generally small (mainly submillimetre) and suspended in the air for periods ranging from days to weeks [9]. Their precursor gases are primarily emitted from fossil fuel combustion, volcanic eruption, biogenic emission, and fire events [10].

The aerosol suspended over a location is the function of activities or processes around the area, including physical, chemical, and biological processes, or combined depending on the sources and the proximity to other potential sources [11]. Thus, aerosols are classified as natural and anthropogenic in emission sources. The aerosol emitted in the process of natural events is called natural aerosols. These categories of particles are emitted independently of human influences, and examples include volcanic ashes, sea salt, deserts, dust, and pollens. They represent the largest source of aerosol emission globally [10], and the impacts on the environment are a function of their individual properties.

In contrast, anthropogenic aerosols occur mainly through human activities and interaction with the natural environment. Examples include fossil fuel, agricultural activities, biomass burning, insecticide or perfume use, and industrial processes. Since humans are the primary driver of anthropogenic aerosols, the variation (over an area) depends on the population, local activities, and proximity to aerosol sources. For instance, aerosols found around residential

areas are habitually different from those observed near an industrial area, although they sometimes have common signature. According to the current trends in aerosol studies, climate scientist still holds anthropogenic aerosols responsible for the imbalance in global climate [12, 13]. However, the issue is still debated critically and has attracted more recent studies globally [11, 14, 15].

Another means of aerosol classification is by employing particle size (diameter or radius) and distribution. However, aerosols are heterogeneous irregular-shaped particles (no specific diameter) in nature. Therefore, to resolve this challenge of non-sphericity and inhomogeneity, an idealisation based on spherical assumption is considered for particle sizing. There are several ways of specifying the particle size in terms of a specific diameter such that the features correspond with the items used as reference (i.e., equivalent diameter). These approaches include aerodynamic diameter, electric mobility, terminal velocity, and density. Subsequently, a size distribution model is used to group aerosols into three distinct groups. A widely used model is the log-normal size distribution model, which is represented by [16, 17];

$$dV = \frac{C_v}{\sigma\sqrt{2\pi}} e^{-\left[\frac{1}{2}\left(\frac{D-D_v}{\sigma}\right)^2\right]} dD, \quad (2.1)$$

then, defining the diameter in the logarithm form gives:

$$\frac{dV}{d\ln D} = \frac{C_v}{\sigma\sqrt{2\pi}} e^{-\left[\frac{1}{2}\left(\frac{\ln D - \ln D_v}{\sigma}\right)^2\right]}, \quad (2.2)$$

where,

$\frac{dV}{d\ln D}$  = the volume distribution

$D$  = the particle diameter

$C_v$  = the volume concentration at the diameter

$D_v$  = the mean diameter

$\sigma$  = the geometric standard deviation of the distribution.

From the log-normal distribution, aerosol particles are mainly categorised into two aerosol modes: fine and coarse mode aerosols. Often, the fine mode is divided as Aitken and accumulation mode aerosols [2, 17]. The Aitken, also called nucleation mode aerosols, consist of ultra-fine particles of diameters typically less than  $0.1\mu\text{m}$ . Meanwhile, the accumulation mode is slightly bigger than the Aitken mode with a size in the range of  $0.1\text{-}2.5\mu\text{m}$ , and the coarse mode particle has an aerodynamic diameter greater than  $2.5\mu\text{m}$  [18, 19]. Figure 2.2 below shows the size distribution of aerosol particles based on the log-normal distribution function. In addition, based on the particle size distribution, aerosol concentration can be expressed by a number, surface area, volume, or mass per unit volume. Therefore, the different aerosol modes and the possible ways of describing the concentration, number concentration is predominantly of fine particles (combined Aitken and accumulation mode aerosols), and coarse mode aerosols dominate mass or volume concentration. Furthermore, aerosol particles of size below  $0.1\mu\text{m}$  in diameter (i.e., typically nucleation mode aerosols) are named particulate matter 0.1 ( $\text{PM}_{0.1}$ ) based on air quality classification. Likewise, particles having a size in the range of  $0.1 < D < 2.5 \mu\text{m}$  (i.e., accumulation mode aerosols) where  $D$  is the diameter are called particulate matter 2.5 ( $\text{PM}_{2.5}$ ). Finally, particulate matter 10 ( $\text{PM}_{10}$ ) is the name given to aerosols of size  $D > 10 \mu\text{m}$  (mainly coarse mode particles). These naming are essential for understanding the aerosol impact on air quality and health, as demonstrated by several studies [20-22].

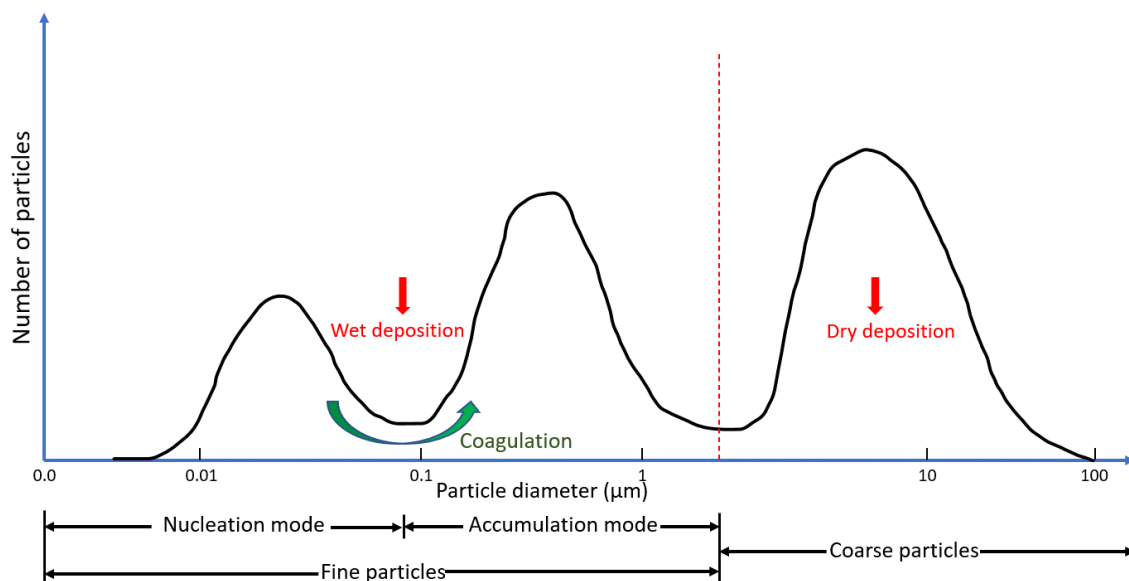


Figure 2.2 Typical aerosol particle size distribution chart based on the log-normal function.

Aerosols classification can also be viewed in terms of the localisation of the particles (i.e., the specific environment where they are found). Different environments are associated with the emission of varying aerosol types, depending on the area's characteristics. For instance, a bustling environment consisting of tarred roads is unlikely to produce much dust compared to an untarred road. On this note, aerosols are classified as continental, urban, rural, maritime, desert, remote continental, free tropospheric, and polar aerosols according to localization. Each aerosol class sometimes contains single or multiple types of aerosols depending on the features of the location, processes, and proximity to a particular aerosol type domain. Table 2.1 below illustrates aerosol classification by locality based on the predominant types of aerosols found in these environments.

Table 2.1 A summary of aerosol types predominantly found in different environments [3, 14, 20].

<b>Locality</b>	Continental	Urban	Semi-urban	Rural	Maritime	Desert	Polar	stratospheric
<b><i>Aerosol type</i></b>								
<i>Mineral dust</i>	✓	-	✓	✓	-	✓	✓	-
<i>Sea spray</i>	-	-	-	-	✓	-	✓	-
<i>Carbonaceous</i>	✓	✓	✓	✓	-	-	-	-
<i>Sulphate</i>	-	✓	✓	-	✓	-	✓	✓
<i>Nitrate</i>	-	✓	✓	✓	-	-	-	-
<i>Biogenic</i>	✓	✓	✓	✓	✓	✓		-
<i>Volcanic</i>	-	-	-	-	-	-	✓	✓

### ***2.1.1 Descriptions of different aerosol types***

Several types of aerosol particles emerging from different emission sources are found in suspension in the atmosphere. A brief description is as follows.

***Mineral dust:*** This includes mineral-rich sand, rock debris, topsoil, and other particles of the earth's crust suspended in the air. They predominantly originate from the desert and other open earth surfaces without vegetation or with less vegetative cover, such as farmland and untarred roads [23, 24]. Their formation mainly results from wind action on desert dust and the weathering of rock surfaces [23]. Mineral dust (MD) comprises fine and coarse mode aerosols but predominantly coarse or larger size particles. Their constituents are mainly compounds of oxides and carbonates like  $\text{Fe}_2\text{O}_3$ ,  $\text{SiO}_2$ ,  $\text{CaCO}_3$ , and  $\text{Al}_2\text{O}_3$ . An essential feature of MD is the possession of high scattering and low absorption characteristics, hence, plays a significant role in reflecting solar radiation and influencing the earth's energy budget [2, 25].

***Sea spray:*** includes sea salt (SS), marine organic, and inorganic matter mainly originating from the sea. Sea sprays are predominantly coarse-mode aerosols when considering the concentration by volume or mass. However, the concentration by number is mainly fine mode like most other aerosol types due to marine organic matter. Sea spray formation occurs in the sea-atmosphere boundary layer through the actions of wave break in releasing its constituents encapsulated in bubbles to the air [2, 26]. This aerosol type just like MD is one of the most important natural aerosol sources characterised by high scattering and low absorbing properties. Besides, SS as a constituent of sea spray, is highly hygroscopic, thereby enhancing the population of large particle aerosol due to swollen process after water intake from the air [27, 28]. Sea spray aerosol, particularly SS, is vital to the earth's radiative forcing (RF) and a critical component for cloud droplet ( $C_d$ ) and precipitation formation through their actions as cloud condensation (CCN) and ice nuclei (IN) [11, 12, 26].

***Carbonaceous aerosols:*** include organic (OC) and black carbon (BC) or elemental carbon (EC), which are mainly products of incomplete combustion of fossil fuels or BB and decay of organic matter [5, 11]. Besides, they are produced as secondary aerosols through atmospheric oxidation of volatile organic compounds (VOC) following chemical reactions or gas-to-particle conversion [29, 30]. Carbonaceous aerosols are mainly fine-mode particles and reside in the air for longer (typically weeks to months). They are the most predominant type of

aerosol associated with anthropogenic sources and constitute the bulk of aerosol particles observed in a densely polluted environment. In terms of natural sources of emission, wild or forest fires constitute the single most significant natural source of carbonaceous aerosol emission. Carbonaceous aerosols are characterised by scattering and high absorption properties, resulting in an impactful effect on incoming solar radiation, global RF and visibility [31, 32]. Also, carbonaceous aerosols are important component of cloud and precipitation formation through their acting as CCN and IN. Besides, this aerosol is one of the chief causes of several health complications due to aerosol through air pollution [33, 34].

***Sulphate aerosols:*** include fine crystallised solid and liquid droplets of sulphate or sulphuric acid neutralised (wholly or partly) by ammonia. They are mainly produced from SO<sub>2</sub> emission by natural sources like volcanic eruption and dimethyl sulphide (DMS) from marine phytoplankton and anthropogenic activities such as BB and fossil fuel combustion [35]. The formation process mainly occurs in the atmosphere following chemical reactions by precursor gases such as SO<sub>2</sub>, HNO<sub>3</sub> and H<sub>2</sub>SO<sub>4</sub> [10]. They are primarily fine-mode aerosols with long residence time in the atmosphere. Likewise, they exhibit an entire scattering of incoming solar radiation across the solar spectrum, with albedo approaching one (i.e.,  $\omega_0 \approx 1.0$ ) and slight absorption at near-infrared wavelengths [36]. Sulphate aerosols are also found to contribute a significant portion of sub-micron aerosol by mass of anthropogenic aerosol loading and RF [37, 38]. Results from several models have demonstrated that sulphate aerosols have net negative RF, thereby causing a cooling effect on the earth [16, 35]. Furthermore, it acts as CCN and IN, forming smaller cloud droplets to influence the precipitation rate. Besides, poor air quality alongside several health risks has been linked to its emission following various studies [16, 33].

***Nitrate aerosols:*** include aerosols formed from chemical reactions through precursor compounds like ammonia and nitric acid in the atmosphere. Their production is predominantly from chemical reactions in the atmosphere during BB, industrial processes, production and application of synthetic fertilisers, and fossil fuel emission [39, 40]. Nitrate aerosols are mainly a mix of coarse and fine-mode aerosols. A high concentration of fine-mode nitrate particles is chiefly associated with industrial activities, while a low concentration of fine-mode aerosols indicates rural areas [21, 36, 41]. They are mainly scattering aerosols and non-absorbing in the visible wavelength band. Nitrate aerosols play a significant role in the earth's RF and the general surface climate. Studies have indicated that

the net radiative effect due to its emission is negative RF with an estimated value ranging from  $-0.03$  to  $-0.22 \text{ Wm}^{-2}$  [36, 42-45]. However, according to the [36] report, the mean direct RF is referenced as  $-10 \text{ Wm}^{-2}$  based on the estimated value at the top of the atmosphere (TOA) since the scattering characteristic is mainly conserved (i.e., absorption is negligible). Apart from the direct radiative effect, nitrate particles act as CCN to modify the microphysical properties of the cloud, hence, indirectly impacting the global climate. Besides, they are notably an important source of air pollution and detrimental to human health [46].

**Biogenic aerosols:** include pollen, spores, bacteria, dandruff, skin remains, fungi, other similar biological materials emitted into the atmosphere. They are a mix of coarse and fine-mode aerosols and typically range in sizes between the nanometres and submillimetres scale [2]. Biogenic aerosols (i.e., primary biogenic aerosols PBA) are mainly emitted directly into the atmosphere from vegetative and marine environments. They are also formed indirectly as biogenic secondary organic aerosols (BSOA) from volatile biogenic gases (VBG) through gas-to-particle conversion. In terms of their impact on the climate system, they interact directly with incoming sun radiation by scattering and absorption and indirectly through the formation of CCN to influence the earth's energy budget [5, 47]. Moreover, they are vital to cloud and precipitation formation through acting as CCN and IN [6]. Biogenic aerosols are also significant in distributing biological and reproductive materials amongst living organisms and enhancing the spread of diseases [10]. Studies have linked several bacteria, fungi, and virus respiratory allergies and other infectious diseases to the presence of biogenic aerosols in the air [20, 46, 48].

**Volcanic aerosol:** also called stratospheric aerosol, includes  $\text{SO}_2$ , volcanic ashes, gases, and debris emitted into the earth's atmosphere in the events of volcanic eruptions. They are sulphur-rich and typically composed of a mix of coarse and fine mode particles, and their constituents often reach the stratosphere due to the extrusive force [2]. A substantial amount of VA, especially  $\text{SO}_2$  gas and  $\text{H}_2\text{S}$  is suspended in the stratosphere and mostly converted into sulphuric acid [49, 50]. The conversion process typically occurs for weeks to months after the first eruption, while the residence period of the resulting particles can reach up to 2 years. A handful portion (mostly MD and volcanic ashes) are found in the troposphere, depending on the extent of the extrusive force. Generally, VA is mainly a reflector of incoming solar radiation and have a net cooling effect on the earth [2, 50]. Through complex chemical

reactions in the stratosphere, VA significantly contributes to the depletion of the ozone layer [49].

### **2.1.2 Importance of aerosol**

Atmospheric aerosols are emitted into the atmosphere, undergo a transformation, and are systemically removed (after residence time) from the air. These processes constitute a vital component of different phenomena occurring on earth and impacting its inhabitants. These include direct, indirect, and semi-direct interactions with solar radiation, thereby affecting changes in climate, formation of clouds, acid deposition, reduced visibility, air quality and human health, and heterogeneous chemistry. Thus, some of the most critical roles of aerosols are briefly discussed below [2, 12].

**Radiative effect:** aerosols are vital in modifying the incoming solar radiation through direct, indirect, and semi-direct interactions, thereby influencing the RF (i.e., causing a cooling or warming effect) and inducing a change in the climate condition. The direct interaction involves scattering, absorption, and reflection of incoming solar radiation leading to the modification of the amount of energy reaching the earth's surface hence, altering the earth's energy budget (EEB) [51, 52]. The indirect interaction involves the formation and modification of microphysical properties of the cloud through their actions as CCN and IN in regulating the incoming sun radiation [47, 53, 54]. Meanwhile, the semi-direct represents the warming of the cloud resulting in its evaporation and affecting the general dynamics to induce climate change [51, 55]. According to IPCC (2013), the direct radiative effect is now referred to as aerosol radiation interaction (ARI), while the indirect and semi-direct effects are defined as aerosol cloud interaction (ACI). Thus, the RF ( $\text{Wm}^{-2}$ ) due to ARI, also called the direct aerosol radiative forcing (DARF) is defined as [56];

$$RF_{atm} = \Delta F_{TOA} - \Delta F_{BOA}, \quad (2.3)$$

where,

$RF_{atm}$  = radiative forcing within the atmosphere,

$\Delta F_{TOA}$  = changes in the net fluxes due to aerosol (i.e., under cloud-free condition) at the top of atmosphere (TOA), and

$\Delta F_{BOA}$  = changes in the net fluxes due to aerosol (i.e., under cloud-free condition) at the bottom of atmosphere (BOA).

Furthermore, each of  $\Delta F_{TOA}$  and  $\Delta F_{BOA}$  are evaluated following the expressions respectively [56];

$$\Delta F_{TOA} = (F_{TOA}^{\downarrow\alpha} - F_{TOA}^{\uparrow\alpha}) - (F_{TOA}^{\downarrow\beta} - F_{TOA}^{\uparrow\beta}), \quad (2.4)$$

and

$$\Delta F_{BOA} = (F_{BOA}^{\downarrow\alpha} - F_{BOA}^{\uparrow\alpha}) - (F_{BOA}^{\downarrow\beta} - F_{BOA}^{\uparrow\beta}), \quad (2.5)$$

where the arrows indicate downward ( $\downarrow$ ) and upward ( $\uparrow$ ) fluxes respectively,  $\alpha$  and  $\beta$  denote conditions with and without aerosol respectively.

**Air quality and human health:** aerosols play a critical role in influencing air quality and subsequently impacting human health. Atmospheric aerosol emission to the air often causes air pollution, especially around the urban and industrialised areas where loads of toxic substances are released into the atmosphere, thus resulting in poor air quality[2, 9]. The persistence of this trend tends to expose humans and animals to different health threats. Several health complications, especially respiratory and heart-related diseases such as cold flu, cough, catarrh, bronchitis, and pneumonia, reported in various health facilities have been linked to air pollution and aerosols [46, 57]. Since aerosols of mostly fine-mode particles with size in the range of  $PM_{0.1}$  and  $PM_{2.5}$  resides much longer in the air, they can penetrate the respiratory organs through inhaling by habitant, thus affecting the wellbeing of the inhaler.

**Cloud formation:** aerosols constitute an essential component in cloud formation through their action as cloud condensation nuclei (CCN) and ice nuclei (IN). Water vapour condenses on the CCN and IN at supersaturation to form cloud droplets that eventually develop into clouds. Studies have shown that the higher the concentration of the aerosol particle at fixed cloud liquid water ( $C_w$ ), the higher the concentration of smaller size cloud droplets [53, 58] and the lesser the rate of coalescence [6, 54]. Consequently, rain-bearing cloud development is affected, and precipitation is delayed or completely suppressed [59, 60]. They increase atmospheric stability by modifying the clouds' microphysical properties to prolong their

lifetime [47, 54]. Aerosols also invigorate existing cloud droplets to enhance their vertical development leading to  $C_w$  growth, thus intensifying rainfall [61, 62].

**Reduce visibility:** intense emission of aerosol, especially fine mode aerosols that typically possess a longer lifetime in the air, reduces visibility through multiple particle reflection and scattering of light, thereby obstructing mobility. Absorption and scattering of light usually result in light extinction capable of degrading visibility up to  $< 1$  km as observed during heavy smoke or smog, thereby hindering traffic flow [23]. Such events are experienced in the natural cause of haze and anthropogenic motivated smoke or pollution, resulting in varying negative incidents like serious motor accidents, flight cancellation, slow traffic movement, and economic hardship [11].

**Environment:** aerosol particles, particularly the coarse mode aerosols, often escape gravity, resulting in gravitational settling on surfaces as observed in dusty and unhealthy environments [11]. Natural and anthropogenic sources often cause this form of aerosol effect, thus frustrating attempts to clean and beautify the environment and aggravate poor health conditions [2, 11]. The impact of atmospheric aerosols on the environment is mainly felt over locations close to sources of MD, such as deserts, quarries, busy untarred roads, and areas with general poor infrastructure (e.g. gravelled roads) [23].

**Acid deposition:** aerosols induce acid deposition in the atmosphere through the emission of toxic compounds such as sulphur dioxide and nitrogen oxides, mostly during industrial processes and fossil fuel combustion. Once these compounds are released into the atmosphere, they undergo chemical conversion to induce secondary pollutants like sulphuric and nitric acid that subsequently dissolve in vapour to produce acid rain, snow, or fog [2, 63]. The acidic water droplets from the chemical conversion are sometimes transported far away from the source by air masses before being precipitated to the earth [6].

**Heterogeneous chemistry:** aerosols create an avenue for chemical reactions to occur in the atmosphere. An example is the ejection of  $SO_2$  and HCl into the atmosphere by volcanic eruptions. In the case of  $SO_2$ , it reacts with vapour to form  $H_2SO_4$  which depletes the ozone layer [6, 63]. As for HCl, the concentration of stratospheric aerosol increases by the ejection process whereby HCl is removed rapidly by liquid water due to its high solubility and active bleaching properties [6, 63]. The output combines with  $SO_2$  to form  $H_2SO_4$  which depletes the ozone [50].

### ***2.1.3 Processes modifying atmospheric aerosol***

Atmospheric aerosol particles suspended in the air are emitted from different sources and environments. Due to varying modifications, they are observed in the atmosphere to change properties subject to the residence environment periodically. These modifications are potentially influential to the resultant impacts on the environment. Some essential processes that influence suspended aerosol include emission, removal, and transportation [2, 10]. Suspended aerosol generally changes characteristics in the event of new emission or formation of new particles from precursor aerosols. An example of such an occasion is the characteristic changes in aerosol suspension and the atmospheric condition during intensified industrialisation (Pro-industrialisation) and new volcanic eruptions [12, 31, 50].

In the case of aerosol removal, suspended particles are systematically ejected from the air mainly by gravitational settling (or sedimentation), wash-out, and cloud deposition. Depending on the aerosol type and period, it often changes the suspended particles and the atmospheric conditions [11]. Sedimentation involves settling particles on surfaces due to gravitational pull toward the earth. An example is the settling of mostly coarse mode aerosols (e.g., MD) on surfaces in a dusty environment, like experienced during the Harmattan period over most sub-Saharan Africa countries [23]. Meanwhile, aerosol removal through precipitation refers to wash-out. Here, the particles removed include those that have acted as CCN or IN and others in their standard form in the air. This removal process spans fine and coarse aerosols and is typically experienced after rainfall, leaving a pristine environment [11]. In cloud deposition, aerosols entrapped in the clouds during cloud formation or scavenging are deposited on highly elevated ecosystems (e.g., hills, vegetation) due to impaction or interception by such platforms [11, 64].

Nevertheless, the removal mode is a function of the aerosol type and the residence time. Thus, the residence time denoted by  $\tau^*$  is the average period of retainment of a particle in the atmosphere and is mathematically expressed as [2];

$$\tau^* = \frac{B}{S} = \frac{B}{R'}, \quad (2.6)$$

where,

$B$  = the vertically integrated particle concentration

$S$  = the source flux, and

$R'$  = the removal or sink flux.

So, particles with a short residence time (mostly coarse particles or with  $D > 1.0 \mu\text{m}$ ) are more removed by dry deposition (i.e., sedimentation) due to their weight. While those having a longer lifetime in the air (aerosols of  $D < 1.0 \mu\text{m}$ ) are mainly ejected from the atmosphere by wet deposition (i.e., wash-out and cloud deposition) [2].

Atmospheric aerosol transport by air masses also plays a crucial part in modifying suspended particles. In or outflux changes (increases or decreases) both the chemical and physical state of the suspended aerosols in the destination or origination point, respectively [11]. A typical example is the motion of MD or BB aerosols from the source region to neighbouring locations, influencing the existing suspended aerosols as observed from various studies [57, 65]. Therefore, understanding the processes inducing aerosol modification and impacts over a region is essential for aerosol modelling, proper evaluation, and prediction of its potential effects on the area under consideration.

#### ***2.1.4 Measurements of aerosol***

Atmospheric aerosols constitute a vital role in transforming the earth and its inhabitants. However, understanding these particles and how they influence the atmosphere are engulfed by several uncertainties such as their role in mixed cloud formation and precipitation suppression. Therefore, prior knowledge of aerosol characteristics is required to evaluate how aerosols impact these components (i.e., the atmosphere and environment). In nature, atmospheric aerosols often exist heterogeneously where several types are mixed in the air, each having distinct chemical and physical features [2, 12]. So, to adequately quantify and understand their net effects, measurements are made to assess their individual and general characteristics. Appropriate measurements are essential in establishing these particles' chemical and physical behaviour in aerosol science.

There are several ways to measure aerosols depending on the interest characteristics and circumstances. Thus, the methods are broadly classified based on the sample size (i.e., ensemble or single sample) and the investigation environment (i.e., field or laboratory) [66, 67]. In terms of the sample size, the ensemble method is more adopted. The ensemble method involves sampling the distribution of aerosols (i.e., particles of different types and sizes) to

provide information on the average characteristic of the sample under investigation [67]. An example of an instrument used for ensemble measurement is the filter sampler. This instrument analyses the size, distribution, and concentration of particles in the air and is most useful for air quality assessment. As for the single sampling technique, only a specific type of aerosol is studied at a time. Hence, not suitable for heterogeneous aerosol as typically observed in a spatial domain [67]. Instead, this method helps analyse a single aerosol type in a controlled environment. Such instruments including a differential mobility analyser (DMA) and optical particle counter (OPC). They offer more detailed information regarding the properties of the sample under investigation [67].

Concerning the investigation environment, laboratory measurements entail evaluating the properties of aerosol under an idealised, controlled environment. This method considers single or collections of aerosol samples subjected to numerous laboratory tests to establish their properties. The technique deployment takes the form of modelling by using known information about the sample combined with physical equations to evaluate specific metrics valuable in describing their properties. Although this measurement approach is most helpful in simulating climate scenarios and prediction, it cannot effectively quantify the aerosol properties in their natural environment [68]. Examples of instruments utilised in laboratory measurements include electron microscope, particle counters, X-ray diffraction (XRD), and radiometers.

On the contrary, field measurements involve observing aerosol properties in their natural environment without removing them. This measurement technique is either deployed by taking the measuring instrument directly in contact with the particles of interest in the atmosphere (in-situ measurement) or remotely interacting with the samples without the device having direct contact with them (remote sensing). As earlier indicated, this method is advantageous over the laboratory approach considering the ability of the measuring instrument to interact with the sample in their most desired form (i.e., natural environment) without altering their existence [66, 67]. Nonetheless, they (in-situ and remote sensing) still have their intuitive disadvantage ranging from high uncertainty in measurement and limited spatio-temporal coverage to cost implication, amongst others depending on the options. Regardless of the associated drawbacks, field measurements still serve as the most adopted method in monitoring and establishing aerosol properties in any environment [67, 69]. Meanwhile, the instruments used in field measurement are mainly similar to those used in the

laboratory evaluation. Particle analysers and radiometric instruments are the most commonly used for this technique.

Following the numerous techniques applied in the measurement of aerosols, most studies consider more than one method in establishing the particle behaviours since no single measurement is suitable to quantify their properties effectively. The reason is that the methods possess different limitations [67] and require varying approaches to take measurements.

### ***2.1.5 In-situ and Remote sensing of aerosol***

In aerosol studies, field measurement comprising in-situ and remote sensing is the most common and vital means of deriving aerosol properties and assessing their impacts. As pointed out earlier, in-situ allows observation of aerosols by direct contact or temporarily removed from their original environment. This method includes the use of mechanical means (e.g., impactors and filters) or electromagnetic radiation (e.g., OPC and spectrometers) to establish the properties of aerosols such as the size distribution. Although confronted by some limitations, in-situ measurement constitutes the most reliable form of observing aerosols [67, 70]. These include poor spatio-temporal coverage, expensive setup cost, laborious and uneasy to manage, and terrain selective. Measurements using this technique are through land-based or airborne setups. The former arrangement follows device installation on surface platforms such as the ground, mast, building tops, and moving vehicles. Meanwhile, the latter requires an instrument attached to a flying object like an aircraft or a weather balloon within the lower atmosphere.

Remote sensing is the fastest growing mode of observing aerosol in recent times and is mainly based on interacting with the samples remotely or indirectly with no physical contact to establish the desired measurements [69]. According to this method, electromagnetic radiation-based instruments are made used of in the process of acquiring information regarding aerosol samples. In terms of accuracy, remote sensing measurements are less accurate than in-situ observation [66, 67]. However, it is advantageous in the aspect of spatial and temporal coverage. Also, it is less expensive in the long run and boasts of flexibility with most terrain [69]. Remote sensing is deployable from the earth's surface (i.e., ground remote sensing), airborne (flying platform in the lower atmosphere), and spaceborne (i.e., satellite remote sensing). Each of these platforms possesses advantages over one another. Hence, they

are often used in tandem with one another to strengthen the reliability of the measurements. Generally, of the three platforms stated earlier, ground and satellite remote sensing are most used for aerosol and climate studies.

Ground-based platforms are less uncertain than satellite instruments of the two commonly used remote sensing methods [11, 71]. One reason is that the ground stationed device can observe aerosols more directly with less interference from the clouds. Besides, they are mostly stationary or sometimes moveable around a small comparable spatial extent to acquire consistent location measurement. Nevertheless, the most critical limitation is the small spatial coverage, as large numbers of this setup are required for sufficient coverage [69]. Also, setup and running costs are high and become more expensive to achieve a large area. As for the satellite platforms, measurements are more uncertain due to clouds and other space interferences. Yet, satellite observation offers broader spatial coverage and is more cost-effective (i.e., one satellite instrument can transverse the entire earth). Furthermore, observation using this medium is relatively stable, providing data without interruption for extended periods [11].

Although, the measurement of atmospheric aerosol has evolved especially over the last few decades with the improvement in model deployment, satellite observations, and increase in the ground monitoring system [11, 69]. However, the challenges posed by considerable uncertainty remain persistent due to the inability of a single instrument to accurately quantify the properties of aerosols in the atmosphere [72]. As mitigation against this drawback, most studies consider more than one instrument in establishing the characteristics and impacts of atmospheric aerosols [11, 73].

## **2.2 Principle of remote sensing**

Remote sensing works based on the interaction of electromagnetic radiation (EMR) or energy (EME) between a device called the sensor and a target object. The knowledge of electromagnetic radiation dates back to the 17th century, following the first publication of its theory [69]. More was known about EMR following the discoveries of infrared and ultraviolet radiation in the 19th century. Subsequently, James Maxwell developed the equation for an electromagnetic field later in the same century [69]. Thus, EMR is mainly waves of electromagnetic fields bearing radiant energy propagating through space at the

speed of light. This radiation consists of both electrical (E) and magnetic (B) fields that vary in magnitudes perpendicularly to the direction of propagation, as shown in Figure 2.3 below.

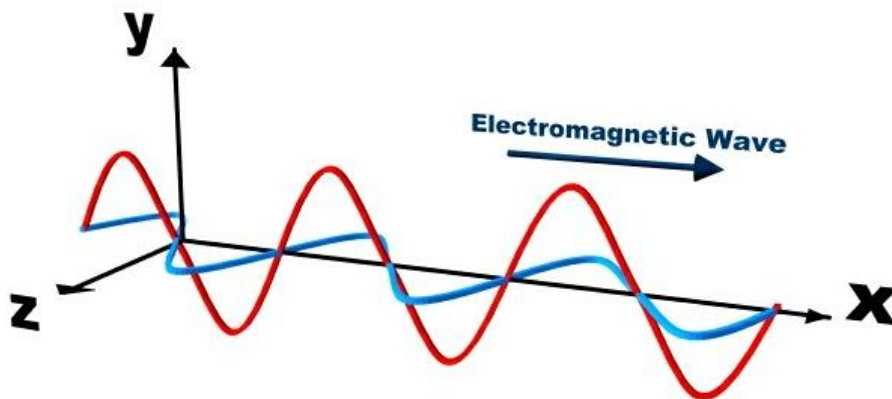


Figure 2.3 An illustration of EMR travelling in the x-direction, with the electric field E (red) and magnetic field B (blue) propagating in directions y and z respectively [74].

EMR possesses fundamental properties, energies, and predictable behaviours. Hence, it is modelled as wave and radiant energy. Since EMR is modellable as a wave, then it can be represented by a sinusoidal wave function [69, 75];

$$y = A \sin\left(\frac{2\pi}{\lambda}x + \varphi\right), \quad (2.7)$$

where,

$A$  = amplitude of the wave

$\lambda$  = wavelength

$x$  = number of oscillations

$\varphi$  = phase.

Thus, three key parameters (i.e., wavelength, amplitude, and phase) in equation (2.7) are essential for characterising EMR. Meanwhile, of the three parameters, the wavelength is a factor that differentiates one EMR from another, as it will be observed from the electromagnetic (EM) spectrum in a subsequent section (i.e., section 2.2.1) [75]. Examples of EMR are the blue and red lights with  $\lambda$  around 450 nm and 650nm respectively and constitute part of the visible light spectrum. Further implications of the differing wavelengths apart from the colour variance will be seen in due course.

Following the wave equation, it is convenient to relate the wavelength to the speed of light ( $c$ ) by defining the period ( $T$ ) of the wave. Thus,  $T$  is the time required to complete a cycle (i.e., attaining one  $\lambda$  of a particular EMR). Then, the frequency  $\nu$  is given by [75];

$$\nu = \frac{1}{T}, \quad (2.8)$$

therefore,

$$c = \nu\lambda. \quad (2.9)$$

Typically,  $c$  is a constant and has a value of 2.98 m/s such that  $\nu$  and  $\lambda$  are inversely related. Hence, the shorter the wavelength, the higher the frequency of the radiation (e.g., blue light possesses higher energy than the red counterpart). In remote sensing, the wavelength is vital to the targeted measurement because different objects interact with EMR differently, giving rise to the importance of EM-spectrum and atmospheric window (see section 2.2.2).

Following equation (2.9) and the ability to represent EMR in terms of energy in a photon, the energy  $E$  held by a photon is quantified by [69, 75];

$$E = h\nu, \quad (2.10)$$

where  $h$  = Planck's constant and  $\approx 6.626 \times 10^{-34}$  Js;  $\nu$  = frequency. Equation (2.10) is further expressed in terms of the speed of light as

$$E = \frac{hc}{\lambda}, \quad (2.11)$$

Also, the momentum  $P$  of the radiation is written as

$$P = \frac{E}{c} = \frac{h}{\lambda}. \quad (2.12)$$

Going by the last two equations, the lower the wavelength, the higher the energy of the photon, and the higher the  $\lambda$ , the lower the values of  $E$  and  $P$  (i.e., lower energy level). Relating these equations to the different EMR leads to the EM-spectrum.

Similarly, because matters possess varying characteristics, like interacting differently with EMR as earlier stated, remote sensing banks on the capabilities of some matters to radiate

EMR in establishing their properties. These categories of matters exhibit molecular agitation, such as the sun, which is the primary source of energy to the earth. Like the sun, several other matters, including some aerosols, absorb radiant energy and re-emit them. Therefore, by exploring the concept of a black body (*BB*) that is a body that can absorb all radiation hitting it (absorption = 1) and is capable of re-emitting such energy (emissivity = 1), conveniently the EMR are related to temperature and associated  $\lambda$ . Thus, further to equation (2.12), the radiant energy can be related to temperature through the wavelength of maximum emission  $\lambda_{max}$  as demonstrated by Wein's law [69]:

$$\lambda_{max} = \frac{b}{T}, \quad (2.13)$$

where

$b$  = constant with value  $\approx 2900 \mu\text{mK}$

$T$  = temperature in Kelvin

and following the Stephan-Boltzmann relation in the evaluation of the temperature of a *BB*

$$E = \sigma T^4, \quad (2.14)$$

where  $\sigma$  is a constant that has a value  $\approx 5.67 \times 10^{-8} \text{ Wm}^{-2}\text{K}^{-4}$ .

Hence, the principles described by equations (2.7-14) are generally explored to evaluate the properties of the various atmospheric phenomenon and their consequential impacts in remote sensing.

### **2.2.1 EM-spectrum**

The EM-spectrum is the band of frequencies and wavelengths of EMR along with their energy levels. The spectrum ranges from low frequencies and the corresponding wavelengths to high frequencies (at smaller wavelengths) separated into different categories based on the radiation characteristics (see Figure 2.4). Thus, according to the hierarchy of their energy levels, the categories include radio waves, microwaves, infrared, visible light, ultraviolet, X-rays, and gamma rays, with each having distinguished properties [64, 69]. As the name implies, the visible light spectrum is the only EMR visible to humans, other bands outside this range are invisible to the eye. Nevertheless, in remote sensing applications, the visible

light spectrum is deemed useful for the purpose. Other bands such as the radio waves and infrared spectra are also explored depending on the target and the propagation medium [69]. Also important, not all wavelengths within each categorised spectral band are suitable for remote sensing. Only a certain fraction of the spectrum is allowable due to atmospheric particles' interaction with the radiant energy [69, 76]. At this point, it is important to introduce the concept of atmospheric windows. To better understand the concept of atmospheric windows, it is essential to describe the mode of interaction of EMR with matters, particularly the atmospheric particles before illustrating the atmospheric windows.

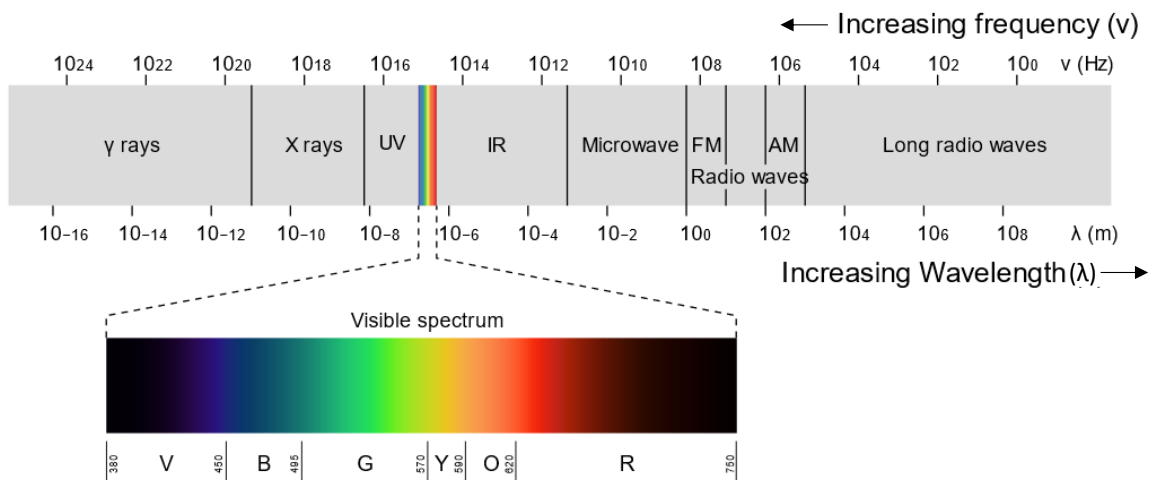


Figure 2.4 An illustration of the EM-spectrum highlighting the visible light spectrum [77].

### 2.2.2 Atmospheric interactions

Solar radiation is the primary source of EMR and energy, as it radiates most types of EMR toward the earth. However, not all radiation from the sun reaches the ground due to the filtering of some spectra (i.e., through absorption and scattering) by atmospheric matter as they approach the surface [76]. Particles including atmospheric components such as gases and aerosols mainly interact with EMR by absorption and scattering [69]. The absorption process occurs when matter absorbs EM energy hitting its surface. Similarly, atmospheric molecules absorb energy from the sun or other sources at varying wavelengths, thus limiting the fractional range of spectrum available for remote sensing [64, 69]. Therefore, the portions of EM-spectrum that is sense-able by remote sensing instruments (i.e., spectral bands at which EMR transmits through atmospheric molecules) are referred to as atmospheric windows, as shown in Figure 2.5.

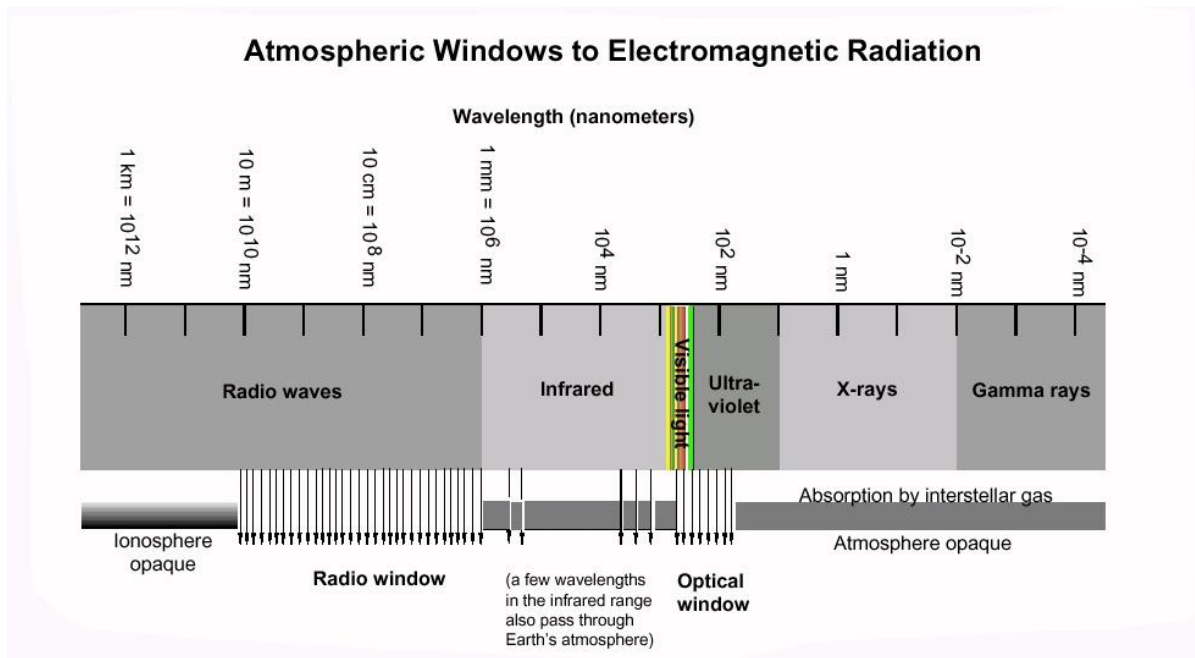


Figure 2.5 The atmospheric windows illustrated from the EM-spectrum [78].

In contrast, the scattering process follows the redirection of EMR from the initial path upon hitting matters. Remote sensing explores the characteristic scattering of EMR from the sun or other energy sources by atmospheric components like aerosols to establish their properties. Different aerosol types and atmospheric particles scatter EME differently therefore categorised into three main types for remote sensing applications: Rayleigh, Mie, and non-selective scatterings [69, 76]. Rayleigh scattering occurs during the interaction between EMR and particles smaller than the radiation wavelength. This type of scattering causes the energy of shorter wavelengths to be scattered greater than longer wavelengths. Hence, this scattering is wavelength dependent, and the intensity  $I$  of the scattered radiation is estimable as [69];

$$I = I_0 \frac{(1 + \cos^2\theta)}{2r^2} \left(\frac{2\pi}{\lambda}\right)^4 \left(\frac{n^2 - 1}{n^2 + 2}\right)^2 \left(\frac{d}{2}\right)^6, \quad (2.15)$$

where,

$I_0$  = intensity of the EMR

$\theta$  = scattering angle

$r$  = distance of scattering from the observation point

$\lambda$  = wavelength of EMR

$n$  = refractive index

$d$  = particle diameter.

Unlike Rayleigh scattering, Mie scattering occurs during the interaction involving EMR and particles with a size equivalent to or bigger than the wavelength of the incident radiation [79]. This scattering mode is often observed in the lower atmosphere, where large-sized particles are predominant. Although Mie scattering is not completely wavelength-dependent, it strongly affects longer wavelength radiation [69, 79]. In aerosol science, Mie scattering is suitable for observing large-sized aerosols such as MD, SS, and specs. The expression for the intensity of scattering at an angle  $\theta$  due to Mie scattering is given as [69];

$$I = I_0 \frac{[f(\theta, m, d_p)_\perp + f(\theta, m, d_p)_\parallel]}{2} \left( \frac{\lambda}{2\pi r} \right)^2, \quad (2.16)$$

where,

$I_0$  = intensity of the EMR

$f$  = a function of  $\theta$ ,  $m$  and  $d_p$  resolved to the perpendicular ( $\perp$ ) and parallel ( $\parallel$ ) based on complex Bessel-Legendre equation

$\theta$  = scattering angle

$m = \frac{m_1}{m_2}$  = ratio of the refractive index of a particle to the refractive index of dispersing medium

$d_p$  = diameter of the particle

$r$  = scattering distance from the observer.

The other form of scattering is the non-selective scattering that occurs due to interaction between EMR and particles of much bigger size relative to the radiation wavelength [69]. This scattering is independent of wavelength within the visible light spectrum as it is scattered at all possible wavelengths evenly in this range [69]. Large MD and water vapor are

prominent particles that initiate non-selective scattering, and a typical example is a whitishness observed from fogs and clouds.

### 2.2.3 Components of remote sensing

Following the different theories that form the basis of remote sensing as earlier illustrated, the setup constitutes certain fundamental components to remotely sense a target in any application, including atmospheric studies. Thus, a typical remote sensing system indicating the basic components is illustrated in Figure 2.6 below.

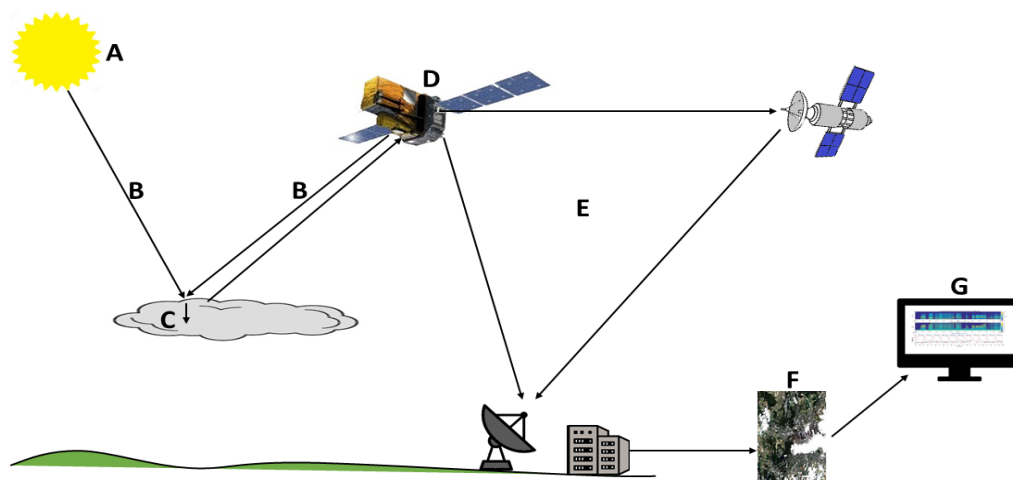


Figure 2.6 A graphical illustration of the basic elements of remote sensing.

The components labelled A-G in Figure 2.6 are described as follow;

Electromagnetic radiation (EMR) source (A): The source of EMR is crucial to a remote sensing system setup because it represents the origin of the energy that will interact with the target and later be measured by the remote sensor. In aerosol science and other atmospheric studies, the sun is the most typical source of EMR to be detected by the sensor [69]. Other sources of EMR include the sensing instrument (i.e., active sensor) and sometimes the target as some of them radiate energies.

EMR (B): The EMR is the required energy that interacts with or emitted from the target object, meant to be measured by the remote sensor to establish the needed characteristics of the target. This component is essential and the basis of remote sensing, as earlier shown from the working principle of remote sensors.

Target (C): The target or the object of interest is the component needed to be studied remotely (i.e., without physical interaction). In atmospheric science, typical targets include aerosols and water vapour.

Sensor (D): The sensor is the intermediary between the object of interest and the data products required to evaluate the properties of the target. It is an instrument or device that detect and measure EMR emanating from a surface based on the various principles of remote sensing described earlier in the previous sections. Examples of sensors include the sun photometer, spectrometer, and laser altimeter.

Transmitter and receiver (E): The transmitter is a device attached to the sensor where data collected by the sensing instruments is transmitted to the processing centre (e.g., Lab and station). Hence, it encodes and facilitates data transmission from the measuring sensor to the processing centre. Meanwhile, the receiver is just the opposite of the transmitter. A receiver collects and decodes data from the transmitter and delivers it to the processing centre in its original form as received by the transmitter from the sensor. Thus, the transmitter and receiver ensure data delivery from the sensor to the data processing centre.

Data products (F): The data products are various measurements of an object of interest made by a remote sensing instrument. These include the qualitative and quantitative properties of the target needful to understand its characteristics and effects.

Data analysis result (G): Data analysis and result involves the process of scrutinising the data products and deriving the appropriate interpretation and conclusion. Here, insightful detail on the target properties and the atmospheric and environmental impacts are revealed.

#### ***2.2.4 Types of remote sensor***

Remote sensors are categorised into two based on the operational mode, either the sun is the source of electromagnetic radiation (EMR) or generating its own EMR) as, active and passive remote sensors. Each type of sensor operates within a specified range of wavelengths in the atmospheric window (i.e., windows of atmospheric transmission within the EM-spectrum) [69]. The wavelength range within the atmospheric windows allowable to each sensor category is illustrated in Figure 2.7 below.

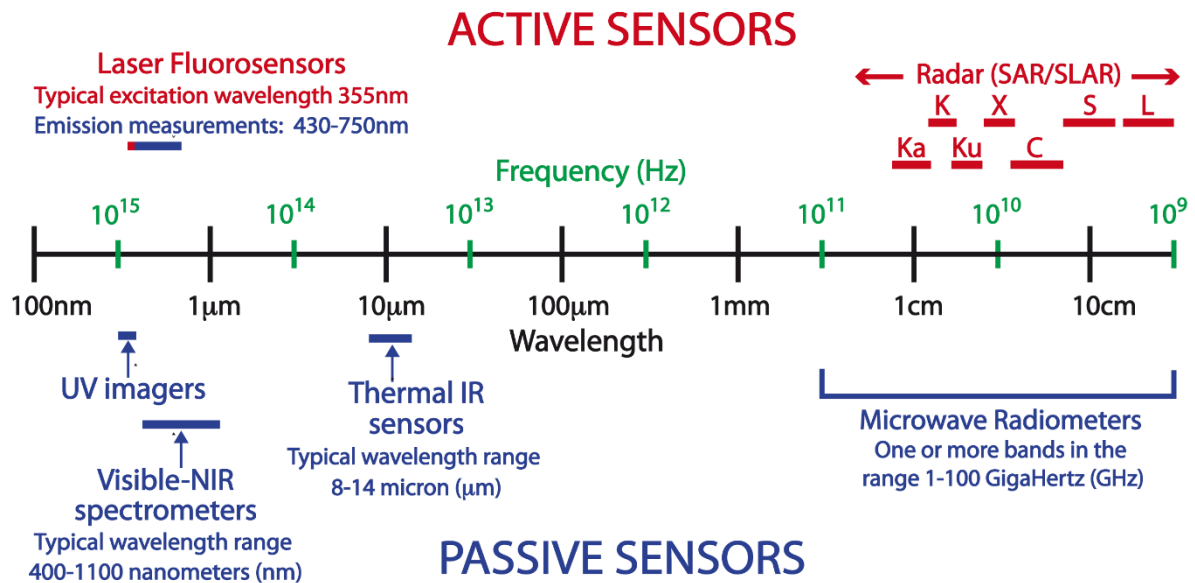


Figure 2.7 Bands of wavelength for different remote sensors within the atmospheric windows of the EM-spectrum [80].

Hence, a brief description of the two types of the remote sensor follows below;

(a) **Active remote sensor:** is a remote sensor that generates its own EMR either as an electromagnetic wave (e.g., radio wave and microwave) or an illumination (e.g., infrared and ultraviolet rays) to interact with the target, then reflected (i.e., energy-carrying information about the target) to be sensed by the sensor [69, 76]. An active remote sensor can measure both the intensity and phase change (i.e., distance and speed) of the target. Also, it possesses capabilities to function both day and night since it generates its own EMR [69]. A simple configuration of active remote sensing is shown in Figure 2.8.

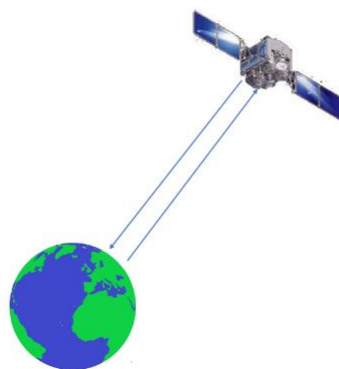


Figure 2.8 An artistic illustration of an active remote sensor setup.

In the general use of active remote sensing instruments, the most common types are Radio detection ranging (RADAR) and Light detection and ranging (LIDAR). In the case of a RADAR, it mainly generates electromagnetic signals in radio waves or microwaves directed towards an object of interest [69]. The reflected radiation (after interaction with the target), called the backscatter ( $\beta$ ), is subsequently received through an antenna or receiver to retrieve the information about the target. RADARs are basically of three subtypes subject to setup, namely

- monostatic (collocated transmitter and receiver)
- bistatic (transmitter separated from the receiver)
- quasi-monostatic (slightly separated transmitter and receiver).

Irrespective of the configuration, they follow the same principle, and the data derived from a RADAR is a function of the power, gain, wavelength, and propagation factor [69, 76]. Thus, the strength of EMR received by a radar system is evaluated as [81];

$$P_r = \frac{P_t G_t A_r \sigma F_t^2 F_r^2}{(4\pi)^2 R_t^2 R_r^2}, \quad (2.17)$$

where,

$P_r$  = receiving power

$P_t$  = transmitting power

$G_t$  = transmitting antenna power gain

$A_r$  = The effective aperture of the receiving antenna; also expressed as  $A_r = \frac{G_r \lambda^2}{4\pi}$

$G_r$  = receiving antenna power gain

$\lambda$  = transmitting wavelength

$\sigma$  = target size

$F_t$  = pattern propagation factor for transmitting antenna-target path

$F_r$  = pattern propagation factor for target-receiving antenna path

$R_t$  = transmitter-target distance

$R_r$  = target-receiver distance

For collocated transmitter and receiver (i.e., monostatic RADAR), the transmitter-target and receiver-target distances are the same (i.e.,  $R_t = R_r = R$ ), also the propagating factors for both transmitter and receiver are the same (i.e.,  $F_t = F_r = F$ ), it is convenient to write equation 2.17 as [81];

$$P_r = \frac{P_t G_t A_r \sigma F^4}{(4\pi)^2 R^4}. \quad (2.18)$$

Then the range  $R$  at which the reflected power =  $P_r$  and the corresponding transmitting power =  $P_t$  is;

$$R = \left[ \frac{P_t G_t A_r \sigma F^4}{P_r (4\pi)^2} \right]^{\frac{1}{4}}. \quad (2.19)$$

The target's speed can also be retrieved from the range by considering the ratio of change in range to the corresponding time change.

LIDAR generates EMR by illumination from a laser producing infrared, ultraviolet, and visible light spectrum. The light pulse energy interacts with the object of interest, while the instrument senses the reflected pulses (i.e.,  $\beta$ ) to establish vital properties of the target, such as distance and speed. The backscatter in this type of remote sensor is mainly received by a large telescope and passed on to the sensor [69, 76]. LIDARs work similarly to RADARs, except they generate EMR through the light spectrum instead of the radio waves or microwaves spectrum. Also, LIDAR is often used to complement a RADAR for data enhancement. Like the RADARs, LIDARs have two sub-categories; monostatic (laser and telescope are collocated) and bistatic (laser and telescope separated) LIDAR [82]. Although LIDAR and RADAR are found on the same principle, the mode of operation differs. Hence, the range  $R$  of a LIDAR is derivable as [82];

$$R = \frac{ct}{2}, \quad (2.20)$$

where  $c$  is the speed of light and constant,  $t$  is the time for the light to travel to and from the sensing instrument. Based on equation 2.20, it is convenient to derive the expression for the LIDAR backscatter power as a function of the range as [82];

$$P(z) = KG(z)\beta(z)T(z). \quad (2.21)$$

Where  $K$  is an experimentally controlled factor given as;

$$K = P_0 \frac{c\tau}{2} A\eta. \quad (2.22)$$

$G(z)$  is a geometry factor that represents the overlap characteristics of the laser beam and the receiver field, hence, given as;

$$G(R) = \frac{O(z)}{z^2}. \quad (2.23)$$

Meanwhile,  $T(z)$  is the transmission term and describe the light pulse lost part, hence, expressed as;

$$T(z, \lambda) = e^{[-2 \int_0^z \alpha(z, \lambda) dz]}. \quad (2.24)$$

Following the last three expressions, equation 2.21 is writable as;

$$P(z, \lambda) = P_0 \frac{c\tau}{2} A\eta \frac{O(z)}{z^2} \beta(z, \lambda) e^{[-2 \int_0^z \alpha(z, \lambda) dz]}, \quad (2.25)$$

where,

$P$  = backscatter power

$P_0$  = emitted laser power

$c$  = the speed of light

$\tau$  = the pulse duration of the laser beam

$A$  = effective telescope area

$\eta$  = system constant

$O$  = the laser beam receiver field of view overlap function

$\alpha$  = extinction coefficient or attenuation coefficient of the atmosphere

$z$  = range

$\beta$  = backscatter coefficient.

**(b) Passive remote sensor:** This type of remote sensor does not generate radiation but depends on the EMR reflected from the surface of a target after interaction due to initial illumination by an external source (e.g., the sun) or the energy radiated initially by the target as shown in Figure 2.9. Unlike an active sensor that can measure both the intensity and phase change of a target, a passive sensor only measures the intensity of the target object [69, 76]. And as such, passive sensors mainly measure an interest object's radiance and irradiance energy. Also, passive sensors are mostly functional during the day alone since it relies on an external source of EMR, primarily the sun [69, 79]. However, exceptional cases occur when it only takes measurements of radiance energy at night if the target radiates energy. The most common form of passive sensing instrument in atmospheric science is the radiometer and spectrometer.

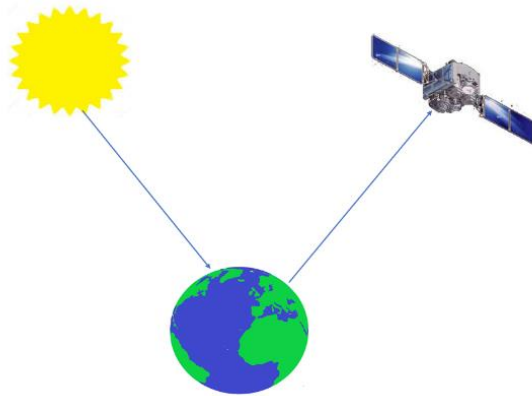


Figure 2.9 An artistic depiction of a passive remote sensing setup.

The radiometer and spectrometer both measure the intensity of EMR based on a similar principle but slightly differ in their mode of operation. The former measure the radiant energy at a specified range of wavelength (e.g., infrared, ultraviolet, or microwave wavelength) and resolve it to the corresponding temperature called the brightness temperature  $T_b$  [83]. Meanwhile, the latter measure the spectral characteristics of the EMR then resolve it into the

corresponding colours within the EM-spectrum depending on the intensity. Therefore, for a radiometer, the equation relating the target's temperature is [83];

$$\frac{T_s}{\sigma_T} = T_s \frac{\sqrt{\tau \Delta \nu}}{T_{sys}}. \quad (2.26)$$

If equation (2.26) is re-arranged, then,

$$\sigma_T = \frac{T_{sys}}{\sqrt{\tau \Delta \nu}}, \quad (2.27)$$

where,

$T_s$  = the signal of the source (target) in terms of temperature

$\sigma_T$  = rms receiver output fluctuations in the system temperature or the noise

$T_{sys}$  = temperature of the system

$\tau$  = time integration

$\Delta \nu$  = receiver bandwidth.

The temperatures listed in the above equation links to the Rayleigh-Jean limit from Plank's *BB* equation [83],

thus, from Plank's quantization of energy emitted by the radiating body

$$E = h\nu = hc/\lambda. \quad (2.28)$$

The energy radiated by a *BB* at a given temperature in terms of frequency is

$$B_\nu(T) = \frac{2h\nu^3}{c^2} \frac{1}{e^{h\nu/KT} - 1}. \quad (2.29)$$

By introducing Rayleigh approximation i.e.,  $\frac{1}{e^{h\nu/KT} - 1} \approx \frac{h\nu}{KT}$  in equation (2.29) then, we obtain;

$$B_\nu(T) = \frac{2\nu^2 KT}{c^2} = \frac{2KT}{\lambda^2}, \quad (2.30)$$

where,

$B_\nu(T)$  = spectral radiance at temperature  $T$

$h$  = Plank's constant

$\nu$  = frequency of the electromagnetic radiation

$c$  = speed of light

$K$  = Boltzmann's constant

$T$  = absolute temperature of the body

$\lambda$  = wavelength.

Since the radiometer measures the intensity in terms of the equivalent temperature of a  $BB$ , then,  $B_\nu(T) = I_\nu$  and  $T = T_b$ , equation (2.30) therefore becomes;

$$T_b = \frac{\lambda^2}{2K} I_\nu, \quad (2.31)$$

where,

$T_b$  = brightness temperature

$I_\nu$  = the intensity.

Following the description of the working principle of remote sensors, the types and processes, Table 2.2 below provide examples of remote sensing instruments and a summary of their operation and working principle.

Table 2.2 Examples of remote sensors and their operational principle [11, 69, 72].

<b>Instrument</b>	<b>Sensor type</b>	<b>Sample application</b>
Lidar	Active	Cloud-Aerosol Lidar and Infrared Pathfinder Satellite Observations (CALIPSO), laser fluorosensor (LF)
Accelerometre	passive	Airborne and satellite instruments
Imaging radiometre	passive	Cameras
Hyperspectral radiometer	passive	Advance CCD Imaging Spectrometre (ACIS), Hyperspectral Ocean Colour Radiometre (HOCR), surveillance camera
Radar	active	Doppler radars, CALIPSO
Radiometer	passive	Sun photometers, Visible Infrared Imaging Radiometre Suite (VIIRS), Along-Track Scanning Radiometre (ATSR)
Spectrometer	passive	TOMS, (Total Ozone Mapping Spectrometre), Airborne Visible/Infrared Imaging Spectrometre (AVIRIS)
Spectroradiometer	passive	Moderate Resolution Imaging Spectroradiometre (MODIS), Multiangle Imaging Spectroradiometre (MISR)
Sounder	Active/ passive	Visible Infrared Spin-Scan Radiometre (VISSR), Stratospheric Aerosol and Gas Experiment (SAGE)
Scatterometer	active	Advance Scatterometre (ASCAT), Rapid Scatterometre (RapidSCAT)

### 2.3 Clouds and classification

Clouds are visible light masses of vapour droplets and ice crystal particles formation suspended in the air. Unlike aerosols, clouds in their appearance do not have physical contact with the earth's surface. This formation of vapour droplets and ice crystal particles varies temporally and spatially depending on the height, size, temperature, pressure profile, aerosol interactions, wind drags, and other atmospheric dynamics and thermodynamics [84]. Cloud constituents (vapour droplets and ice crystals particles) possess a long residence time in the atmosphere. The formation of clouds fundamentally occurs from cool, saturated air along with water vapour or ice crystal and microscopic particles (i.e., CCN and IN) called hygroscopic nuclei [6, 63]. They grow big due to coalescing and collisions of particles, cloud droplets, or smaller neighbouring clouds. Further growth of cloud droplets (typically radius < 1 to 50  $\mu\text{m}$ ) along with rapid atmospheric dynamics and thermodynamics leads to raindrops (typically radius > 0.5 mm) forming, which are eventually removed by precipitating [72, 85].

Basically, clouds exist in various forms, possess diverse characteristics, and interact differently with the earth's climate. They are mainly described and classed based on their physical structure, shape, size, thickness, height, and ability to produce rainfall [6, 63]. Furthermore, clouds primarily reside within the troposphere and stratosphere and are mostly found between 0-11 km above sea level [63, 84]. Internationally, the most adopted cloud classification system is with respect to their structure, shape, and altitude above the sea [6, 84]. Hence, with their heights, they are generally classified into three distinct layers; high clouds (e.g., cirrus clouds), middle clouds (e.g., altostratus), and low clouds (e.g., cumulus clouds). Then in terms of shapes, they are classified as cirrus, stratus, and cumulus clouds. Also important, the cloud base height varies with latitude leading to a considerable difference in height range for any cloud class over different latitudes [84, 86]. A summarised description of the factors considered in the classification clouds considering their latitudinal variance where applicable is presented in Tables 2.3 and 2.4 below.

Table 2.3 Cloud classification by altitude over different latitudes [63, 84].

Cloud class	High cloud	Middle cloud	Low cloud
Altitude (ft)	16000-50000	6000-23000	Below 6500
Tropics (ft)	> 23000	6000-23000	Below 6500
Mid-latitude (ft)	> 20000	6000-20000	Below 6500
High latitude	> 16000	6000-16000	Below 6500
Cloud type	cirrus, cirrocumulus and cirrostratus	altostratus and altocumulus	cumulus, stratocumulus, stratus, nimbostratus and cumulonimbus

Table 2.4 Cloud classification by structure [63, 84].

Cloud class	Cirrus	Stratus	Cumulus
Description	They earned their name from having a hairy wispy shape and are mainly found as high clouds.	Possess a layer formation or forms as a group of layers. This type of cloud is found in all levels of cloud formation.	Adopts their name from being puffy and the general heaped fluffy shaped. Mainly found in all altitudes of cloud formations.
Cloud type	cirrus, cirrocumulus and cirrostratus	stratus, cirrostratus, altostratus, stratocumulus and nimbostratus	cirrocumulus, altocumulus, stratocumulus, cumulus and cumulonimbus

### 2.3.1 Types of clouds

Clouds are formed in the atmosphere, and they vary in shape, size, and altitude above sea level. There are ten different genera of cloud formation founded on the primary characteristics described in Tables 2.3 & 2.4 above, as observed in the atmosphere. The naming of each cloud systemically follows the names of the primary features by including the base name and prefixes, hence, described as follows [84];

***Cirrus clouds:*** These are high clouds with a wispy hairy feature and are mainly made up of ice crystals. They are found highest in altitude above the sea level over the tropics, with the base sometimes exceeding 13 km. Also, they are mainly thin, light in structure, and have a low temperature of about -100 K. They are generally non-precipitating cloud systems but sometimes produce droplets that do not reach the ground. Cirrus clouds form under fair weather conditions and occasionally during warm front when they become more significant over time.

***Cirrocumulus clouds*** are puffy-shaped high clouds, usually whitish in colour but occasionally grey. They are approximately similar in size and generally smaller than other cloud systems. Cirrocumulus clouds are often aligned in parallel rows and do not precipitate. Instead, they are more associated with fair cold weather and commonly occur during winter.

***Cirrostratus clouds:*** Another category of high-thin clouds, white and often cover most or all the sky in a veil-like style. They usually produce halos such that the outline of the sun and moon are visible through them. Cirrostratus clouds are predominantly made-up of ice crystals and often indicate an approaching front (i.e., usually precede heavy rain or snowstorm).

***Altostratus clouds:*** are mixed-phase (i.e., contains both ice crystals and water droplets) mid-level clouds that often cover the entirety of the sky. Grey or blue-grey colour, altostratus clouds mostly hid the sun and moon, but their illumination still passes through and mainly appears dim behind the clouds. Although these clouds are not precipitating one, however, their occurrence (especially when they become thicker) often indicates the coming of a stormy continuous light precipitation.

***Alto cumulus clouds:*** are patchy greyish white mid-level clouds predominantly made-up of water droplets but occasionally precipitate. They have a woolly appearance and often form in groups that subsequently grow thick to the extent capable of completely hiding the sun and moon.

***Cumulus clouds:*** are low puffy clouds, mainly whitish or greyish, with a fluffy shape found in the altitude range of 1 to 2 km from the base above the sea level. These clouds often resemble floating cotton with a flat bottom and are mainly formed due to rising air due to temperature increase during surface heating. Cumulus cloud is associated with the fair weather condition and sometimes results in light showers.

***Stratocumulus clouds:*** predominantly greyish with traces of whiteness, fluffy low-level clouds that tend to be darker as they grow bigger. They are associated with a cloudy appearance with less sunny and eventually obscure the sun or moon as they become thicker. Stratocumulus clouds mainly consist of water droplets formed closer to the top of the boundary layer but produce more drizzling than precipitation, especially in the hills.

***Stratus clouds:*** often grey in colour and thin, the low-level clouds are known for partly or fully covering the sky to the extent that they obscure the sun or moon when thick. They have a resemblance to fog but do not extend to the ground. Stratus clouds do not usually precipitate, but once they become very thick, they can produce a significant amount of light precipitation, particularly around hills and coastal environments.

***Nimbostratus clouds:*** are thick dark grey clouds that often blot out the sun or moon and cover the entire sky. They are primarily associated with continuous moderate to heavy precipitation. Nimbostratus clouds are usually fused such that their individuals are difficult to pick out and classified as low or mid-level clouds.

***Cumulonimbus clouds:*** are large, towering clouds mainly formed due to the development of deep convection and can reach a very significant vertical extent towards the tropopause. They often possess an anvil-like appearance at the top caused by high winds flattening. Cumulonimbus clouds consist of liquid droplets at the bottom and tend towards mixed-phase to glaciated clouds with altitude. Besides, they are characterised mainly by thunderstorms, lightning, and heavy precipitation.

The pictorial illustration of the described ten (10) predominant types of clouds is shown in Figure 2.10 below.

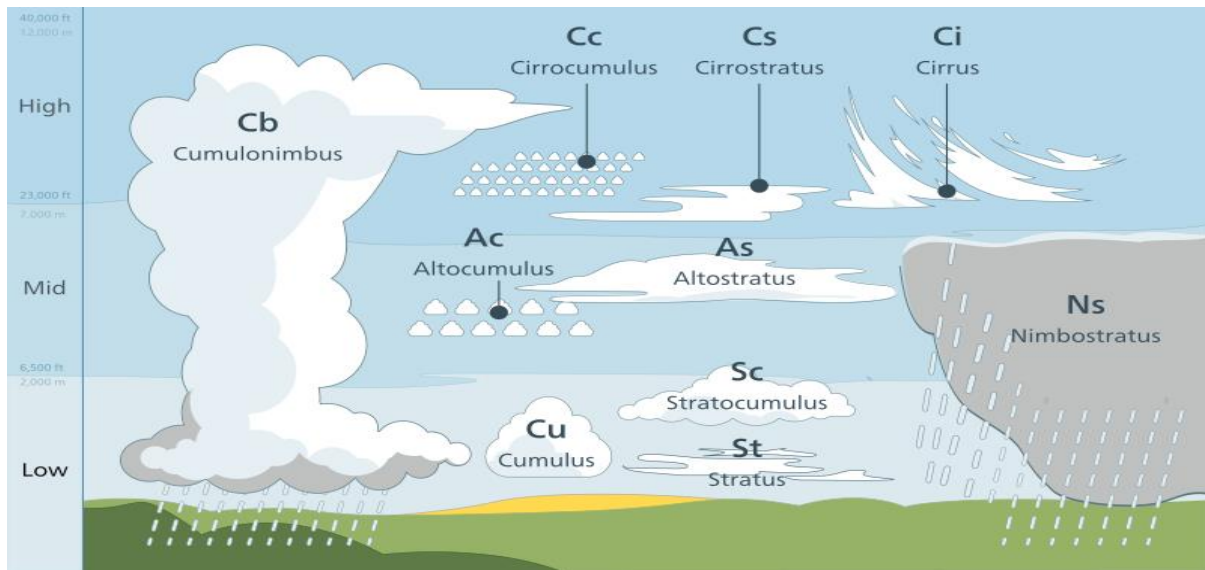


Figure 2.10 A graphical display of the ten types of clouds along with their altitude and shapes [87].

### 2.3.2 Importance of clouds

Through their formation, dynamic and thermodynamic processes, clouds play an essential role in controlling the earth's climate system. Every slight change in their physical and microphysical processes fuel different and significant feedback mechanisms that influence the earth's climate conditions. As a reflection, some of the importance of the clouds are described below.

**Earth's energy budget (EEB):** clouds constitute a significant control effect on the Earth's radiative budget by regulating the amount of solar radiation reaching the earth's surface. By reflecting, absorbing, and reemitting incoming solar energy, they regulate energy received by the planet from the sun [11, 51]. Invariably, the changes in the properties of the clouds translate to the corresponding variation in the solar energy the earth gets.

**Radiative forcing (RF):** as the sun emits shortwave radiation (SWR) towards the earth, the earth reciprocates by emitting longwave radiation (LWR) in the direction of space; meanwhile, the clouds influence how much of either radiation cross over. In this circumstance, the clouds play a crucial role in regulating the net energy flux into the earth's atmosphere, mainly referred to as the earth's energy balance [12, 36]. An event of the planet receiving more SWR than it successfully emits LWR to space results in net energy gain and warming effect, referred to as positive radiative forcing. The reverse leads to net energy loss and cooling effect tagged a negative radiative forcing.

**Precipitation formation and hydrology cycle:** essential processes leading to the formation and initiation of all forms of precipitation occur in the clouds. Therefore, the characteristics and morphology of the clouds define water mobility to and fro between the surface and atmosphere. So, clouds are the bearer of precipitation and an essential driver of the global hydrology cycle.

**Aerosol removal:** Atmospheric aerosols are emitted into the air and subsequently removed systematically from the atmosphere. Clouds constitute an essential means of aerosol removal from the atmosphere through scavenging and in the process of nucleating CCN and IN [11, 12].

**Heat redistribution and climate dynamics:** The clouds aid the redistribution of extra heat towards the poles from the equator. Besides, they serve as a way to regulate the global average temperature [6]. Furthermore, they indicate the type of atmospheric process ongoing at a given time, such as atmospheric turbulence and heating.

### ***2.3.3 Processes modifying the clouds***

The clouds frequently change in characteristics on a timely scale, yielding a corresponding change in the climate dynamics and the atmospheric conditions because of the role played by clouds. Meanwhile, several factors lead to clouds modification, including aerosol emission, precipitation, atmospheric dynamics, and thermodynamics, among others [53, 54]. Regarding aerosols, they influence the composition and radiative properties of clouds through their roles as CCN and IN [72]. The influx of newly emitted aerosols (mainly resulting in a high concentration of small size CCN) into the clouds depending on the type can invigorate cloud development and precipitation formation [85]. Similarly, the reverse could occur when freshly emitted aerosols alter the thermal structure of the clouds, therefore, suppressing convective development [72].

Another important process that alters the state of the clouds is precipitation. Heaps of cloud often reduce or sometimes clear off following precipitation events. Since the size of the clouds reduces substantially due to rainfall or snow, the properties (i.e., macro and microphysical) consequently change [84]. Similar to cloud alteration due to precipitation, atmospheric dynamics such as air movement plays a significant role in the motion and distribution of clouds. Both horizontal and vertical motion of air, depending on their velocities, are crucial to the development and spread of clouds globally [84, 85].

In terms of thermodynamics effect, changes in the atmospheric heating rate cause a shift in the cloud's thermodynamic properties, including altering the cloud radiative properties and their entire thermal structure [85]. As an influential factor, the clouds respond by modifying all processes (e.g., freezing, condensation, evaporation, and precipitation) within them. Besides, this effect often falls back to influencing atmospheric circulation [84].

#### ***2.3.4 Measurements of cloud***

To monitor and understand the behaviour of the clouds and how they influence different atmospheric and climate processes, the need to observe and evaluate their activities becomes essential. Just as in aerosol measurements described in the previous sections (section 2.1.4-2.1.5), clouds properties are established similarly. In most cases, the measurement techniques of aerosols and clouds overlap; hence, they often share the same instruments since both phenomena are mainly studied in tandem. Also, most instruments (in-situ, airborne, ground, and satellite) have multi-spectral, frequency, and size compatibilities suitable to detect various aerosol and cloud properties. Examples of cloud measuring instruments include particle counters, RADARs, LIDARs and radiometers.

### **2.4 Precipitation**

Precipitation is the droplets of condensed water vapour in liquid or solid form that falls from the atmosphere to the ground. As a process, precipitation constitutes an essential part of the global hydrology cycle (i.e., global water drive through-formation and occurrence) and is a vital source of fresh water. Precipitation occurs in different forms, including rain, drizzle, snow, hail, and sleet [63]. The emergence structure is a function of the characteristics of the clouds formed during the period [84, 85]. The precipitation formations start with the absorption of water by air to form water vapour through evaporation, followed by the elevation of vapour to a higher altitude through airlifting. The raised vapour eventually reaches saturation point and condenses on particles of aerosols (i.e., CCN and IN), activating them into cloud droplets that form the clouds [84]. Because the cloud droplets are too tiny and light to escape gravity, they grow in the clouds by collision and coalescence to become big enough to fall as precipitation [72, 85]. Therefore, the aerosol types and atmospheric dynamics are crucial to the development of precipitation-bearing clouds and their precipitation occurrence.

### ***2.4.1 Types of precipitation***

Different types of precipitation occur depending on the cloud's characteristics, particularly the mode of air uplift (i.e., vertical motions) [85]. According to the way of vertical air motions, precipitation is mainly of three types; convective, cyclonic, and orographic [63], hence, describe as follows;

**Convective precipitation:** is a showery to heavy form of precipitation associated with towering cumulus-scale (e.g., cumulus congestus and cumulonimbus) clouds in unstable air. The spatial organisation and degree of this precipitation type depend on the convective instability of the atmosphere ushered by intense heating of the land surface when the temperature in the upper troposphere is very low [84]. This process eventually leads to the development of scattered convective cells, individually resulting in heavy rain or sometimes hailstorm [63]. In some circumstances, deep convective cloud gathers as cumulonimbus cell (e.g., tropical cyclones) to descend through prolonged heavy rainfall [85]. Also, convective precipitation results from the passage of colder convective cells over a warmer surface, causing showers of rain or snow covering a wide area. In general, convective precipitation usually covers small regions not more than 10 km<sup>2</sup> in size [63, 84].

**Cyclonic or stratiform precipitation:** is a less intense or moderate form of continuous precipitation occurring over extensive large areas [84]. Unlike the convective type, the formation involves weak upward air motion through largescale horizontal convergence over a low-pressure area [63].

**Orographic precipitation:** a distinct type of precipitation associated with orographic barriers (e.g., mountains, hills, and slopes) influencing atmospheric instability to cause downpours. The mechanism of this precipitation type is based on the adiabatic cooling of an airstream forced to ascend an elevation such as a mountain and undergoes condensation to form precipitation [63, 84]. Alternatively, an orographic barrier often obstructs the airflow, leading to forceful airlifting that triggers convective instability that yields condensation and precipitation [63].

A graphical description of the three types of precipitation is illustrated in Figure 2.11 below.

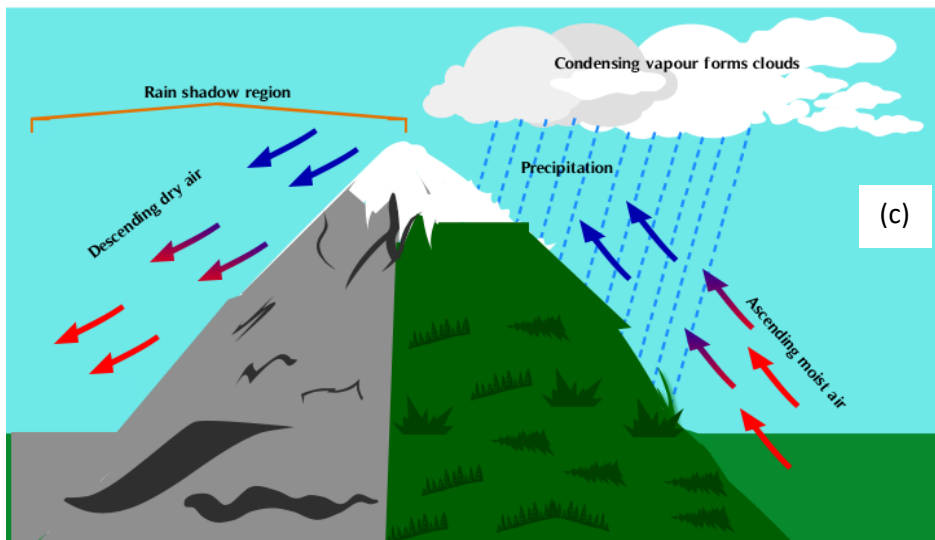
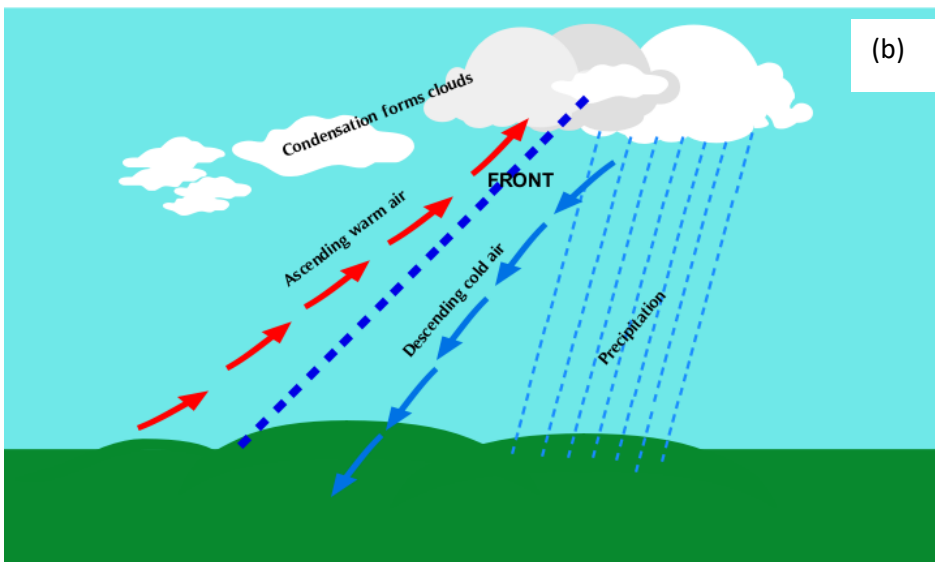
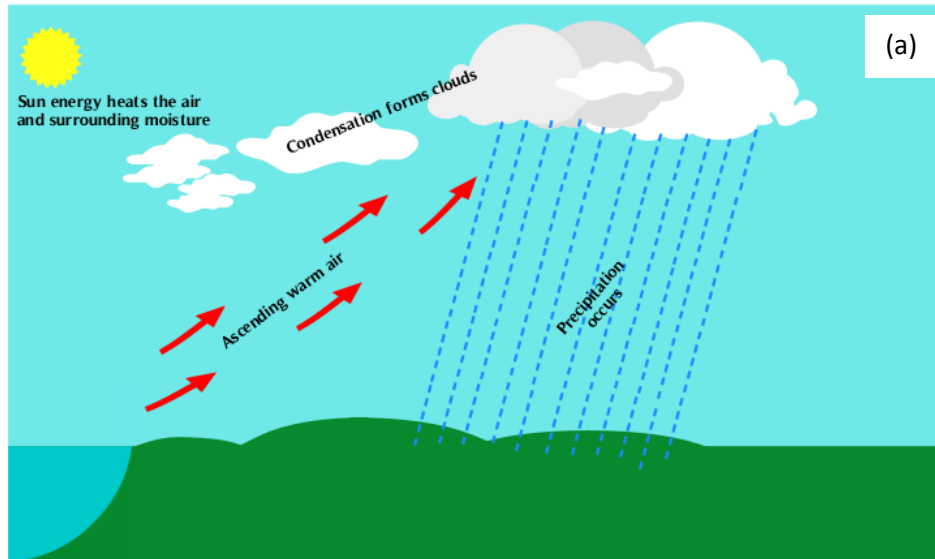


Figure 2.11 An illustration of the types of precipitation; (a) convective, (b) cyclonic and (c) orographic precipitation systems.

### ***2.4.2 Importance of precipitation***

Precipitation occurrence on earth owes enormous importance to the habitability and sustainability of the planet. Some of the significance are briefly highlighted below.

**Source of fresh water:** precipitation is a crucial source of fresh water to the planet. The process enhances the supply of fresh water to estuaries and serves as a source of water replenishment to the earth.

**Climate regulator:** events of precipitation influence the climate condition through the formation and discharging of the clouds, thereby initiating changes in the atmosphere, land, and oceans.

**Hydrology cycle:** precipitation constitutes a significant component in the global hydrology cycle by reinstating water to the earth after removal by evaporation.

**Global energy regulation:** precipitation aids the distribution of energy across the earth through changes in the cloud structure, thereby modifying the mean energy flux to the planet. Also, precipitation influences temperature distribution in the atmosphere and sea to alter the atmospheric circulation pattern [64].

**Aerosol removal:** precipitation is an essential means of aerosol removal through wet deposition, therefore, improving the air quality [11].

### ***2.4.3 Processes that modify precipitation***

Precipitation occurrence varies spatial-temporarily and is generally influenced by different atmospheric and environmental changes. One critical component that alters precipitation patterns is the cloud's properties. Through the dynamic and thermodynamic process of cloud development, the atmospheric stability systematically changes (i.e., becomes stable or unstable) leading to the suppression or enhancement of precipitation-bearing clouds [38, 72]. This phenomenon is typically observable during the process of convergence or sometimes the discarding of already converged precipitation-bearing clouds [72, 85].

Another vital component that alters precipitation is aerosol emission. Aerosols are emitted from natural and anthropogenic sources, thus acting as CCN and IN to alter the clouds' microphysical properties [38]. Through this process, aerosols modify both the composition

and radiative properties of deep and shallow clouds, thereby affecting precipitation formation, occurrence, and intensity [85]. A typical example of this effect on precipitation is the event of low rainfall or drought where the clouds are unable to deliver sufficient amount of precipitation or result in dryness.

#### ***2.4.4 Measurements of precipitation***

Observation and measurement of precipitation are mainly established through in-situ methods using a standard gauge (e.g., rain gauge, snow gauge) usually placed at weather stations. The gauge measures the depth or intensity of precipitation in millimetres or inches to generate hourly or daily averages depending on defined timing. Standard gauges are mainly of two categories, the recording and non-recording gauges as shown in Figure 2.12 below. The former continuously measures and records precipitation intensity automatically using an inbuilt recorder until the observer physically visits the site to collect such data [88]. Examples of the recording type are the siphon and the tipping bucket gauges. The recorded data is remotely retrieved through various data transmissions in modern designs. As for the latter, precipitation intensity is measured manually using a cylindrical or ordinary gauge. The non-recording gauge typically consists of an inner calibrated cylinder measuring up to 25 mm (1 inch). Rain overflows into a bigger (e.g., 200 mm) outer container when it gets filled. Measurement and recording are then physically taken by measuring and cumulatively adding up the contents of both containers [88].



Figure 2.12 Images of a recording (left) and non-recording (right) gauges.

Apart from the in-situ measurement of precipitation, remote sensing techniques including ground, airborne, and satellite instruments are also used in inferring the occurrence and intensity [84, 88]. The principle and method are the same as earlier described in the previous sections under measurements of aerosols and clouds. In remote sensing of precipitation, instruments such as LIDAR and RADAR observe the formed clouds to estimate the amount of rain or snow expected to fall over an area [84]. Essentially, the theoretical equation for evaluating precipitation is embedded in the RADAR or LIDAR equation to measure the precipitation rate or intensity. The precipitation intensity ( $\text{mmd}^{-1}$ ) defined as the precipitation flux over a horizontal surface is expressible in terms of size distribution function  $N(D)$  as [84];

$$I_p = \frac{\pi}{6} \int_0^{\infty} N(D) D^3 u(D) dD, \quad (2.32)$$

where,

$I_p$  = equivalent precipitation rate

$D$  = melted diameter

$u(D)$  = fall velocity of droplet size  $D$ ,

such that  $\rho_w$  is water density, while other parameters retain their previous definitions.

Then, the precipitation water content  $L$  (i.e., precipitation amount independent of fall velocity in  $\text{gm}^{-3}$ ) is defined by [84];

$$L = \frac{\pi}{6} \rho_w \int_0^{\infty} N(D) D^3 dD. \quad (2.33)$$

For instance, from the radar equation in (2.18), the average receiving power associated to a given range is expressed by [84];

$$\bar{P}_r \cong \frac{P_t (G_t \lambda)^2 F^4}{(4\pi)^3 R^4} \sum \sigma, \quad (2.34)$$

where  $\sum \sigma$  is the sum of the backscatter cross-sections of the total particles within the resolution volume. Thus, for a single scatterer small compared to the radar wavelength,  $\sigma$  is linked to the sphere radius  $r_0$  by;

$$\sigma = 64 \frac{\pi^5}{\lambda^4} |K|^2 r_0^6, \quad (2.35)$$

where,  $K = \frac{(m^2-1)}{(m^2+2)}$  and  $m = n - ik$  is the sphere complex index of refraction such that  $n$  and  $k$  are respectively the refractive index and absorption coefficient. This is a typical representation of Rayleigh scattering law; thus, particles are approximate Rayleigh scatterers [84].

Now, for the collection of spherical precipitation droplets with the above defined size, combining (2.34) and (2.35) gives;

$$\bar{P}_r \cong \frac{P_t (G_t \lambda)^2 F^4}{(4\pi)^3 R^4} 64 \frac{\pi^5}{\lambda^4} |K|^2 \sum r_0^6. \quad (2.36)$$

By considering the droplet diameters, (2.36) becomes;

$$\bar{P}_r \cong \frac{P_t (G_t)^2 \pi^5 F^4}{(4\pi)^3 R^4 \lambda^2} |K|^2 \sum D^6. \quad (2.37)$$

Hence, the mean power received for the small spherical scatterers compared to the wavelength is a function of the radar parameters, range, and values of  $|K|^2$  and  $\sum D^6$  (i.e., two factors dependent on the scatterers). Due to the factor  $\sum D^6$ , it is essential to define a new quantity  $Z$  ( $\text{mm}^6/\text{m}^3$ ), the reflectivity factor such that [84];

$$Z = \sum_v D^6 = \int_0^{\infty} N(D) D^6 dD, \quad (2.38)$$

where,

$\sum_v$  = summation over unit volume

$N(D)dD$  = number of scatterers per unit volume with diameters in  $dD$

$N(D)$  = drop-size (for raindrops) or melted diameters (for snowflakes) distribution.

Now, the radar equation as a function of  $Z$ , plus the small correction due to a Gaussian beam pattern becomes;

$$\bar{P}_r \cong \frac{\pi^3 c}{1024 \ln 2} \underbrace{\left[ \frac{P_t (G_t)^2 \tau \theta^2 F^4}{\lambda^2} \right]}_{\text{RADAR}} \underbrace{\left[ |K|^2 \frac{Z}{R^4} \right]}_{\text{TARGET}}, \quad (2.39)$$

where,  $c\tau = h$  (i.e., the pulse length) and  $\theta$  (the beamwidth) are parameters estimated from the contributing volume  $V \approx \pi \left( \frac{r\theta}{2} \right)^2 \frac{h}{2}$ .

Therefore, the  $Z$ - $I_p$  relationship for rain is approximately expressed by [84];

$$Z = 200 I_p^{1.6}, \quad (2.40)$$

while for snow, the approximate relation is given by;

$$Z = 2000 I_p^2. \quad (2.41)$$

Similarly, the empirical relations between  $Z$  and  $L$  (precipitation content) for rain is;

$$Z = 2.4 \times 10^4 L^{1.82}, \quad (2.42)$$

And for snow,

$$Z = 3.8 \times 10^4 L^{2.2}. \quad (2.43)$$

## 2.5 Aerosol-cloud-precipitation interaction (ACPI): A general review

Atmospheric aerosols are usually emitted into the atmosphere, where they initiate interactions with clouds and precipitation to consequently impact the climate. Even with this fundamental knowledge of aerosol-cloud-precipitation interactions (ACPI) and the observed effects on surface climate, not much is understood about the mechanism regarding how they interact to induce different climate conditions due to significant uncertainties. However, many studies have investigated ACPI and associated primary physical mechanisms both on regional and global scales, which has led to tremendous progress and a significant improvement in the understanding. Nevertheless, the current understanding of the interactions still lacks the adequate knowledge required to effectively describe several phenomena (e.g., mixed-phase

cloud formation and convective cloud invigoration by fresh aerosol emission) linked to climate change, therefore hindering efficient projection [12, 85].

Fundamentally, the process of aerosols as associated with ACPI and how they influence global climate are broadly classified into direct, indirect, and semi-direct effects, where each category plays a vital role in altering the earth's radiation budget [36]. In the aerosol direct or radiative effect, now referred to as aerosol radiative interaction (ARI), incoming solar radiation is absorbed or scattered, leading to change in the atmospheric and cloud conditions (e.g., surface temperature, stability, cloud properties) [12]. More importantly, the effect of ARI can result in either negative or positive net radiative forcing (RF), thus influencing the average global temperature and other climate components [51, 52]. Negative net RF is noted by the cooling effect of the earth when the outgoing radiative flux (i.e., longwave radiation LWR) exceeds the incoming shortwave radiation (SWR). The reverse is net positive RF associated with warm effect such that SWR exceeds LWR. Whether the net RF results in a negative or positive, the outcome affects the cloud's features (i.e., dynamic, and thermodynamic states) that subsequently impact precipitation and the general climate [12].

Regarding the indirect and semi-direct effects, aerosols act as CCN and IN to alter the cloud's microphysical properties, resulting in Twomey or albedo effect which represents an increase in cloud reflectance due to a rise in the droplet number as a function of reducing droplet size [89]. Furthermore, changes in the cloud's microphysical properties increase cloud lifetime and cloudiness [54] and sometimes initiate cloud burn-off initiated by heating [55], therefore suppressing or delaying precipitation [72, 90]. These effects are jointly referred to as aerosol-cloud interaction (ACI) according to the [12] report. Like ARI, ACI consequentially induces RF (cooling or warming effect) on the planet, thereby affecting the precipitation pattern and other climate components [72, 85]. A pictorial illustration of the effects pivoted on aerosol emission is displayed in Figure 2.13.

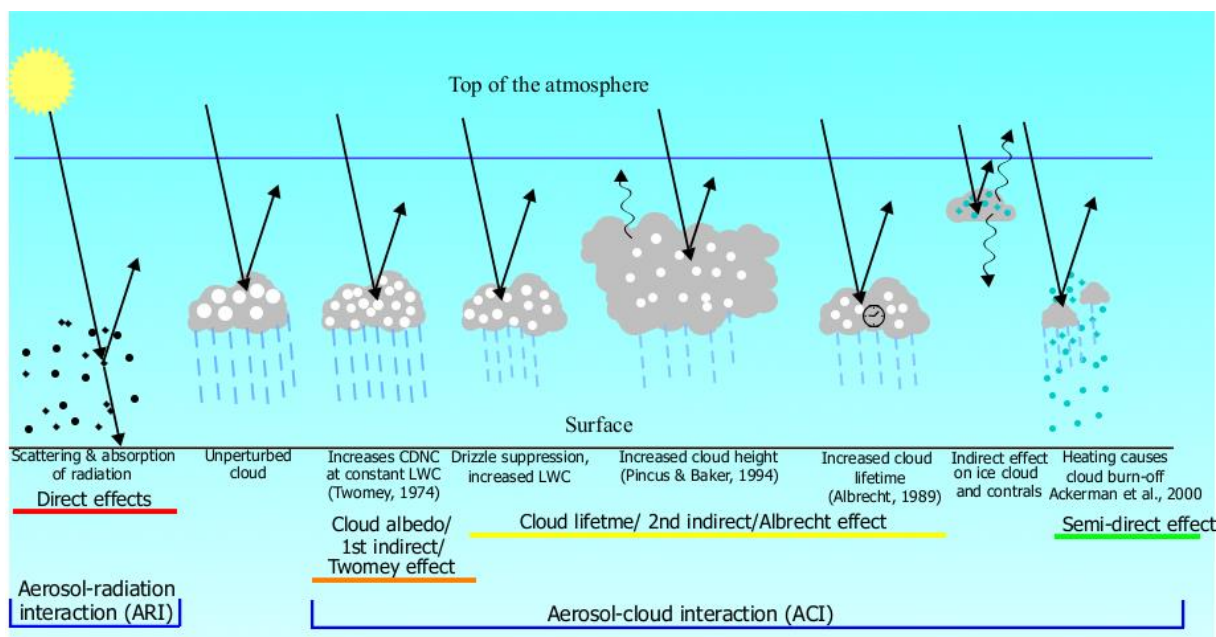


Figure 2.13 A graphical description of ARI and ACI modified from [36].

Importantly, studying ARI and ACI in tandem is the panacea to fully understanding ACPI. Although, both individual interactions (i.e., ARI and ACI) are associated with large uncertainty, especially regarding their impacts on radiative forcing and cloud morphology, however, ARI is more understood than ACI to a considerable extent [12, 72, 85]. Since RF depends on anthropogenic aerosol emission, quantifying the net emission due to anthropogenic sources alone constitutes a challenge [12, 36]. Similarly, aerosols mainly exist heterogeneously in the atmosphere hence, the inability to accurately account for the aerosol types present in an environment and their properties (e.g., size distribution, concentration, and refractive indices) contributes to the uncertainty in evaluating the net RF. Nevertheless, numerous observational studies have attempted to estimate better the aerosol types and the net radiative effects over different environments [3, 42, 91-93]. However, their results are insufficient to fill the knowledge gap instated by the various uncertainties. Therefore, more efforts are required to accurately estimate the RF due to aerosol for better modelling and future climate projection.

For ACI with a more complicated mechanism regarding changes in the microphysical, dynamics and thermodynamics structures due to aerosol impacts, the understanding is extremely complex and constitutes the largest part of uncertainty associated with ACPI. Several bottlenecks including estimating the number of aerosol particles recruited as CCN

and IN, disentangling their impacts on the cloud radiative properties and net RF, and effects on different cloud development amongst others contributes to our poor understanding and parametrisation of the processes from meteorological to climate effects [58, 59, 61, 94]. In the last decade, intensified observations and modelling studies have yielded tremendous progress in each of the identified factors mentioned. For instance, more insight had been gained regarding the number concentration of aerosols elevated to the status of CCN and IN, and their linkage to the formation, size, and number concentration of cloud droplets, through observation and numerical simulation [95-100]. However, the impacts of changing aerosol loading on cloud and precipitation based on ACI varies among the different cloud types, especially those that are strongly driven by atmospheric dynamics and thermodynamics processes, yielding further complexity [85, 101-103].

Hence, in cloud evolving study, aerosols impact on deep convective clouds requires more understanding. Besides, more insights are needed into aerosols microphysical, dynamic, and thermodynamics influence on the transition from shallow to deep clouds [85, 104]. Although some studies have suggested that aerosol suppresses warm rain and consequently increases cloud buildup through the lifting of more cloud water to a freezing height where more latent heat is released, therefore invigorating convection [105-107]. However, several modelling studies have hinted a convection suppression is more likely for such convective thermodynamic invigoration than increasing cloud buildup, especially for clouds with considerable wind shear or dry conditions or cold base [59, 102, 108]. Yet some observational studies report that cloud fraction (CF) and top height (CTH) often increase due to increasing aerosol loading [109, 110]. Other investigations found the rising CCN concentration accompanied by a drop in shallow cumulus cloud and increasing deep convection due to notable evaporation-entrainment feedback [111-113]. One obvious observation from the various studies is the complex nature of the mechanisms and processes that lead to conflicting results [85, 103, 114, 115] focused upon in chapter 3 of this work.

Apart from the complex nature of several mechanisms and processes concerning ACI, poor measurements and parameterisation of aerosol and cloud properties constitutes another crucial factor that affects our ability to disentangle ACI processes effectively [12]. In-situ and ground observation of aerosol and cloud properties offer reduced uncertainties but limited spatio-temporal coverage [116-118]. Meanwhile, satellite observations promise better coverage but are prone to more significant uncertainties [12, 36]. Numerous studies have

attempted to validate satellite data against ground and in-situ observation to enhance satellite retrieval of aerosol and cloud properties on a regional and global scale, thereby improving the efficiency of models and general studies on ACPI [98, 119-121]. However, most studies found that the uncertainties due to satellite observation vary with the properties of interest, terrain, surface type (e.g., land or water), level of atmospheric contamination, and instrument calibration [72, 98, 119]. Therefore, more validation exercises are needed mainly on a regional scale to amplify the progress in the betterment and reliability of satellite measurements, upon which chapter 4 of this work focus. In general, intensified research by carefully diagnosing the several obstacles (under diverse scenarios) identified to hinder the complete understanding of climate dynamics from the perspective of ACPI becomes a necessity for meaningful advancements in climate projection and potential impacts on the environment.

## References

- [1] J.P. Putaud, European aerosol phenomenology-3: Physical and chemical characteristics of particulate matter from 60 rural, urban, and kerbside sites across Europe, *Atmospheric Environment* 44 (2010) 13.
- [2] O. Boucher, *Atmospheric aerosols: Properties and climate impacts*, 1 (Ed.), Springer, Netherlands, 2015.
- [3] A. Smirnov, B.N. Holben, O. Dubovik, R. Frouin, T.F. Eck, I. Slutsker, Maritime component in aerosol optical models derived from Aerosol Robotic Network data, *J Geophys Res-Atmos* 108 (2003).
- [4] UIUC, *Atmospheric aerosol*, in: P. Sharply (Ed.), University of Illinois, Illinois, USA, 2011.
- [5] U. Pöschl, *Atmospheric aerosols: Composition, transformation, climate and health effects.*, *Angewandte Chemie International Edition* 44 (2005) 7520-7540.
- [6] O. Boucher, D. Randall, P. Artaxo, C. Bretherton, G. Feingold, P. Forster, V.-M. Kerminen, Y. Kondo, H. Liao, U. Lohmann, P. Rasch, S.K. Satheesh, S. Sherwood, B. Stevens, X.Y. Zhang, *Clouds and Aerosols*, in: T.F. Stocker, D. Qin, G.-K. Plattner, M. Tignor, S.K. Allen, J. Boschung, A. Nauels, Y. Xia, V. Bex, P.M. Midgley (Eds.), *Climate*

Change 2013: The Physical Science Basis. Contribution of Working Group I to the Fifth Assessment Report of the Intergovernmental Panel on Climate Change, Cambridge University Press, Cambridge, United Kingdom and New York, NY, USA, 2013, pp. 571–658.

[7] A.A. Lushnikov, Introduction to aerosols, in: I. Agranovski (Ed.), *Aerosol-Science and Technology*, Wiley-VCH Verlag GmbH & Co., Weinheim, 2010, pp. 41.

[8] B. Ervens, B.J. Turpin, R.J. Weber, Secondary organic aerosol formation in cloud droplets and aqueous particles (aqSOA): A review of laboratory, field and model studies, *Atmospheric Chemistry and Physics*, 11 (2011) 11069-11102.

[9] G. Myhre, C.E.L. Myhre, B.H. Samset, T. Storelvmo, Aerosols and their relation to global climate and climate sensitivity, *Nature Education Knowledge* 4 (2013).

[10] C. Tomasi, A. Lupi, Atmospheric Aerosols, in: C. Tomasi, S. Fuzzi, A. Kokhanovsky (Eds.), *Life Cycles and Effects on Air Quality and Climate.*, John Wiley & Sons, New York, 2016.

[11] A.T. Yakubu, N. Chetty, Optical properties of atmospheric aerosol over Cape Town, Western Cape of South Africa: Role of biomass burning, *Atmósfera* 34 (2020) 395–416.

[12] IPCC, *Climate Change 2013: The Physical Science Basis. Contribution of Working Group I to the Fifth Assessment Report of the Intergovernmental Panel on Climate Change*, Cambridge University Press, Cambridge, United Kingdom and New York, NY, USA, 2013.

[13] IPCC, Anthropogenic and Natural Radiative Forcing, in: T.F. Stocker, D. Qin, G.-K. Plattner, M. Tignor, S.K. Allen, J. Boschung, A. Nauels, Y. Xia, V. Bex, P.M. Midgley (Eds.), *Climate Change 2013 - The Physical Science Basis*, Cambridge University Press, Cambridge, United Kingdom and New York, NY, USA, 2014, pp. 659-740.

[14] Ø. Hodnebrog, G. Myhre, P.M. Forster, J. Sillmann, B.H. Samset, Local biomass burning is a dominant cause of the observed precipitation reduction in southern Africa, *Nature Communications* 7 (2016) 11236.

[15] G.D. Thornhill, Ryder, C. L., Highwood, E. J., Shaffrey, L. C., Johnson, B. T., The effect of South American biomass burning aerosol emissions on the regional climate, *Atmos Chem Phys* 18 (2018) 5321–5342.

- [16] K.T. Whitby, The physical characteristics of sulfur aerosols, *Atmospheric Environment* (1967) 12 (1978) 135-159.
- [17] J. Heintzenberg, Properties of the log-normal particle size distribution, *Aerosol Science and Technology* (1994) 3.
- [18] K. Willeke, K.T. Whitby, Atmospheric aerosols: Size distribution interpretation., *Journal of the Air Pollution Control Association* 25 (1975) 529-534.
- [19] M. Kulmala, H. Vehkamäki, T. Petaja, M. Dal Maso, A. Lauri, V.M. Kerminen, W. Birmili, P.H. McMurry, Formation and growth rates of ultrafine atmospheric particles: A review of observations, *Journal of Aerosol Science* 35 (2004) 143-176.
- [20] J. Douwes, P. Thorne, N. Pearce, D. Heederik, Bioaerosol health effects and exposure assessment: progress and prospects., *Annals of Occupational Hygiene* 47 (2003) 187-200.
- [21] J.P. Putaud, F. Raes, R. Van Dingenen, E. Brüggemann, M.C. Facchini, S. Decesari, S. Fuzzi, R. Gehrig, C. Hüglin, P. Laj, G. Lorbeer, W. Maenhaut, N. Mihalopoulos, K. Müller, X. Querol, S. Rodriguez, J. Schneider, G. Spindler, H. Ten Brink, K. Tørseth, A. Wiedensohler, European aerosol phenomenology-2: chemical characteristics of particulate matter at kerbside, urban, rural and background sites in Europe., *Atmos. Environ.* 38 (2004) 2579–2595.
- [22] D. Wang, B. Jiang, F. Li, W. Lin, Investigation of the air pollution event in Beijing-Tianjin-Hebei region in December 2016 using WRF-Chem, *Advances in Meteorology* 2018 (2018) 1-12.
- [23] O.A. Falaiye, A.T. Yakubu, F.O. Aweda, O.J. Abimbola, Mineralogical characteristics of harmattan dust in Ilorin, Sub-Saharan Africa, *Ife Journal of Science* 15 (2013) 175-181.
- [24] C.L. Ryder, E.J. Highwood, P.D. Rosenberg, J. Trembath, J.K. Brooks, M. Bart, A. Dean, J. Crosier, J. Drorsey, H. Brindley, J. Banks, J.H. Marsham, J.B. McQuaid, H. Sodemann, R. Washington, Optical properties of Saharan dust aerosol and contribution from the coarse mode as measured during the Fennec 2011 aircraft campaign, *Atmos. Chem. Phys.* 13 (2013) 303-325.

- [25] D. Tanré, Y.J. Kaufman, B.N. Holben, B. Chatenet, A. Karnieli, F. Lavenu, L. Blarel, O. Dubovik, L.A. Remer, A. Smirnov, Climatology of dust aerosol size distribution and optical properties derived from remotely sensed data in the solar spectrum, *Journal of Geophysical Research: Atmospheres* 106 (2001) 18205-18217.
- [26] G. de Leeuw, E.L. Andreas, M.D. Anguelova, C.W. Fairall, E.R. Lewis, C. O'Dowd, M. Schulz, S.E. Schwartz, Production flux of sea spray aerosol, *Rev Geophys* 49 (2011).
- [27] J.A. Oregon, R.J. Charlson, Implications for models and measurements of chemical inhomogeneities among cloud droplets, *Tellus* 44B (1992) 489-502.
- [28] A. Massling, S. Leinert, A. Wiedensohler, D. Covert, Hygroscopic growth of sub-micrometer and one-micrometer aerosol particles measured during ACE-Asia, *Atmos. Chem. Phys* 7 (2007) 3249-3259.
- [29] M.C. Jacobson, -C. Hansson H, K.J. Noone, R.J. Charlson, Organic atmospheric aerosols: review and state of the science., *Rev. Geophys.* 38 (2000) 267-294.
- [30] H. Ni, R.J. Huang, J. Cao, J. Guo, H. Deng, U. Dusek, Sources and formation of carbonaceous aerosols in Xi'an, China: primary emissions and secondary formation constrained by radiocarbon., *Atmos. Chem. Phys* 19 (2019) 15609-15628.
- [31] R.J. Charlson, S.E. Schwartz, J.M. Hales, R.D. Cess, R.D. Coakley, J.E. Hansen, D.J. Hofmann, Climate forcing by anthropogenic aerosols, *Science* 255 (1992) 423-430.
- [32] M. Kulmala, A. Asmi, H.K. Lappalainen, K.S. Carslaw, U. Poschl, U. Baltensperger, Ø. Hov, J.L. Brenquier, S.N. Pandis, M.C. Facchini, H.C. Hansson, A. Wiedensohler, C.D. O'Dowd, Introduction: European Integrated Project on Aerosol Cloud Climate and Air Quality Interactions (EUCAARI)-integrating aerosol research from nano to global scales, *Atmos Chem Phys* 9 (2009) 2825-2841.
- [33] M.T. Freiman, S.J. Piketh, Air transport into and out of the industrial Highveld region of South Africa, *Journal of Applied Meteorology* 42 (2003) 994-1002.
- [34] A.P. Sati, M. Mohan, Analysis of air pollution during a severe smog episode of November 2012 and the Diwali Festival over Delhi, India, *International Journal of Remote Sensing* 35 (2014) 6940-6954.

- [35] O. Boucher, C. Moulin, S. Belviso, O. Aumont, L. Bopp, E. Cosme, R. Von Kuhlmann, M.G. Lawrence, M. Pham, M.S. Reddy, J. Sciare, C. Venkataraman, DMS atmospheric concentrations and sulphate aerosol indirect radiative forcing: a sensitivity study to the DMS source representation and oxidation., *Atmos Chem Phys* 3 (2003) 49-65.
- [36] IPCC, The Physical Science Basis. Contribution of Working Group I to the Fourth Assessment Report of the Intergovernmental Panel on Climate Change Cambridge University Press, Cambridge, 2007.
- [37] P.B. Russell, J. Heintzenberg, An overview of the ACE-2 clear sky column closure experiment (CLEARCOLUMN). *Tellus B* 52 (2000) 463-483.
- [38] V. Ramanathan, P.J. Crutzen, J.T. Kiehl, D. Rosenfeld, Aerosols, climate, and the hydrological cycle, *Science* 294 (2001) 2119-2124.
- [39] A.F. Bouwman, D.S. Lee, W.A.H. Asman, F.J. Dentener, K.W.V.D. Hoek, J. Olivier, A global high-resolution emission inventory for ammonia, *Global Biogeochemical Cycles* 11 (1997) 561-587.
- [40] S.E. Bauer, D. Koch, N. Unger, D.T. Metzger, D.T. Shindell, D.G. Streets, Nitrate aerosols today and in 2030: A global simulation including aerosols and tropospheric ozone., *Atmos. Chem. Phys* 7 (2007) 5043-5059.
- [41] W.C. Malm, B.A. Schichtel, M.L. Pitchford, L.L. Ashbaugh, R.A. Eldred, Spatial and monthly trends in speciated fine particle concentration in the United States, *Journal of Geophysical Research: Atmospheres* 109 (2004).
- [42] M.Z. Jacobson, Global direct radiative forcing due to multicomponent anthropogenic and natural aerosols, *Journal of Geophysical Research: Atmospheres* 106 (2001) 1551-1568.
- [43] P.J. Adams, J.H. Seinfeld, D. Koch, L. Mickley, D. Jacob, General circulation model assessment of direct radiative forcing by the sulfate-nitrate-ammonium-water inorganic aerosol system., *Journal of Geophysical Research* 106 (2001) 1097-1112.
- [44] S.T. Martin, H.M. Hung, R.J. Park, D.J. Jacob, R.J.D. Spurr, K.V. Chance, M. Chin, Effects of the physical state of tropospheric ammonium-sulfate-nitrate particles on global aerosol direct radiative forcing., *Atmos. Chem. Phys.* 4 (2004) 183-214.

- [45] H. Liao, J.H. Seinfeld, Global impacts of gas-phase chemistry/aerosol interactions on direct radiative forcing by anthropogenic aerosols and ozone., *J. Geophys. Res.* 110 (2005).
- [46] C.A. Pope, R.T. Burnett, M.J. Thun, E.E. Calle, D. Krewski, K. Ito, G.D. Thurston, Lung Cancer, Cardiopulmonary Mortality, and Long-term Exposure to Fine Particulate Air Pollution, *JAMA* 287 (2002) 1132-1141.
- [47] U. Lohmann, J. Feichter, Global indirect aerosol effects: a review, *Atmos Chem Phys* 5 (2005) 715-737.
- [48] J. Peccia, M. Hernandez, Incorporating polymerase chain reaction-based identification, population characterization, and quantification of microorganisms into aerosol science. a review., *Atmos. Environ.* 40 (2006) 3941-3961.
- [49] S. Muthers, F. Arfeuille, C.C. Raible, E. Rozanov, The impacts of volcanic aerosol on stratospheric ozone and the Northern Hemisphere polar vortex: separating radiative-dynamical changes from direct effects due to enhanced aerosol heterogeneous chemistry, *Atmos Chem Phys* 15 (2015) 11461-11476.
- [50] S. Andersson, B. Martinsson, J. Vernier, Significant radiative impact of volcanic aerosol in the lowermost stratosphere., *Nature Communications* 6 (2015) 7692
- [51] J. Hansen, M. Sato, R. Ruedy, Radiative forcing and climate response, *Journal of Geophysical Research: Atmospheres* 102 (1997) 6831-6864.
- [52] J. Haywood, O. Boucher, Estimates of the direct and indirect radiative forcing due to tropospheric aerosols: A review, *Rev Geophys* 38 (2000) 513-543.
- [53] S. Twomey, Influence of Pollution on Shortwave Albedo of Clouds, *Journal of the Atmospheric Sciences* 34 (1977) 1149-1152.
- [54] B.A. Albrecht, Aerosols, Cloud Microphysics, and Fractional Cloudiness, *Science* 245 (1989) 1227-1230.
- [55] A.S. Ackerman, O.B. Toon, D.E. Stevens, A.J. Heymsfield, V. Ramanathan, E.J. Welton, Reduction of Tropical Cloudiness by Soot, *Science* 288 (2000) 1042-1047.

- [56] R. Boiyo, K.R. Kumar, T. Zhao, J. Guo, A 10-Year Record of Aerosol Optical Properties and Radiative Forcing Over Three Environmentally Distinct AERONET Sites in Kenya, East Africa, *Journal of Geophysical Research: Atmospheres* 124 (2019) 1596-1617.
- [57] T.N. Carlson, J.M. Prospero, The largescale movement of Sahara air outbreak over the Northern Equatorial Atlantic., *Journal of Applied Meteorology* II (1972) 283-297.
- [58] Y.C. Chen, L. Xue, Z.J. Lebo, H. Wang, R.M. Rasmussen, J.H. Seinfeld, A comprehensive numerical study of aerosol-cloud-precipitation interactions in marine stratocumulus, *Atmos Chem Phys* 11 (2011) 9749-9769.
- [59] J.W. Fan, L.R. Leung, Z.Q. Li, H. Morrison, H.B. Chen, Y.Q. Zhou, Y. Qian, Y. Wang, Aerosol impacts on clouds and precipitation in eastern China: Results from bin and bulk microphysics, *J Geophys Res-Atmos* 117 (2012).
- [60] I. Koren, G. Dagan, O. Altaratz, From aerosol-limited to invigoration of warm convective clouds, *Science* 344 (2014) 1143-1146.
- [61] M.W. Christensen, G.L. Stephens, Microphysical and macrophysical responses of marine stratocumulus polluted by underlying ships: 2. Impacts of haze on precipitating clouds, *J Geophys Res-Atmos* 117 (2012).
- [62] Y.-C. Chen, M.W. Christensen, D.J. Diner, M.J. Garay, Aerosol-cloud interactions in ship tracks using Terra MODIS/MISR, *Journal of Geophysical Research: Atmospheres* 120 (2015) 2819-2833.
- [63] R.G. Barry, R.J. Chorley, *Atmosphere, weather and climate*, 8 ed., Routledge, London, 2003.
- [64] M.L. Salby, *Fundamentals of Atmospheric Physics*, Academic Press, San Diego, 1996.
- [65] S.J. Piketh, R.J. Swap, W. Maenhaut, H.J. Annegam, P. Formenti, Chemical evidence of long-range atmospheric transport over southern Africa, *J Geophys Res-Atmos* 107 (2002).
- [66] T.J. O'hern, D.J. Rader, Practical application of in-situ aerosol measurement. , Halon Alternatives Technical Working Conference Albuquerque, Mexico, 1993, pp. 275-289.

- [67] P.H. McMurry, A review of atmospheric aerosol measurements., *Atmospheric Environment* 34 (2000) 1959-1999.
- [68] J.B. Burkholder, J.P.D. Abbatt, I. Barnes, J.M. Roberts, M.L. Melamed, M. Ammann, A.K. Bertram, C.D. Cappa, A.G. Carlton, L.J. Carpenter, J.N. Crowley, Y. Dubowski, C. Geoge, C.E. Heard, H. Herrmann, F.N. Keutsch, J. Kroll, V.F. McNeill, N.L. Ng, S.A. Nizkorodov, J.J. Orlando, C.J. Percival, B. Picquet-Varrault, Y. Rudich, P.W. Seakins, J.D. Surratt, H. Tanimoto, J.A. Thornton, Z. Tong, G.S. Tyndall, A. Wahner, C.J. Weschler, K.R. Wilson, P.J. Ziemann, The essential role for laboratory studies in atmospheric chemistry, *Environmental Science Technology* 51 (2017) 2519-2528.
- [69] K. Tempfli, N. Kerle, G.C. Huurneman, L.L.F. Janssen, *Principles of remote sensing*, The International Institute for Geo-Information Science and Earth Observation (ITC), Enschede, The Netherlands, 2009.
- [70] P. Kulkarni, P.A. Baron, *An Approach To Performing Aerosol Measurements.*, In: P. Kulkarni, P.A. Baron, K. Willeke (Eds.), *Aerosol Measurement: Principles, Techniques, and Applications.*, John Wiley & Sons, Hoboken, New Jersey, 2011.
- [71] M. Tesfaye, V. Sivakumar, J. Botai, G. Mengistu Tsidu, Aerosol climatology over South Africa based on 10 years of Multiangle Imaging Spectroradiometer (MISR) data, *Journal of Geophysical Research: Atmospheres* 116 (2011).
- [72] D. Rosenfeld, M.O. Andreae, A. Asmi, M. Chin, G. de Leeuw, D.P. Donovan, R. Kahn, S. Kinne, N. Kivekäs, M. Kulmala, W. Lau, K.S. Schmidt, T. Suni, T. Wagner, M. Wild, J. Quaas, Global observations of aerosol-cloud-precipitation-climate interactions, *Rev Geophys* 52 (2014) 750-808.
- [73] J.P. Sherman, P. Gupta, R.C. Levy, P.J. Sherman, An Evaluation of MODIS-Retrieved Aerosol Optical Depth over a Mountainous AERONET Site in the Southeastern US, *Aerosol and Air Quality Research* 16 (2016) 3243-3255.
- [74] SUT, Swinburne University of Technology, Available: <https://astronomy.swin.edu.au/cosmos/e/Electromagnetic+Radiation> [Accessed November 2021]

- [75] P.P. Urone, R. Hinrichs, K. Dirks, M. Sharma, College physics, OpenStax, Houston, Texas, 2012.
- [76] E.C. Barrett, L.F. Curtis, Introduction to environmental remote sensing, Chapman & Hall, London, New York, 1992.
- [77] WIKIPEDIA, Wikimedia Foundation, Incorporation, Available: [https://en.wikipedia.org/wiki/Electromagnetic\\_radiation](https://en.wikipedia.org/wiki/Electromagnetic_radiation) [Accessed November 2021].
- [78] NASA, National Aeronautics and Space Administration, Available: <https://radiojove.gsfc.nasa.gov/education/activities/iono.html> [Accessed September 2021].
- [79] W.C. Hinds, Aerosol Technology, Properties, Behavior, and Measurement of Airborne Particles, 1 ed., John Wiley & Sons, Inc.1982.
- [80] SEOS, Science Education through Earth Observation for High Schools, Available: <https://seos-project.eu/marinepollution/marinepollution-c01-s02-p01.html> [Accessed September 2021].
- [81] L.V. Blake, A guide to basic pulse-radar maximum-range calculation, Naval Research Laboratory (NRL), Washington, D.C., 1969.
- [82] U. Wandinger, Introduction to lidar, in: C. Weitkamp (Ed.), Lidar: Range-resolved optical remote sensing of the atmosphere, Springer, New York, 2005.
- [83] M.A. Janssen, An introduction to the passive microwave remote sensing of atmospheres, in: M.A. Janssen (Ed.), Atmospheric remote sensing by microwave radiometry, John Wiley & Sons, New York, 1993.
- [84] R.R. Rogers, M.K. Yau, A short course in cloud physics, 3 ed., Butterworth-Heinemann, UK, 1996.
- [85] J. Fan, Y. Wang, D. Rosenfeld, X. Liu, Review of Aerosol–Cloud Interactions: Mechanisms, Significance, and Challenges, Journal of the Atmospheric Sciences 73 (2016) 4221-4252.

- [86] Y. Liang, X.J. Sun, S.D. Miller, H.R. Li, Y.B. Zhou, R.W. Zhang, S.H. Li, Cloud base height estimation from ISCCP cloud-type classification applied to A-train data, *Advances in Meteorology* 2017 (2017) 14
- [87] WIKIPEDIA, Wikimedia Foundation, Incorporation, Available: [https://en.wikipedia.org/wiki/List\\_of\\_cloud\\_types](https://en.wikipedia.org/wiki/List_of_cloud_types) [Accessed November 2021].
- [88] I. Strangeways, *Precipitation: Theory, Measurement and Distribution*, Cambridge University Press, 2006.
- [89] S. Twomey, Pollution and the planetary albedo, *Atmospheric Environment* (1967) 8 (1974) 1251-1256.
- [90] D. Rosenfeld, TRMM observed first direct evidence of smoke from forest fires inhibiting rainfall, *Geophysical Research Letters* 26 (1999) 3105-3108.
- [91] Y.J. Kaufman, D. Tanré, O. Dubovik, A. Karnieli, L.A. Remer, Absorption of sunlight by dust as inferred from satellite and ground-based remote sensing, *Geophysical Research Letters* 28 (2001) 1479-1482.
- [92] A. McComiskey, S.E. Schwartz, B. Schmid, H. Guan, E.R. Lewis, P. Ricchiazzi, J.A. Ogren, Direct aerosol forcing: Calculation from observables and sensitivities to inputs, *J Geophys Res-Atmos* 113 (2008).
- [93] K.R. Kumar, N. Kang, V. Sivakumar, D. Griffith, Temporal characteristics of columnar aerosol optical properties and radiative forcing (2011–2015) measured at AERONET's Pretoria\_CSIR\_DPSS site in South Africa, *Atmospheric Environment* 165 (2017) 274-289.
- [94] J. Quaas, Y. Ming, S. Menon, T. Takemura, M. Wang, J.E. Penner, A. Gettelman, U. Lohmann, N. Bellouin, O. Boucher, A.M. Sayer, G.E. Thomas, A. McComiskey, G. Feingold, C. Hoose, J.E. Kristjánsson, X. Liu, Y. Balkanski, L.J. Donner, P.A. Ginoux, P. Stier, B. Grandey, J. Feichter, I. Sednev, S.E. Bauer, D. Koch, R.G. Grainger, Kirkev, and aring, A. g, T. Iversen, Ø. Seland, R. Easter, S.J. Ghan, P.J. Rasch, H. Morrison, J.F. Lamarque, M.J. Iacono, S. Kinne, M. Schulz, Aerosol indirect effects – general circulation model intercomparison and evaluation with satellite data, *Atmos Chem Phys* 9 (2009) 8697-8717.

- [95] T. Eidhammer, P.J. DeMott, A.J. Prenni, M.D. Petters, C.H. Twohy, D.C. Rogers, J. Stith, A. Heymsfield, Z. Wang, K.A. Pratt, K.A. Prather, S.M. Murphy, J.H. Seinfeld, R. Subramanian, S.M. Kreidenweis, Ice Initiation by Aerosol Particles: Measured and Predicted Ice Nuclei Concentrations versus Measured Ice Crystal Concentrations in an Orographic Wave Cloud, *Journal of the Atmospheric Sciences* 67 (2010) 2417-2436.
- [96] C. Genz, R. Schrödner, B. Heinold, S. Henning, H. Baars, G. Spindler, I. Tegen, Estimation of cloud condensation nuclei number concentrations and comparison to in situ and lidar observations during the HOPE experiments, *Atmos Chem Phys* 20 (2020) 8787-8806.
- [97] J. Quaas, A. Arola, B. Cairns, M. Christensen, H. Deneke, A.M.L. Ekman, G. Feingold, A. Fridlind, E. Gryspeerdt, O. Hasekamp, Z. Li, A. Lipponen, P.-L. Ma, J. Mülmenstädt, A. Nenes, J.E. Penner, D. Rosenfeld, R. Schrödner, K. Sinclair, O. Sourdeval, P. Stier, M. Tesche, B. van Dierenhoven, M. Wendisch, Constraining the Twomey effect from satellite observations: issues and perspectives, *Atmos Chem Phys* 20 (2020) 15079-15099.
- [98] J. Schmale, S. Henning, B. Henzing, H. Keskinen, K. Sellegri, J. Ovadnevaite, A. Bougiatioti, N. Kalivitis, I. Stavroulas, A. Jefferson, M. Park, P. Schlag, A. Kristensson, Y. Iwamoto, K. Pringle, C. Reddington, P. Aalto, M. Aijala, U. Baltensperger, J. Bialek, W. Birmili, N. Bukowiecki, M. Ehn, A.M. Fjaeraa, M. Fiebig, G. Frank, R. Frohlich, A. Frumau, M. Furuya, E. Hammer, L. Heikkinen, E. Herrmann, R. Holzinger, H. Hyono, M. Kanakidou, A. Kiendler-Scharr, K. Kinouchi, G. Kos, M. Kulmala, N. Mihalopoulos, G. Motos, A. Nenes, C. O'Dowd, M. Paramonov, T. Petaja, D. Picard, L. Poulain, A.S. Prevot, J. Slowik, A. Sonntag, E. Swietlicki, B. Svenningsson, H. Tsurumaru, A. Wiedensohler, C. Wittbom, J.A. Ogren, A. Matsuki, S.S. Yum, C.L. Myhre, K. Carslaw, F. Stratmann, M. Gysel, Collocated observations of cloud condensation nuclei, particle size distributions, and chemical composition, *Sci Data* 4 (2017) 170003.
- [99] W. Tan, G. Zhao, Y. Yu, C. Li, J. Li, L. Kang, T. Zhu, C. Zhao, Method to retrieve cloud condensation nuclei number concentrations using lidar measurements, *Atmospheric Measurement Techniques* 12 (2019) 3825-3839.
- [100] B. Zhao, Y. Wang, Y. Gu, K.N. Liou, J.H. Jiang, J. Fan, X. Liu, L. Huang, Y.L. Yung, Ice nucleation by aerosols from anthropogenic pollution, *Nat Geosci* 12 (2019) 602-607.

- [101] G.H. Li, Y. Wang, R.Y. Zhang, Implementation of a two-moment bulk microphysics scheme to the WRF model to investigate aerosol-cloud interaction, *J Geophys Res-Atmos* 113 (2008).
- [102] Z.J. Lebo, H. Morrison, J.H. Seinfeld, Are simulated aerosol-induced effects on deep convective clouds strongly dependent on saturation adjustment?, *Atmos Chem Phys* 12 (2012) 9941-9964.
- [103] C. Barthlott, C. Hoose, Aerosol effects on clouds and precipitation over central Europe in different weather regimes, *J. Atmos. Sci.* 75 (2018) 4247–4264.
- [104] G.S. Fanourgakis, M. Kanakidou, A. Nenes, S.E. Bauer, T. Bergman, K.S. Carslaw, A. Grini, D.S. Hamilton, J.S. Johnson, V.A. Karydis, A. Kirkevag, J.K. Kodros, U. Lohmann, G. Luo, R. Makkonen, H. Matsui, D. Neubauer, J.R. Pierce, J. Schmale, P. Stier, K. Tsigaridis, T. van Noije, H. Wang, D. Watson-Parris, D.M. Westervelt, Y. Yang, M. Yoshioka, N. Daskalakis, S. Decesari, M. Gysel-Beer, N. Kalivitis, X. Liu, N.M. Mahowald, S. Myriokefalitakis, R. Schrodner, M. Sfakianaki, A.P. Tsimpidi, M. Wu, F. Yu, Evaluation of global simulations of aerosol particle and cloud condensation nuclei number, with implications for cloud droplet formation, *Atmos Chem Phys* 19 (2019) 8591-8617.
- [105] J.C. Lin, T. Matsui, R.A. Pielke, C. Kummerow, Effects of biomass-burning-derived aerosols on precipitation and clouds in the Amazon Basin: a satellite-based empirical study, *J Geophys Res-Atmos* 111 (2006).
- [106] S.C. van den Heever, G.G. Carrió, W.R. Cotton, P.J. DeMott, A.J. Prenni, Impacts of Nucleating Aerosol on Florida Storms. Part I: Mesoscale Simulations, *Journal of the Atmospheric Sciences* 63 (2006) 1752-1775.
- [107] D. Rosenfeld, U. Lohmann, G.B. Raga, C.D. O'Dowd, M. Kulmala, S. Fuzzi, A. Reissell, M.O. Andreae, Flood or drought: how do aerosols affect precipitation?, *Science* 321 (2008) 1309-1313.
- [108] Z.J. Lebo, J.H. Seinfeld, Theoretical basis for convective invigoration due to increased aerosol concentration, *Atmos Chem Phys* 11 (2011) 5407-5429.
- [109] Z. Li, F. Niu, J. Fan, Y. Liu, D. Rosenfeld, Y. Ding, Long-term impacts of aerosols on the vertical development of clouds and precipitation, *Nature Geoscience* 4 (2011) 888-894.

- [110] F. Niu, Z. Li, Systematic variations of cloud top temperature and precipitation rate with aerosols over the global tropics, *Atmos Chem Phys* 12 (2012) 8491-8498.
- [111] Z.J. Lebo, The sensitivity of a numerically simulated idealized squall line to the vertical distribution of aerosols, *J. Atmos. Sci.* 71 (2014) 4581–4596.
- [112] S.M. Saleeby, S.R. Herbener, S.C. van den Heever, T. L’Ecuyer, Impacts of Cloud Droplet–Nucleating Aerosols on Shallow Tropical Convection, *Journal of the Atmospheric Sciences* 72 (2015) 1369-1385.
- [113] P.J. Marinescu, S.C. van den Heever, S.M. Saleeby, S.M. Kreidenweis, P.J. DeMott, The Microphysical Roles of Lower-Tropospheric versus Midtropospheric Aerosol Particles in Mature-Stage MCS Precipitation, *Journal of the Atmospheric Sciences* 74 (2017) 3657-3678.
- [114] J.W. Fan, T.L. Yuan, J.M. Comstock, S. Ghan, A. Khain, L.R. Leung, Z.Q. Li, V.J. Martins, M. Ovchinnikov, Dominant role by vertical wind shear in regulating aerosol effects on deep convective clouds, *J Geophys Res-Atmos* 114 (2009).
- [115] P.J. Marinescu, S.C. van den Heever, M. Heikenfeld, A.I. Barrett, C. Barthlott, C. Hoose, J. Fan, A.M. Fridlind, T. Matsui, A.K. Miltenberger, P. Stier, B. Vie, B.A. White, Y. Zhang, Impacts of Varying Concentrations of Cloud Condensation Nuclei on Deep Convective Cloud Updrafts—A Multimodel Assessment, *Journal of the Atmospheric Sciences* 78 (2021) 1147-1172.
- [116] W.A. Abdou, D.J. Diner, J.V. Martonchik, C.J. Bruegge, R.A. Kahn, B.J. Gaitley, K.A. Crean, L.A. Remer, B. Holben, Comparison of coincident Multiangle Imaging Spectroradiometer and Moderate Resolution Imaging Spectroradiometer aerosol optical depths over land and ocean scenes containing Aerosol Robotic Network sites, *Journal of Geophysical Research* 110 (2005).
- [117] E. Gryspeerd, P. Stier, D.G. Partridge, Satellite observations of cloud regime development: the role of aerosol processes, *Atmos Chem Phys* 14 (2014) 1141-1158.
- [118] R.A. Kahn, B.J. Gaitley, M.J. Garay, D.J. Diner, T.F. Eck, A. Smirnov, B.N. Holben, Multiangle Imaging SpectroRadiometer global aerosol product assessment by comparison with the Aerosol Robotic Network, *Journal of Geophysical Research* 115 (2010).

[119] Y.J. Kaufman, D. Tanré, H.R. Gordon, T. Nakajima, J. Lenoble, R. Frouin, H. Grassl, B.M. Herman, M.D. King, P.M. Teillet, Passive remote sensing of tropospheric aerosol and atmospheric correction for the aerosol effect, *Journal of Geophysical Research: Atmospheres* 102 (1997) 16815-16830.

[120] S.-W. Kim, S.-C. Yoon, J. Kim, S.-Y. Kim, Seasonal and monthly variations of columnar aerosol optical properties over east Asia determined from multi-year MODIS, LIDAR, and AERONET Sun/sky radiometer measurements, *Atmospheric Environment* 41 (2007) 1634-1651.

[121] S.M. Loría-Salazar, H.A. Holmes, W. Patrick Arnott, J.C. Barnard, H. Moosmüller, Evaluation of MODIS columnar aerosol retrievals using AERONET in semi-arid Nevada and California, U.S.A., during the summer of 2012, *Atmospheric Environment* 144 (2016) 345-360.

## Chapter 3 –

# **A decadal assessment of the climatology of aerosol and cloud properties over South Africa**

Abdulaziz Tunde Yakubu<sup>1</sup> and Naven Chetty<sup>1,\*</sup>

<sup>1</sup>School of Chemistry and Physics, University of KwaZulu-Natal, Pietermaritzburg 3209, South Africa.

\*Correspondence: chettyn3@ukzn.ac.za; Tel.: +27-33-260-5660

### **3.1 Abstract**

Aerosol-cloud interaction (ACI) plays an essential role in understanding precipitation occurrence and climate change but remains poorly understood. Conducting a climatology study on a regional or global scale constitutes a prospect of better understanding ACI and its influence on precipitation and climate. This study analysed the characteristics of ACI over South Africa based on two instruments Moderate Resolution Imaging Spectroradiometer (MODIS) and Multiangle Imaging Spectroradiometer (MISR) onboard Terra satellite, and ground-based meteorology data from South Africa Weather Service (SAWS) between 2007-2016. The region mainly splits into the upper, central, and lower sub-regions based on aerosol loading characteristics. Findings from the study show that depending on the atmospheric conditions, aerosol exhibits dual features of increasing and decreasing the potential formation of precipitating clouds. However, more often, fine-mode predominated aerosols suppress rain-bearing clouds. Furthermore, cloud top height (CTH) demonstrates an upward increment from the lower to the upper part of the region, and the cloud fraction (CF) is in the downward direction. Both the CF and CTH display the characteristic enhancers of the precipitation intensity, mainly when the initial conditions necessary for rain-bearing occurs. Besides, cloud optical depth (COD) depends significantly on the liquid water path (LWP) and is suggestively associated with the aerosol-vapour ratio ingested into the cloud. Also notably, the temperature over the entire region generally increased steadily and continuously from 2013.

### **3.2 Introduction**

The interaction between the atmospheric aerosol and cloud forms a vital driving force influencing climate change. Therefore, assessing aerosol and cloud formation over time is crucial to understanding climate variability on a regional and global scale [1]. Aerosols interact with solar radiation directly through scattering and absorption and indirectly with the cloud through cloud condensation nuclei (CCN) and ice nuclei (IN) formation to modify the earth's radiative budget [2, 3]. Through their interactions and solar radiation, aerosols and clouds influence changes in the hydrology cycle and climate pattern [4, 5]. Besides, they impact the reception and distribution of incoming solar radiation, thereby modifying the earth's energy budget [6]. Various studies (e.g., [7, 8]) attempt to quantify the effect of aerosol-cloud interaction on the earth's radiative forcing. However, the understanding remains challenging due to enormous associate uncertainty. To this end, understanding the

climatology of aerosol and cloud over a region is vital to evaluating their roles on the earth's energy budget.

According to [1], aerosol impact on climate mainly linked to their influence on radiative forcing through absorption and scattering of solar radiation represents the aerosol radiative interaction (ARI). Also, aerosols and clouds interaction that induces changes in the climate pattern by modifying the earth's energy budget and surface precipitation is the effective radiative forcing due to aerosol and cloud interaction (ERF<sub>aci</sub>). Thus, due to the complex and constant changes in aerosol and cloud properties within the shortest time, the net effect on radiative forcing remains ambiguous and wrapped by huge uncertainty [1]. Besides, the task of unwrapping the complex link between the impact of aerosols and meteorology on cloud evolution constitutes a significant challenge towards understanding aerosol-cloud-climate interaction [9, 10]. Since aerosols and clouds formation varies rapidly over a short time depending on the atmospheric emission sources, assessing the climatology over time can be highly useful for modelling and identifying potential impacts over time and future projection. Therefore, a comprehensive assessment of aerosol and cloud climatology over time is crucial to understanding how climate change from small to significant scale impacts. The fundamental idea of the whole concept is to incorporate observation over a given long range of time to improve climate models on the impacts of aerosol-cloud interaction on climate change to enhance future variation prediction.

Regional climate system offers a real advantage in understanding climate change holistically because of the distinct spectral and temporal differences in aerosol and cloud properties [11, 12] usher by the variation of anthropogenic influences over different regions. Besides, knowledge of regional climate coupled with global average will enhance the quality of general climate models. Furthermore, regional climate study will better understand how different weather and climate respond to varying atmospheric phenomena. For instance, previous studies have identified a high population of fine mode particles results in reduced droplet size under a constant liquid water path [13] and precipitation suppression due to less coalescence [14]. Similarly, other studies found a large concentration of aerosol to invigorate cloud droplet concentration, increasing their vertical development and precipitation formation [15, 16]. Therefore, the impact of aerosol-climate interaction depends on multiple parameters that vary regionally due to distinct atmospheric and environmental conditions. For better

quantification of ACI impacts on a global scale, detailed regional evaluation becomes a necessity.

Although Africa mainly remains understudied in atmospheric and climate science, even though identified to be highly vulnerable to climate change impacts. Over South Africa, a reasonable number of previous works have examined aerosol properties and, to some extent, cloud mostly over parts of the region. Studies, however, show that a considerable amount of aerosol dominates the northern part of the region. In contrast, low aerosol loading dominates the middle and lower part of the country [12, 17]. Nonetheless, the main discussion of many studies has focused on sources and the transport characteristics of aerosols. At the same time, their influence on the formation and evolution of clouds remains less investigated. Furthermore, the feedback effect of cloud and precipitation on aerosol distribution, such as the effect of wet deposition on climatology, has not been quantified. Therefore, to significantly enhance our knowledge and improve climate models, the behavior of aerosols over sites within the source proximity, the cloud response, and resulting climatic perturbation, more studies are needed around aerosol-cloud climatology.

This work presents the effect of aerosol-cloud interaction on climate variability based on the climatology of aerosol and cloud over South Africa. This effort aimed towards improving our knowledge gap on the process of aerosol and cloud formation and feedback along with proximity, including the climate impacts. Although climatology study is not holistic to diagnose the challenge of climate change, it identifies the next level of research that will clarify things for better understanding. Besides, the result from such a study, once factored into the process of aerosol-cloud interaction, helps improve the general climate model. The study region is a suitable experimental environment to investigate aerosol-cloud interactions and how they influence the climate over proximity spatial domain. In this study, the region is divided into three parts based on differences in the aerosol loading as reported by previous study [17] and as shown in Figure 3.1. The area generally shares the same climate pattern as the southern hemisphere regions. It possesses two distinct sub-climates divided along the upper, central, and lower parts of the region, a feature unique for the natural exploration of the effects of aerosol and cloud properties changes in the same season. Perhaps, a specific site like this will be suitable to understand the impact of seasonal changes on how aerosols are being transported or removed and the adverse effect on the cloud properties.

Consequently, the climate system over South Africa follows the characterisation by summer (December – February), fall (March-May), Winter (June-August), and spring (September-November) such that two periods of rainfall exist split along the upper, central, and lowest parts of the region. Hence, a duo biomass burning tenure occurs over the area. The upper and central parts experience summer rainfall and biomass burning during spring in preparation for the farming season. In contrast, the lower part receives rain during the winter and incidence of biomass burning during mid-summer till early fall. The influence of aerosols from one location on another is critical to understanding climate variability over the region.

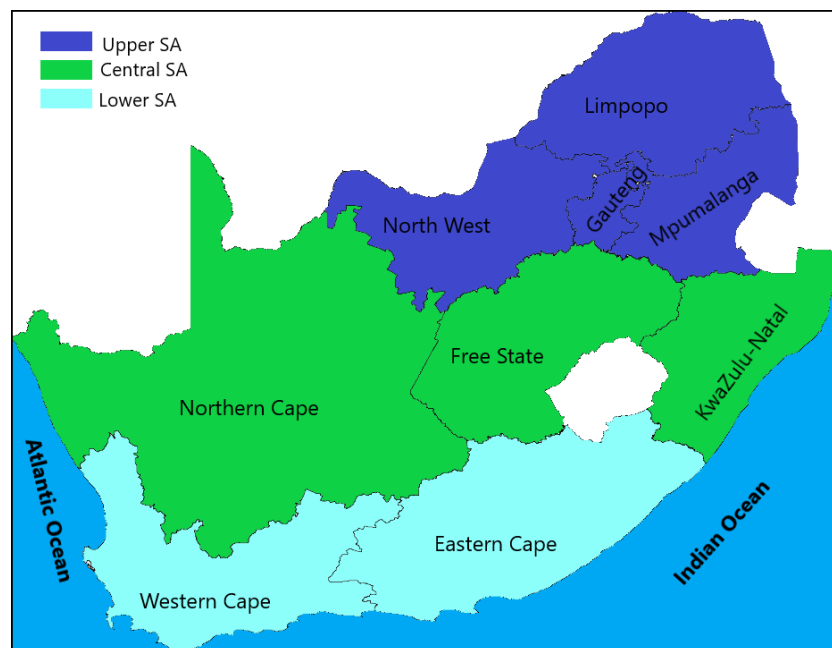


Figure 3.1 Map of South Africa divided into three sub-regions based on the distribution of aerosol loading.

### 3.3 Data and methods

The datasets presented in this study are based on measurements from the observations of two instruments on-board the Terra satellite, namely Multiangle Imaging Spectroradiometer (MISR) and Moderate Resolution Imaging Spectroradiometer (MODIS). In addition, data from the South Africa Weather Service (SAWS) was utilized to evaluate the meteorological impact over the region.

#### 3.3.1 MISR

The MISR instrument launched more than two decades ago is equipped with nine cameras pointed at the earth at nine distinct angles; one at nadir, then forward, and afterward

directions at 26.1°, 45.6°, 60.0° and 70.5° above the planet to monitor the climate trends. The instrument measures the solar radiation reflected by or the brightness of the earth with each of its nine cameras at four wavelengths to include blue (443nm), green (555nm), red (670nm), and infrared (865nm). MISR acquires spatial samples every 275m and for 7-minutes to cover a 360km swath view of the earth's surface at each camera [18]. Furthermore, following careful calibration, the instrument operates at optimal accuracy to provide high spatial resolution data. Consequently, MISR can retrieve several aerosols and clouds properties, including distinguishing different aerosols, clouds, and surfaces. In this work, level-3 monthly data at a resolution of 0.5° x 0.5° for aerosol optical depth (AOD), Ångström exponent (AE), and absorbing AOD ( $A_{abs}$ ).

### **3.3.2 MODIS**

MODIS (Terra) measures the radiances from the earth's surface to acquire data in 36 spectral bands from 0.4 to 14.4 $\mu$  to provide information on the state of atmosphere, land, and ocean. Of the 36 wavelengths, two bands image at a nominal resolution of 250m, five other bands at 500m, and the 29 remaining bands at 1km. The instrument achieves a 2330km viewing swath and reaching near-global coverage every 1 to 2 days. MODIS provides different scientific data products from monitoring global dynamics and processes spanning the atmosphere, land, and the ocean. Each data products are available to the science community at different processed levels. For this study, datasets from MODIS level-3 monthly aerosol and cloud product MOD08 were used to present additional results. Datasets including cloud optical thickness (COD), cloud fraction (CF), cloud top height (CTH), liquid water path (LWP), cloud effective radius (CER), and atmospheric water vapour content (AWV) at 1° x 1° horizontal resolution.

### **3.3.3 Meteorology data**

Data obtained from SAWS stations were utilized to examine the impacts of aerosol and cloud on the meteorological condition over the region. SAWS monitors and provides weather information services at several ground measurements stations across the nine provinces. The agency provides different ranges of data, from hourly to monthly data. The datasets used in this study include surface precipitation (PRECP), wind speed (WS), and ambient temperature (TEMP).

### **3.4 Results and discussion**

#### ***3.4.1 Climatology of aerosol properties***

Aerosol optical depth (AOD) still represents an important parameter in estimating the extent of aerosol loading over an area. Figure 3.2 shows the monthly averages for ten years (2007-2016) of MISR AOD measurement at 555nm over South Africa. The adoption of AOD and other aerosol properties data from MISR instrument against that of MODIS lies on the higher grid resolution ( $0.5^\circ \times 0.5^\circ$ ) of the former compared to the latter, which is coarser ( $1^\circ \times 1^\circ$ ). Besides, previous studies demonstrated that MISR retrieved aerosol properties are in better agreement with ground-based instruments such as Aerosol Robotic Network (AERONET) than MODIS [17, 19-21]. As earlier pointed, the season over South Africa is typically similar to what is obtainable over the Southern hemisphere region such that summer begins in December to February, fall from March to May, winter from June through August, and spring from September to November. However, the meteorology characteristics are divided into two such that the upper and central parts mainly experience hot wet summer and cold, dry winter. Contrarily, the lower parts experience warm, dry summer, and cold, wet winter, which influences the characteristics of aerosol emission over the different parts of the region. Also, the population and number of industrial activities in the upper part are more than the central, followed by the lower location.

Subsequently, from Figure 3.2, AOD shows seasonality for the entire region. Hence, an increase in July through September (mainly during the spring months) followed by a general decline from October through June (mainly in winter). The maximum aerosol loading (AOD > 0.25) occurred during the September months and was primarily associated with biomass burning in the upper part of the country and the surrounding bordering countries. Besides, aerosol emissions emerging from industrial and other human activities aggravate the aerosol particle suspension over the northern-most part of the region. Perhaps the dryness condition extending through the spring is instrumental in enhancing aerosol build-up, especially around Richard Bay (central east of the country), where a coal loading bay and other industrial emissions occur. Aerosol particles removal by wet deposit is absent at this period of the year, thereby allowing these particles to remain in the air for a more extended period. Furthermore, there are drifts of aerosol particles transported by air masses from the Northern to Southern part of the region. Most of these particles are fine mode aerosols such as aged smoke and

dust particles of coal debris emitted into the atmosphere in the upper area and undergoes different interaction and complex reactions along the transit path.

Meanwhile, the minimum AOD (typically  $< 0.05$ ) is observed in June months and is mainly linked with aerosol removal process (e.g., dry and wet deposition, cloud scavenging) and less biomass burning activities. This result is similar to the observation of [12] and [17] that high aerosol loading of mainly biomass burning and industrial smoke originating from Northern and border communities dominate aerosol loading over South Africa. Over the lower or southernmost part, biomass burning due to forest fire and industrial activity emissions also account for aerosol emission from November to March. However, due to the low turbidity, the effect is minimal compared to the central and upper parts. Furthermore, the region's central sub-region, especially around the west, contributes significantly to mineral dust (MD) suspension due to its arid nature. However, the impact is weaker compared to other forms of aerosols over the region. The weakness could be due to the coarse nature of MD aerosol and the susceptibility to dry deposition. Although the process of aerosol removal or exit has not received much attention over South Africa (SA), there is a need for such study to give a better insight into the mechanism of aerosol emission, residence, and removal over the region.

To complement the possible identification of biomass burning and general smoke emission observed from the AOD variation, Figure 3.3 illustrates the absorbing aerosol optical depth ( $A_{\text{abs}}$ ). Like the AOD, the  $A_{\text{abs}}$  demonstrates a seasonality pattern such that an increase is observed from July to September then decreases from October through June. The maximum  $A_{\text{abs}}$  ( $> 0.025$ ) occurs in September and the minimum ( $< 0.005$ ) during the January months. This variation indicates a concurrent increase in AOD and  $A_{\text{abs}}$  during the spring season, thus demonstrating a significant increase in absorbing aerosol emissions such as biomass burning, fossil fuel combustion smokes, and carbon-related fine mode particles. Also, two essential characteristics of the  $A_{\text{abs}}$  observation include revealing the period of high AOD associated with massive emission of absorbing aerosol particles and the area dominating in concentration level. High absorbing properties appear more at the upper parts, then towards the central and lowest at the southernmost sub-region. Interestingly, a more significant portion of the absorbing trait is around the eastern parts than the west. Hence, considering the timing and location of peak values, biomass burning activities during the pre-farming period around Limpopo and bordering countries such as Botswana, Mozambique, and Zimbabwe contribute significantly [12, 22, 23].

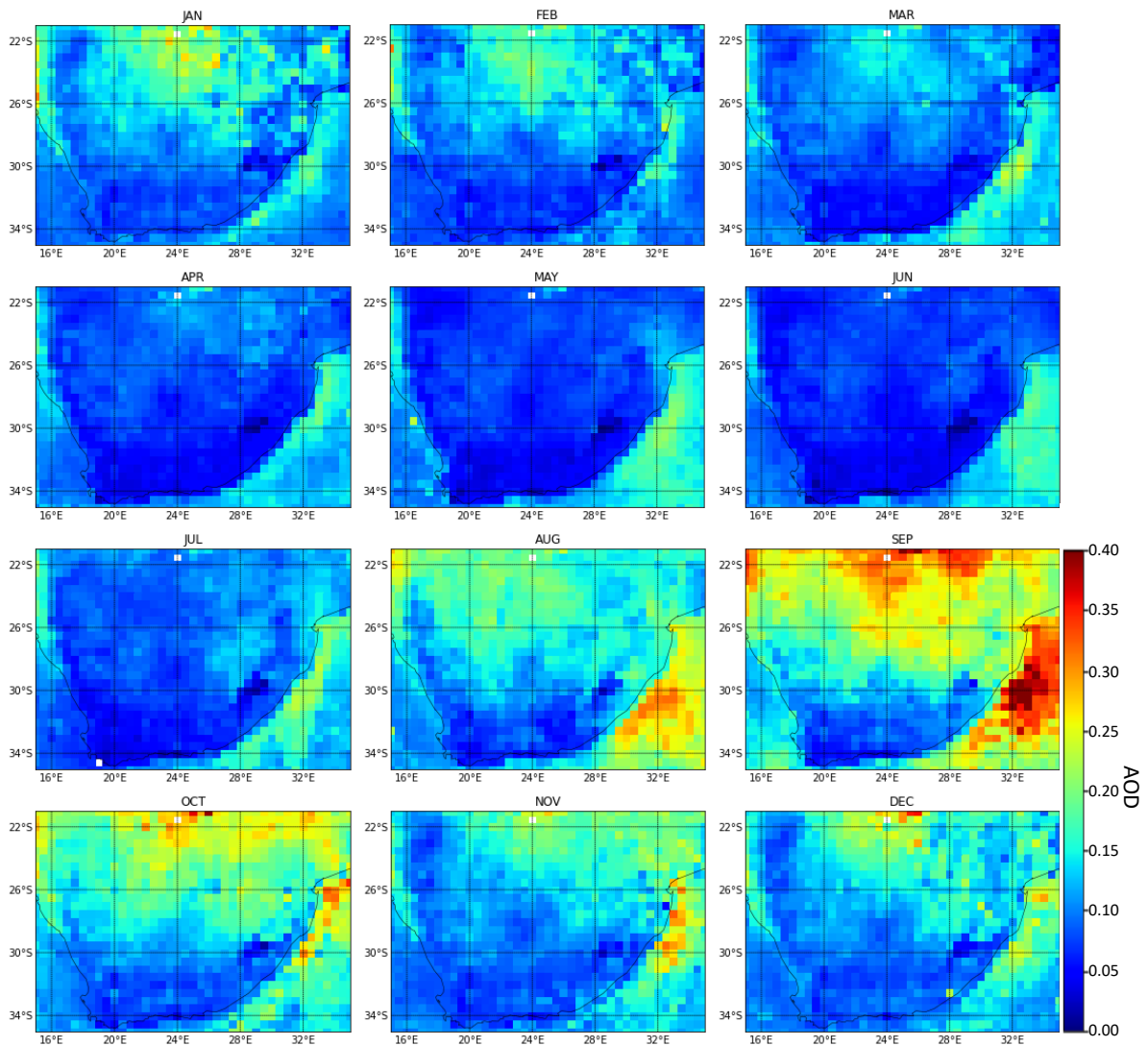


Figure 3.2 Average spatial distribution of aerosol optical depth (AOD) at  $\lambda = 555\text{nm}$  over South Africa from MISR data for 10 years.

The variation of Ångström exponent (AE) in Figure 3.4 shows the predominance of fine mode aerosol in most periods of the year. An increase in fine mode aerosols from January to September, followed by a decrease during October to December, is evident over the region. The maximum AE value ( $AE > 1.7$ ) is obtained chiefly during the August months, and the minimum ( $AE < 0.5$ ) occurred in December. This observation is consistent with the changes in AOD and  $A_{\text{abs}}$  in the previous figures. There are strong indications from both figures (Figures 3.2 and 3.3) that activities such as biomass burning, smoke emission from industries, and carbon-related dust samples are responsible for high aerosol loading over the area. Besides, the regime of high aerosol loading exhibit seasonality pivoted around the summer and usually diffuse from the upper through the centre then to the lower parts aided by the

motion of air masses. Nevertheless, the lower and a fraction of the central sub-region are more of coarse mode and less absorbing aerosol dominated areas. The characteristics of aerosol particles over this area earned their influence from proximity to the ocean, where sea salt aerosols are prevalent, and the arid region with a significant presence of MD, respectively. Furthermore, some element of high presence of fine mode particles is noticeable around the coasts. Perhaps, these cases may be prompted by the occasional inflow of aged smoke over the Atlantic Ocean from the Amazon Forest to the west coast (see [12, 24]) and the spread of aerosols to the Indian Ocean through the East coast.

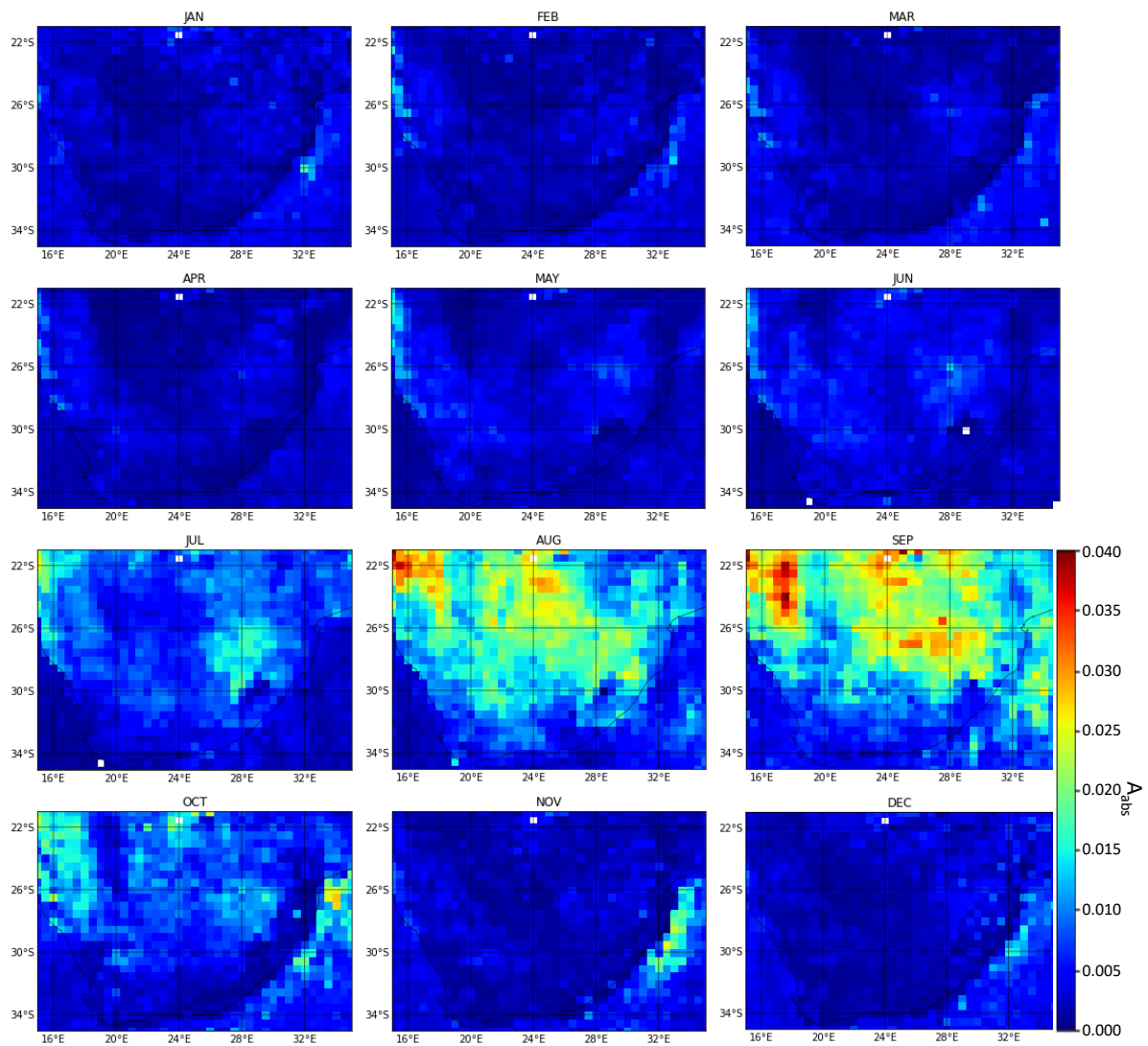


Figure 3.3 Average aerosol absorbing optical depth ( $A_{abs}$ ) over South Africa from MISR data for 10 years.

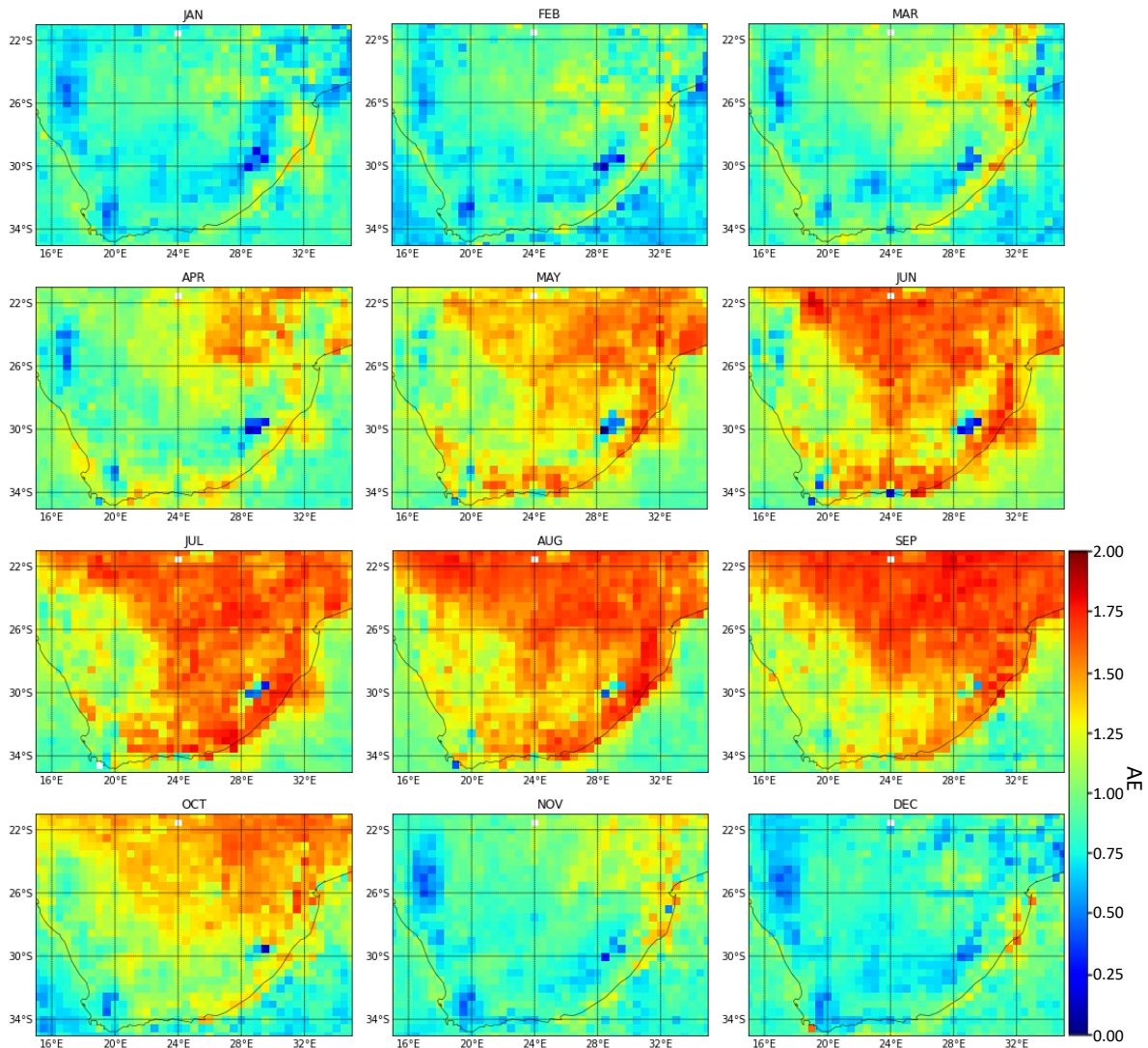


Figure 3.4 Average Ångström exponent (AE) over South Africa from MISR data for 10 years.

### 3.4.2 Climatology of the atmospheric vapour and cloud optical properties

In this section, all parameters are based on MODIS instrument measurement and characterised by a horizontal resolution of  $1^\circ \times 1^\circ$  as earlier explained. The variation of atmospheric water vapour (AWV) or precipitable water is as shown in Figure 3.5. The observation of high precipitable water during summer is evident and low towards winter for all parts of the region. The highest vapour value (AWV > 3.5cm) occurs during the January months and the lowest (AWV < 2.3cm) in August. The evidence of seasonality in the pattern of atmospheric vapour is apparent here. Generally, AWV decline from February to August then rises from September through January. One important thing worthy of observation is that high atmospheric vapour during the summer coincides with the precipitation season over the summer rainfall areas (mainly the upper and central parts of the region). Perhaps, there are chances of the high amount of vapour enhancing rainfall intensity over the region. Another

important observation from the AWW variation is that it declines from north to south similarly to AOD, except for the coastal environments where the vapour content is relatively higher than the lower inland areas. The high value of vapour in summer in contrast to other seasons is due to warmer air conditions since warm air expands more and possesses the capabilities to hold more water than cold air. A similar pattern is noticeable over the oceans around the region. AWW is higher over the Indian Ocean coast due to the warm air front from that direction than the lower value seen over the Atlantic Ocean, where cold wind emerges to the region. Earlier studies have demonstrated the seasonality of water vapour following the plunge to a minimum in June and rises to the maximum value in January [24]. Apart from the observation over this region, globally, AWW is found to increase in most areas during the summer, which is often associated with higher air temperature [25-27].

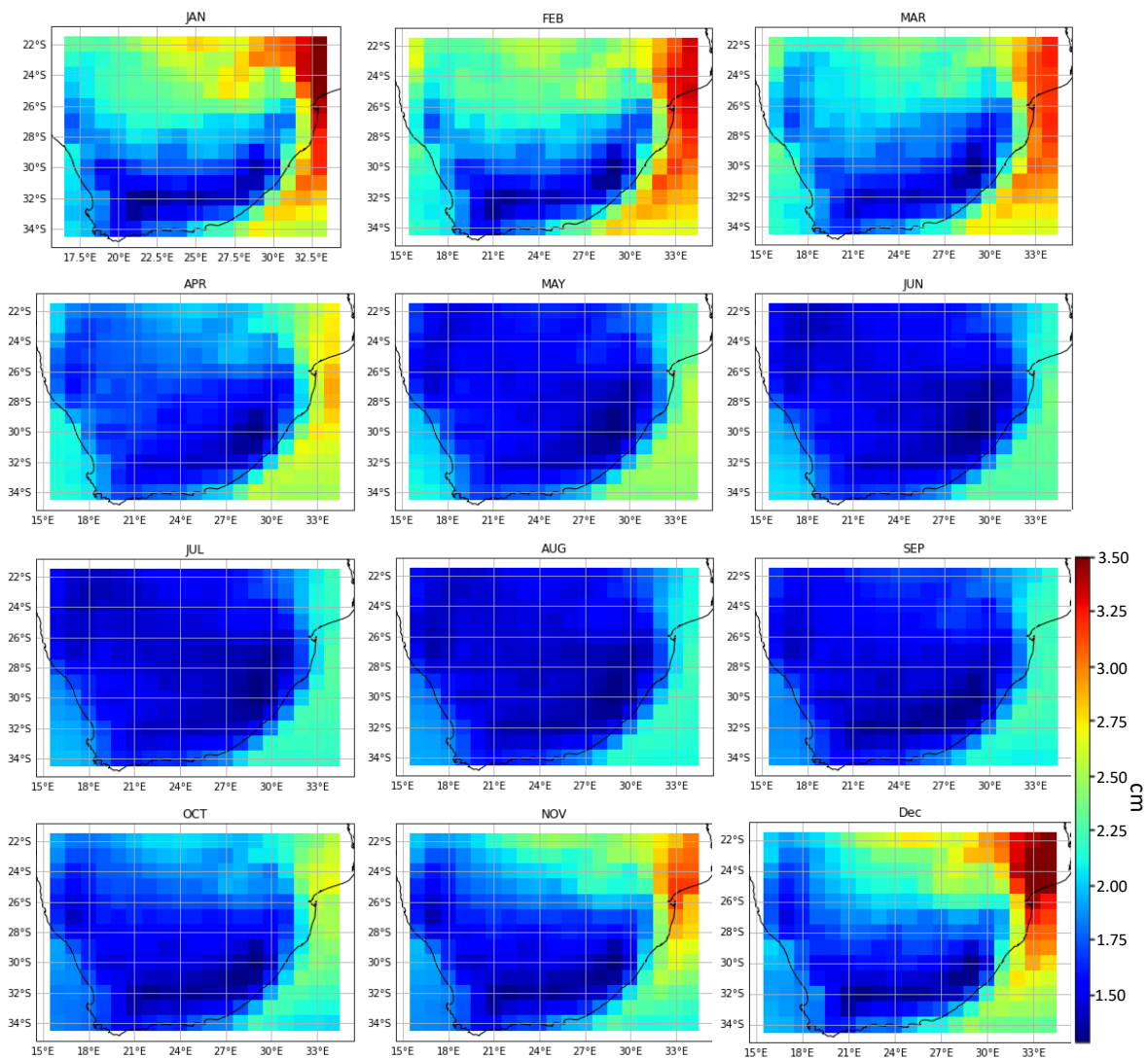


Figure 3.5 Average spatial distribution of atmospheric water vapour (AWW) in cm over South Africa from MODIS data for 10 years.

For the liquid water path (LWP) over South Africa, Figure 3.6 shows the distribution of cloud liquid content over the country. During winter months with extension to May and September, LWP is mainly low over the inland areas except for the coastal locations where relatively or higher values prevail. During this period, the values around the coasts reaches more than 40% higher than measurements obtained inland and most pronounced in June months. In contrast, LWP is more distributed over the entire region during summer, including November to April. The maximum values ( $LWP > 20.0 \text{ gm}^{-2}$ ) are witnessed during the June months and are mainly associated with the region's coasts. The minimum values ( $LWP < 10.0 \text{ gm}^{-2}$ ) are predominant over the inland areas, particularly in August. Interestingly, both maximum and minimum occurred in the same seasonal period. Although the min-max happened during the same temporal domain seasonally, their spatial spaces are exclusively different. Meanwhile, the pattern demonstrated by LWP over this region does not show a discernible link with AWV especially considering the distribution of both parameters over the country. While AWV is more distributed spatially over the central and upper sub-regions, LWP is more around the lower area. Nevertheless, carefully observing the variation of AWV and LWP, mainly during the summer and autumn seasons, gives further insight. There is a sign AWV influences the changes in LWP, but other factors such as the aerosol types and perhaps temperature could be significant. For instance, there are periods of low AWV noticeably corresponding to relatively high LWP. Previous studies have identified less water vapour condensation resulting from less hygroscopic aerosols accountable for this feature [28, 29]. This observation is analogous to the spotted variation over South Africa, taking into account the high values of LWP over sea salt endowed lower parts compare to the inland (mainly central and upper) areas.

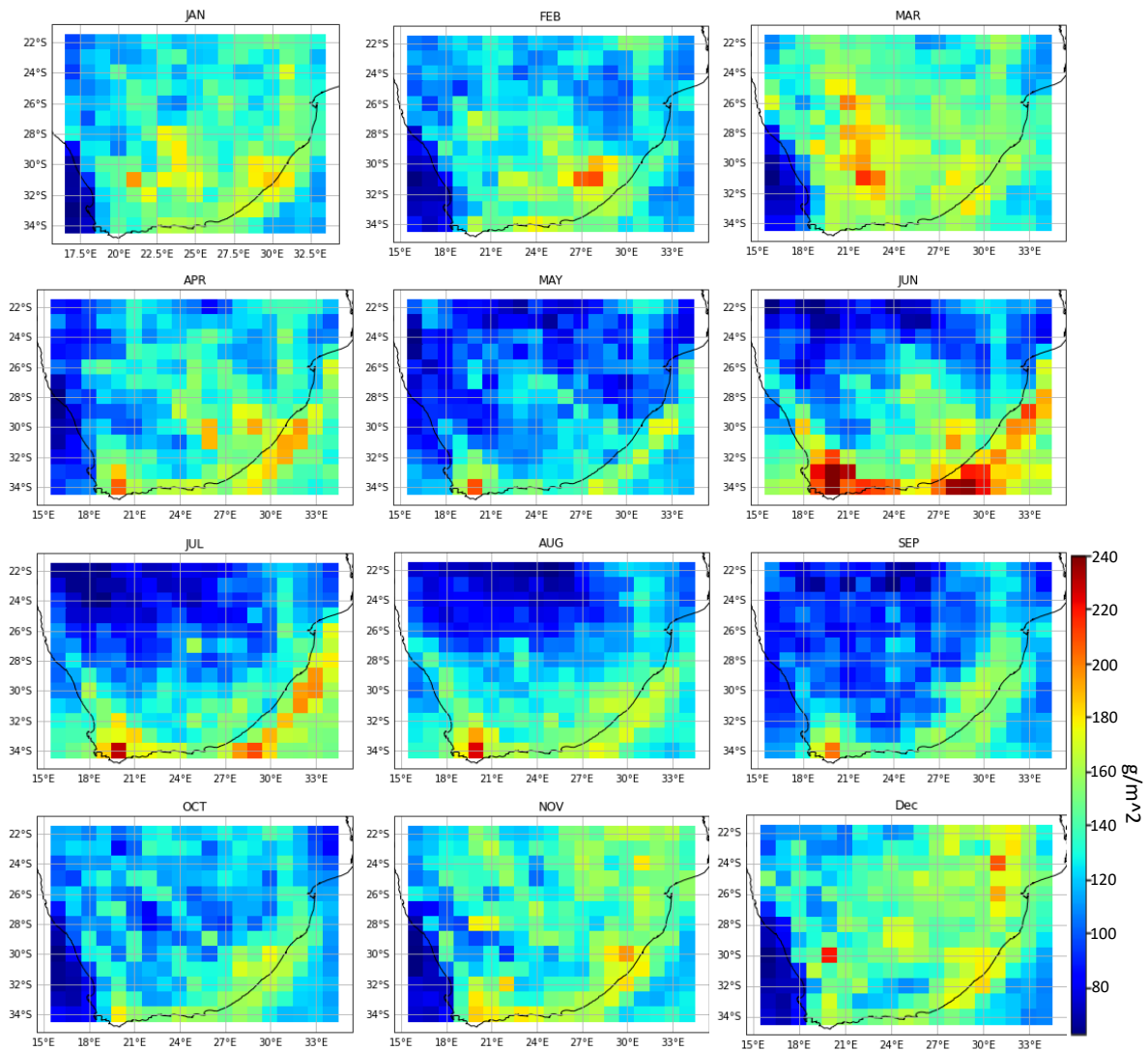


Figure 3.6 Average cloud water path (LWP) in  $\text{gm}^{-2}$  over South Africa from MODIS data for 10 years.

In Figure 3.7, the variation of cloud optical depth (COD) is illustrated. Therein, COD is high mainly around the coastal areas compared to the inland environments. Besides, the eastern parts of the country domicile most optical thick clouds while the western parts of the region, except for the lower coastal parts, are more optical thinner clouds. Over the 10-years study period, COD sparingly shows seasonality trends with the alternating increase and decrease in COD across the seasons. Higher values are seen mainly during summer and spring, then around the early parts of winter and fall. Meanwhile, the May, August, and September months are also characterised by the lower value of COD. The high COD value with extension to autumn corresponds to high atmospheric vapour and low aerosol turbidity during

summer. In contrast, high COD during the spring season overlaps with the emission of a considerable amount of aerosol, predominantly fine mode particles. In the two cases, there are possibilities that the high AWV and fine AOD significantly influenced the high COD, respectively. Meanwhile, the increase observed during winter might be accountable to cloud scavenging since both AWV and AOD are generally low at this period. Hence, there is a need for specific studies to understand aerosol removal processes over South Africa better. The maximum COD ( $> 22.0$ ) occurred in June and the minimum ( $< 7.0$ ) in May, just like the LWP. The high value of COD during winter and, to some extent, in autumn correspond to the period of high LWP and low AWV. In contrast, during the spring and summer seasons, high COD coincide with high LWP and increasing AWV. In the two cases, there is evidence of robust affinity between the variation of LWP and COD. By mapping the idea of aerosols acting as nucleating seeds during cloud formation, the variation demonstrates the albedo effect proposed by [13]. However, the exception lies in the constant LWP in Twomey's postulation, which differs from the variation of this parameter as observed over the study region. Observations from other studies have also shown that COD increases with LWP, especially when there is a proportionate rise in  $N_d$  [30, 31].

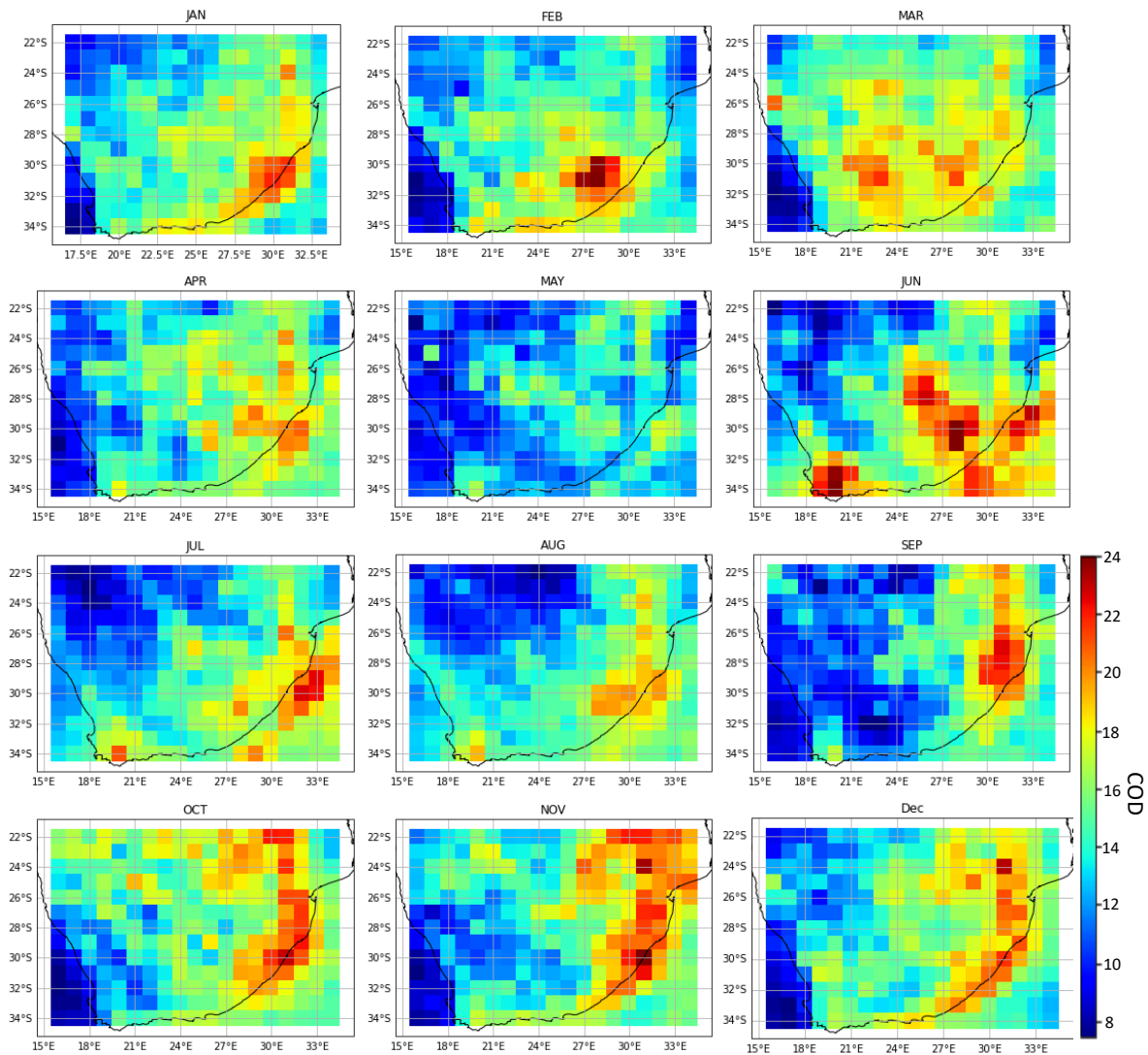


Figure 3.7 Average cloud optical depth (COD) over South Africa from MODIS data for 10 years.

Evaluation of the amount of cloud cover based on the cloud fraction in Figure 3.8 shows high value spreading from over the coastal environments towards the inland areas. Also, more cloud cover is observable around the upper eastern parts than the central and lower western parts except for the marine areas. Furthermore, high CF occurs during the summer and spring months and often declines towards autumn and winter, then rises through spring to summer again. The maximum values ( $CF > 0.7$ ) were mainly recorded during the December months, while the minimums ( $CF < 0.25$ ) were often around the August periods. A vital outlook from the CF trend is that it increases with AWW. The fraction of cloud covered plays a crucial role in the amount of solar radiation reaching the surface, hence can significantly influence the thermodynamics of the clouds depending on cloud type. Large cloud cover often reduces the

amount of solar radiation per unit area reaching the earth's surface. At the same time, lesser CF will enhance the quantity of incoming sun energy arriving on the earth. Although, there are other several important cloud properties such as the COD, the number of cloud droplets ( $N_d$ ), and droplet size distribution that influences the solar radiative energy over the earth. However, based on the surface area and relationship with cloud albedo, CF is an important factor defining the amount of sunlight reaching the ground [32-34]. Over South Africa, a lower temperature generally prevails during most of the year. The high-altitude feature of the region is one known factor that influences the low temperature. However, a rise in solar intensity is not uncommon over South Africa during the winter and spring months, which give rise to high temperatures during the day. During these periods, the low CF over the region could enhance the temperature profile, thereby causing a slight warmth in the afternoon. Also, the eastern coast of the region is warmer than its western counterpart. The two air fronts from India (warm Agulhas current) and Atlantic Oceans (cold Benguela current) respectively are accountable for this and constitute the significant differences in climate and vegetation over the region [35].

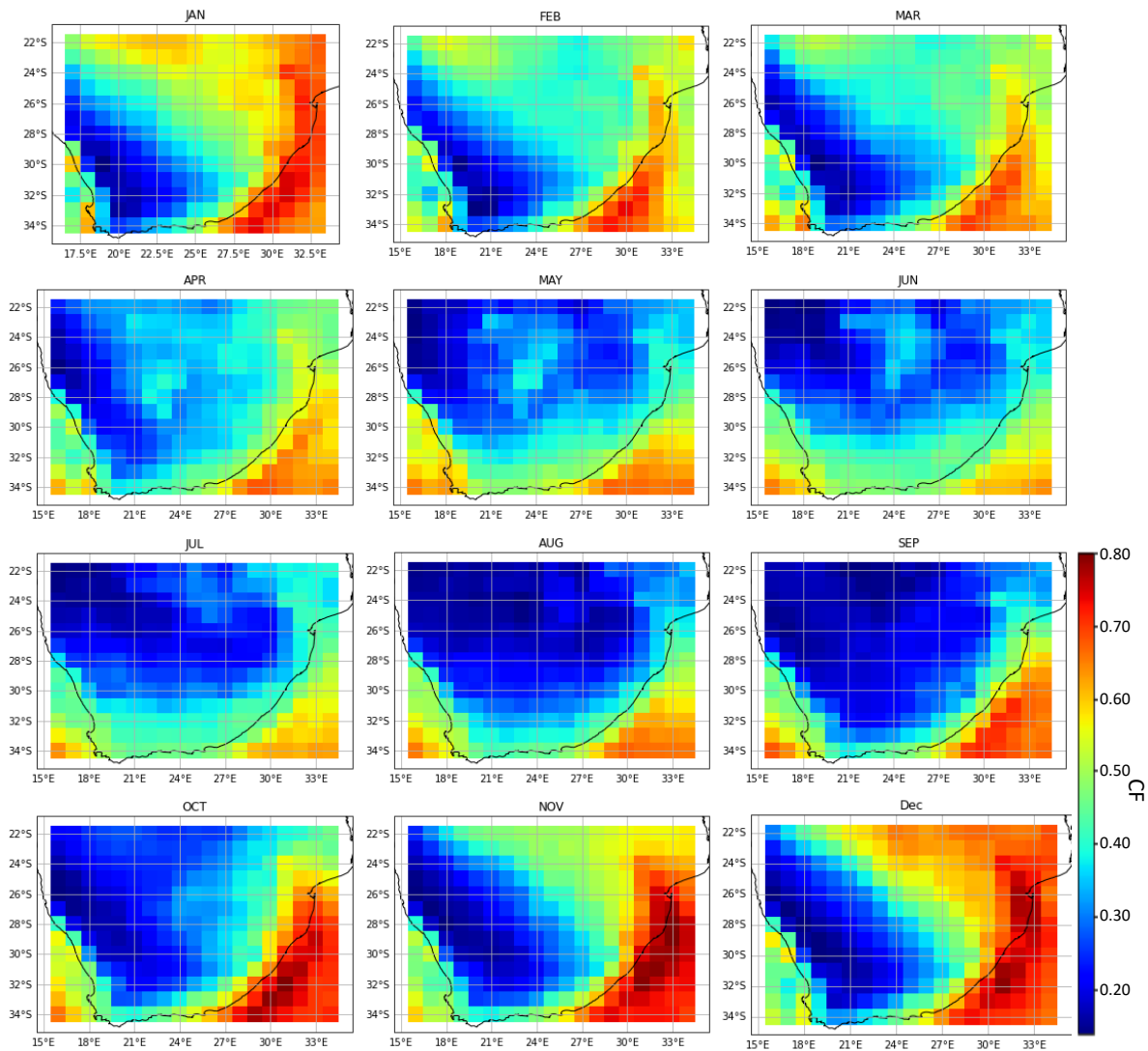


Figure 3.8 Average spatial distribution of cloud fraction (CF) over South Africa from MODIS data for 10 years.

As shown in Figure 3.9, the cloud effective radius (CER or  $R_e$ ) is highest over the surrounding oceans and the coastal environment compared to the country's inland areas. Besides,  $R_e$  is generally lower at the upper parts of the country and increases navigating through the central location to the southernmost parts where values are maximum. Furthermore, high  $R_e$  values are more spread over the western parts of the region than the eastern parts. In terms of temporal variation, CER basically increase during the autumn months and extends till winter. Then a declining pattern follows from the spring months till the end of summer in February. Also over the upper and central parts,  $R_e$  is slightly higher than the lower location during the summer. Thus, the maximum values ( $R_e > 15\mu\text{m}$ ) are mainly observed during the June months, while the minimums ( $R_e < 11\mu\text{m}$ ) are more during the July months. The high value of  $R_e$  over the coastal area could be linked to the

considerable presence of larger particle size aerosols, mostly of sea salt. In contrast, the lower value at the upper and central sub-regions, particularly towards the east, is associable with the dominance of fine mode particles. Several studies have elaborated on the role of cloud droplet size influencing the effective radius (e.g., [16, 36, 37]). Hence, the dominance of  $N_d$  by large-sized particles will result in  $R_e$  having high values, and small particles accounting for the most  $N_d$  will most result in low  $R_e$ . The variation played out over this region significantly aligned with the conventional theory by comparing the fine mode aerosol dominated upper and central parts with low CER values and the coarse mode associated lower parts with high CER.

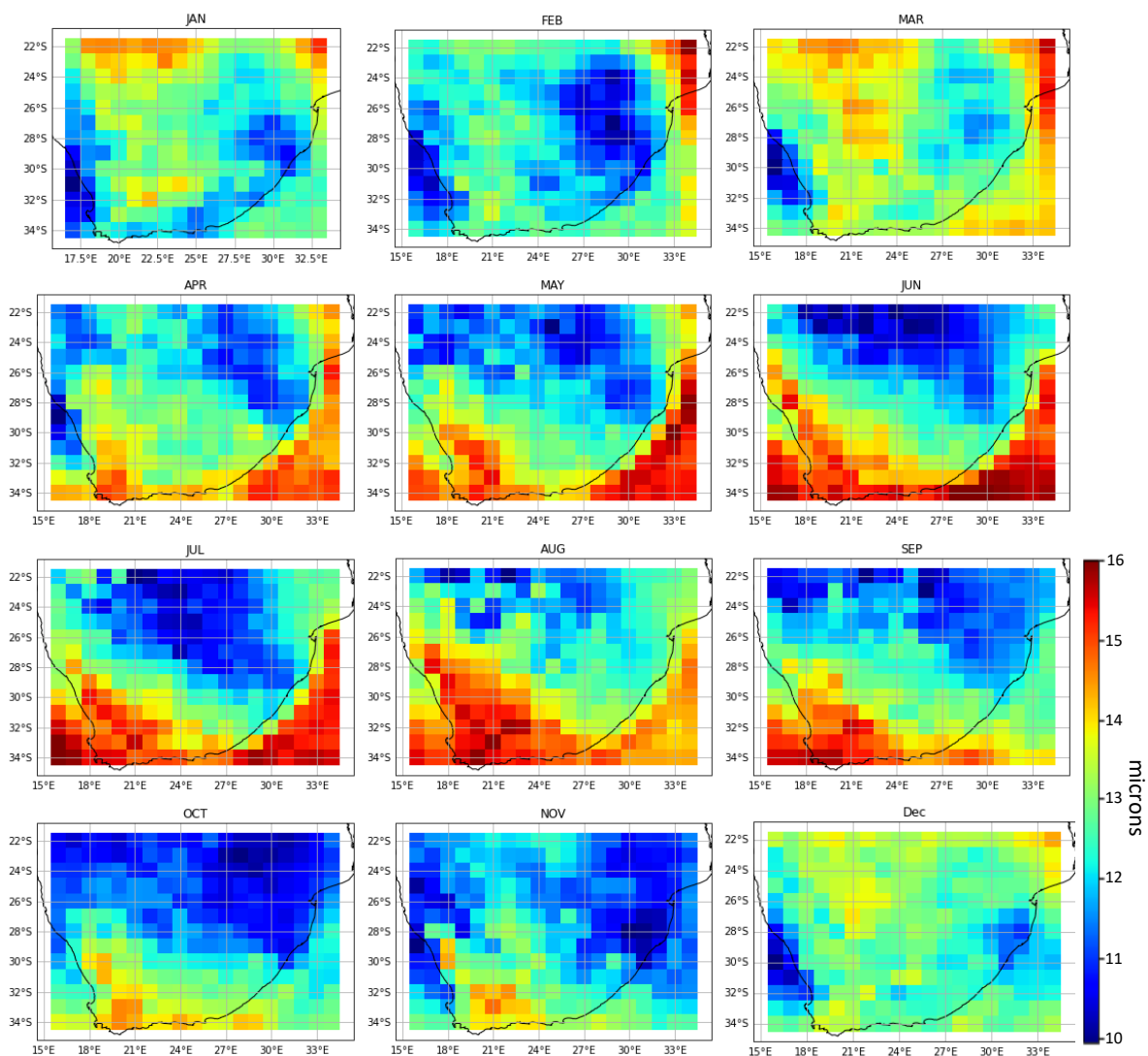


Figure 3.9 Average cloud effective radius (CER) in  $\mu\text{m}$  over South Africa from MODIS data for 10 years.

The distribution of cloud top height (CTH) over the region is illustrated in Figure 3.10. As expected, CTH is low over the ocean and to an extent at the coasts. Over the inland areas, CTH is more than two times greater than the height over the sea, depending on the period of the year. Temporally, CTH shows strong seasonality such that elevation increase during the spring months through summer, then declines in autumn through winter. Also, cloud top height is highest over the upper, followed by the central and lower parts. The maximum value for the cloud top height (CTH > 7500m) occurred during the summer months, especially in January, and the minimum (CTH < 4000m) in the winter period, mainly in the July months. A comparable variation is noticeable between AWW and CTH following their dramatic seasonal changes. Perhaps this characteristic could represent an increase in AWW, aiding more cloud development, especially at high updraft velocity.

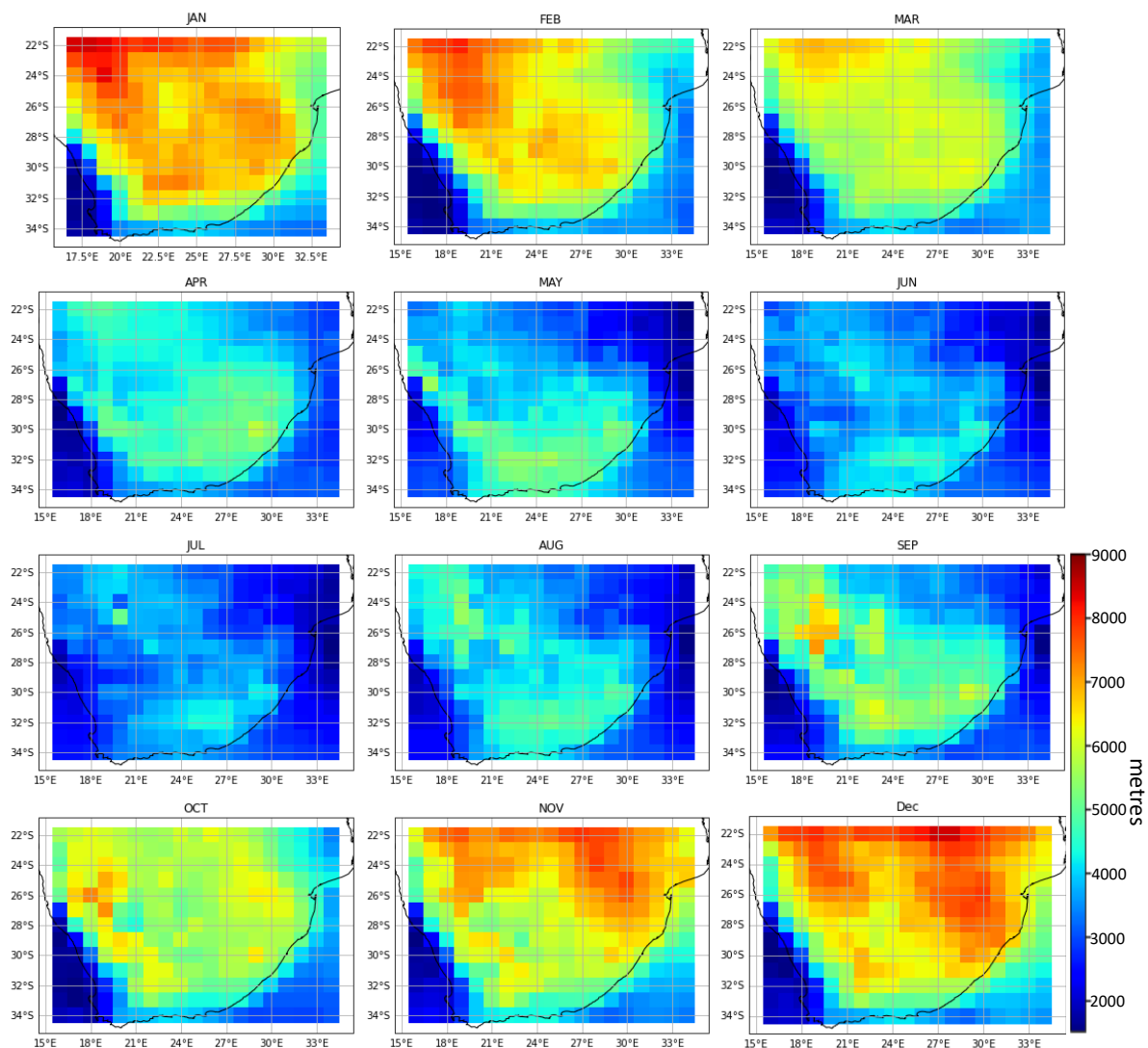


Figure 3.10 Average cloud top height (CTH) over South Africa from MODIS data for 10 years.

### ***3.4.3 Climatology of aerosol-cloud interrelationship and meteorology characteristics***

This section examines various aerosol and cloud properties observations based on the current understanding of aerosol-cloud interaction (ACI) and perhaps other distinct observable characteristics peculiar to the study region. The analysis attempts to enhance the knowledge of the influence of aerosol climatology on clouds and the reverse impacts (cloud effects on aerosol) during different temporal periods. Further, this will provide an insight on the possible response of precipitation which is valuable for future studies. The previous sections identified AOD as mainly high during the spring (August – November) and lowest in the winter season. To examine the interrelations amongst aerosol and cloud properties, Figure 3.11 shows the monthly mean variations of all parameters under consideration generated by statistical averaging of measurements over selected locations (Johannesburg 26.25° S, 28.05° E; Polokwane 23.90° S, 29.44° E; Nelspruit 25.47° S, 30.96° E; Mafikeng 25.81° S, 25.50° E) in each of the province within the upper part. Critically scrutinising the three aerosol properties (AOD,  $A_{\text{abs}}$  and AE), one can generally split the variation into two cases based on the combined AE- $A_{\text{abs}}$  relationship with AOD. The first case (case-I) represents the period (April-October) of changes in AOD associated with  $AE > 1.0$  and corresponding variation in aerosol absorbing properties (AOD influenced by  $A_{\text{abs}}$  increase). In comparison, the second case (case-II) represents the change in AOD with low  $AE < 1.0$  with no significant influence of absorbing aerosol as seen during November to March.

In terms of the atmospheric vapour, case-I represents the relationship between AWV and AOD. From observation, AOD changes in the same manner (increase or decrease) as atmospheric vapour while the particle size is increasing/decreasing accordingly. This characteristic demonstrates a shift in the optical properties of aerosol particles (e.g., size and scattering albedo) due to water uptake. In the presence of high AWV, as particles with high affinity for water increase in size, AOD simultaneously increased, and AE decreases. The described pattern is especially true for an environment dominated by hygroscopic aerosol and under humid conditions [38-40]. Subsequently, the particles act as cloud condensation or ice nuclei (CCN or IN) and are later activated to cloud droplets at supersaturation by vapour condensation. The continuous and rapid growth of these cloud droplets explains the strong dependency of CF on AWV and AOD. In contrast, case-II illustrates AOD variation in response to rising absorbing particles such as organic carbon (OC) and black carbon (BC),

where AWV is low. One should note the increasing particle size ( $AE > 1.0$ ) and sharp drop of CF with AWV. Coalescence of cloud droplets formed reduces, compelling a proportionate reduction in the cloud cover (CF decreases). Besides, at the intersecting peak (in September) of the aerosol properties, a slight rise in vapour does not immediately increase particle size due to overwhelmed atmospheric water by fine mode aerosols.

Cloud thickness has been explained to be influenced by LWP in the previous section. Hence, considering case-I, COD and LWP demonstrate strong dependency, suggesting proportionate cloud water to nucleating particle ratio. Contrarily, the dependence of the parameters (COD and LWP) is relatively weak during case-II, such that the LWP does not directly quantify COD. Instead, cloud thickness increases with the aerosol particle size, and mostly the same for cloud droplets. Also, one can relate this to the variation of the CER in case-I, where COD is closely dependent on LWP correspond to a high effective radius ( $R_e > 12\mu\text{m}$ ), hence large cloud droplet size and more cloud growth due to increase collision and coalescence. Furthermore, the increase in cloud top height along the effective radius and thickness will likely enhance radiative cooling at the top due to increasing cloud albedo. Interestingly, the surface temperature is relatively high to invigorate a convective scene, prompting corresponding precipitation dynamics over the upper SA. Therefore, any shortfall in these parameters (CER, LWP, COD, CTH) to commiserate the aerosol concentration could be detrimental to precipitation occurrence.

During case II, AOD is predominantly fine mode and mainly influenced by absorbing particles. Vapour is generally low, same as COD and LWP compared to the aerosol loading that can potentially act as CCN. This situation is portrayable as a polluted condition whereby aerosols nucleate a more significant amount of smaller cloud droplets, thereby affecting the alignment of LWP and COD, resulting in lower CER and cloud cover. Consequently, cloud droplets collision and coalescence rate are slower while cloud albedo increases according to the Twomey effect causing warm rain suppression [14, 41]. A vital observation is the radiative effect ushered by the smaller cloud droplets amid low surface temperatures. Radiative cooling at cloud-top along low surface temperatures enhances atmospheric stability and creates an unsuitable condition for convective developments [42].

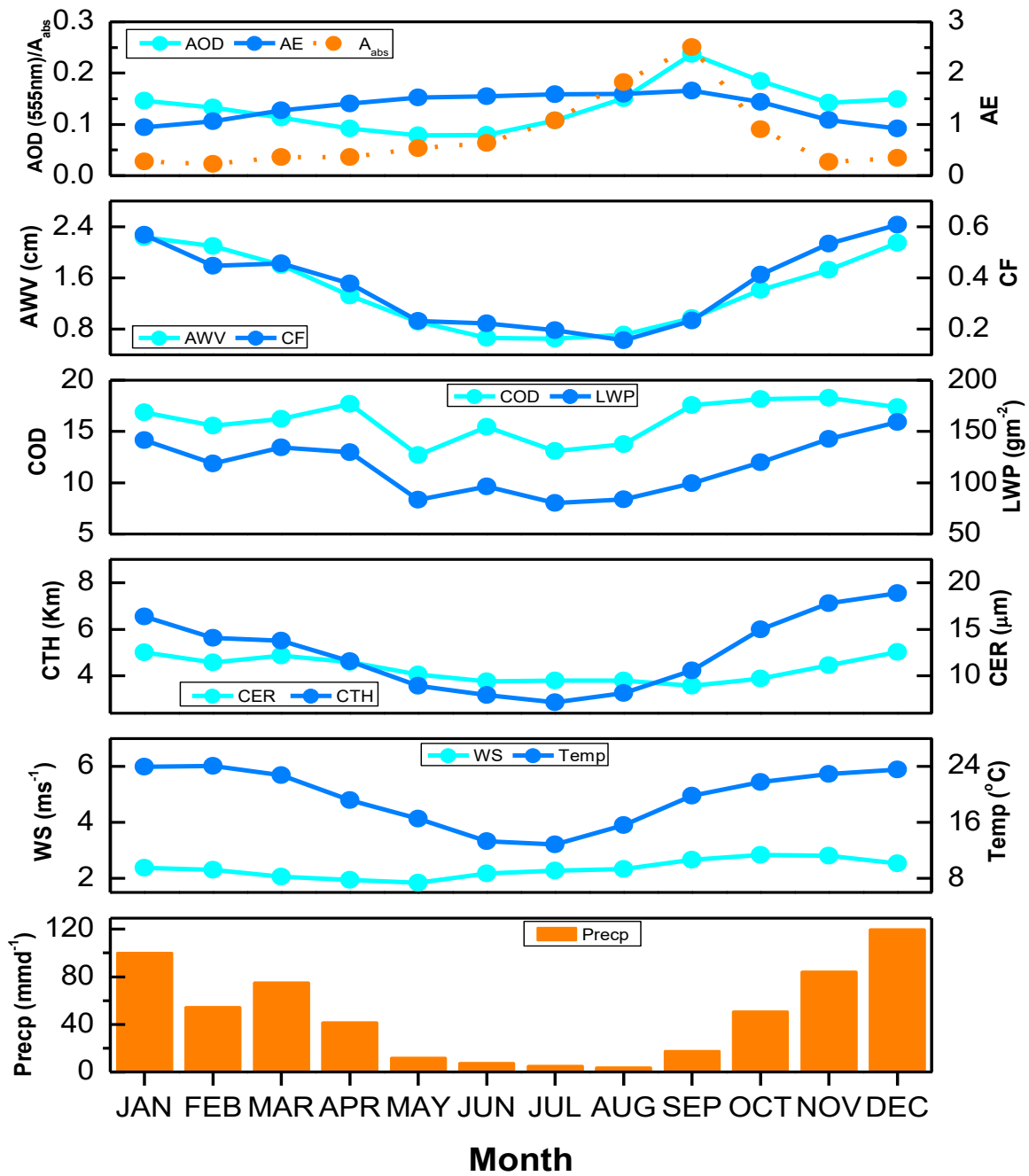


Figure 3.11 Intercomparison of average monthly variation of aerosol (AOD, AE, A<sub>abs</sub>), AWW, cloud (CF, LWP, COD, CTH, CER) and meteorology (WS, TEMP, PRECIP) parameters over upper South Africa.

In Figure 3.12 representing the variation over the central part made up of Bloemfontein (29.12° S, 26.22° E), Durban (29.92° S, 31.01° E) and Upington (28.39° S, 21.27° E). The dynamic is not much diverging from the upper part considering the drift of aerosol southward of the region and their sharing of similar meteorology conditions. Here, the aerosol-cloud interaction regime can be divided into two case studies as done for the upper part. Case-I

covers the period (November to April) of high aerosol loading dominated by large size particles (i.e.,  $AE < 1.0$ ) and generally low absorbing aerosols. Meanwhile, case-II is the period (May to October) where aerosol loading is fine particle dominated and linked with absorbing aerosol emission. Just as for upper SA, the vapour is higher during case-I, and CF maintains close variation as AWV. Cloud thickness significantly varies with cloud water following changes in AOD. A rise in AOD at high AWV corresponds to increasing COD, LWP, CER, CTH, and more precipitation. This process possibly follows the formation of larger size cloud droplets due to the concentration of bigger-sized particles yielding a proportionate increase in LWP and COD with a high value of CER and CTH, thereby leading to more precipitation. The ambient temperature and wind speed are relatively high to drive the dynamic and thermodynamic aspects of the process. Noteworthy is the changes in precipitation rate due to characteristics features of aerosol-cloud interaction.

For the second pattern (case-II) covering May to October, AOD shows substantial variation with absorbing aerosols and is primarily fine mode particle dominated. The meteorological condition is characterised by general low precipitation, temperature drop, and a slight reduction of horizontal wind speed. An increase in aerosol loading mainly corresponds to a decrease in COD and LWP. Besides, CER generally decreases while CF and CTH decline in most parts of the period. On account of generally low AWV during case-II, CF and CTH decreased to a minimum but increased as AOD even in the presence of less water vapour around September. From the pattern, precipitation formation is motivated by relatively larger cloud droplet size (higher CER), high atmospheric water, and ambient temperature. COD and LWP increased and maintained proportionate variation, coupled with a slight increase in temperature, serving as potential invigorator of atmospheric instability, thereby raising the precipitation chances.

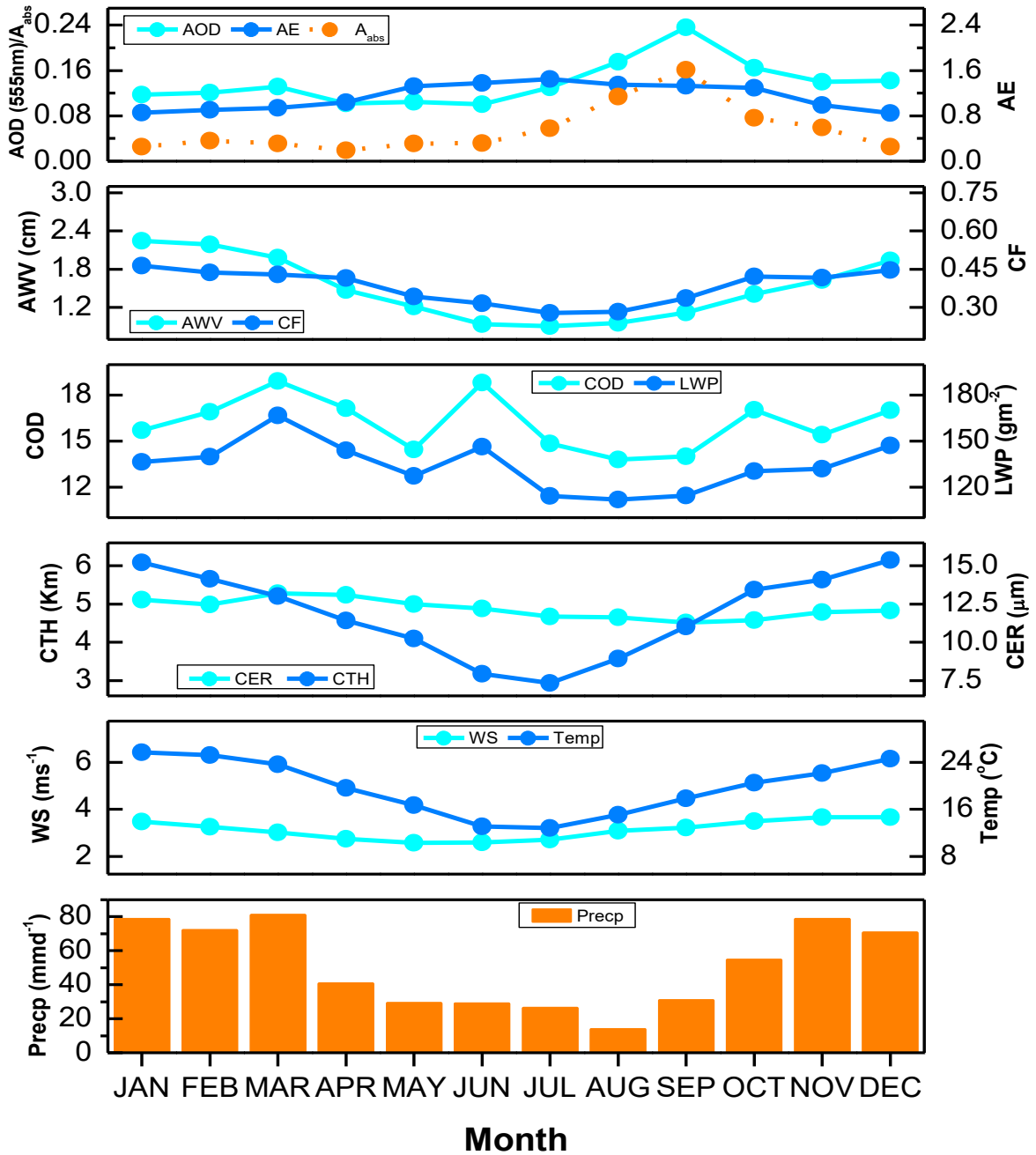


Figure 3.12 Intercomparison of average monthly variation of aerosol (AOD, AE, A<sub>abs</sub>), AWW, cloud (CF, LWP, COD, CTH, CER) and meteorology (WS, TEMP, PRECP) parameters over central South Africa.

Over the lower part (Cape Town 33.92° S, 18.42° E and Port Elizabeth 33.95° S, 25.59° E) in Figure 3.13, the aerosol loading is generally low (AOD < 0.1) and further characterised by low cloud (CTH < 3km) typical of marine environments. Amazingly, this part presents high atmospheric vapour, ambient temperature, and wind speed during the summer and spring as the other parts (upper and central) yet low precipitation. Following a convention similar to the other parts, case-I represents the period between October and March where lower

absorbing properties and  $AE \leq 1.0$  typify aerosol while rainfall is deficient. In contrast, case-II during April – September demonstrates an increase in precipitation, absorbing aerosols and  $AE > 1.0$  with AWP and temperature lower. During case-I, the general low aerosol loading corresponds to clouds with less water (low LWP) even though the cloud is optically thicker ( $COD > 15.0$ ). There is notable contrast in the proportionate variation of LWP and COD coupled with low effective radius ( $CER < 14\mu\text{m}$ ). Precipitation decline here is linkable with low cloud water, droplet size, and reduced CER. The size of cloud droplet effective radius plays a vital role in precipitation forming clouds. A low value in shallow clouds, particularly less than  $14\mu\text{m}$ , leads to slower collision and coalescence rates and precipitation suppressing. Because more evaporation occurs in smaller size cloud droplets when mixing with dry ambient air, thus causing loss of cloud water. Several studies, including modelling experiments, have presented similar observations [16, 43, 44].

Meanwhile, case-II presented an increased aerosol loading period dominated by fine mode particles with strong absorbing properties where atmospheric vapour slightly dropped. Here, a rise in cloud water is observable and proportionately varies with cloud depth while the ambient temperature dropped to minimal along with a slight decrease in wind speed. More importantly, CER is greater than  $14\mu\text{m}$ , and cloud height averagely increased sparingly. Thus, precipitation here is boosted by the increase in CER and LWP coupled with the low ambient temperature that will enhance the faster reach of supersaturation level. Because of the rise in CER, collision and coalescence will increase along cloud water since the coalescence rate is a function of droplet size.

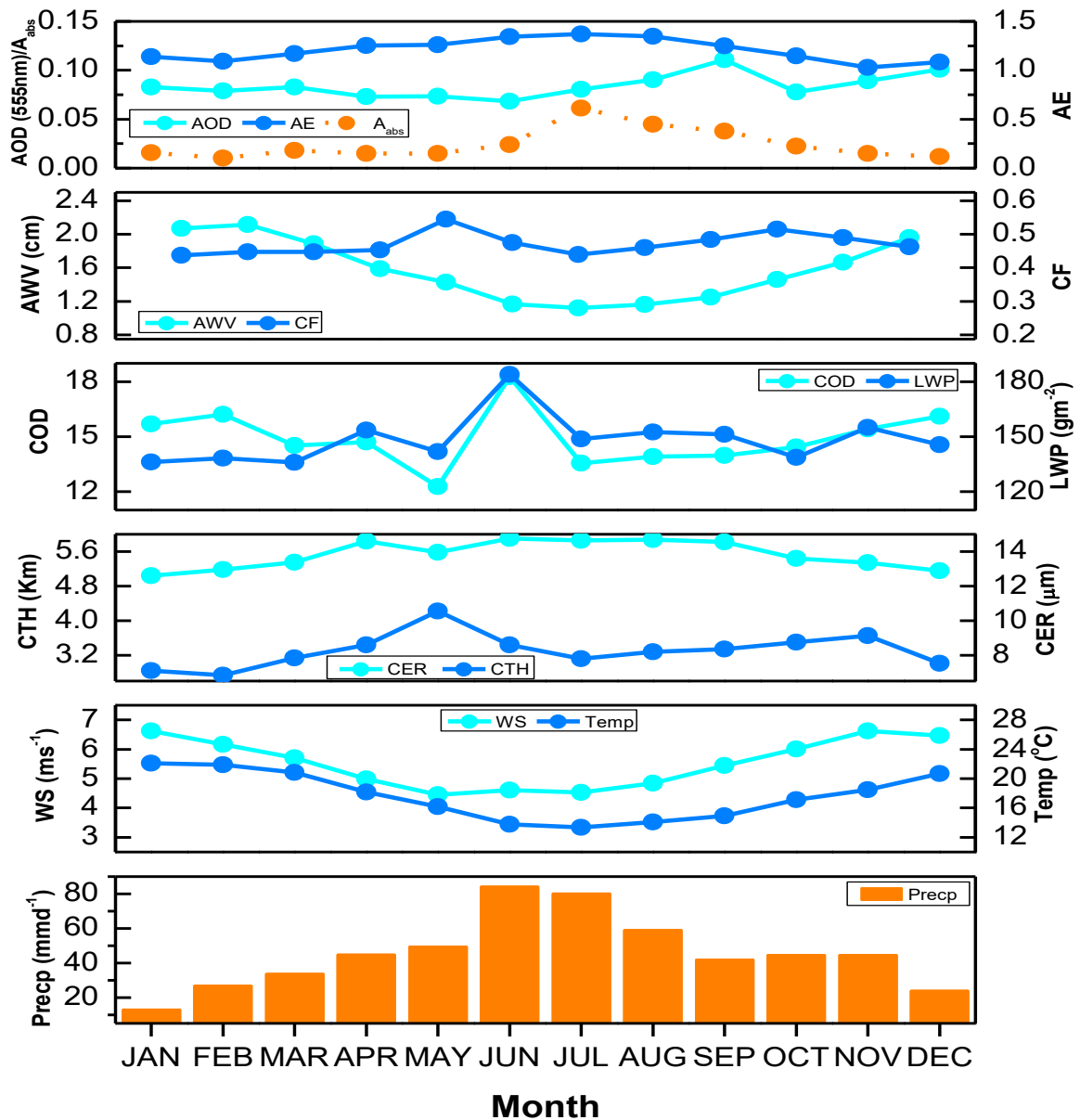


Figure 3.13 Intercomparison of average monthly variation of aerosol (AOD, AE,  $A_{abs}$ ), AWP, cloud (CF, LWP, COD, CTH, CER) and meteorology (WS, TEMP, PRECIP) parameters over lower South Africa.

### 3.4.4 Interannual characteristics of aerosol, cloud, and meteorology parameters

In Similarities in the weather characteristics over central and upper South Africa constitute a vital outlook in the interannual variation in Figure 3.14. Critically observing the figure, the meteorological state of the region shows close relationship amongst temperature (TEMP), wind speed (WS) and AWP, and a general increasing tendency from 2013. AOD, AE and  $A_{abs}$  show a similar declining trend between 2012 – 2013, then increasing tendencies during 2008 – 2010 and 2013 – 2015 over the lower area. Aerosol loading is generally low over this part (mostly  $AOD < 0.1$ ), which is typical of a maritime environment [45]. Even though a

substantial amount of anthropogenic aerosols is emitted internally in this environment due to the high human population and industrial activities, long-range external emissions mainly trigger the aerosol loading and fine mode particles concentration [17, 46]. Cloud cover and top height over the lower sub-region experienced increments to two major peaks in 2009 and 2015, coinciding with the rise in AOD. An increase in aerosol loading can enhance CF and CTH through the addition of CCN, invigorate existing cloud droplet concentration ( $N_d$ ) to enhance vertical development [47]. The case is typical of warm clouds such as shallow cumuli and stratocumuli found over the marine environment as observed by previous studies [38, 48]. For atmospheric vapour, a distinct rise to the highest value in 2010 corresponds to high AOD, CF and CTH. Meanwhile, CER, LWP, and COD increased in 2008 and during 2012 – 2014, which fall into the years of moderate to highest rainfall and lower aerosol loading and AE. Likewise, less precipitating years such as 2010 and 2015, mainly associated with drought events across the region [24], coincide with high AOD and AE, while effective radius, cloud water, and optical thickness are lower.

Over the central and upper sub-regions, AOD follows a series of increase and decrease almost along subsequent years. Nevertheless, AOD, AE, and  $A_{abs}$  simultaneously rose to peaks in 2010 and 2015, just as water vapour. During these peaks, cloud cover is high over both upper and central parts except for the sharp drop at the upper area in 2015. Consequently, the growth in aerosol loading over these sub-regions mainly enhanced by fine mode particles generally result in more cloud covers. In contrast, increasing aerosol loading largely negatively impacts cloud water and optical depth over the central sub-region, which resembles the trend over lower SA. However, the reverse is mostly the case over upper SA. The disparity in aerosol-cloud interaction behaviour might be due to differences in particle size distribution and the general aerosol composition over each area. As for the effective radius, an overall decrease prevailed during years associated with rising aerosol loading over the central and upper sub-regions. This feature is more evident for 2010 and 2015 and consistent with observation over the lower sub-region.

From the interannual variations, several distinct characteristics of aerosol and cloud over each sub-region are noticeable apart from the dynamics of aerosol-cloud interaction. For instance, the hierarchy by location of aerosol loading and optical depth of absorbing particles demonstrate a declining trend from upper to lower. Meanwhile, for most cloud parameters, the reverse is the case such that an increasing trend prevails from upper to lower area.

Furthermore, parameters like CER, CTH, and CF are higher over the lower, followed by the central and upper. These characteristics alone tend to set varying conditions for precipitation to occur.

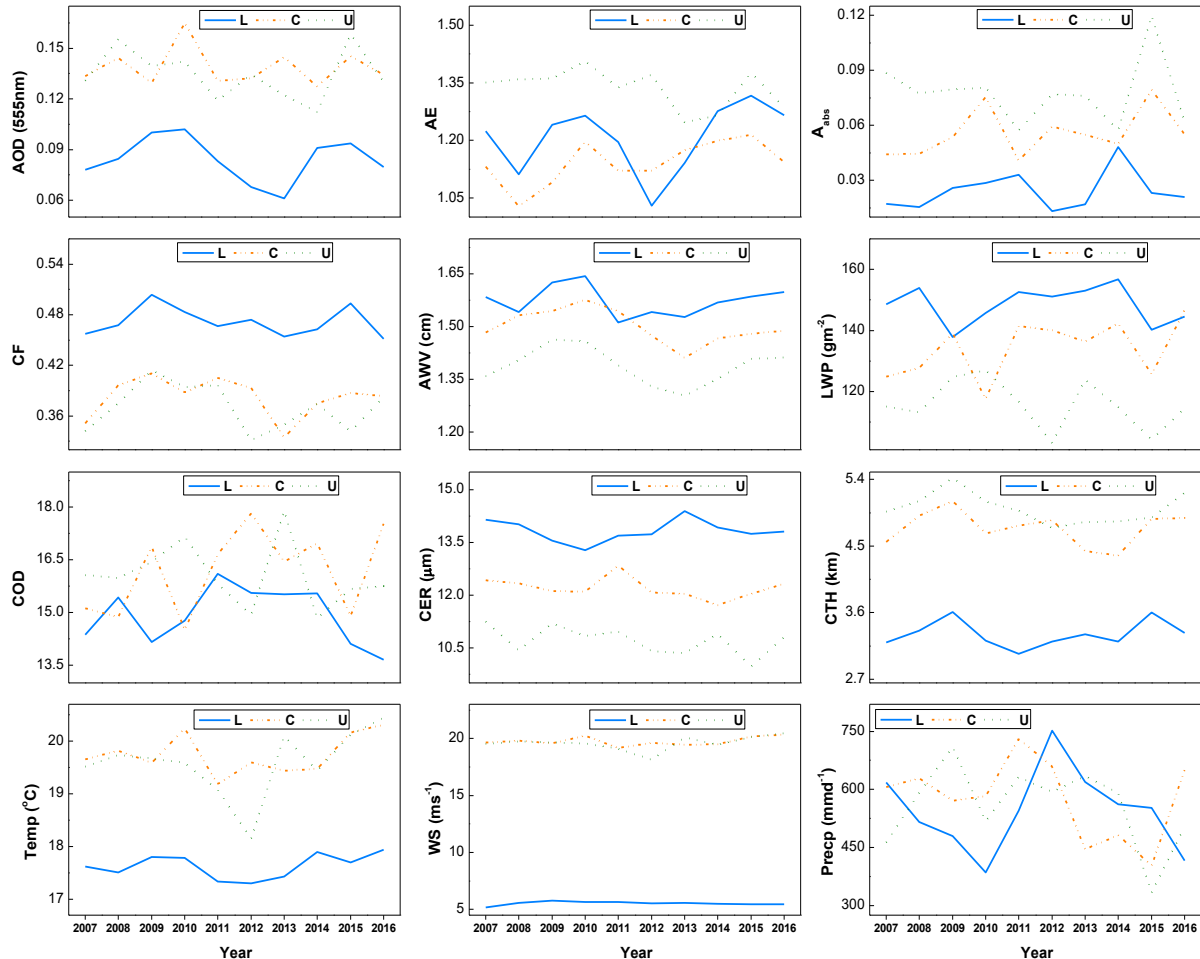


Figure 3.14 Interannual variation of monthly means for aerosol (AOD, AE,  $A_{abs}$ ), cloud (CF, LWP, COD, CTH, CER) and meteorology (WS, TEMP, PRECP) parameters over upper (U), central (C) and lower (L) South Africa.

### 3.4.5 Correlation analysis of parameters

From the previous section, different mechanisms of precipitating and non-precipitating conditions based on the aerosol characteristics and atmospheric states are elaborated for the region. The upper and central parts share a similar trend and have the same precipitation pattern, while the lower part differs in drift and rainfall patterns. This section presents the correlation analysis of aerosol-cloud and cloud-precipitation interactions to understand the aerosol-cloud interaction over the region better. Since particle size distributions tremendously influence cloud properties, the correlation analysis for aerosol properties includes AOD and

aerosol index (AI). Figure 3.15a shows the correlation between AOD and cloud properties (COD, LWP, CER, CF, and CTH). The correlations between AOD and cloud properties are generally low, ranging between 0 and  $\pm 0.39$ . However, the most significant is the relationship between AOD, COD, LWP, and CER, with correlations predominantly between -0.2 to -0.4 for all parts of the region under consideration. A closer look at these three crucial cloud parameters further reveals CER to be the top influenced parameter by aerosol loading with negative correlation. An increase in aerosol loading often results in a smaller size cloud droplet concentration, reducing the effective radius of the cloud.

Similarly, both LWP and COD demonstrated a negative correlation such that for the former, an increase in aerosol also results in loss of cloud water. Thus, together with low CER often result in increasing albedo, just as postulated by [13]. For the latter, the persistence rise in AOD sometimes results in cloud burnout due to the absorbing effect. Although one will envisage a linear relationship between AOD and COD based on the expected inheritance of aerosol characteristics by cloud, aerosols inhibit cloud development through the warming effect [49, 50]. In general, several studies have demonstrated the impact of increasing aerosol loading on the decrease of LWP and CER, thereby suppressing rainfall [14, 51, 52]. The relationships between AI and cloud properties in Figure 3.15b show notably positive correlations over the central part with weak positivity ( $< 1.5$ ) for CER, COD, and LWP. Meanwhile, negative correlations dominate the upper part, except for COD that portrays an extremely weak positivity ( $\approx 0.03$ ). As for the lower area, CER, COD, and LWP are negatively correlated with AI, while CF and CTH showed extremely weak positive correlations.

A positive correlation existed between all considered cloud properties and precipitation for the entire region, as illustrated in Figure 3.15c. Most of the correlation values range from moderate to strong ( $\approx 0.4 - 0.7$ ) except for the lower part, where the relationship between precipitation and each of COD, CF, and CTH is relatively weak ( $r < 1.8$ ). The weak correlation between rainfall and these parameters lies mainly in this area's low and shallow cloud characteristics. Notably, the significance of increasing cloud water and effective radius in enhancing precipitation is evident according to this chart as it cut across the entire region. Hence, as observed from this region, CER and LWP have demonstrated a critical role in deep and shallow clouds.

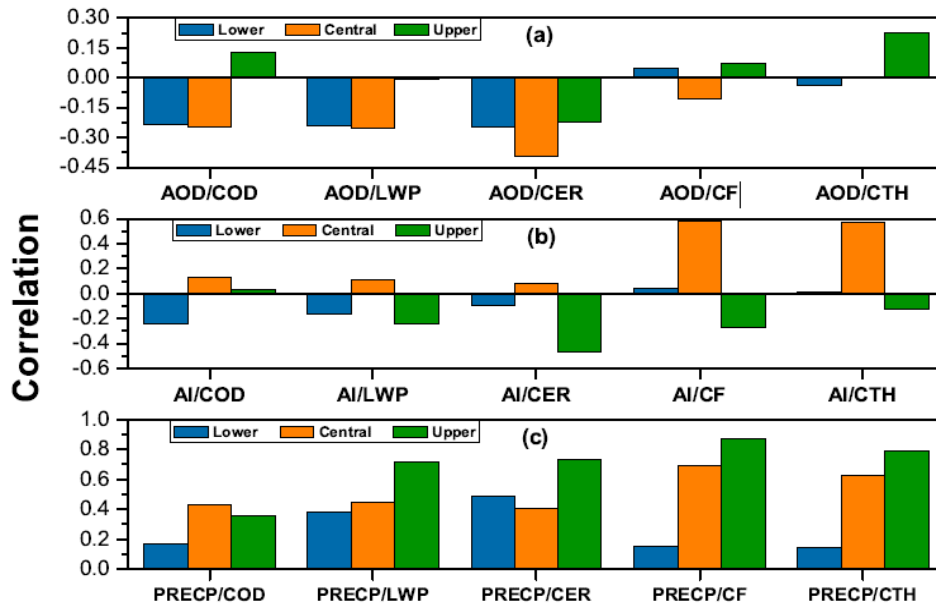


Figure 3.15 Correlation analysis of (a) AOD vs cloud (CF, LWP, COD, CTH, CER) properties, (b) AI vs cloud (CF, LWP, COD, CTH, CER) properties, and (c) PRECP vs cloud (CF, LWP, COD, CTH, CER) properties for upper, central and lower South Africa.

In general, based on the climatology of aerosol and cloud as described in the previous sections, precipitation formation is a function of the characteristics of aerosol-cloud interaction. ACI leading to varying states of cloud properties, particularly CER, LWP, CF, and CTH, have differing effects on precipitation, hence, summarized in Table 1.

Table 3.1 A summary of the different states of cloud properties and the corresponding effects on precipitation over the region.

Properties	CER/LWP	CF/CTH	PRECP	Characteristics
1.	$\uparrow_{TH}$	$\uparrow$	$\uparrow$	Moderate to heavy precipitation
2.	$\uparrow_{TH}$	$\downarrow$	$\uparrow$	Light to moderate precipitation
3.	$\downarrow_{TH}$	$\uparrow$	$\downarrow$	Cloudiness/non-drizzling to light precipitation
4.	$\downarrow_{TH}$	$\downarrow$	$\downarrow$	Clear sky/non-drizzling

\*Note:  $\uparrow_{TH}$  and  $\downarrow_{TH}$  respectively represent increment above and decrement below the threshold.

### 3.5 Summary and conclusion

Air pollution through aerosol emission over the South Africa region consistently maintains a reoccurrence pattern centred around a sharp increase in spring. The bulk of these pollutants are transported to the area by air masses mostly originating from the bordering countries. Domestic emissions mainly mix with transported incoming aerosols, hence, inducing a characteristic change in the atmospheric and environmental conditions. Nonetheless, the interaction between aerosol and the cloud is driven by the dynamic and thermodynamic processes of the atmosphere, with aerosol and vapour acting as feedstocks.

Even though aerosol-cloud interaction appears complex, the deduction from the analysis presented in this study shows that cloud formation and evolution is a function of the amount of aerosol and vapour integrated into the cloud system. Besides, the process itself follows certain conditions that define the cloud properties and the ability to precipitate. Thus, infusing a proportionate concentration of aerosols and vapour into the cloud will enhance cloud water and effective radius (increase LWP and CER). Likewise, integrating a disproportionate amount of the duo will suppress rain-bearing cloud development because excess aerosol will result in smaller cloud droplets and lesser LWP. In contrast, extreme cloud water with fewer particles will surmount to the nucleation of fewer but bigger size droplets. Although, an increase in fine mode dominated aerosol corresponds to lower CER and LWP, resulting in lower rain, as seen in this study. However, cases of predominated small size aerosol concentration leading to rising rainfall were also registered.

Based on these assessments, the potential to precipitate is mainly the function of CER, LWP, and COD over the entire region. An increase in the three parameters increases the chances of rain-bearing cloud formation. Furthermore, the threshold for shallow lower subregion cloud for rain occur is  $CER > 14 \mu\text{m}$ , while the central and upper areas with more deep cloud possess a threshold of  $CER > 11 \mu\text{m}$ . Meanwhile, the average value for precipitating cloud water over SA seems uniform for all the locations and corresponds to  $LWP > 100 \text{ gm}^{-2}$ .

Both CF and CTH influence more of the precipitation intensity. Both cloud cover and top height increase for high precipitating clouds and the reverse for low precipitating clouds. Nevertheless, the primary conditions ( $CER > \text{threshold}$ ;  $LWP > \text{threshold}$ ) for rain-bearing needed attainment before an increase in CF and CTH result in a pronounced rise in

precipitation. So, an increase in cloud cover and depth will necessarily not yield rainfall but mainly will increase the quantity.

Surface temperature and wind speed mainly increased with atmospheric vapour. Due to the measurement altitude of both quantities (< 100 m above the ground), the influence is not much observed on aerosol loading and cloud development. Also important, temperature generally rises continuously in 2013 over the region.

### **Acknowledgment**

The authors gratefully acknowledge the NASA Langley Research Centre Atmospheric Science Data Centre (ASDC) for providing the MISR and LAADS for the MODIS data. The authors also appreciate the support of the South Africa Weather Service (SAWS) for making the meteorology data available.

### **Reference**

- [1] IPCC, Climate Change 2013: The Physical Science Basis. Contribution of Working Group I to the Fifth Assessment Report of the Intergovernmental Panel on Climate Change, Cambridge University Press, Cambridge, United Kingdom and New York, NY, USA, 2013.
- [2] V. Ramanathan, P.J. Crutzen, J.T. Kiehl, D. Rosenfeld, Aerosols, climate, and the hydrological cycle, *Science* 294 (2001) 2119-2124.
- [3] IPCC, The Physical Science Basis. Contribution of Working Group I to the Fourth Assessment Report of the Intergovernmental Panel on Climate Change Cambridge University Press, Cambridge, 2007.
- [4] U. Lohmann, J. Feichter, Global indirect aerosol effects: a review, *Atmos Chem Phys* 5 (2005) 715-737.
- [5] M. Kamala, A. Asmi, L. H.K., K.S. Carslaw, U. Poschl, U. Baltensperger, O. Hov, J.-L. Brenquier, P. S.N., M.C. Facchini, H.-C. Hansson, A. Wiedensohler, D. C.D.O., Introduction: European integrated project on aerosol cloud climate and air quality interactions (EUCAARI)-integrating aerosol research from nano global scales, *Atmos. Chem. Phys* 9 (2009) 2825-2841.

- [6] J. Haywood, O. Boucher, Estimates of the direct and indirect radiative forcing due to tropospheric aerosols: A review, *Rev Geophys* 38 (2000) 513-543.
- [7] J. Quaas, Y. Ming, S. Menon, T. Takemura, M. Wang, J.E. Penner, A. Gettelman, U. Lohmann, N. Bellouin, O. Boucher, A.M. Sayer, G.E. Thomas, A. McComiskey, G. Feingold, C. Hoose, J.E. Kristjánsson, X. Liu, Y. Balkanski, L.J. Donner, P.A. Ginoux, P. Stier, B. Grandey, J. Feichter, I. Sednev, S.E. Bauer, D. Koch, R.G. Grainger, Kirkev, amp, aring, A. g, T. Iversen, Ø. Seland, R. Easter, S.J. Ghan, P.J. Rasch, H. Morrison, J.F. Lamarque, M.J. Iacono, S. Kinne, M. Schulz, Aerosol indirect effects – general circulation model intercomparison and evaluation with satellite data, *Atmos Chem Phys* 9 (2009) 8697-8717.
- [8] T.A. Jones, S.A. Christopher, Statistical properties of aerosol-cloud-precipitation interactions in South America, *Atmos Chem Phys* 10 (2010) 2287-2305.
- [9] B. Stevens, G. Feingold, Untangling aerosol effects on clouds and precipitation in a buffered system, *Nature* 461 (2009) 607-613.
- [10] A. Sorooshian, A.B. MacDonald, H. Dadashazar, K.H. Bates, M.M. Coggon, J.S. Craven, E. Crosbie, S.P. Hersey, N. Hodas, J.J. Lin, A. Negron Marty, L.C. Maudlin, A.R. Metcalf, S.M. Murphy, L.T. Padro, G. Prabhakar, T.A. Rissman, T. Shingler, V. Varutbangkul, Z. Wang, R.K. Woods, P.Y. Chuang, A. Nenes, H.H. Jonsson, R.C. Flagan, J.H. Seinfeld, A multi-year data set on aerosol-cloud-precipitation-meteorology interactions for marine stratocumulus clouds, *Sci Data* 5 (2018) 180026.
- [11] S.J. Piketh, R.J. Swap, W. Maenhaut, H.J. Annegam, P. Formenti, Chemical evidence of long-range atmospheric transport over southern Africa, *J Geophys Res-Atmos* 107 (2002).
- [12] P. Formenti, H. Winkler, P. Fourie, S. Piketh, B. Makgopa, G. Helas, M.O. Andreae, Aerosol optical depth over a remote semi-arid region of South Africa from spectral measurements of the daytime solar extinction and the nighttime stellar extinction, *Atmospheric Research* 62 (2002) 11-32.
- [13] S. Twomey, Influence of Pollution on Shortwave Albedo of Clouds, *Journal of the Atmospheric Sciences* 34 (1977) 1149-1152.

- [14] B.A. Albrecht, Aerosols, Cloud Microphysics, and Fractional Cloudiness, *Science* 245 (1989) 1227-1230.
- [15] M.W. Christensen, G.L. Stephens, Microphysical and macrophysical responses of marine stratocumulus polluted by underlying ships: 2. Impacts of haze on precipitating clouds, *J Geophys Res-Atmos* 117 (2012).
- [16] J. Fan, Y. Wang, D. Rosenfeld, X. Liu, Review of Aerosol–Cloud Interactions: Mechanisms, Significance, and Challenges, *Journal of the Atmospheric Sciences* 73 (2016) 4221-4252.
- [17] M. Tesfaye, V. Sivakumar, J. Botai, G. Mengistu Tsidu, Aerosol climatology over South Africa based on 10 years of Multiangle Imaging Spectroradiometer (MISR) data, *Journal of Geophysical Research: Atmospheres* 116 (2011).
- [18] D.J. Diner, J.C. Beckert, T.H. Reilly, C.J. Bruegge, J.E. Conel, R.A. Kahn, J.V. Martonchik, T.P. Ackerman, R. Davies, S.A.W. Gerstl, H.R. Gordon, J.P. Muller, R.B. Myneni, P.J. Sellers, B. Pinty, M.M. Verstraete, Multiangle Image Spectroradiometer (MISR) instrument description and experiment overview, *IEEE T. Geosci. Remote* 36 (1998) 1072–1087.
- [19] W.A. Abdou, D.J. Diner, J.V. Martonchik, C.J. Bruegge, R.A. Kahn, B.J. Gaitley, K.A. Crean, L.A. Remer, B. Holben, Comparison of coincident Multiangle Imaging Spectroradiometer and Moderate Resolution Imaging Spectroradiometer aerosol optical depths over land and ocean scenes containing Aerosol Robotic Network sites, *Journal of Geophysical Research* 110 (2005).
- [20] R.A. Kahn, B.J. Gaitley, M.J. Garay, D.J. Diner, T.F. Eck, A. Smirnov, B.N. Holben, Multiangle Imaging SpectroRadiometer global aerosol product assessment by comparison with the Aerosol Robotic Network, *Journal of Geophysical Research* 115 (2010).
- [21] A. de Meij, J. Lelieveld, Evaluating aerosol optical properties observed by ground-based and satellite remote sensing over the Mediterranean and the Middle East in 2006, *Atmospheric Research* 99 (2011) 415-433.
- [22] M.T. Freiman, S.J. Piketh, Air transport into and out of the industrial Highveld region of South Africa, *Journal of Applied Meteorology* 42 (2003) 994-1002.

- [23] B.I. Magi, P. Ginoux, Y. Ming, V. Ramaswamy, Evaluation of tropical and extratropical Southern Hemisphere African aerosol properties simulated by a climate model, *Journal of Geophysical Research* 114 (2009).
- [24] A.T. Yakubu, N. Chetty, Optical properties of atmospheric aerosol over Cape Town, Western Cape of South Africa: Role of biomass burning, *Atmósfera* 34 (2020) 395–416.
- [25] G.L. Stephens, On the Relationship between Water-Vapor over the Oceans and Sea-Surface Temperature, *Journal of Climate* 3 (1990) 634-645.
- [26] C.L. Shie, W.K. Tao, J. Simpson, A note on the relationship between temperature and water vapor over oceans, including sea surface temperature effects, *Adv Atmos Sci* 23 (2006) 141-148.
- [27] T.-B. Zhao, Correlation between Atmospheric Water Vapor and Diurnal Temperature Range over China, *Atmospheric and Oceanic Science Letters* 7 (2014) 369-379.
- [28] J.W. Fan, L.R. Leung, Z.Q. Li, H. Morrison, H.B. Chen, Y.Q. Zhou, Y. Qian, Y. Wang, Aerosol impacts on clouds and precipitation in eastern China: Results from bin and bulk microphysics, *J Geophys Res-Atmos* 117 (2012).
- [29] O. Alizadeh-Choobari, M. Gharaylou, Aerosol impacts on radiative and microphysical properties of clouds and precipitation formation, *Atmospheric Research* 185 (2017) 53-64.
- [30] R. Wood, Cancellation of aerosol indirect effects in marine stratocumulus through cloud thinning, *Journal of the Atmospheric Sciences* 64 (2007) 2657-2669.
- [31] Y.-C. Chen, M.W. Christensen, D.J. Diner, M.J. Garay, Aerosol-cloud interactions in ship tracks using Terra MODIS/MISR, *Journal of Geophysical Research: Atmospheres* 120 (2015) 2819-2833.
- [32] Y. Liu, W. Wu, M.P. Jensen, T. Toto, Relationship between cloud radiative forcing, cloud fraction and cloud albedo, and new surface-based approach for determining cloud albedo, *Atmos Chem Phys* 11 (2011) 7155-7170.
- [33] R. Muller, T. Behrendt, A. Hammer, A. Kemper, A new algorithm for the satellite based retrieval of solar surface irradiance in spectral bands, *Remote Sensing* 4 (2012) 622–647.

- [34] C.J. Smith, J.M. Bright, R. Crook, Cloud cover effect of clear-sky index distributions and differences between human and automatic cloud observations, *Solar Energy* 144 (2017) 10-21.
- [35] M.C. Wicking-Baird, M.G. De Villiers, R.K. Dutkiewicz, Cape Town brown haze study, Energy Research Institute, University of Cape Town, Cape Town, South Africa, 1997, pp. 79.
- [36] D. Rosenfeld, Y.J. Kaufman, I. Koren, Switching cloud cover and dynamical regimes from open to closed Benard cells in response to the suppression of precipitation by aerosols, *Atmos Chem Phys* 6 (2006) 2503-2511.
- [37] W.I. Gustafson Jr, L.K. Berg, R.C. Easter, S.J. Ghan, The Explicit-Cloud Parameterized-Pollutant hybrid approach for aerosol–cloud interactions in multiscale modeling framework models: tracer transport results, *Environmental Research Letters* 3 (2008).
- [38] C. Pilinis, J.H. Seinfeld, D. Grosjean, Water content of atmospheric aerosols, *Atmospheric Environment* (1967) 23 (1989) 1601-1606.
- [39] P.R. Nair, K.K. Moorthy, Effects of changes in atmospheric water vapor content on physical properties of atmospheric aerosols at a coastal station, *Journal of Atmospheric and Solar-Terrestrial Physics* 60 (1998) 563-572.
- [40] Z.J. Wu, J. Chen, Y. Wang, Y.S. Zhu, Y.C. Liu, B. Yao, Y.H. Zhang, M. Hu, Interactions between water vapor and atmospheric aerosols have key roles in air quality and climate change, *National Science Review* 5 (2018) 452-454.
- [41] A.S. Ackerman, O.B. Toon, D.E. Stevens, A.J. Heymsfield, V. Ramanathan, E.J. Welton, Reduction of Tropical Cloudiness by Soot, *Science* 288 (2000) 1042-1047.
- [42] X. Yang, M. Ferrat, Z. Li, New evidence of orographic precipitation suppression by aerosols in central China, *Meteor. Atmos. Phys.* 119 (2013) 17–29.
- [43] G. Feingold, A.A. Hill, H. Jiang, The Influence of Entrainment and Mixing Assumption on Aerosol–Cloud Interactions in Marine Stratocumulus, *Journal of the Atmospheric Sciences* 66 (2009) 1450-1464.

- [44] Y.C. Chen, M.W. Christensen, L. Xue, A. Sorooshian, G.L. Stephens, R.M. Rasmussen, J.H. Seinfeld, Occurrence of lower cloud albedo in ship tracks, *Atmos Chem Phys* 12 (2012) 8223-8235.
- [45] A. Smirnov, B.N. Holben, O. Dubovik, R. Frouin, T.F. Eck, I. Slutsker, Maritime component in aerosol optical models derived from Aerosol Robotic Network data, *J Geophys Res-Atmos* 108 (2003).
- [46] C. Ichoku, L.A. Remer, Y.J. Kaufman, R.C. Levy, D.A. Chu, D. Tanré, B.N. Holben, MODIS observation of aerosols and estimation of aerosol radiative forcing over Southern Africa during SAFARI 2000, *J. Geophys. Res.* 108 (2003).
- [47] F. Niu, Z.Q. Li, Systematic variations of cloud top temperature and precipitation rate with aerosols over the global tropics, *Atmos Chem Phys* 12 (2012) 8491-8498.
- [48] I. Koren, G. Dagan, O. Altaratz, From aerosol-limited to invigoration of warm convective clouds, *Science* 344 (2014) 1143-1146.
- [49] J.E. Ten Hoeve, L.A. Remer, M.Z. Jacobson, Microphysical and radiative effects of aerosols on warm clouds during the Amazon biomass burning season as observed by MODIS: impacts of water vapor and land cover, *Atmos Chem Phys* 11 (2011) 3021-3036.
- [50] M.Z. Jacobson, Investigating cloud absorption effects: Global absorption properties of black carbon, tar balls, and soil dust in clouds and aerosols, *J Geophys Res-Atmos* 117 (2012).
- [51] J.H. Jiang, H. Su, S.T. Massie, P.R. Colarco, M.R. Schoeberl, S. Platnick, Aerosol-CO relationship and aerosol effect on ice cloud particle size: Analyses from Aura Microwave Limb Sounder and Aqua Moderate Resolution Imaging Spectroradiometer observations, *Journal of Geophysical Research* 114 (2009).
- [52] Z.J. Lebo, H. Morrison, J.H. Seinfeld, Are simulated aerosol-induced effects on deep convective clouds strongly dependent on saturation adjustment?, *Atmos Chem Phys* 12 (2012) 9941-9964.

## Chapter 4 –

# **Atmospheric aerosol optical properties and radiative forcing over two metros in South Africa**

Abdulaziz Tunde Yakubu<sup>1</sup> and Naven Chetty<sup>1,\*</sup>

<sup>1</sup>School of Chemistry and Physics, University of KwaZulu-Natal, Pietermaritzburg 3209, South Africa.

\*Correspondence: chettyn3@ukzn.ac.za; Tel.: +27-33-260-5660

## 4.1 Abstract

Aerosol Robotic Network (AERONET) measurements and the validation of two prominent satellite retrieval, Multiangle Imaging Spectroradiometer (MISR) and Moderate Resolution Imaging Spectroradiometer (MODIS), are used to examine the properties of aerosols and the direct influence on radiative forcing (RF) over two metropolitan cities, Cape Town (CPT) and Pretoria (PRT) in South Africa. The synoptic characteristics of aerosols over CPT for 2015-2019 indicate a general low aerosol optical depth (AOD) of an average of  $0.08 \pm 0.014$  and are prevalently sea salt (SS) aerosols. In contrast, a high AOD value with an average of  $0.23 \pm 0.050$  was observed over PRT between 2011-2019 and predominated by sulphate/nitrate aerosols. MISR and MODIS satellite retrieval validation demonstrated better accuracy over the land than in the maritime environment. MISR over estimated AOD by  $\approx 40\%$  but generally reported better precision across the board compared to MODIS instrument. Further investigation into the seasonal variation of aerosols over the two locations identified seasonality changes in the characteristics of aerosols mainly influenced by transport of high absorbing biomass burning aerosols. Finally, this work shows that the RF over CPT and PRT is a net cooling effect. However, this effect is motivated by distinct aerosol types in each location.

## 4.2 Introduction

Atmospheric aerosols are known to influence global weather and climate conditions. However, the extent of this influence solely and relatively to other phenomena that impact observable changes in the weather and climate system forms a significant source of ambiguity [1, 2]. Aerosol particles significantly interact with incoming solar radiation directly through scattering and absorption and indirectly by modifying the clouds microphysical properties [3], thus serving as cloud condensation and ice nuclei (CCN and IN) during cloud formation [4, 5]. Also, aerosols interact with terrestrial radiation (longwave radiation) via absorption and re-emission of electromagnetic radiation [6]. The interaction of these particles with solar as the primary energy source and terrestrial radiations results in the earth's energy budget perturbation, hence, driving the changes in weather and climate conditions [3, 6]. More so, aerosols influence differing atmospheric and environmental challenges ranging from poor air quality, health problems, low visibility, and a dusty environment [7-9] which are detrimental to human survival and general well-being. In contrast, aerosols are vital components of cloud formation and rainfall and sometimes serve

as an essential source of soil nutrients favourable to humans [9, 10]. Therefore, regular qualitative and quantitative assessments are crucial for properly managing its consequences regarding their impacts on the earth's energy budget and inhabitants.

Aerosols are emitted from different sources, vary in types and properties, and the distribution is susceptible to spatio-temporal changes [11]. Also, based on the listed characteristics, aerosol particles influence the earth and its atmosphere to a varying degrees on a regional and global scale [1]. However, due to the poor understanding of how different aerosol characteristics translate to differing atmospheric and climate phenomena, their impacts are associated with significant uncertainty [1, 12]. Proper measurements and assessments become critical in characterising aerosols and their corresponding effects efficiently.

Over the years, various approaches have been employed to measure and determine aerosol characteristics, including in-situ measurement, ground, and satellite remote sensing, modelling, and prediction [13-15]. Each process has distinct drawbacks ranging from spatial coverage, temporal stability, and sensitivity. In-situ or field campaigns are the most accurate method of monitoring aerosol but have significant disadvantages of limited spatio-temporal coverage [16-18]. Thus, in practice, remote sensing from both ground and satellite platforms constitutes the most commonly used method of aerosol measurement [11]. These methods are mainly advantageous due to their effectiveness in measuring the total column values of aerosol and non-intrusiveness [19]. Besides, they possess considerably high stability in terms of temporal and spatial coverage. Although ground observation is still ranked the most effective remote form of observing aerosol properties, they are yet faced with the limitation of poor spatial coverage. Satellite-measured aerosol properties are less efficient, though they possess an uninterrupted temporal and broader spatial range [11, 20]. Therefore, ground and satellite remote sensing synergy for aerosol monitoring has demonstrated promising results [21]. Meanwhile, modelled generated aerosol data is also stable temporally and spatially but prone to several errors since such data depends on in-situ, ground, and satellite data. Applying any or the synergy of these methods has helped describe aerosol characteristics and investigate its impacts on climate [11, 20, 22].

Both natural and anthropogenic aerosols are found as a mix globally. However, several studies have argued that the increase in anthropogenic aerosols leads to the current challenge posed by climatic change [1, 23, 24]. Previous studies have demonstrated that the aerosol suspension over an area is a function of both localised generated and in-ward transported

aerosols from the external origin [11]. Hence, the characteristics of aerosol suspended can be predominantly localised generated aerosols or influx of transported aerosol. Several studies have shown that internally generated aerosols that mainly form a canopy over urban/industrialised environments emerge mainly from anthropogenic sources [23-25]. However, the occasional influx of transported aerosols also increases the aerosol suspended in rare cases. In contrast, rural and semi-urban areas are dominated by natural aerosols and mainly account for the sharp increase in aerosol suspension due to the influx of transported particles [18, 26]. As an advance, the different aerosol suspension has differing impacts on the region. Studies around various parts of the world have shown fine mode particles with generally absorbing characteristics and mainly originating from anthropogenic sources dominate urban/industrial sites [1, 11]. The typical impact associated with this aerosol environment is an increase or decrease in the radiative forcing [4, 25] due to the absorbing or scattering nature of the predominant particles, depending on the composition of the suspended aerosols.

Studies around urban/industrial areas such as America [18], Europe [7, 27] and Central Asia [25] have shown that the impact of suspension due to urban/industrial aerosols on radiative forcing is positive due to the strong absorption features of the constituents. Meanwhile, related studies in a similar setting have observed the reverse [28]. More so, polluted environments have been presented to suppress precipitation formation [10, 29]. However, some studies have also found precipitation enhancement by high aerosol loading [10, 30]. Studies have consistently explained the two situations to be mainly influenced by atmospheric dynamics and thermodynamics [10, 31].

Over South Africa (SA), some studies have been carried out on the characterisation of atmospheric aerosols suspended in the region. These include aerosol optical properties, the effect on radiative forcing, impacts on cloud and precipitation, and air pollution, among others [16, 17, 32, 33]. Generally, from previous studies, aerosols over SA exhibit seasonality centred around spring and aerosol loading is highest in the upper parts compared to the lower areas [11, 33, 34]. Similarly, these studies show that the upper parts are distinctly dominated by fine mode aerosol, while the lower parts are a mix of coarse and fine aerosols. The primary sources of aerosols identified by studies depend on the level of industrialisation, population and other related human activities. They are sometimes enhanced by seasonal biomass burning aerosol from neighbouring communities.

Regarding spatial coverage, most studies have investigated aerosol activities in fewer locations based on ground data such as AERONET [35, 36] and more multilocation studies using satellite instruments [33, 34]. However, validation of satellite aerosol retrieval over SA is still minimal, and most studies using ground instruments such as sun photometers are mainly single location-based observations. Only a few studies [11, 32] have examined the validation of satellite measurement over the region to date which is limited to small spatial coverage and often involve selected parameters. With the growing industrialisation and population across the region, urban expansion calls for more climate actions, hence, understanding aerosol properties and the accompanying impacts become essential. Besides, more study is needed towards the validation of satellite retrieved and modelled generated data considering the huge gap set by satellite-based predominated studies over the region. This approach will enhance the reliability of satellite-based observations in studying aerosol regionally and globally.

This work investigates aerosol optical characteristics and the consequential impacts on radiative forcing over two metropolises in South Africa with distinct industrial and population footprints. Each of the two study areas represents the upper and lower part of the country, respectively and is strategic to entire Southern Africa. Furthermore, the areas are host to AERONET sun photometers and boast relatively consistent data in terms of availability amongst peers. The study explores the advantages of these two sites' attributes (as mentioned above) to understand the aerosol characteristics and radiative effects of locally generated and inward transported aerosols. The role of naturally emitted and anthropogenic aerosols over each environment and proxy location is examined. Equally important, data from two satellite instruments over the sites will be validated using the AERONET data. The results present a comprehensive insight into identifying the types and sources of aerosols in South Africa and their effects on the region. Further, the study will assist in deciding on an appropriate measure to tackle the climate change issue. Also, this output portrays a significant advance towards optimising satellite retrieval of aerosol measurements over Africa and enhancing modelling of the same over the region. Subsequently, section two describes the data, sources, and general approach to this study. Sections three and four give the study's detailed methodology and general discussion. Finally, the summary and a brief conclusion of the outcomes of this work are presented in section five.

## 4.3 Method

### 4.3.1 Sites

This study focused on two strategic metros (Pretoria and Cape Town) in South Africa, separated  $\approx$  by 2000km within the region's geographical space (see Figure 4.1). Cape Town ( $33.92^\circ$  S,  $18.42^\circ$  E) is one of the largest metropolitan areas in SA, located in the southernmost and coastal parts of the region. The area has a mountainous and hilly landscape, including the famous Table Mountain, a popular tourist site. Also, the environment is typically a marine environment due to the nearness to the coast of South Africa. Cape Town is home to several industrial and commercial activities and represents the economic centre of the Western Cape Province. The area with a population of over 2 million people is involved in different industrial and domestic activities that result in the emission of a considerable amount of aerosols. Aerosols such as  $\text{SO}_2$ , NO, black (BC) and organic carbons (OC) are typical of this location. Some aerosol impacts in this area include increased air pollution, weather changes, and associated health implications. Between the years 2013 and 2015, the region experienced low rainfall and was potentially prone to drought [11]. Similarly, a slight rise in air pollution and poorer air quality are observed during the period 2014 to 2018.

Pretoria ( $25.75^\circ$  S,  $28.28^\circ$  E) is in Gauteng province north-east of South Africa, with another metropolis, Johannesburg, known as the country's economic capital. Due to the proximity to another metro city (i.e., Johannesburg), the neighbouring city's population and activities significantly influence this area. Pretoria, popularly known as the administrative domain of SA, is home to extensive industrial activities, particularly the heavy steel industries. Mining activities and the coal power plant around the area are also essential sources of aerosol emission. In the last two decades, the city has suffered climate change impacts such as heat waves, precipitation drops, and drought. Considering the notion of aerosols inducing changes to the climate pattern in an environment, thus, understanding the characteristics of aerosols over an area and the associating impacts is crucial for effectively mitigating the possible negative influences. Besides, this study will enhance the characterisation of aerosols regionally and globally.

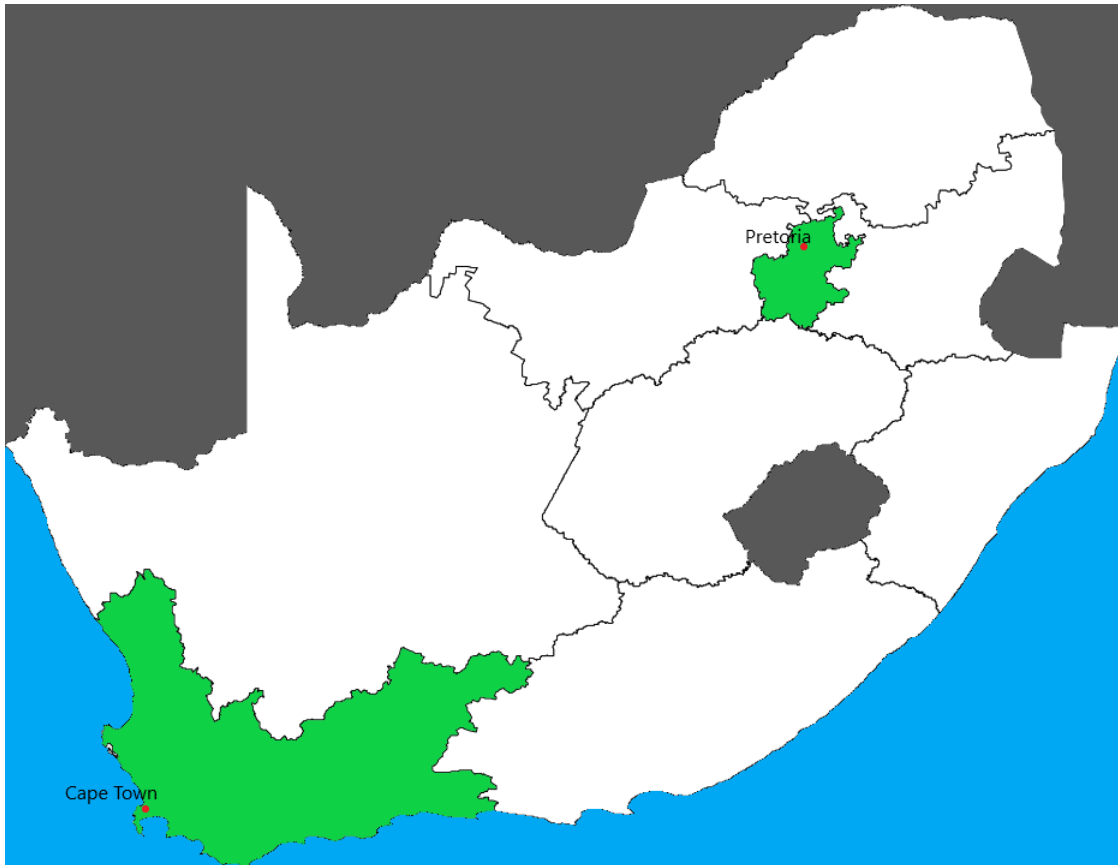


Figure 4.1 A map of South Africa showing the locations of Cape Town and Pretoria.

#### **4.3.2 Data**

For a detailed understanding of the aerosol properties and their corresponding impacts, this study utilises data from ground and satellite platforms to demonstrate the result presented in this work. The ground observation data is from the AERONET (Aerosol Robotic Network) stations in both locations. AERONET is a ground-based network of sun photometers that monitors the near real-time global distribution of aerosol spectral optical thickness through measurements of the direct sun collimated and sky radiance. The radiometers within the network take measurements at eight spectral bands: 340 nm, 440 nm, 500 nm, 675 nm, 870 nm, 970 nm and 1020 nm. The direct sun radiation is measured in all eight spectra, while the sky radiation is obtained at four wavelengths (440 nm, 670 nm, 870 nm and 1020 nm). Furthermore, AERONET provides aerosol optical depth (AOD) measurement at seven spectral bands and a nominal uncertainty of  $\approx \pm 0.01-0.02$  [37, 38]. From the AOD measurements at two reference wavelengths, another vital parameter, the Ångström exponent (AE), which gives some insight into the size characteristics of aerosols, is obtained. Also, from the spectral deconvolution algorithm (SDA), other properties such as the fine mode

fraction (FMF) and AOD ( $\tau_f$ ) are inferred from AERONET sun photometers measurements. Apart from the optical parameters, the network of radiometers produces microphysical parameters, including the volume size distribution, single scattering albedo (SSA), refractive indices (RI), and absorbing AOD ( $\tau_{\text{abs}}$ ), amongst others, using the flexible inversion algorithm and the sky radiance measurement as input. Several works have documented a detailed description of the retrieval method and products following the flexible inversion algorithm [11, 14]. In this work, the level 1.5 scientific datasets from AERONET measurements for Pretoria and Simons Town sites were utilised to present the documented results. The preference for level 1.5 (cloud screen only) over level 2.0 (cloud screen and quality assurance) datasets is due to the size of datasets offered by the former and the consistency level ( $> 90\%$ ) compared with the latter, as observed from the two sites. Generally, the AERONET data is vital to this study as it creates an insightful view of aerosol optical and microphysical properties over the locations and acts as a validator to satellite and modelled derived data.

Both satellite data used in this study are measurements obtained from two instruments on board the Terra satellite, one of the A-train constellation satellites. The Multiangle Imaging Spectroradiometer (MISR) instrument measures the reflected solar radiation from the earth's surface by nine different cameras positioned at different angles; nadir,  $\pm 26.1^\circ$ ,  $\pm 45.6^\circ$ ,  $\pm 60.0^\circ$  and  $\pm 70.5^\circ$ , to monitor changes in global climate. Each of the nine cameras operates at four wavelengths; blue (443 nm), green (555 nm), red (670 nm), and infrared (865 nm) to provide various scientific datasets on aerosol and cloud properties beneficial for the proper characterisation of their impact on global climate. MISR possesses the advantage of being carefully calibrated to operate at optimal accuracy to provide data at high spatial resolution. Besides, the instrument offers the classification of aerosol particle size distribution among its peers. In the present study, level 3 daytime daily and monthly data at a spatial resolution of  $0.5^\circ \times 0.5^\circ$  are utilised to present additional results.

On the other hand, Moderate Resolution Imaging Spectroradiometer (MODIS) possesses the radiometric capabilities to measure the reflectance from both cloud and earth surface at 36 different spectrums ranging from visible to infrared wavelengths. The instrument monitors the activities of aerosol and cloud at a horizontal resolution between 250 m and 1 km. Datasets from MODIS instrument form the basis of several studies, particularly over vast areas with no ground instruments. Hence, it is crucial to validate the data available from this

instrument over all possible locations to assess the credibility in evaluating the past, present and future states of the atmosphere. Daily and monthly standard level 3,  $1^\circ \times 1^\circ$  gridded datasets are used for the analysis presented in this paper.

## 4.4 Results

### 4.4.1 Aerosol optical properties statistics

The monthly averages of the parameters AOD, AE, FMF, AOD<sub>abs</sub>, SSA and WVC over the study period 2015-2019 for Cape Town (CPT) and 2011-2019 for Pretoria (PRT) are presented in Figures 4.2 and 4.3. Generally, aerosol loading measured by AOD is lower in CPT (AOD<sub>av\_440</sub> =  $0.08 \pm 0.014$ ), typical of the maritime environment [18], compared to PRT ( $0.23 \pm 0.050$ ), which boasts of more industrial activities, especially in the heavy metal industries. These observed values agree well with reported ones from previous studies [11, 36]. Also, noticeably, the two locations differ in the period of min-max occurrence of aerosol loading due to slight differences in climate patterns. Remarkably, the meteorological states are critical to aerosol characterisation owing to their roles in suspension and removal from the atmosphere. CPT is associated with the winter rainfall season resulting in the increase in aerosol removal by scavenging clouds ahead of the rainy season and is suggestively accountable for the minimum AOD (0.060) in April, as shown in Figure 4.2a, while the continuous suspension and the influx of air masses carrying aerosol is linked to maximum AOD (0.103) in August and most parts of spring.

Meanwhile, the case slightly differs from Pretoria, as illustrated by Figure 4.2b, such that the minimum AOD (0.159) occurred in June and the maximum (0.341) in September extending the spring season like in CPT and often associated with the events of biomass burning (BB) during the pre-farming season. Studies have repeatedly linked the BB events accounting for the high aerosol turbidity over the two springs locations, mainly emanating from the northern parts of South Africa and neighbouring countries. The concentration over each site is a function of the proximity [11, 16, 32, 39].

Following the characteristic aerosol loading over the study sites, CPT demonstrated the predominance of coarse particles (i.e.,  $AE < 1.0$ ) with a multiyear monthly average of  $0.733 \pm 0.128$ . At the same time, PRT tends more toward fine mode aerosols (i.e.,  $AE > 1.0$ ) with an average value of  $1.517 \pm 0.072$ . From Figure 4.2c, the minimum monthly mean AE (0.504 in March) and general lower AE over Cape Town occurs during the summer and autumn

months and coincide with the period of lower aerosol loading over the site. This variation significantly portrays the feature of a typical maritime site with the predominance of sea salt (SS) aerosol. Several studies over similar sites [18, 40] and this current site [11] have demonstrated comparable variation and linked to a coastal site predominated by coarse aerosol of sea salt origin. Similarly, the maximum monthly mean (0.929 in September) represents finer particles and corresponds to the period of high atmospheric turbidity and consists mainly of the spring months characterised by biomass burning and fossil fuel combustion. In contrast, aerosol suspension over Pretoria is chiefly dominated by fine mode aerosols, the mean monthly average AE (1.52). Emissions from industrial activities, vehicular movement, and other domestic activities are more likely to account for this variation. Meanwhile, the minimum AE (1.409 in July) and during the summer months suggest more coarse particles, mainly mineral dust (MD), due to the high AOD. The maximum (1.597 in December) and generally from spring to autumn indicates the enhanced emission and suspension of fine mode particles, which is also influenced by the BB influx from external sources. This AE characteristic over PRT is consistent with the observation from a previous study over the site [36].

To further examine the particle size characteristics over the study sites, the FMF variation from the spectral deconvolution algorithm (SDA) for the sites is presented in Figures 4.2d and e (i.e., for CPT and PRT, respectively). Coarse mode dominates atmospheric aerosol suspension over CPT, with FMF mostly less than 0.5 during most months of each season, such that the monthly average value ( $0.45 \pm 0.056$ ) reflects the dominance. This observation, coupled with the AOD and AE variation earlier described, strongly demonstrates SS as the primary aerosol type over the region. Hence, the minimum average FMF (0.360 in March) and most months display the strong dominance of SS aerosol over the area with less pollution, while the maximum mean (0.542 in September) and a large part of winter signify an increase in pollution and considerably align with the earlier description in this work and hypothesis from a previous study [11] of the influx of polluted air mass mainly linked to BB aerosol (i.e., aged smoke) from the northern part of South Africa. Contrastingly, FMF variation over PRT with a monthly mean value ( $0.780 \pm 0.029$ ) further illustrates the predominance of fine mode aerosol in the site. The minimum FMF (0.730 in November) represent the period of less influx of external air pollution (such as aged smoke), while the maximum (0.821 in September) demonstrates the enhancement of internal pollution suspension by the external influx of aerosol particles.

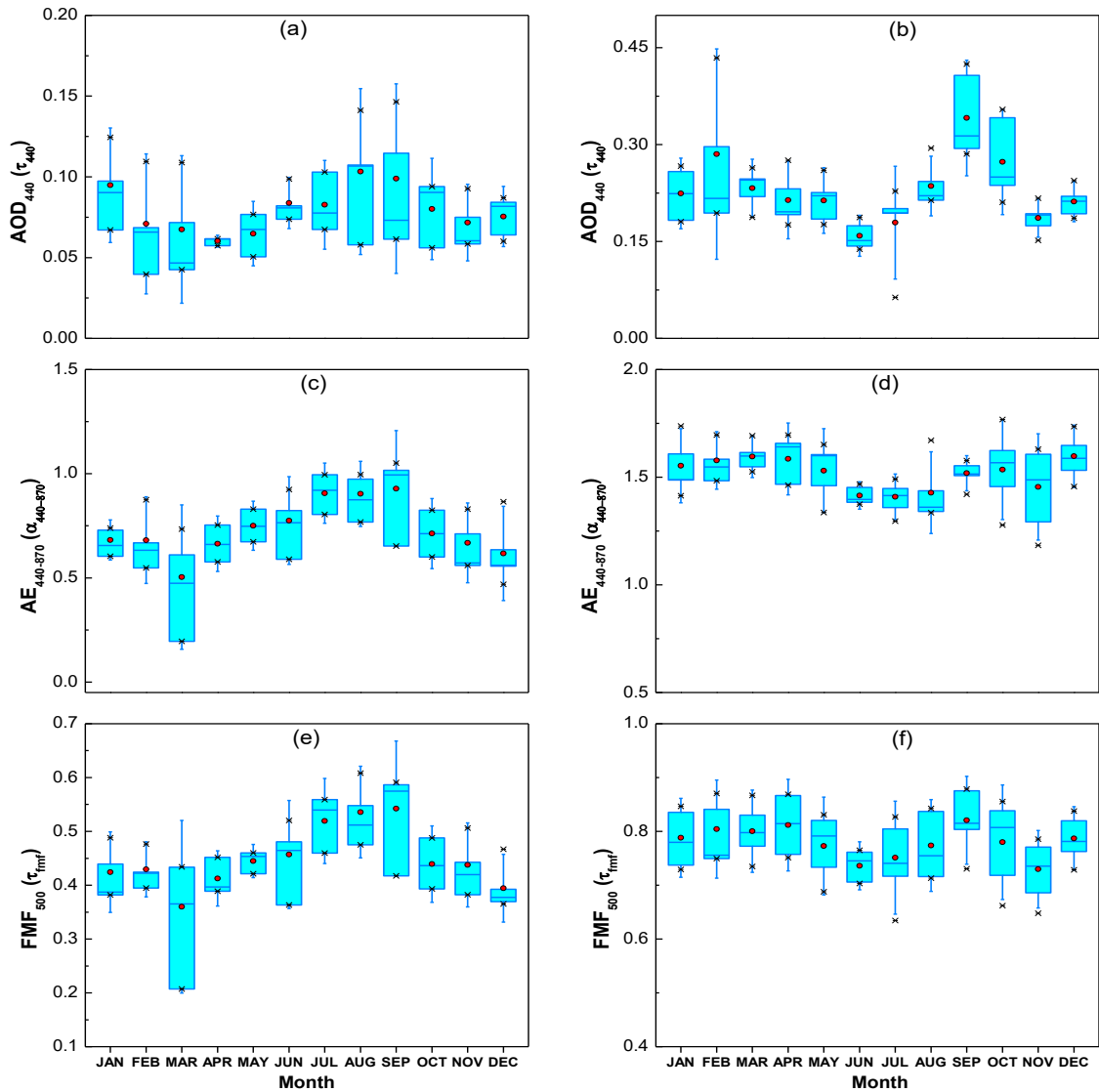


Figure 4.2 The graphs of the multiyear monthly mean AOD, AE and FMF for Cape Town; (a), (c) and (e), and Pretoria; (b), (d) and (f).

Figures 4.3a and 4.3b illustrate the variation of absorbing AOD ( $AOD_{abs}$  or  $\tau_{abs}$ ) over Cape Town and Pretoria, respectively.  $AOD_{abs}$  also constitute a vital property in aerosol characterisation and enhance the identification of different aerosol types. Aerosols such as carbon soot (CS) and black carbon (BC) are strong absorbers of solar radiation, hence, identifiable by high  $\tau_{abs}$ . Low or relatively moderate  $\tau_{abs}$  can infer moderately absorbing aerosols such as organic carbon (OC) and MD; those with poor absorbing properties are differentiable by extremely low  $AOD_{abs}$ . On this note,  $\tau_{abs}$  is generally low over CPT (mean  $\tau_{abs} = 0.005 \pm 0.002$ ) compared to PRT (mean  $\tau_{abs} = 0.019 \pm 0.009$ ) with  $\approx 4$ -times absorbing characteristics of CPT. The features presented by the  $AOD_{abs}$  variations in the two locations support the pattern demonstrated by AOD, AE and FMF. Also, the differences in  $\tau_{abs}$  between

the two sites beam more insight into the role of proximity in the aerosol characteristics over each location.

Similar but opposite to  $\tau_{\text{abs}}$ , the single scattering albedo (SSA or  $\omega$ ) variation over the study locations is described in Figures 3a and b for CPT and PRT, respectively. Over CPT, the monthly mean  $\omega$  value is  $0.932 \pm 0.022$  suggesting a considerable dominance of scattering suspensions. Factoring the variations portrayed by AOD, AE, FMF, and AOD<sub>abs</sub>, the evidence of SS matching the predominance aerosol type over the Cape Town site is more apparent. The finding is consistent with the previous studies on the location [11]. Nevertheless, it is vital to note from the min-max SSA (i.e., 0.897- 0.967) that aerosol suspended over this site sometime constitutes the mix of coarse-fine mode particles leading to characteristics shift in the value of SSA from strong to less scattering. Internal emissions such as domestic and industrial emissions and aged smoke-bearing air mass influx are often liable to these changes.

Similarly monthly mean  $\omega$  in PRT is  $0.899 \pm 0.027$ , thus indicating a more absorbing-scattering mix typical of an urban-industrial location. The minimum average SSA (0.860) occurs in August, and the maximum value (0.948) is recorded in December. Minimum SSA and lower values are chiefly associated with the winter and spring months, coinciding with the pre-planting period in South Africa and bordering countries. SSA variation combined with other aerosol properties over Pretoria gives a clearer picture of the dominance of Sulphate and nitrate and the influence of less scattering and more absorbing aerosols (black and organic carbon) around the winter and spring, thereby changing the spectral properties of suspended particles.

Figures 3e and f illustrate the variations of atmospheric water vapour content (WVC) for CPT and PRT. AWV or precipitable water for both locations are similar in interpretation such that atmospheric vapour is lowest during winter (i.e., CPT - 1.17 cm and PRT - 0.67 cm, both in July) and highest in summer (CPT - 1.99 cm in January and PRT – 2.05 cm in December). This pattern is typical for all parts of South Africa, where WVC is all high during summer and lowest in winter. The monthly average WVC for the sites is  $1.52 \pm 0.29$  cm and  $1.35 \pm 0.54$  cm for Cape Town and Pretoria, respectively. Notably, WVC over CPT is larger than the value for PRT and is linkable to the nearest to the ocean.

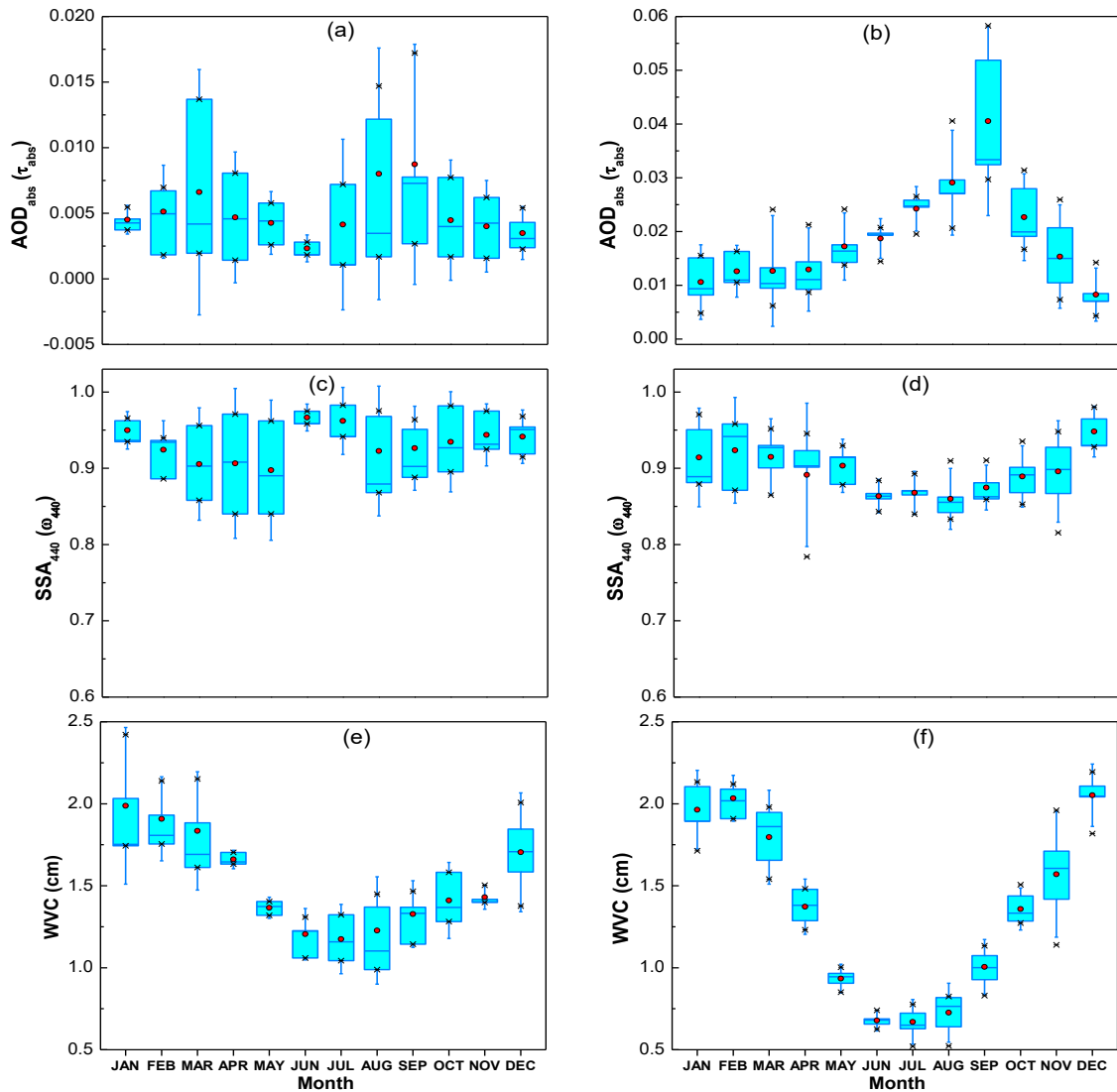


Figure 4.3 The plot of monthly mean AOD<sub>abs</sub>, SSA<sub>440</sub> and WVC for Cape Town; (a), (c) and (e), and Pretoria; (b), (d) and (f) over their respective study periods.

#### 4.4.2 Validation of satellite retrieved data

Figure 4 shows the validation of satellite observation of aerosol parameters over the locations under investigation in this work against ground measured values. Figures 4.4a and 4.4b represent Cape Town and Pretoria, respectively, and the AOD from MODIS and MISR are validated against AERONET observation. For measurement over CPT, MISR observation demonstrate better agreement with AERONET with correlation (R) and significance (P) values  $R = 0.60$  and  $P = 0.04$  than MODIS ( $R = 0.48$  and  $P = 0.12$ ). However, MISR tends to overestimate AOD by over 40% compared to AERONET measurement at the location. As for MODIS, the mean-min-max values are slightly closed to that of AERONET but with inconsistent factors (i.e., by -3%; < -11%; > 4% for mean; min; max). Similarly, MISR

accuracy ( $R = 0.75$ ;  $P = 0.005$ ) is slightly better than MODIS ( $R = 0.74$ ;  $P = 0.006$ ) over PRT. Both instruments underestimated (MISR averagely by -14% and MODIS by -47%) AOD compared to AERONET measurement.

AE measurements from the two instruments (MISR AND MODIS) over the locations under investigation are compared to AERONET obtained measurement is presented in Figures 4.4c (CPT) and 4.4d (PRT). MODIS shows better accuracy ( $R = 0.54$ ;  $P = 0.07$ ) compared to MISR ( $R = 0.01$ ;  $P = 0.97$ ) measurement of AE over CPT. The cause of this low accuracy demonstrated by MISR for AE estimate over CPT results from poor aerosol properties retrieval over the water surface, mainly owing to the location's closeness to the sea. However for PRT the pattern quite differs with MISR portraying stronger but negative correlation (i.e.,  $R = -0.48$ ;  $P = 0.12$ ) with AERONET compared to MODIS ( $R = 0.33$ ;  $P = 0.30$ ) measurement. The cause of the negative R-value in the case of MISR is not immediately clear. Still, suggestively, such divergence is likely to be inherited from the uncertainty in AOD retrieval, probably at one of the adopted wavelengths.

The validation of  $AOD_{abs}$  for the satellite instruments over CPT and PRT is illustrated in Figures 4.4e and 4.4f, respectively. From the figures, again MISR dataset shows far better consistency with  $R = 0.42$ ;  $P = 0.17$  compared to MODIS ( $R = 0.052$ ;  $P = 0.87$ ). Although both instruments demonstrate poor performances in terms of statistical significance, their datasets still provide useful insights regarding aerosol absorbing properties over the region. As for PRT, the instruments still demonstrate their properties of better performance over land than over water surfaces. MISR maintain the lead in accuracy with  $R > 0.85$ ;  $P \ll 0.001$  as validated against AERONET measured values. In contrast, MODIS also post a strong accuracy ( $R = 0.70$ ;  $P = 0.011$ ) over the region.

According to the SSA variation over CPT in Figure 4.4g, both instruments recorded negative and weak relationships against the AERONET dataset. MODIS measured  $\omega$  displayed a stronger relationship (i.e.,  $R = -0.34$ ;  $P = 0.28$ ) with the ground instrument compared to MISR ( $R = -0.23$ ;  $P = 0.48$ ). The negative correlation, which in this case represents the disagreement level exhibited by the satellite instruments, probably results from the sensitivity error over the observed environment. Meanwhile, the satellite instruments demonstrated far better accuracy against the ground instrument measurement of  $\omega$  over PRT, as observed from Figure 4.4h, than observation over CPT. The SSA measurement over PRT by the MODIS instrument is more consistent (i.e.,  $R = 0.80$ ;  $P = 0.002$ ) than MISR obtained measurements

(i.e.,  $R = 0.71$ ;  $P = 0.009$ ). Overall, it is convenient to deduce that the accuracy of the instruments is significantly influenced by the environment and surface type, as observed from the two site measurements.

Figures 4.4i and 4.4j illustrate the comparisons between MODIS and AERONET precipitable water measurements for CPT and PRT, respectively. The satellite (MODIS) instrument shows robust agreement with the ground counterpart in the two locations. As expected, the accuracy over PRT ( $R = 0.99$ ;  $P \ll 0.0001$ ) supersede that of CPT ( $R = 0.97$ ;  $P \ll 0.0001$ ), and obviously accountable to the satellite instrument retrieval precision over land compared to water surface. This result consistently agrees with previous global studies [11, 41, 42].

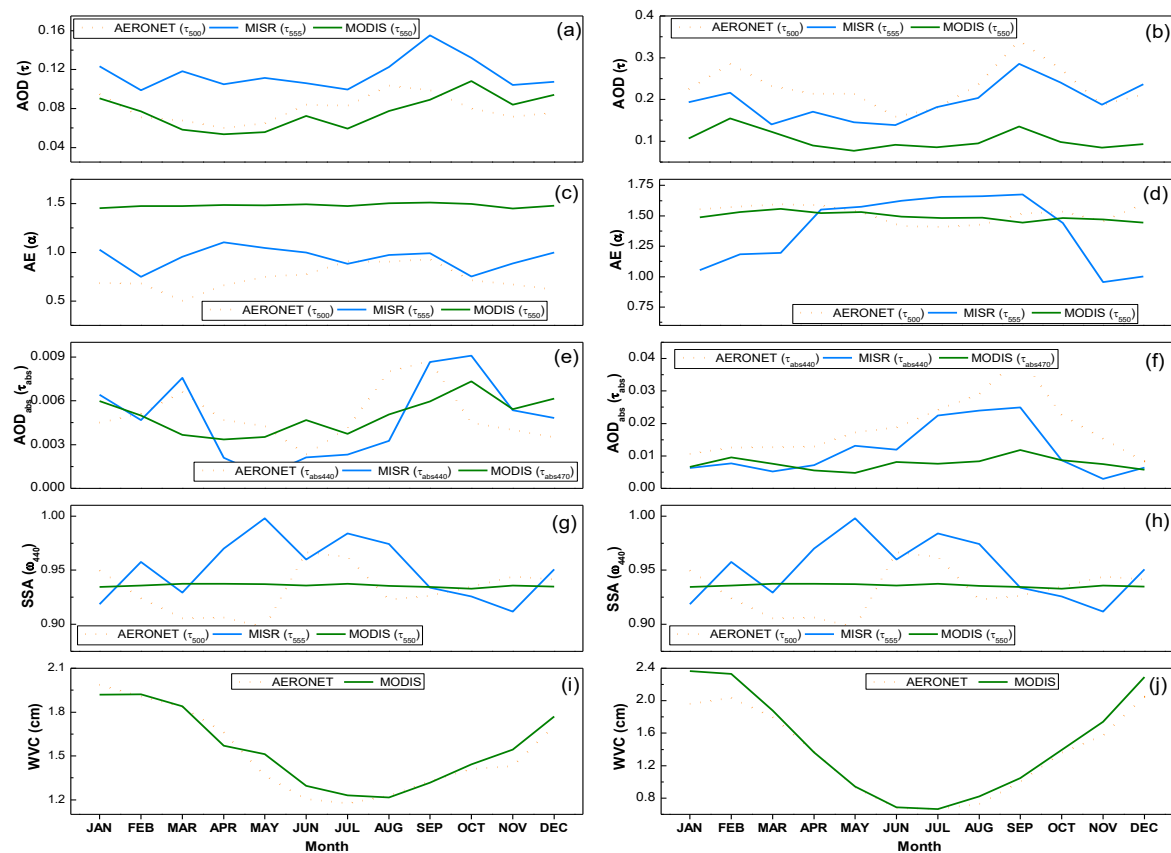


Figure 4.4 The plots of comparisons amongst AERONET, MISR and MODIS instrument data on AOD, AE, AOD<sub>abs</sub>, SSA and WVC for CPT (left panels) and PTR (right panels).

#### 4.4.3 Relationships amongst optical properties

In this section, the relationships AE vs AOD, SSA vs AOD, AE vs AOD<sub>abs</sub> and aerosol index (AI) vs WVC are presented in Figure 4.5 to further understand the aerosol characteristics over the study locations through examining the interrelations among previously observed parameters. AI represent a new parameter defined as  $AOD * AE$  to factor the aerosol loading

along with the size distribution in a single term. Figure 4.5a shows the relationship between AOD and AE for Cape Town. Mainly, low aerosol loading is characterised by small particle size (i.e.,  $\tau_{440} < 0.1$  mostly for  $\alpha_{440-870} < 1.0$ ), AOD between 0.1 and 0.15 consist more mixed particle size (coarse and fine) and high atmospheric pollution over the location is dominated by fine-mode aerosols ( $\tau_{440} > 0.15$  correspond to  $\alpha_{440-870} > 1.0$ ). Similarly and more obviously, low aerosol loading over Pretoria is dominated by coarse-mode aerosols (i.e.,  $\tau_{440} < 0.1 \equiv \alpha_{440-870} < 1.0$ ) and  $\tau_{440} > 0.2 \equiv \alpha_{440-870} > 1.0$  as observed from Figure 4.5b.

The plot of SSA vs AOD for CPT in Figure 4.5c demonstrate predominant scattering (i.e.,  $\omega > 0.9$ ) for  $\tau_{440} < 0.2$ , then the region of  $\omega < 0.9$  characterised by  $\tau_{440} > 0.2$  and the cluster of  $\omega > 0.9$  with mostly high aerosol loading (i.e.,  $\tau_{440} > 0.15$ ). The first described region exhibits the characteristic of SS aerosols, the next is likened to carbon emission (including carbon soot, OC, and BC), and the last segment depicts sulphate and nitrate presence. This observation is consistent with the findings in the previous section and earlier study [11], considering the environmental characteristics of CPT, the biomass activities (including forest fire), the influx of aged smoke, and the level of industrial activities. For Pretoria in Figure 4.5d, again the variation is more obvious with the predominant spread of  $\text{SSA} > 0.9$  extending from low to high aerosol loading (i.e.,  $0.15 < \tau_{440} < 1.20$ ) and the region of  $\omega < 0.9$  for  $0.15 < \tau_{440} < 0.90$ . The first segment depicts the dominance of aerosols mostly from fossil fuel (FF) combustion (both domestic and industrial settings), such as sulphate and nitrate. The second part represents more mixed emissions from combustion activities (such as BB and FF) and mineral dust (MD). The characteristics of  $\omega$  vs  $\tau_{440}$  provide considerable evidence of CPT being SS rich, receiving low-moderate FF emissions and is seasonally polluted by the combined internal and external low emissions from BB. In contrast, PRT demonstrates a large suspension of sulphate and nitrate aerosols through regular emissions from FF activities and seasonal enhanced pollution by a large concentration of BB aerosol constituents (like BC, OC and soot).

The relationship between particle size and absorption strength for CPT in Figure 4.5e shows relatively higher  $\tau_{\text{abs}}$  ( $> 0.02$ ) are mainly fine-mode aerosols such as BC and OC. At the same time, the lower absorbing feature is associated with predominantly coarse mode aerosols suspected to be SS and considerable fine-mode concentration typical of FF combustion emission (sulphate and nitrate). In the case of PRT (Figure 4.5f), aerosols of low absorption dominate the location. Hence, lower  $\tau_{\text{abs}}$ -value mainly coincide with smaller sized particles

( $AE > 1.0$ ), likewise for  $AOD_{abs}$  with higher value ( $\tau_{abs} > 0.04$ ). The first feature is typical of sulphate and nitrate aerosols, and the second is more of BC and soot. Meanwhile, the cluster of  $AE < 1.0$  and  $AOD_{abs} < 0.02$  comprises coarse non-absorbing aerosols such as mainly MD considering the geographic location and presence of SS aerosol.

Figure 4.5g and h respectively illustrate the variation of AI with WVC for CPT and PRT. For CPT, increasing vapour content is accompanied by a moderate rise in the AI, especially in the range of implies growth in the particle sizes due to water intake. Similarly, hygroscopic particle growth is evident for PRT following the rise in AI with WVC. This observation supports the evidence of  $WVC = 1$  to  $2.5$  cm, which the predominance of SS aerosols in CPT and sulphate-nitrate combination in the case of PRT, as depicted by the earlier figures (i.e., Figures 5a-f).

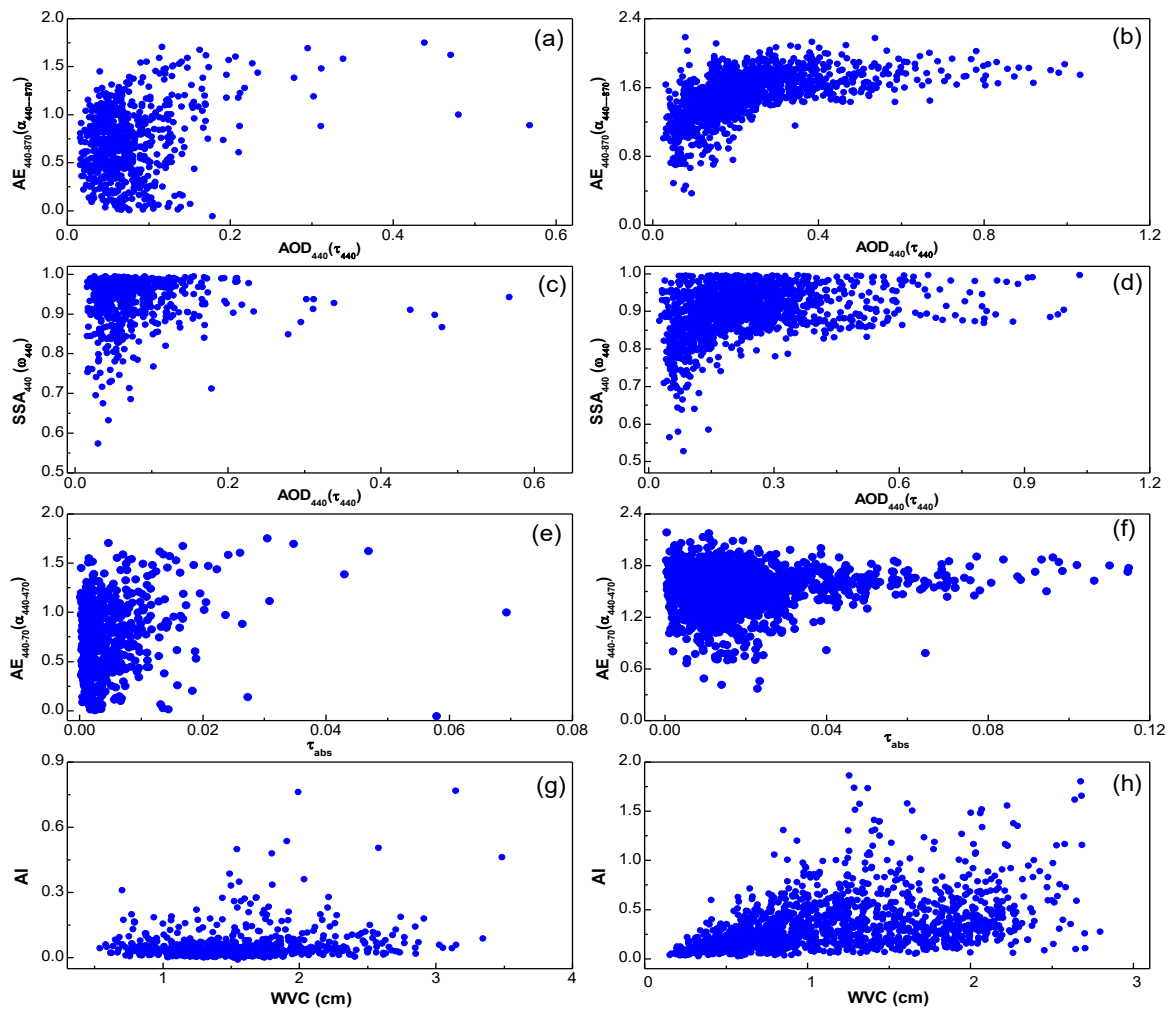


Figure 4.5 The plots of the relationships between AERONET, MISR and MODIS instrument measurement of the parameters AE vs AOD, SSA vs AOD, AE vs  $AOD_{abs}$  and AI vs WVC for CPT; (a), (c), (e) and (g), and PRT; (b), (d), (f) and (h).

#### ***4.4.4 Particle size distributions***

The multiyear monthly average particle size distribution (PSD) for CPT in Figures 4.6a and 4.6b mainly displays bimodal characteristics distinctly signifying fine and coarse mode particles. Remarkably, the fine mode represents the region of radius ( $r$ )  $< 0.4\mu\text{m}$ , and the coarse mode is marked by  $r > 0.4\mu\text{m}$ . Obviously, from the PSD variation in the figures, the coarse mode aerosol demonstrates the predominance and association with SS and possibly traces of MD. Several studies have shown that CPT is not prone to MD aerosol due to its general environmental characteristics, including not being within the proxies of any desert region and possession of paved and tarred roads, such that the main dust source is through occasional sedimentary weathering of rocks [11, 34]. The rise in the buildup of coarse mode volume concentration is observed in March and January, while a significant increase in fine mode particles is noticeable July-September. These features are more apparent in the seasonal variation in Figure 4.6e, where distinct intensification of coarse mode particles is visible for summer, and peak concentration of fine mode aerosols is detectable in winter.

A substantial and distinct rise in the fine mode aerosol concentration (i.e.,  $r < 0.6\mu\text{m}$ ) is evident in February and September over PRT, thus demonstrating the predominance of fine particles as illustrated by the monthly average in Figures 4.6c and 4.6d. Additionally, several other peaks are observable in the region of  $r > 0.6\mu\text{m}$ , particularly for May, June, and September, as seen in the figures. These peaks represent the suspension of a significant amount of large-sized particles mainly due to hygroscopic growth of hydrophilic aerosols (such as sulphate and nitrate) and emission from biomass burning activities (carbon soot), including from internal and external sources (i.e., considering the period of peak). This finding agrees well with the observation from several existing studies on the location [33, 36, 42]. Further to the monthly variation of PDS over PRT, Figure 4.6f display the seasonal changes in the bimodal characteristics of the PSD. The highest concentration of both coarse and fine mode aerosols are registered in spring which depicts a scenario of mixed aerosol types linked to biomass burning and hydrophilic aerosols.

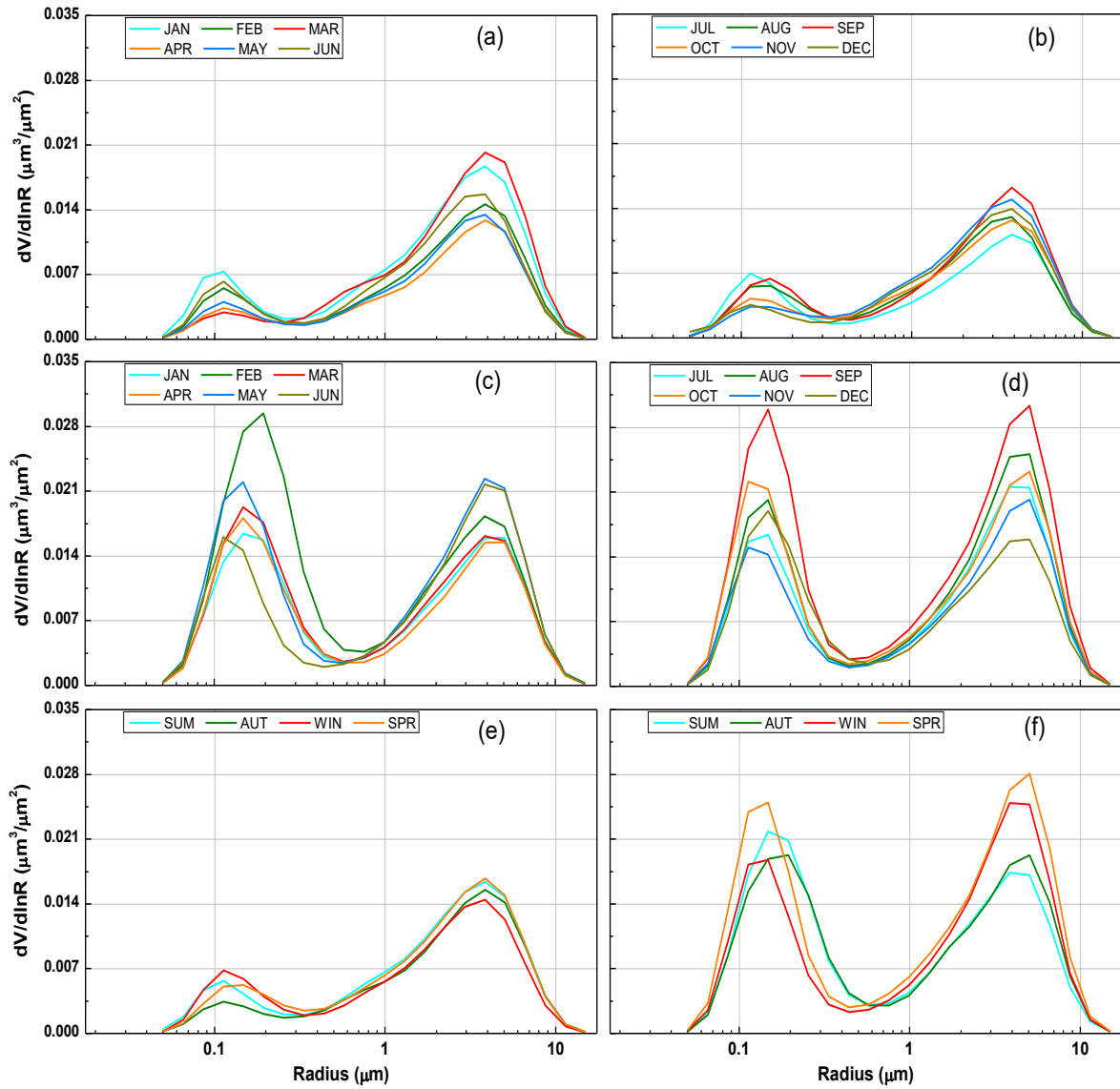


Figure 4.6 The illustration of monthly and seasonal average particle size distribution for CPT; (a), (b) and (e), and PRT; (c), (d) and (f).

#### 4.4.5 Spectral Characteristics

The spectral behaviour of aerosol particles over the study location is examined for wavelengths between 440-1020 $\mu\text{m}$  and AERONET, MISR, and MODIS instruments. Figures 4.7a and 4.7b present the spectral characteristics of CPT and PRT, respectively. SSA in Figure 4.7a shows moderate spectral dependence such that  $\omega$  is approximately steady between 440 and 680 nm, then slightly decreases with increasing wavelength at  $\lambda > 680$  nm. This variation represents the mix of non-/absorbing aerosol typical for an urban-industrial setting like CPT. Meanwhile, the satellite observations of the spectral variation differ because both satellite instruments demonstrate an increasing to steady  $\omega$  value with  $\lambda$ . Satellite

observation from the MISR instrument shows a similar pattern but approximate flatness as the wavelength changes. However, for MODIS, a strong spectral dependence of increasing  $\omega$  with  $\lambda$  is visible for the few wavelengths range (i.e., 440-660nm) available for the instrument. Similarly, Figure 4.7b displays SSA's moderate spectral dependence on wavelength, following  $\omega$  sparingly decrease with  $\lambda$  mainly at  $\lambda > 800$  nm. This again indicates mixed-type aerosols of non-absorbing and absorbing properties which is consistent with the environmental situation of the PTR. MISR again exhibits closer similarity with the AERONET variation for the satellite instruments, while MODIS is more divergent, just as experienced for CPT.

The variation of absorbing AOD for CPT illustrated in Figure 4.7c exhibits some spectral dependency, mainly around  $\lambda < 680$ nm for the three instruments. An approximately steady value is noticeable for  $\lambda > 680$ nm. This variation shows the dominance of absorbing aerosol by fine particles and scattering aerosols by mainly coarse mode. The result from the previous studies on this site has demonstrated similar variation. Meanwhile, a strong spectral dependence is shown by  $AOD_{abs}$  over PRT in Figure 4.7d.  $AOD_{abs}$  decrease with increasing  $\lambda$ , and the pattern tends to be more evident at  $\lambda < 680$ nm. Like the pattern shown for CPT, smaller aerosol particles demonstrated higher absorption characteristics than larger ones. The  $AOD_{abs}$  spectral variation in PRT indicates a significant presence of absorbing fine-mode aerosols such as BC and OC. Also, similarly to the observation for CPT, the spectral characteristics of  $AOD_{abs}$  retrieved from MISR and MODIS instruments agree well with the AERONET measurement.

Apart from the spectral characteristics of  $\omega$  and  $\tau_{abs}$  that provide an insight into the scattering and absorption properties of particles for possible identification of aerosol types, the refractive indices (i.e., the real and imaginary refractive index RI) further reveals the absorption/scattering and size features for different aerosol types. Thus, the CPT's real refractive index ( $RI_r$ ) in Figure 4.7e exhibits significant spectral changes such that  $RI_r$  decreases with increasing wavelength. Since  $RI_r$  tends more toward the particle size, the variation thus demonstrates the presence of a substantial amount of fine mode aerosols. In contrast, the  $RI_r$  for PRT in Figure 4.7f does not show strong spectral dependence as seen in the  $RI_r$  for CPT. The  $RI_r$  is almost steady for all wavelengths for seasons (i.e., winter and spring) associated with the intense mix of BB aerosol and particles from incomplete

combustion of fossil fuel (FF). Regarding the other two seasons, only  $RI_r$  at shorter wavelengths ( $\lambda < 650\text{nm}$ ) exhibit relatively observable spectral dependence.

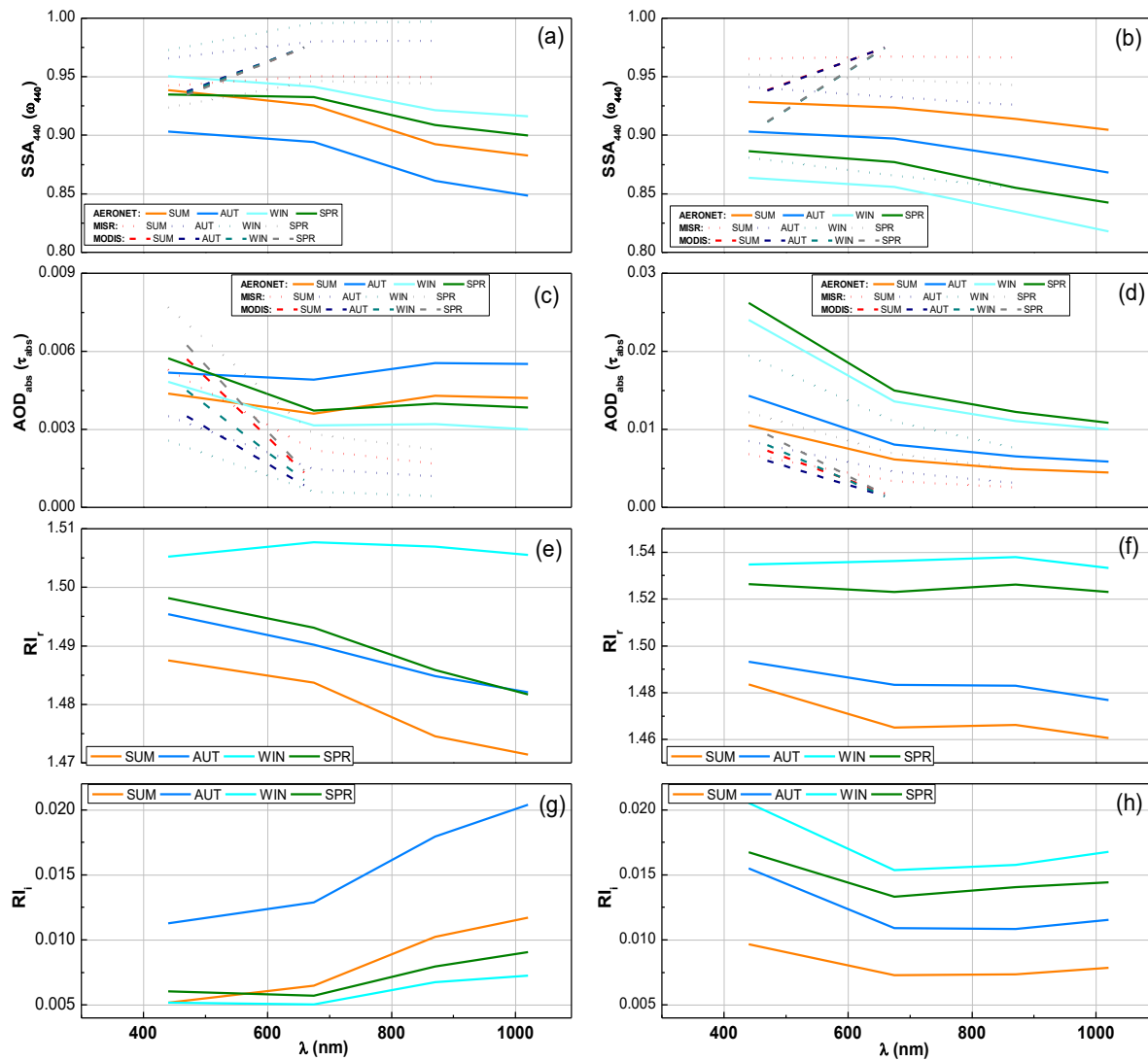


Figure 4.7 The graph showing the monthly and seasonal average spectral variation of  $SSA_{440}$ ,  $AOD_{abs}$ ,  $RI_r$  and  $RI_i$ .

#### 4.4.6 Identification of different aerosol types

Following the different aerosol properties examined in the previous sections, this section is intended to identify the prime aerosol types found in the locations currently under investigation. According to the behaviour of aerosol particles, the size, absorption/scattering properties, and the effect on light extinction constitute a vital and well-established method of partially inferring an aerosol type. This is because different particles type earns these attributes in a differing magnitude though each attribute cannot fully ascribe an aerosol type due to complex inter-similarities amongst particle type. Several studies have explored similar

methods to distinguish the different aerosol types in an environment [18, 36, 43]. However, these studies consider mainly particle size and aerosol loading or size and absorbing/scattering only. In this work, the particle size (FMF), effect on light extinction (AOD), and absorption/scattering ( $\omega$  and  $AOD_{abs}$ ) are considered simultaneously to enhance the identification of the different aerosol types. Figure 4.8a shows the relationships between AOD,  $\omega$ , and  $\tau_{abs}$  for Cape Town. The cluster bounded by the red box represents the region of high scattering ( $\omega > 0.89$ ), low aerosol loading ( $\tau_{440} < 0.10$ ) and very low absorbing particles ( $AOD_{abs} < 0.01$ ), which satisfy the features of SS aerosols and constitute the major aerosol type over the site. The yellow box corresponding to high aerosol loading ( $AOD > 0.10$ ), scattering ( $\omega > 0.90$ ) and low absorption ( $AOD_{abs} < 0.02$ ) is linked to sulphate and nitrate aerosols. The orange box represents  $AOD < 0.02$ ,  $\omega > 0.80$  and  $AOD_{abs} < 0.02$  resembles more MD. Also, the black box bounding particles with relatively high SSA ( $\omega < 0.80$ ), low to very high absorption, and AOD matches carbonaceous soot and OC. While the cluster of  $AOD > 0.10$ , high absorbing and  $\omega < 0.90$  (purple) coincide with BC.

Figure 4.8b illustrates the identification of the different aerosol types over Pretoria based on the plot of AOD, SSA, and  $AOD_{abs}$ . From the figure, the smallest cluster (yellow box) of particles with high scattering and low absorption ( $\omega > 0.9$ ,  $AOD_{abs} < 0.02$  and  $AOD < 0.01$ ) constitutes SS aerosols. The red box bounding high scattering aerosols with low absorption and AOD extending to high-value matches sulphate and nitrate aerosols. Similarly, the region of high scattering, AOD and moderate to low absorbing feature correspond to MD aerosols (orange box). Also, the cluster of particles having  $\omega < 0.90$ , low to moderate  $AOD_{abs}$ -values and AOD ranging from low to very high values bounded by the black box matches carbonaceous soot.

Meanwhile, the segment of high absorbing, low scattering, and high aerosol loading indicated by the purple box correspond to OC and BC mix. Hence from the identification process, sulphate and nitrate aerosols demonstrate to be the predominant aerosol types in the region which is consistent with the urban-industrialised characteristic of the location. Likewise significant is the identification of a substantial amount of carbonaceous aerosols (soot, OC and BC) being in suspension over the region and earlier suggested to result from locally and externally activities of BB. Summarily, the results from aerosol observations and identifications for the two locations are in close agreement with several studies conducted over these sites and elsewhere globally [11, 18, 36, 43].

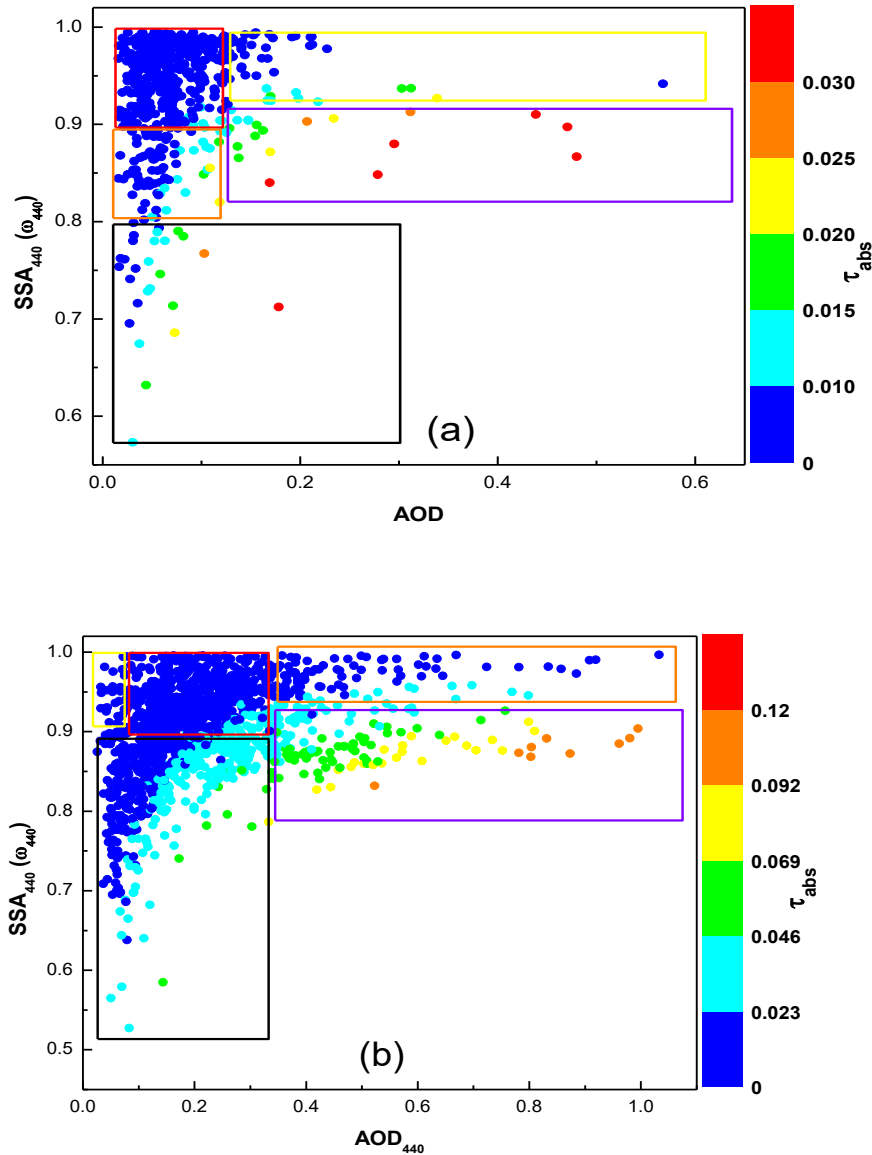


Figure 4.8 The plot of SSA, AOD and  $\tau_{\text{abs}}$  (colourbar) for (a) CPT and (b) PTE.

#### 4.4.7 Radiative forcing (RF)

A critical impact of aerosol on the earth associated with huge uncertainties is the radiative forcing (RF) effects. The RF, which constitutes the primary factor that influences the global average temperature, is a function of the amount of incoming shortwave (SWR)solar radiation and outgoing longwave (LWR) terrestrial radiation [1, 26]. The effective RF mainly results in a net cooling effect when incoming SWR is lesser than outgoing LWR, piloted by predominated scattering aerosols. In contrast, a net warming effect occurs when  $\text{SWR} > \text{LWR}$  is mainly enhanced by absorbing particles [36, 44]. Estimating the average RF (ARF) over a region follows the expression below [36, 43];

$$ARF = RF_{TOA} - RF_{BOA}, \quad (1)$$

where,

$RF_{BOA}$  = radiative forcing at the top of the atmosphere

$RF_{BOA}$  = radiative forcing at the bottom of the atmosphere.

Therefore, Figure 4.9 displays the multiyear average monthly RF for Cape Town and Pretoria as observed from the AERONET instrument at each site. In Figure 4.9a, the RF at the bottom of the atmosphere for CPT generally demonstrated a warming effect over the region with an overall average of  $10.41 \pm 1.93 \text{Wm}^{-2}$ . The maximum monthly average of  $13.37 \text{Wm}^{-2}$  in September corresponds to the period of high aerosol loading associated with the influx of aged smoke from BB activities outside the region. In comparison, the minimum  $7.75 \text{Wm}^{-2}$  in May coincides with the period of low aerosol loading. Similarly, for Pretoria in Figure 4.9b, a positive RF of a monthly average of  $22.81 \text{Wm}^{-2}$  is observed at  $RF_{BOA}$  leading to a warming effect. The maximum RF ( $40.56 \text{Wm}^{-2}$ ) recorded in September is linked to the activities of BB in the region and from boundary communities. Also, the peak coincides with the maximum over CPT, emphasising the drift of BB aerosol from the dominating sources in the north to the southern part of Southern Africa. Meanwhile, the minimum monthly value ( $16.35$ ) occurs in January tallies, with the period dominated by internally generated aerosols.

Figure 4.9c illustrates the RF at the top of the atmosphere, in contrast to the pattern depicted in Figure 4.9a, a negative forcing is displayed over CPT at the top of the atmosphere (TOA). The average monthly RF for the multiyear statistics is  $-5.34 \pm 1.09 \text{Wm}^{-2}$ , representing a cooling effect. From the chart, the maximum cooling effect ( $-6.49 \text{Wm}^{-2}$ ) occurs in September, while the minimum ( $-3.36 \text{Wm}^{-2}$ ) is recorded in March. For the PRT station, Figure 4.9d display a similitude variation as earlier seen in the case of CPT. A cooling effect with a multiyear monthly average value of  $-10.30 \text{Wm}^{-2}$  is observed at the top of the atmosphere over PRT. Meanwhile, the maximum negative RF at TOA is  $-14.20 \text{Wm}^{-2}$  in February, and the minimum cooling effect is  $-7.56 \text{Wm}^{-2}$  which occurs in June. Therefore, the variation of RF at TOA demonstrated by both locations depicts the consequences of predominance scattering initiated by a differing factor such that coarse aerosol (SS) is linked to CPT and fine particles (sulphate and nitrate aerosol) are associated with PRT.

According to the expression in equation (1), the effective RF for the study locations is shown in Figures 4.9e and 4.9f, where they apparently display net cooling effects (negative RF) over the two sites. For the net effect over CPT in Figure 4.9e, an average net cooling effect of value  $-15.75 \pm 2.44 \text{Wm}^{-2}$  is deduced over the study period. The maximum cooling effect ( $-19.82 \text{Wm}^{-2}$ ) is attained during September, and the minimum ( $-11.71 \text{Wm}^{-2}$ ) is reached in April. Figure 4.9f shows a net cooling effect averaged at  $-33.11 \pm 8.04$  in PRT during the study period. The monthly mean cooling effect at maximum ( $-53.69 \text{Wm}^{-2}$ ) occurs in September, coinciding with the month of higher aerosol loading. And as expected, the minimum cooling effect ( $-25.92 \text{Wm}^{-2}$ ) occurred during January, which is identified for low AOD. One can see that the net RF over the two locations result in a practical cooling effect. The magnitude of cooling is higher over PRT than CPT, and significantly depends on the aerosol loading and the predominance of aerosol types suspended over the regions.

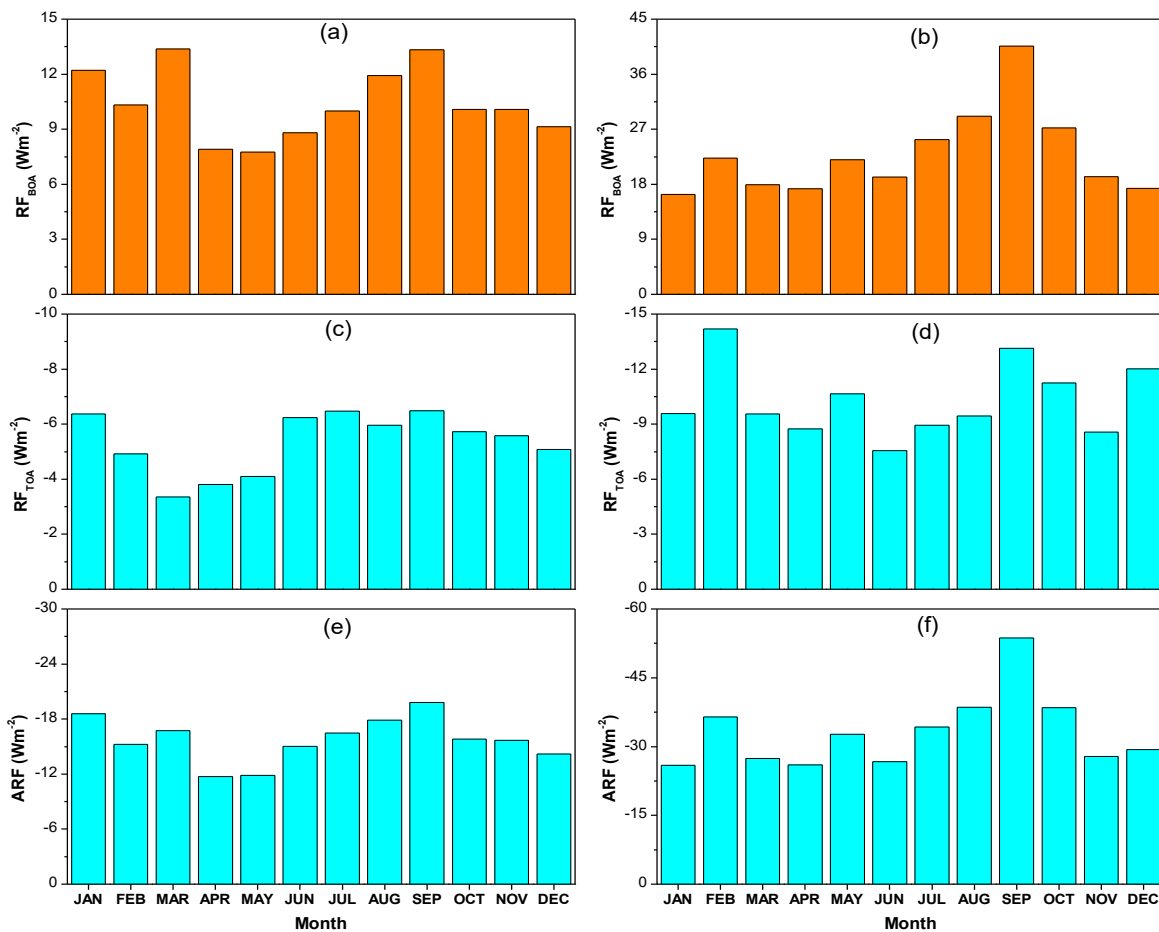


Figure 4.9 The graph of RF at BOA, TOA and average over CPT (a, c and e) and Pretoria (b, d and f).

## 4.5 Conclusion

The optical properties and the consequential radiative effect of aerosol are investigated in Cape Town (CPT) and Pretoria (PRT), two renowned metropolitans with distinct background aerosol types and commonly influenced by biomass burning (BB) activities from the northern part of South Africa. Apart from the background aerosol, they differ in meteorological and climate circumstances due to geographical stance and internal activities. Thus, the followings are deduced from the observations.

Cape Town is mainly characterised by low aerosol loading predominated by coarse particles identified as sea salt (SS). In contrast, Pretoria is found to experience high aerosol loading, largely fine mode particles ailing from different combustion activities (i.e., BB and fossil fuel combustion). Furthermore, the aerosol loading over the two metropolitans is frequently influenced by BB activities emitted north of South Africa, including PRT during the pre-farming season in September.

Aerosol suspension over CPT and PRT mainly demonstrated strong scattering characteristics and low absorption properties. While the high scattering and low absorption characteristics in CPT are linked to coarse mode aerosols mainly identifiable as sea salt (SS) aerosols, PRT is more of fine mode particles associated ascribed to sulphate and nitrate aerosols. Further, the absorption feature is found to increase in both locations during the period identified for predominance BB activities, with the extent more obvious for PRT.

The amount of columnal precipitable water increases sharply over the two locations during summer, which represents more than 65% compared to the values in other sea seasons. Also, the average value for WVC is slightly higher in CPT than in PRT. Cape Town's nearness to the ocean is suggested to account for the increase.

Validation of satellite instrument measurements of aerosol parameters against the AERONET datasets shows considerable agreement. However, some parameters such as AE and  $AOD_{abs}$  for a specific location (i.e., CPT) but the different platforms. On a general note, MISR outperformed MODIS based on the instrument performance, exception for vapour measurement, which is unavailable for MISR. Considering the two locations, the satellite retrieval possesses better accuracy in PRT (mainly land surface) than for CPT (water environment). Also important is that the MODIS instrument is most accurate in atmospheric vapour measurement (i.e., for WVC,  $R > 0.95$ ) over both locations.

According to the relationships amongst the optical parameters and the spectral characteristics of SSA, AOD<sub>abs</sub>, RI<sub>r</sub> and RI<sub>i</sub>, the aerosol suspended over CPT is dominated by SS such that the prominence of aerosol types follows the hierarchy MD < OC < BC < sulphate/nitrate < SS. As for PRT, sulphate/nitrate aerosols are the chief aerosol type over the site; hence, the order of prominence follows SS < MD < OC < BC < sulphate/nitrate aerosols.

The effective radiative forcing over the two locations is negative RF, therefore, resulting in a net cooling effect over the regions. Over CPT, the predominance of coarse, low absorbing and high scattering SS aerosols is responsible for the net cooling effect experienced in the location. Meanwhile, the prevalence of fine mode, highly scattering, and lower absorption sulphate/nitrate aerosols are responsible for the net cooling effect over the location.

### **Acknowledgments**

The authors appreciate the principal investigators of the Simons Town and Pretoria AERONET site and the entire AERONET team for their support. We also appreciate the MISR, MODIS and NASA/GSFC/ESDIS team for the use of data. The authors would also like to acknowledge anonymous reviewers for their insightful comments and suggestions for improved clarification of this paper.

### **References**

- [1] IPCC, Climate Change 2013: The Physical Science Basis. Contribution of Working Group I to the Fifth Assessment Report of the Intergovernmental Panel on Climate Change, Cambridge University Press, Cambridge, United Kingdom and New York, NY, USA, 2013.
- [2] O. Boucher, Atmospheric aerosols: Properties and climate impacts, 1 ed., Springer, Netherlands, 2015.
- [3] J. Haywood, O. Boucher, Estimates of the direct and indirect radiative forcing due to tropospheric aerosols: A review, *Rev Geophys*, 38 (2000) 513-543.
- [4] S. Twomey, Influence of Pollution on Shortwave Albedo of Clouds, *Journal of the Atmospheric Sciences*, 34 (1977) 1149-1152.
- [5] A.S. Ackerman, O.B. Toon, D.E. Stevens, A.J. Heymsfield, V. Ramanathan, E.J. Welton, Reduction of Tropical Cloudiness by Soot, *Science*, 288 (2000) 1042-1047.

- [6] J. Hansen, M. Sato, R. Ruedy, Radiative forcing and climate response, *Journal of Geophysical Research: Atmospheres*, 102 (1997) 6831-6864.
- [7] J.P. Putaud, European aerosol phenomenology-3: Physical and chemical characteristics of particulate matter from 60 rural, urban, and kerbside sites across Europe, *Atmospheric Environment*, 44 (2010) 13.
- [8] C.A. Pope, R.T. Burnett, M.J. Thun, E.E. Calle, D. Krewski, K. Ito, G.D. Thurston, Lung Cancer, Cardiopulmonary Mortality, and Long-term Exposure to Fine Particulate Air Pollution, *JAMA*, 287 (2002) 1132-1141.
- [9] O.A. Falaiye, A.T. Yakubu, F.O. Aweda, O.J. Abimbola, Mineralogical characteristics of harmattan dust in Ilorin, Sub-Sahara Africa, *Ife Journal of Science* 15 (2013) 175-181.
- [10] J. Fan, Y. Wang, D. Rosenfeld, X. Liu, Review of Aerosol–Cloud Interactions: Mechanisms, Significance, and Challenges, *Journal of the Atmospheric Sciences*, 73 (2016) 4221-4252.
- [11] A.T. Yakubu, N. Chetty, Optical properties of atmospheric aerosol over Cape Town, Western Cape of South Africa: Role of biomass burning, *Atmósfera*, 34 (2020) 395–416.
- [12] M.Z. Jacobson, Global direct radiative forcing due to multicomponent anthropogenic and natural aerosols, *Journal of Geophysical Research: Atmospheres*, 106 (2001) 1551-1568.
- [13] A. de Meij, J. Lelieveld, Evaluating aerosol optical properties observed by ground-based and satellite remote sensing over the Mediterranean and the Middle East in 2006, *Atmospheric Research*, 99 (2011) 415-433.
- [14] O. Dubovik, M.D. King, A flexible inversion algorithm for retrieval of aerosol optical properties from Sun and sky radiance measurements, *Journal of Geophysical Research: Atmospheres*, 105 (2000) 20673-20696.
- [15] E. Drury, D.J. Jacob, J. Wang, R.J.D. Spurr, K. Chance, Improved algorithm for MODIS satellite retrievals of aerosol optical depths over western North America, *Journal of Geophysical Research: Atmospheres*, 113 (2008).
- [16] P. Formenti, H. Winkler, P. Fourie, S. Piketh, B. Makgopa, G. Helas, M.O. Andreae, Aerosol optical depth over a remote semi-arid region of South Africa from spectral

measurements of the daytime solar extinction and the nighttime stellar extinction, *Atmospheric Research*, 62 (2002) 11-32.

[17] C. Ichoku, L.A. Remer, Y.J. Kaufman, R.C. Levy, D.A. Chu, D. Tanré, B.N. Holben, MODIS observation of aerosols and estimation of aerosol radiative forcing over Southern Africa during SAFARI 2000, *J. Geophys. Res.*, 108 (2003).

[18] A. Smirnov, B.N. Holben, O. Dubovik, R. Frouin, T.F. Eck, I. Slutsker, Maritime component in aerosol optical models derived from Aerosol Robotic Network data, *J Geophys Res-Atmos*, 108 (2003).

[19] A. Smirnov, B.N. Holben, O. Dubovik, N.T. O'Neill, T.F. Eck, D.L. Westphal, A.K. Goroch, C. Pietras, I. Slutsker, Atmospheric Aerosol Optical Properties in the Persian Gulf, *Journal of the Atmospheric Sciences*, 59 (2002) 620-634.

[20] J.P. Sherman, P. Gupta, R.C. Levy, P.J. Sherman, An Evaluation of MODIS-Retrieved Aerosol Optical Depth over a Mountainous AERONET Site in the Southeastern US, *Aerosol and Air Quality Research*, 16 (2016) 3243-3255.

[21] Y.J. Kaufman, B.N. Holben, D. Tanré, I. Slutsker, A. Smirnov, T.F. Eck, Will aerosol measurements from Terra and Aqua Polar Orbiting satellites represent the daily aerosol abundance and properties?, *Geophysical Research Letters*, 27 (2000) 3861-3864.

[22] G.L. Schuster, Vaughan, M., MacDonnell, D., Su, W., Winker, D., Dubovik, O., Lapyonok, T., and Trepte, C., Comparison of CALIPSO aerosol optical depth retrievals to AERONET measurements, and a climatology for the lidar ratio of dust, *Atmos Chem Phys*, 12 (2012) 7431-7452.

[23] R.J. Charlson, S.E. Schwartz, J.M. Hales, R.D. Cess, R.D. Coakley, J.E. Hansen, D.J. Hofmann, Climate forcing by anthropogenic aerosols, *Science*, 255 (1992) 423-430.

[24] S.E. Schwartz, Harshvardhan, C.M. Benkovitz, Influence of anthropogenic aerosol on cloud optical depth and albedo shown by satellite measurements and chemical transport modeling, *Proc Natl Acad Sci U S A*, 99 (2002) 1784-1789.

- [25] D. Wang, B. Jiang, F. Li, W. Lin, Investigation of the air pollution event in Beijing-Tianjin-Hebei region in December 2016 using WRF-Chem, *Advances in Meteorology*, 2018 (2018) 1-12.
- [26] IPCC, The Physical Science Basis. Contribution of Working Group I to the Fourth Assessment Report of the Intergovernmental Panel on Climate Change in, Cambridge University Press, Cambridge, 2007.
- [27] A.M. Sayer, Hsu, N. C., Eck, T. F., Smirnov, A., and Holben, B. N, AERONET-based models of smoke-dominated aerosol near source regions and transported over oceans, and implications for satellite retrievals of aerosol optical depth, *Atmos Chem Phys*, 14 (2014) 11493-11523.
- [28] L. Yun, W. Yuan, P. Bowen, H. Jiayi, G. Song, L.Z. Misti, T. Pengfei, S. Qiong, J. Yuemeng, G.-Z. Mario, H. Min, Z. Renyi, Formation , radiative forcing, and climatic effects of severe regional haze, *Atmos. Chem. Phys*, 22 (2022) 4951-4967.
- [29] D. Rosenfeld, TRMM observed first direct evidence of smoke from forest fires inhibiting rainfall, *Geophysical Research Letters*, 26 (1999) 3105-3108.
- [30] M.W. Christensen, G.L. Stephens, Microphysical and macrophysical responses of marine stratocumulus polluted by underlying ships: 2. Impacts of haze on precipitating clouds, *J Geophys Res-Atmos*, 117 (2012).
- [31] D. Rosenfeld, M.O. Andreae, A. Asmi, M. Chin, G. de Leeuw, D.P. Donovan, R. Kahn, S. Kinne, N. Kivekäs, M. Kulmala, W. Lau, K.S. Schmidt, T. Suni, T. Wagner, M. Wild, J. Quaas, Global observations of aerosol-cloud-precipitation-climate interactions, *Rev Geophys*, 52 (2014) 750-808.
- [32] S.P. Hersey, R.M. Garland, E. Crosbie, T. Shingler, A. Sorooshian, S. Piketh, R. Burger, An overview of regional and local characteristics of aerosols in South Africa using satellite, ground, and modeling data, *Atmos Chem Phys*, 15 (2015) 4259-4278.
- [33] A.J. Adesina, K.R. Kumar, V. Sivakumar, Aerosol-Cloud-Precipitation Interactions over Major Cities in South Africa: Impact on Regional Environment and Climate Change, *Aerosol and Air Quality Research*, 16 (2016) 195-211.

- [34] M. Tesfaye, V. Sivakumar, J. Botai, G. Mengistu Tsidu, Aerosol climatology over South Africa based on 10 years of Multiangle Imaging Spectroradiometer (MISR) data, *Journal of Geophysical Research: Atmospheres*, 116 (2011).
- [35] A.J. Queface, S.J. Piketh, T.F. Eck, S.C. Tsay, A.F. Mavume, Climatology of aerosol optical properties in Southern Africa, *Atmospheric Environment*, 45 (2011) 2910-2921.
- [36] K.R. Kumar, N. Kang, V. Sivakumar, D. Griffith, Temporal characteristics of columnar aerosol optical properties and radiative forcing (2011–2015) measured at AERONET's Pretoria\_CSIR\_DPSS site in South Africa, *Atmospheric Environment*, 165 (2017) 274-289.
- [37] T.F. Eck, B.N. Holben, J.S. Reid, M.M. Mukelabai, S.J. Piketh, O. Torres, H.T. Jethva, E.J. Hyer, D.E. Ward, O. Dubovik, A. Sinyuk, J.S. Schafer, D.M. Giles, M. Sorokin, A. Smirnov, I. Slutsker, A seasonal trend of single scattering albedo in southern African biomass-burning particles: Implications for satellite products and estimates of emissions for the world's largest biomass-burning source, *Journal of Geophysical Research: Atmospheres*, 118 (2013) 6414-6432.
- [38] B.N. Holben, T.F. Eck, I. Slutsker, D. Tanré, J.P. Buis, A. Setzer, E. Vermote, J.A. Reagan, Y.J. Kaufman, T. Nakajima, F. Lavenue, I. Jankowiak, A. Smirnov, AERONET—A Federated Instrument Network and Data Archive for Aerosol Characterization, *Remote Sensing of Environment*, 66 (1998) 1-16.
- [39] Ø. Hodnebrog, G. Myhre, P.M. Forster, J. Sillmann, B.H. Samset, Local biomass burning is a dominant cause of the observed precipitation reduction in southern Africa, *Nature Communications*, 7 (2016) 11236.
- [40] G. de Leeuw, E.L. Andreas, M.D. Anguelova, C.W. Fairall, E.R. Lewis, C. O'Dowd, M. Schulz, S.E. Schwartz, Production flux of sea spray aerosol, *Rev Geophys*, 49 (2011).
- [41] R.A. Kahn, B.J. Gaitley, M.J. Garay, D.J. Diner, T.F. Eck, A. Smirnov, B.N. Holben, Multiangle Imaging SpectroRadiometer global aerosol product assessment by comparison with the Aerosol Robotic Network, *Journal of Geophysical Research*, 115 (2010).
- [42] A.T. Yakubu, N. Chetty, A decadal assessment of the climatology of aerosol and cloud properties over South Africa, *Atmos. Chem. Phys. Discuss.*, 2022 (2022) 1-36.

[43] R. Boiyo, K.R. Kumar, T. Zhao, J. Guo, A 10-Year Record of Aerosol Optical Properties and Radiative Forcing Over Three Environmentally Distinct AERONET Sites in Kenya, East Africa, *Journal of Geophysical Research: Atmospheres*, 124 (2019) 1596-1617.

[44] U. Lohmann, J. Feichter, Global indirect aerosol effects: a review, *Atmos Chem Phys*, 5 (2005) 715-737.

## Chapter 5 –

# Machine Learning-Based Precipitation Prediction Using Cloud Properties

Abdulaziz Tunde Yakubu<sup>1</sup>[0000-0002-7417-9045], Abdultaofeek Abayomi<sup>2</sup>[0000-0003-3129-5246], and  
Naven Chetty<sup>3</sup>\*[0000-0002-0916-578X]

<sup>1,3</sup>Discipline of Physics, School of Chemistry and Physics, University of KwaZulu-Natal, Private Bag  
X01, Scottsville, 3209, Pietermaritzburg, South Africa

<sup>2</sup>Department of Information and Communication Technology, Mangosuthu University of Technology,  
P.O. Box 12363 Jacobs, 4026 Durban, South Africa

\*chettyn3@ukzn.ac.za

**5.1 Abstract.** Developing a forecast model with a high accuracy and consistency level continues to be of global interest in weather prediction and climate projection studies. Precipitation constitutes one of the critical components of weather, surrounded by huge uncertainties but requires adequate information to enhance water resources management and sustainability of life. Machine learning techniques as data-driven tools have been found worthy in addressing these challenges and have shown promising results over the years, particularly in their robustness and moderate resources requirement. In this current study, two machine learning algorithms, including multiple linear regression (MLR) and multilayered perceptron artificial neural network (MLP-ANN), are deployed to develop a model for daily precipitation prediction based on cloud properties. The algorithms using cloud parameters comprising of cloud optical thickness (COT), cloud effective radius (CER), cloud top temperature (CTT), cloud top pressure (CTP), and liquid water path (LWP) as inputs performed well to produce models with good accuracies up to  $R > 0.7$  and generally  $RMSE < 5.5$ . In all, the models produced by MLP-ANN prove to be more accurate with higher R-values and low errors for location-specific training and prediction. At the same time, MLR shows more consistent traits based on a multilocation forecast. Besides, the location with the highest number of samples results in better models compared to areas with lower data samples. Results obtained are helpful to weather and climate change stakeholders for accurate prediction of daily precipitation and management of water resources to support the ecosystem.

**Keywords:** Cloud Parameters, Climate Change, Ecosystem, Precipitation, Prediction, Weather

## **5.2 Introduction**

As an element of weather, precipitation plays a vital role in the global hydrology cycle and the earth's climate system. The habitability and sustainability of life on the planet significantly depend on its occurrence and intensity. Precipitation constitutes one of the primary sources of freshwater available to humans for survival. It does have essential impacts on human livelihoods as well as several other aspects of their lives. These include but are not limited to agriculture, water availability, transportation, hygiene, environmental conditions, and socio-economic values, amongst others. Prolonged precipitating or non-precipitating

events could result in extreme weather conditions such as flooding and drought, thus, causing damage to the environment and hardship to the habitats [1]. Therefore, there is a need for an accurate forecast of precipitation for effective climate projection, adaptive strategies, and disaster and water resources management in a manner suitable for promoting stability and sustainability on the earth.

Due to the complex nature and high precipitation variability caused by changes in the atmospheric condition, accurate and timely prediction of the event is highly challenging. It has also raised concerns both on regional and global scales [2, 3]. Different prediction methods have been employed for general weather and climate forecasts. These include modelling, data assimilation, and machine learning techniques, amongst others [4, 5, 6]. However, regardless of the adopted method, specific climate parameters are considered as input to be fed into the predicting model. These include meteorology parameters like surface temperature, relative humidity (RH), wind speed, solar irradiance, atmospheric parameters such as cloud properties, atmospheric pressure, ocean features like ocean circulation, sea surface temperature, and sea salinity that interact with precipitation.

### **5.3 Literature Review**

Most studies that have employed a machine learning approach for precipitation prediction focused mainly on meteorology parameters, while the other climate parameters received less attention. Yet, to effectively describe precipitation in regional and global climate studies, the cloud is very critical to understanding the process.

The cloud is crucial to precipitation formation processes, including the timing, distribution, and intensity of the event over any geographical environment. Studies have demonstrated the strong dependency of precipitation on variations in cloud macro and microphysical properties [7,8]. Besides, the clouds serve as incubation ground and a significant driver of precipitation production. Several studies have identified the influence of different cloud properties on precipitation development and how they induce changes to the pattern [9,10]. Therefore, these properties are valuable pathways in predicting both the occurrence and intensity of precipitation. They also constitute an important input toward regional and global climate change projection and the general assessment of possible extreme weather events. Following the advent of satellite observation of the earth, several cloud measurements capable of providing helpful information on its condition and clues regarding the expected precipitation

type becomes increasingly available. In addition, satellite measurement offers more spatial and temporal coverage of cloud measurements, allowing precipitation forecasting over any area and time, especially over remote locations without a weather station. However, there are some setbacks in the extent of accuracy relative to other measurement platforms.

Indeed, the robust data archive offered by satellite remote sensing becomes the height of advantage in utilising machine learning techniques as standard methods of precipitation prediction and widely used tools in different forms of prediction and classification problems. Machine learnings are particularly suitable for dealing with problems that involve non-linear, highly dynamic variables like precipitation. These methods have been employed in a wide range of applications such as medical diagnosis, online marketing, stock analysis, engineering, and weather forecasting [11,12,13]. In terms of weather forecasting, machine learning is gaining more attention within the global community as a widely used method of forecasting precipitation events because of its robustness merged with moderate resource requirements [14].

Several studies have applied machine learning techniques to forecast precipitation events and have yielded promising results. In the work of [15], RNN (recurrent neural network) and ANN machine learning techniques were used to predict hourly rainfall in southern Taiwan and yielded valuable results.

Similarly, [16] applied the combined backpropagation-genetic algorithm, a modified form of ANN, to estimate the monthly rainfall pattern over the city of Tehran. One common feature of most of these studies is that meteorology parameters have been used as the input towards precipitation prediction parameters; hence, cloud parameters have mainly gained less attention. Since the cloud is critical to understanding climate and plays a crucial role in precipitation formation, a land-breaking outcome could also emanate by prioritising cloud properties as an essential input for precipitation prediction. Even in general climate models, the cloud is treated as a high-priority component necessary in defining any weather element.

This current study develops a forecasting model for precipitation using two machine learning techniques based on cloud parameters as input over three cities in South Africa, namely Durban, Cape Town, and Port Elizabeth. The study will investigate the capability of cloud-measured properties as effective variables in predicting precipitation events over multilocation sites. Besides, the rich data archive of satellite observation will be used to

evaluate how accurate precipitation prediction can be achieved over locations without a weather station.

## **5.4 Materials and Method**

### ***5.4.1 Study Areas' Descriptions***

The study is conducted in three cities in the lower part of South Africa, namely, Cape Town (CPT), Durban (DBN), and Port Elizabeth (PTE), as shown in Figure 5.1. The cities have several features in common, including coastal sites, metropolitans, and the economic hubs of their respective provinces/region. Hence, precipitation forecast is typically crucial in these environments for adequately managing their waterfronts and protecting their socio-economic activities, which could endanger the entire province. Cape Town (33.92S 18.42E) is in the Western Cape province of the country and is home to several domestic, commercial, and industrial activities. The city is surrounded by two major oceans and endowed with mountainous and plain land, making it a favorite tourist destination. Besides being a commercial and industrialised region, the city also boasts massive agricultural activities, especially in the citrus and winery industries, which depend on the adequate water supply to boost production. The city is characterised by winter rainfall and experiences an annual rainfall of 470.5mm (average over 1981-2010), while it also often experiences low rainfall that sometimes leads to drought and water shortages.

Durban (29.86S 31.01E) is in the KwaZulu-Natal province and is renowned for its commercial and industrial bustling. The city is surrounded by the Indian Ocean and shares the same climate as most parts of South Africa. DBN, experiences summer precipitation mainly from November-February and receive the highest amount of rainfall annually of the three locations under investigation, with thirty years average of 806.8mm. The region is also known for some agricultural activities, mainly around the outskirts. Even though Durban sometimes experiences precipitation decrease like other parts of South Africa, the area is known for flooding activities, resulting in damages and substantial economic loss. Port Elizabeth (33.95S 25.59E) is also notable for commercialisation and industrialisation. The region shares a similar rainfall pattern with Cape Town and receives an average of 540.6mm of downpour annually. Like Cape Town, Port Elizabeth faces the challenges of low rainfall and water shortages on a timely basis. Therefore, the need for an accurate forecast model to

enhance water resources and environmental management in the regions under study cannot be overemphasised.

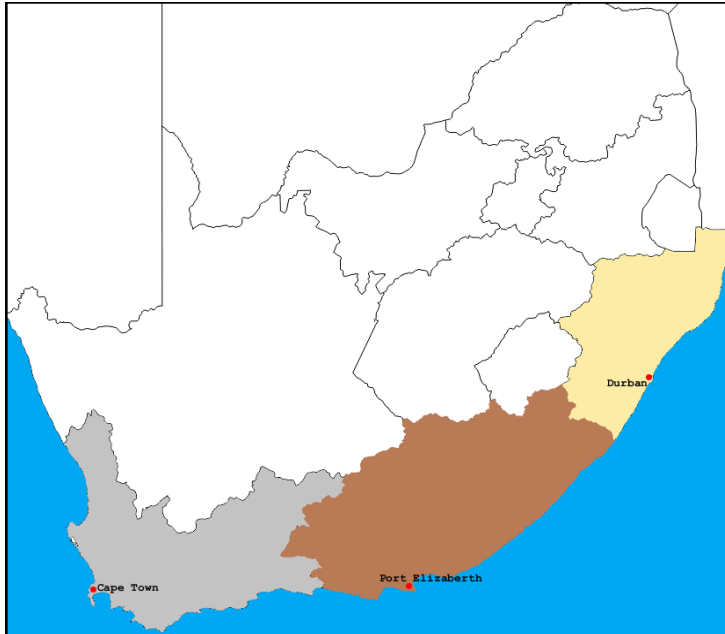


Figure 5.1 Map of South Africa showing the study areas locations.

#### ***5.4.2 Data Acquisition and Processing***

The data used in this study are obtained from MODIS (Moderate Resolution Imaging Spectrometer) satellite and POWER (Prediction of Worldwide Energy Resources) project, two platforms known for their global coverage and temporal stability. MODIS onboard Aqua and Terra satellites are one of the A-train constellation satellites that swath the earth to observe the current conditions of the atmosphere, land, and ocean. The satellite swath the entire earth every 1-2 days to retrieve helpful information about the current conditions. This includes monitoring aerosol activities as well as cloud properties and atmospheric dynamics. The instrument provides daily, weekly, and monthly data products at three distinct levels (levels 1-3). However, the level 3 data is based on a  $1^{\circ} \times 1^{\circ}$  grid system of cloud properties comprising cloud optical thickness (COT), effective cloud radius (CER), cloud top temperature (CTT), cloud top pressure (CTP), and liquid water path (LWP) are employed towards this study.

POWER project data provided by NASA (National Aeronautics and Space Administration) is processed using the data assimilation technique to produce global meteorology information

based on the grid system. The technique generates new datasets from historical observation of different meteorology parameters, producing current daily, weekly, monthly, and yearly data. Therefore, the precipitation data for the study locations are obtained from the POWER database. The daily datasets from both platforms (MODIS and POWER) obtained for over seven years from 2004-2011 (representing 2556 days) are used in this study. Furthermore, a correlation analysis is computed to evaluate the consistency of the datasets, and the result shows significant relationships amongst the parameters. While correlations amongst some parameters are strong ( $R > 0.6$ ), others are observed to be weak-moderate ( $|R| > 0.25$ ). A visual summary of the correlation between cloud parameters and precipitation (the target) is illustrated in the heatmap plot in Figure 5.2.

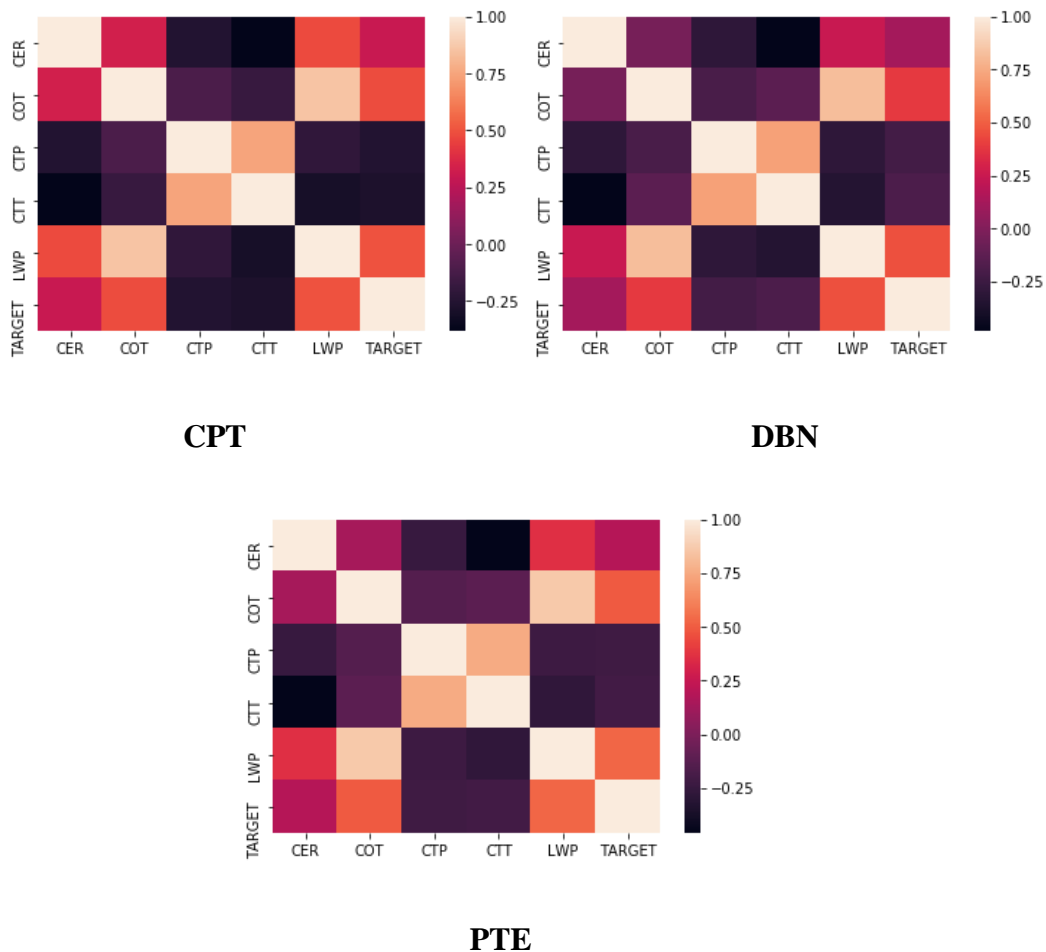


Figure 5.2 Summary of the correlations between the predictors and the targets.

The raw dataset collected from the two platforms is initially processed by filtering samples with missing or void values for any parameter. Consequently, Cape Town accounts for the

highest population sample with 2111 data points, followed by Port Elizabeth (1895) and Durban (1794). A statistical summary of the filtered data for the study locations is shown in Table 5.1.

Table 5.1 The statistical summary of filtered data samples available for each location.

	<b>CPT</b>	<b>DBN</b>	<b>PTE</b>
<b>Sample count</b>	<b>2111</b>	<b>1794</b>	<b>1895</b>
<b>Precipitating</b>	<b>1041</b>	<b>1319</b>	<b>1104</b>
<b>Non-Precipitating</b>	<b>1070</b>	<b>475</b>	<b>791</b>
<b>Mean</b>	<b>1.60</b>	<b>2.87</b>	<b>1.69</b>
<b>Standard Deviation</b>	<b>4.21</b>	<b>5.44</b>	<b>4.04</b>
<b>Minimum</b>	<b>0</b>	<b>0</b>	<b>0</b>
<b>Maximum</b>	<b>67.60</b>	<b>72.04</b>	<b>56.04</b>
<b>25<sup>th</sup> Percentile</b>	<b>0.02</b>	<b>0.16</b>	<b>0.03</b>
<b>50<sup>th</sup> Percentile</b>	<b>0.18</b>	<b>0.93</b>	<b>0.35</b>
<b>75<sup>th</sup> Percentile</b>	<b>1.18</b>	<b>3.20</b>	<b>1.66</b>

The datasets are then subjected to training and testing processes using two machine learning techniques: multiple linear regression (MLR) and artificial neural network (ANN), which are deployed from MATLAB neural network toolbox and PYTHON software, respectively to develop a model for precipitation prediction. The MLR algorithm, an advanced form of

simple linear regression, is a statistical tool used to linearly model the relationship between a target (dependent variable) and multiple predictors (independent variables). Therefore, the algorithm is suitable for stochastic systems such as precipitation and has yielded promising results. The MLR model for k-number of predictors  $P_1, P_2, P_3, \dots, P_k$ , and a target T is thus expressed as follows:

$$T = \beta_0 + \beta_1 P_1 + \beta_2 P_2 + \beta_3 P_3 + \dots + \beta_k P_k + \varepsilon \quad (1)$$

where  $\beta_0, \beta_1, \beta_2, \beta_3, \dots, \beta_k$  are the regression coefficients,  $\varepsilon$  is the residual, and other parameters (T, k and  $P_1, P_2, P_3, \dots, P_k$ ) are as earlier defined.

On the other hand, ANN is a machine learning technique used in the classification and prediction of a non-linear dynamic system. The network of neurons imitates the human brain function to detect the relationship between an input and a target by learning the patterns using a concept of weight and bias estimation and passing through an activation function to link the target [17]. The network consists of layers in which input data are processed and matched with the appropriate output data. During the training process in ANN, the input information is scaled based on random weight and bias and passed through the activation function, which evaluates the compatibility with the target. In this work, the network used comprises two layers consisting of an input layer and one hidden layer with various neurons. The hidden layer uses the sigmoid function as the activation function based on the Levenberg-Marquardt algorithm. The input layer consists of the five cloud parameters: cloud optical thickness (COT), effective cloud radius (CER), cloud top temperature (CTT), cloud top pressure (CTP), and liquid water path (LWP) fed into the network as input features of each sample to be trained/tested. The output layer implements a linear function and represents the predicted precipitation value. An illustration of the network is shown in Figure 5.3.

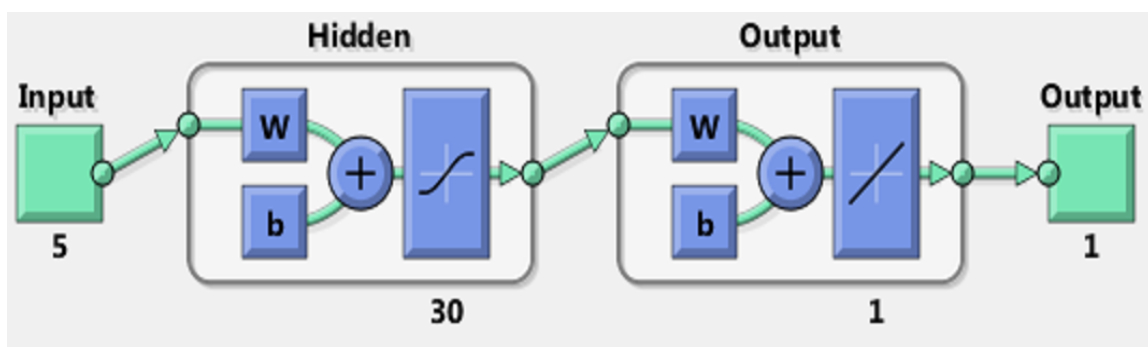


Figure 5.3 The ANN architecture for precipitation prediction.

For a model to be widely accepted as an appropriate tool for predicting an event such as precipitation, certain conditions are fundamental, including the accuracy, error value, and level of consistency. To this effect, two experimental procedures are employed to develop a precipitation prediction model suitable for a multilocation forecast. The term ‘‘multilocation’’ prediction refers to the prediction made on any other locations with a model developed from data from another area. For instance, using a model created using the data of Durban (a location) to predict any other sites globally. The first procedure involves splitting the dataset for each location into training and testing partitions (according to split ratio), then processing using both machine learning methods earlier described, one at a time to obtain the most suitable prediction model. For instance, Cape Town, with a total sample size of 2111, will have 1689 (80%) samples for training and 422 (20%) for testing the MLR model.

Consequently, two sets of models emerged per location, consisting of a model resulting from each learning process initiated by the algorithms. In the second procedure, the models generated for each site in the first procedure are used to predict precipitation events over the other locations. During the machine learning process for each method, some specific training parameters are randomly varied along with trials. These include the split ratio (SR), numbers of random states (MLR model), or neurons (ANN). For MLR, SR between 70:30 and 80:20 is chosen for better performance. This value is based on the outcome of a preliminary investigation that shows values outside this range to perform poorly or result in overfitting. Also, the random state is selected between 20-30 according to data size for the adequate spread of data features.

Similarly, for ANN, SR follows the same rule as MLR, and the number of hidden neurons between 10-30 generated better models. Outcast values are either poorly performed or yield no improvement. Also, the adoption of the sigmoid function lies in its capability to extract more features compared to its peers. Meanwhile, the number of epochs is fixed at 1000 for the entire process. The experiment involves several trials to obtain the most relevant and consistent results. Evaluation of the accuracy of the results is based on the correlation value R and root mean square error (RMSE) metrics and is described in the next section.

## **5.5 Results and Discussion**

Modelling a complex variable such as precipitation can be rigorous and highly challenging; hence, identifying suitable proxies will significantly ease the task. In this manner, this work

evaluates the strength of cloud properties as predicting variable for precipitation. Besides, the MLR algorithm is compared with ANN. On a broad scale, the models generated from the experiments in this study averagely have  $R > 0.50$  and  $RMSE < 5.0$  for location-based prediction. This result is an indication of cloud properties being potentially suitable for precipitation forecasts using machine learning techniques. Furthermore, the model developed based on ANN shows better accuracy with an R-value in the range of 0.39 - 0.72 and RMSE between 2.90 – 5.76 than the R-value range of 0.44 - 0.55 and RMSE 3.39 – 4.90 recorded by MLR. A summary of the model performances is shown in Table 5.2 below.

Table 5.2 Summary of training parameters and results of the models for the locations.

Site	Model	Training parameters			Model outcome		Other site's outcome (R/RMSE)		
		SR	NRS	Neurons	R	RMSE	CPT	DBN	PTE
CPT	MLR	80/20	25	-	0.54	3.53	-	0.44/4.89	0.53/4.44
DBN		70/30	25	-	0.46	4.83	0.50/3.64	-	0.51/3.48
PTE		80/20	23	-	0.55	3.39	0.53/3.33	0.44/4.90	-
CPT	ANN	80/10/10	-	30	0.72	2.90	-	0.39/5.38	0.53/3.96
DBN		70/15/15	-	20	0.62	4.26	0.48/5.40	-	0.44/4.49
PTE		80/10/10	-	30	0.67	2.99	0.50/3.69	0.39/5.76	-

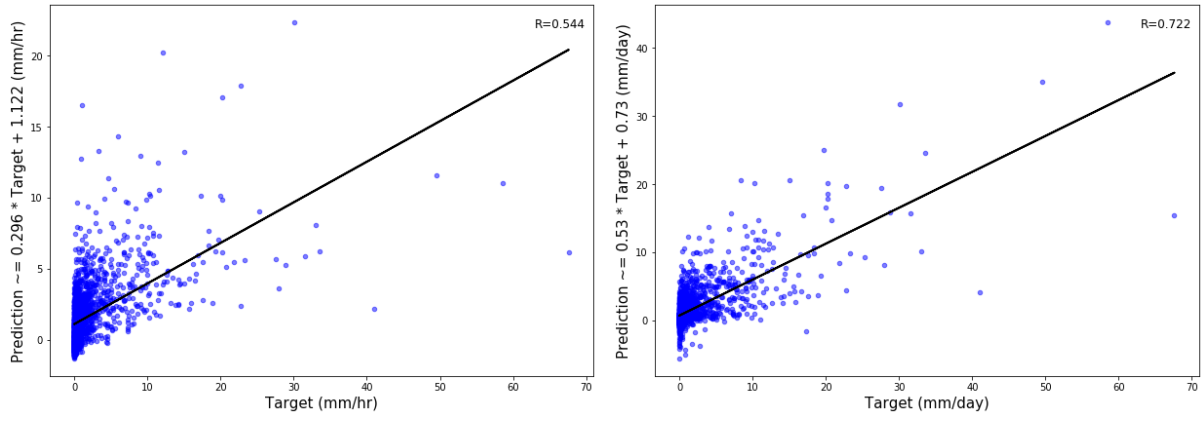
\*SR= split ratio and NRS= number of random states.

Furthermore, while ANN prediction models are more accurate location-wise (over dedicated location), the MLR model seems better for a multilocation forecast. These features are well observed for all sites, with ANN losing strength up to 30% for multilocation prediction, while the MLR model is approximately stable in a similar condition. In terms of consistency, the MLR model performs better since it is more generalised if found to predict accurately over all domains. On the other hand, ANN may possess high accuracy for domesticated prediction, but the substantial divergence in the case of the multilocation forecast is a severe setback. Perhaps introducing additional parameters in the process of developing the model could enhance the detection of more features between the input parameters and target by the machine learning process, leading to more stable prediction in the case of ANN and general improvement in accuracy for the MLR.

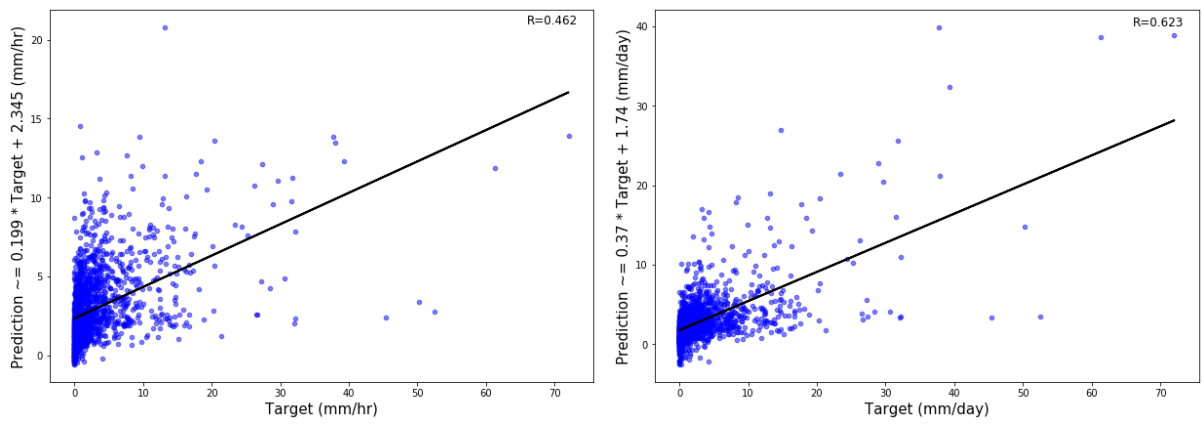
In Figure 5.4, the fittings for the prediction models for all three locations under investigation are shown. Cape Town is observed to possess the most accurate prediction model with  $R > 0.7$  and  $RMSE < 3.00$ , followed by Port Elizabeth with  $R = 0.67$  and  $RMSE < 3.00$ , while Durban is making the least, have values  $R < 0.65$  and  $RMSE > 3.00$ , according to ANN learning process. One noteworthy fact is that Cape Town has the highest population sample while Durban has the least. This observation is consistent with the result from typical machine learning studies whereby a huge amount of data yields a better model than a lesser number of samples [18,19]. In the case of MLR model, the pattern is slightly different with Durban ( $R = 0.46$ ,  $RMSE = 4.83$ ) still the least accurate but, Port Elizabeth ( $R = 0.55$ ,  $RMSE = 3.39$ ) slightly surpass Cape Town ( $R = 0.54$ ,  $RMSE = 3.53$ ). The prediction models are thus summarised in Table 5.3, and a year observation-prediction plot for the period January-December 2005 is shown in Figure 5.5.

Table 5.3 Summary of models.

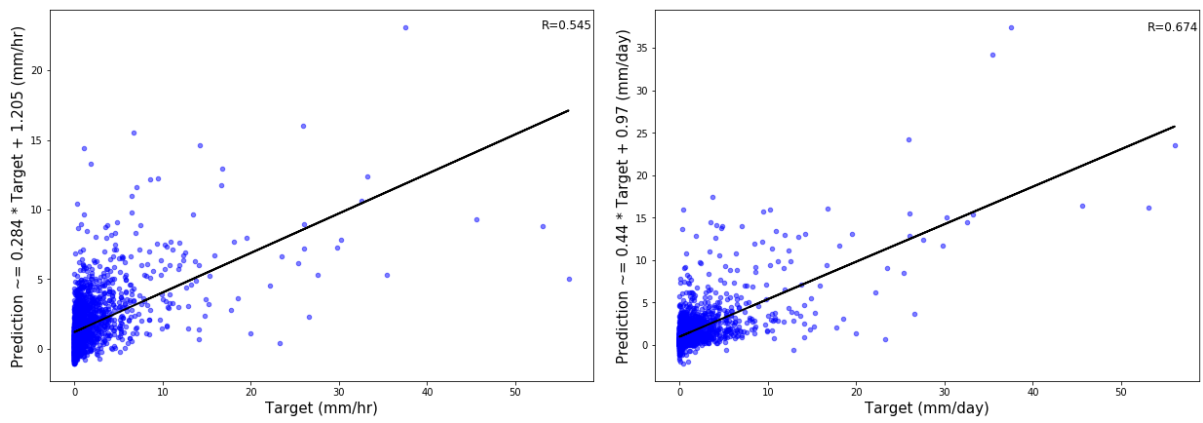
<b>Location</b>	<b>MLR-model Output</b>	<b>ANN-model Output</b>
<b>CPT</b>	<b><math>0.296T + 1.112</math></b>	<b><math>0.53T + 0.73</math></b>
<b>DBN</b>	<b><math>0.199T + 2.345</math></b>	<b><math>0.37T + 1.74</math></b>
<b>PTE</b>	<b><math>0.284T + 1.205</math></b>	<b><math>0.44T + 0.97</math></b>



(a)

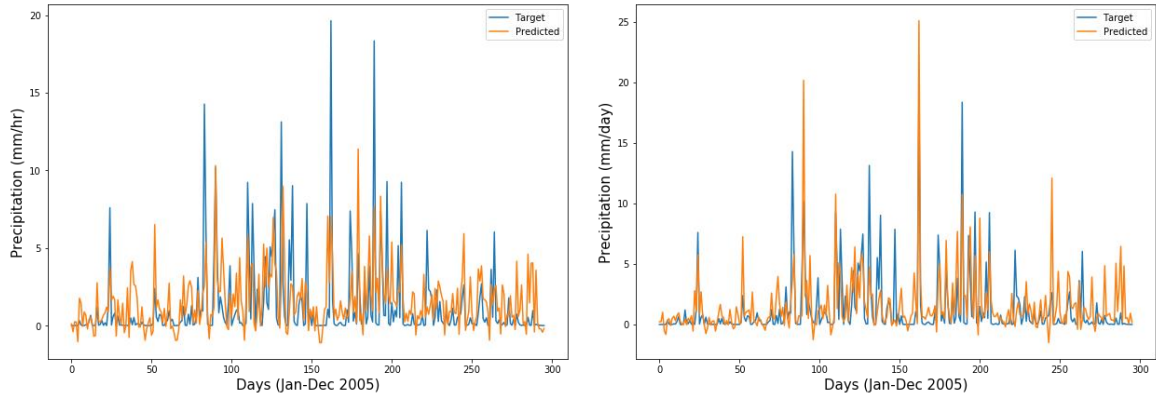


(b)

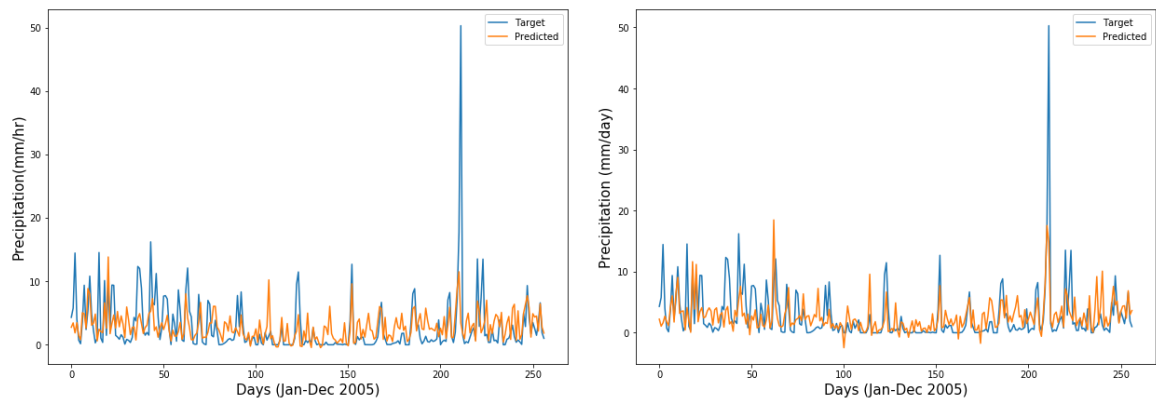


(c)

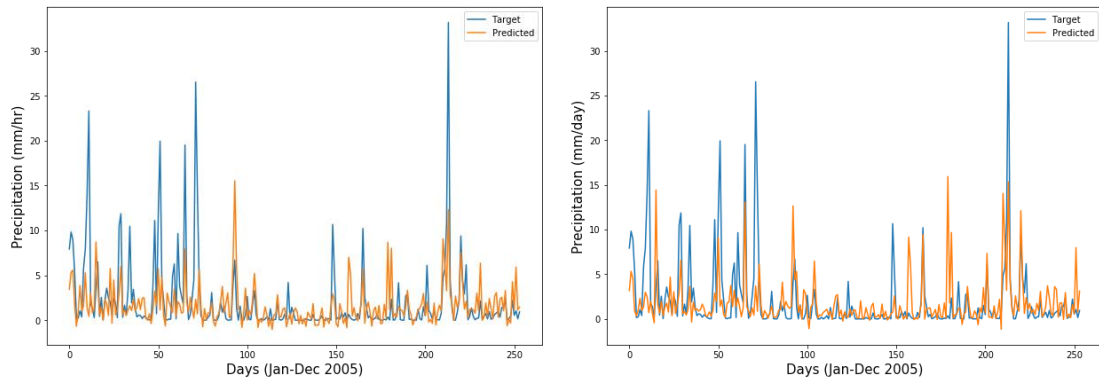
Figure 5.4 Plots of model outputs based on MLR (left panels) and ANN (right panels) for (a) CPT (b) DBN, and (c) PTE.



(a)



(b)



(c)

Figure 5.5 Comparison plots of observed precipitation and prediction for MLR (left panels) and ANN (right panels) models for January – December 2005: (a) CPT (b) DBN (c) PTE.

## 5.6 Conclusion

The capability of cloud properties as a potential predictor in the daily prediction of precipitation events is demonstrated using two machine learning techniques: multilinear regression (MLR) and artificial neural network (ANN) algorithms. Generally, cloud properties significantly proved valuable for multilocation precipitation forecast considering the measured accuracy (averagely, R-value is  $> 0.50$  and RMSE relatively small in the order of  $< 5.00$ ) across all the locations. Subsequently, the model produced by ANN demonstrated better accuracy than MLR on a broad scale. However, MLR proves to be more stable for multilocation prediction. Besides, model accuracy tends to depend on the data size available for the learning process and consequently a reduction in error. Therefore, the results obtained suggest that a more accurate, consistent, and negligible error model can be developed by factoring in more closely related input parameters.

## References

1. IPCC, Climate Change 2013: The physical science basis. Contribution of working group I to the fifth assessment report of the Intergovernmental Panel on Climate Change. Cambridge, United Kingdom and New York, USA. 2013.
2. Rajeevan, M., Prediction of Indian summer monsoon: Status, problems and prospects. *Current Science*, vol. 81, pp. 1451–1457, 2001.
3. Schleiss, M., Chamoun, S. and Berne, A., Stochastic simulation of intermittent rainfall using the concept of dry drift. *Water Resources Research*, vol. 50, pp. 2329–2349, 2014.
4. Dee, D.P., Uppala, S., Simmons, A., Berrisford, P., Poli, P., Kobayashi, S., Andrae, U., Balmaseda, M., Balsamo, G., Bauer, D.P., et al., The ERA-Interim reanalysis: Configuration and performance of the data assimilation system. *Quarterly Journal of the Royal Meteorological Society*, vol. 137, pp. 553–597, 2011.
5. Deo, R.C. and Şahin, M., Application of the extreme learning machine algorithm for the prediction of monthly effective drought index in eastern Australia. *Atmospheric Research*, vol. 153, pp. 512–525, 2015.

6. Hashim, R., Roy, C., Motamedi, S., Shamshirband, S., Petković, D., Gocic, M., and Lee, S., Selection of meteorological parameters affecting rainfall estimation using neuro-fuzzy computing methodology. *Atmospheric Research*, vol. 171, pp. 21–30, 2016.
7. Alizadeh-Choobari, O. and Gharaylou, M., Aerosol impacts on radiative and microphysical properties of clouds and precipitation formation. *Atmospheric Research*, vol. 185, pp. 53–64, 2017.
8. Padmakumari, B., Maheskumar, R.S., Anand, V. and Axisa, D., Microphysical characteristics of convective clouds over ocean and land from aircraft observations. *Atmospheric Research*, vol. 195, pp. 62–71, 2017.
9. Freud, E. and Rosenfeld, D., Linear relation between convective cloud drop number concentration and depth for rain initiation. *Journal of Geophysical Research: Atmospheres*, vol. 117, no. D02207, 2012.
10. Rosenfeld, D., Andreae, M.O., Asmi, A., Chin, M., de Leeuw, G., Donovan, D.P., Kahn, R., Kinne, S., Kivekäs, N., Kulmala, M., Lau, W., Schmidt, S.K., Suni, T., Wagner, T., Wild, M. and Quaas, J., Global observations of aerosol-cloud-precipitation climate interactions. *Reviews of Geophysics*, vol. 52, pp. 750–808, 2014.
11. Lu, Z., Szafron, D., Greiner, R., Lu, P., Wishart, D.S., Poulin, B., Anvik, J., Macdonell, C. and Eisner, R., Predicting subcellular localization of proteins using machine-learned classifiers. *Bioinformatics* vol. 20 no. 4, pp. 547–556, 2004.
12. Ahmadi, M.A., Soleimani, R., Lee, M., Kashiwao, T. and Bahadori, A., Determination of oil well production performance using artificial neural network (ANN) linked to the particle swarm optimization (PSO) tool. *Petroleum*, vol. 1, no. 2, pp. 118–132, 2015.
13. Popova, M., Isayev, O. and Tropsha, A., Deep reinforcement learning for de novo drug design. *Science Advances*, vol. 4, eaap7885, 2018.
14. Lee, J., Kim, C., Lee, J., Kim, N. and Kim, H., Application of artificial neural networks to rainfall forecasting in the Geum River Basin, Korea. *Water*, vol. 10, 1448, 2018.
15. Yen, M., Liu, D., Hsin, Y., Lin, C. and C. Chen, Application of the deep learning for the prediction of rainfall in Southern Taiwan. *Scientific Report*, vol. 9, 12774, 2019.

16. Gholizadeh, M.H. and Darand, M., Forecasting precipitation with artificial neural networks (Case Study: Tehran). *Journal of Applied Sciences*, vol. 9, pp. 1786–1790, 2009.
17. Mislán, M., Havaluddin, H., Hardwinarto, S., Sumaryono, M.S. and Aipassa, M.I., Rainfall monthly prediction based on artificial neural network: A case study in Tenggara Station, East Kalimantan – Indonesia. *Procedia Computer Science*, vol. 59, pp. 142 – 151, 2015.
18. Benevides, V.P., Catalao, J. and Nico, G., Neural network approach to forecast hourly intense rainfall using GNSS precipitable water vapor and meteorological sensors. *Remote Sensing*, vol. 11, 966, 2019.
19. Tokar, A.S and Johnson, P.A., Rainfall-runoff modeling using artificial neural networks. *Journal of Hydrologic Engineering*, vol. 4, pp. 232–239, 1999.

## Chapter 6 –

# Summary and challenges

### 6.1 Summary

This work described the grand challenge associated with climate change, such as poor assessment and vulnerability, and the components involved, like aerosols, based on existing literature (see Chapter 1). The research further presented an insightful description of the various elements that drive climate change (such as aerosol, cloud, and precipitation), illustrated their interactions and methods of measurements, and the current understanding of their processes (Chapter 2). Subsequently, the project examined the mechanism and processes of atmospheric aerosols from emission to their role in clouds and precipitation formation in South Africa (SA). The research provided answers and clarification to the cause of some identified climate change impacts such as low precipitation and drought, flooding, and surface temperature rise experienced over the region. Further insight into aerosol-cloud-precipitation interactions (ACPI) is provided using SA as a case study. Also evaluated is the effective radiative forcing over the region and the cause, including identification and the emission sources. Furthermore, the study assessed the accuracy of satellite instruments in retrieving aerosol optical and spectral properties over the region. Finally, the research demonstrated the capabilities and improvement of satellite retrieved cloud properties to accurately and timely predict precipitation using machine learning techniques.

Fundamentally, atmospheric aerosols and greenhouse gases (GHG) are significant influencers of changes in global climate and regional weather conditions. Conventionally, GHG is established to possess a net positive radiative (warming) effect on global climate, and it is well represented in global climate models mainly due to its homogeneous characteristics. However, quantifying the aerosol impact on climate constitutes considerable vagueness due to their heterogeneous characteristics as a function of multiple types mixed in the natural environment. Different aerosol types basically exhibit distinct features and interact differently with the environment, making evaluating their impacts complex in space and time. With the deployment of more satellite instruments and earth observing systems, a sharp rise in the amount of data available to monitor the activities of aerosols and clouds, including extensive spatio-temporal coverage, set a new era in the attempt to understand ACPI and climate change better. However, this advancement cannot adequately address the existing challenges

owing to the unreliable data retrieved from satellite measurements. Therefore, enhancing the capabilities through intensified research of existing infrastructures, especially satellite systems, in evaluating earth changes is essential.

As a progress, the project in Chapter 3 examining ACPI using satellite data identified flooding, drought and steady temperature rise over the years as the critical impacts of climate change in SA. Further findings from the study show that the high temporal variability in aerosol emissions consistently influences specific atmospheric parameters like the cloud water and droplet size to drive changes that causes flooding and sometimes drought experienced in SA. The chapter further presented a new knowledge of a threshold for liquid water path and a dynamic minimum for cloud effective radius depending on cloud type for precipitation to occur as part of understanding ACPI better. The project in Chapter 4 identified sulphate, nitrate, sea salt and black and organic carbon as the significant aerosol types found over SA and mainly result from anthropogenic and natural sources. Also, these aerosols predominantly originate from the northern parts of the region. Furthermore, the study found the accuracy of satellite instruments observation of aerosol properties varies amongst parameters and surface type. Finally, the project in Chapter 5 demonstrated the capabilities of predicting daily rainfall from satellite retrieved cloud properties using machine learning (ML) methods. The chapter concluded that considering more cloud parameters and more sophisticated ML algorithm will enhance the prediction of weather and climate variation.

## **6.2 Challenges**

Acquiring the appropriate information and tools to sufficiently characterise, model, and understand the coupling effect amongst the atmosphere, land and oceans constitute a contending challenge. Any attempt to define the relationship amongst the components that drive climate change requires analysing a vast amount of data and solving complex physics equations. Yet, not all available data is suitable to characterise the mechanism and process as they influence climate change. Therefore, the transformation of data is a typical challenge during this research. Another crucial challenge involves the computational aspect because one way to handle the huge data requires high-level programming. Therefore, one needs to be acquainted with one or more programming languages. Finally, acquiring data through in-situ and ground remote sensing instruments to enhance satellite data is the most challenging aspect. Satellite instruments are poor in measurements and therefore require proper

calibration and validation. Meanwhile, ground data are scanty and limited in coverage but are highly necessary for the reliability of research.

### **6.3 Future work**

In this project, I provided a better insight into the process and mechanism of aerosol-cloud-precipitation interactions (ACPI) in the context of drought and flooding events and the implications of climate change. Unlike in my previous work, this research considered other factors, including the atmospheric dynamic and thermodynamics, to better explain and understand events around precipitation development and occurrences. Also, I have improved aerosols' characterisation, which will enhance the accuracy of satellite observations in yielding better data quality and spatiotemporal coverage. One other critical component that drives global climate is the oceans. Therefore, in the future, I will focus more on the ocean dynamics and thermodynamics impacts on coastal and continental climates. The expected results will explore improving modelling of the coupling effect of the atmosphere, land, and ocean on climate change. Furthermore, future work will improve instruments and methods of aerosol and cloud evaluation, especially regarding the qualitative and quantitative tropospheric-stratospheric gas exchange and concentration of greenhouse gases. This will provide a clearer understanding of climate change and further close the gap of uncertainty.